Macromolecules Containing Metal and Metal-Like Elements

Volume 2

Macromolecules Containing Metal and Metal-Like Elements

Volume 2

Organoiron Polymers

Edited by

Alaa S. Abd-El-Aziz
Department of Chemistry, The University of Winnipeg, Winnipeg, Manitoba, Canada

Charles E. Carraher Jr.
Department of Chemistry and Biochemistry, Florida Atlantic University, Boca Raton, Florida

Charles U. Pittman Jr.
Department of Chemistry, Mississippi State University, Mississippi State, Mississippi

John E. Sheats
Department of Chemistry, Rider University, Lawrenceville, New Jersey

Martel Zeldin
Department of Chemistry, Hobart and William Smith Colleges, Geneva, New York

WILEY-INTERSCIENCE
A John Wiley & Sons, Inc., Publication

Published by John Wiley & Sons, Inc., Hoboken, New Jersey.
Published simultaneously in Canada.

Library of Congress Cataloging-in Publication Data:

ISBN 0-471-45078-2
ISSN 1545-438X

Printed in the United States of America.

10 9 8 7 6 5 4 3 2 1

Contributors

Alaa S. Abd-El-Aziz, Department of Chemistry, The University of Winnipeg, Winnipeg, Manitoba, Canada R3B 2E9 (a.abdelaziz@uwinnipeg.ca)

Lan Cao, Department of Chemistry, University of Toronto, 80 St. George Street, Toronto, Ontario, Canada M5S 3H6

Paul Cyr, Department of Chemistry, University of Toronto, 80 St. George Street, Toronto, Ontario, Canada M5S 3H6

Mark A. Hempenius, Department of Chemical Technology, University of Twente and MESA$^+$ Research Institute, PO Box 217, 7500 AE Enschede, The Netherlands

E. Stefan Kooij, Department of Chemical Technology, University of Twente and MESA$^+$ Research Institute, PO Box 217, 7500 AE Enschede, The Netherlands

Igor Korczagin, University of Twente and MESA$^+$ Research Institute, PO Box 217, 7500 AE Enschede, The Netherlands

Heinz-Bernhard Kraatz, Department of Chemistry, University of Saskatchewan, 110 Science Place, Saskatoon, Saskatchewan, Canada S7N 5C9

Rob G. H. Lammertink, University of Twente and MESA$^+$ Research Institute, PO Box 217, 7500 AE Enschede, The Netherlands

Ian Manners, Department of Chemistry, University of Toronto, 80 St. George Street, Toronto, Ontario, Canada M5S 3H6 (imanners@chem.utoronto.ca)

Masaki Murata, Department of Chemistry, School of Science, The University of Tokyo, 7-3-1 Bunkyo-ku, Tokyo, Japan 113-0033

Hiroshi Nishihara, Department of Chemistry, School of Science, The University of Tokyo, 7-3-1 Bunkyo-ku, Tokyo, Japan 113-0033

Rawda M. Okasha, Department of Chemistry, The University of Winnipeg, Winnipeg, Manitoba, Canada R3B 2E9

Han Peng, Department of Chemistry, Institute of Nano Science and Technology and Open Laboratory of Chirotechnology of the Institute of Molecular Technology for Drug Discovery and Synthesis, Hong Kong University of Science and Technology, Clear Water Bay, Kowloon, Hong Kong, China

Mária Péter, Department of Chemical Technology, University of Twente and MESA$^+$ Research Institute, PO Box 217, 7500 AE Enschede, The Netherlands

David Rider, Department of Chemistry, University of Toronto, 80 St. George Street, Toronto, Ontario, Canada M5S 3H6

Neil S. Robins, Department of Chemical Technology, University of Twente and MESA$^+$ Research Institute, PO Box 217, 7500 AE Enschede, The Netherlands

Qunhui Sun, Department of Chemistry, Institute of Nano Science and Technology and Open Laboratory of Chirotechnology of the Institute of Molecular Technology for Drug Discovery and Synthesis, Hong Kong University of Science and Technology, Clear Water Bay, Kowloon, Hong Kong, China

Ben Zhong Tang, Department of Chemistry, Institute of Nano Science and Technology and Open Laboratory of Chirotechnology of the Institute of Molecular Technology for Drug Discovery and Synthesis, Hong Kong University of Science and Technology, Clear Water Bay, Kowloon, Hong Kong, China (tangbenz@ust.hk)

Erin K. Todd, Department of Chemistry, The University of Winnipeg, Winnipeg, Manitoba, Canada R3B 2E9

G. Julius Vancso, Department of Chemical Technology, University of Twente and MESA$^+$ Research Institute, PO Box 217, 7500 AE Enschede, The Netherlands

Xiao-Song Wang, Department of Chemistry, University of Toronto, 80 St. George Street, Toronto, Ontario, Canada M5S 3H6

Mitchell A. Winnik, Department of Chemistry, University of Toronto, 80 St. George Street, Toronto, Ontario, Canada M5S 3H6 (mwinnik@chem.utoronto.ca)

Kaitian Xu, Department of Chemistry, Institute of Nano Science and Technology and Open Laboratory of Chirotechnology of the Institute of Molecular Technology for Drug Discovery and Synthesis, Hong Kong University of Science and Technology, Clear Water Bay, Kowloon, Hong Kong, China

Contents

Preface

This is the second volume in the series, *Macromolecules Containing Metal and Metal-like Elements.* The first volume presented a half-century, historical perspective of metal- and metalloid-containing polymers. This tome on iron-containing polymers represents the first of several thematic volumes that will be published within this series. The lead chapter highlights the development of organoiron polymers since the early 1950s. It also describes many of the different classes of these macromolecules and the current trends in the field. The subsequent 10 chapters review many of the important findings from research groups from around the world.

Two different classes of organoiron polymers are the focus of this volume: ferrocene-based macromolecules and polymers containing cationic arene cyclopentadienyliron complexes incorporated into their structures. Ferrocene-based polymers are the best-examined class of organo-transition-metal polymer. Since they were first examined in the 1950s, this class of organoiron polymer has been synthesized by almost all imaginable polymerization techniques.

Since the early 1990s, significant advances have been made in the synthesis of new classes of high-molecular-weight ferrocene-based polymers. This has led to countless examples of homo- and copolymers with well-defined structures. These materials exhibit attractive electrochemical, optical, thermal, biological, and magnetic properties. New structurally defined copolymers have also been shown to possess interesting morphologies. While arene complexes have also been known since the 1950s, polymers containing these cationic cyclopentadienyliron moieties in their structures were not reported until the 1990s.

Alaa S. Abd-El-Aziz
Charles E. Carraher Jr.
Charles U. Pittman Jr.
John E. Sheats
Martel Zeldin

Series Preface

Most traditional macromolecules deal with less than 10 elements (mainly C, H, N, O, S, P, Cl, F), whereas metal and semi-metal-containing polymers allow properties that can be gained through the inclusion of nearly 100 additional elements. Macromolecules containing metal and metal-like elements are widespread in nature with metalloenzymes supplying a number of essential physiological functions including respiration, photosynthesis, energy transfer, and metal ion storage.

Polysiloxanes (silicones) are one of the most studied classes of polymers. They exhibit a variety of useful properties not common to non-metal-containing macromolecules. They are characterized by combinations of chemical, mechanical, electrical, and other properties that, when taken together, are not found in any other commercially available class of materials. The initial footprints on the moon were made by polysiloxanes. Polysiloxanes are currently sold as high-performance caulks, lubricants, antifoaming agents, window gaskets, O-rings, contact lens, and numerous and variable human biological implants and prosthetics, to mention just a few of their applications.

The variety of macromolecules containing metal and metal-like elements is extremely large, not only because of the larger number of metallic and metalloid elements, but also because of the diversity of available oxidation states, the use of combinations of different metals, the ability to include a plethora of organic moieties, and so on. The appearance of new macromolecules containing metal and metal-like elements has been enormous since the early 1950s, with the number increasing explosively since the early 1990s. These new macromolecules represent marriages among many disciplines, including chemistry, biochemistry, materials science, engineering, biomedical science, and physics. These materials also form bridges between ceramics, organic, inorganic, natural and synthetic, alloys, and metallic materials. As a result, new materials with specially designated properties have been made as composites, single- and multiple-site catalysts, biologically active/inert materials, smart materials, nanomaterials, and materials with superior conducting, nonlinear optical, tensile strength, flame retardant, chemical inertness, superior solvent resistance, thermal stability, solvent resistant, and other properties.

There also exist a variety of syntheses, stabilities, and characteristics, which are unique to each particular material. Further, macromolecules containing metal and metal-like elements can be produced in a variety of geometries, including linear, two-dimensional, three-dimensional, dendritic, and star arrays.

In this book series, macromolecules containing metal and metal-like elements will be defined as large structures where the metal and metalloid atoms are (largely) covalently bonded into the macromolecular network within or pendant to the polymer backbone. This includes various coordination polymers where combinations of ionic, sigma-, and pi-bonding interactions are present. Organometallic macromolecules are materials that contain both organic and metal components. For the purposes of this series, we will define metal-like elements to include both the metalloids as well as materials that are metal-like in at least one important physical characteristic such as electrical conductance. Thus the term includes macromolecules containing boron, silicon, germanium, arsenic, and antimony as well as materials such as poly(sulfur nitride), conducting carbon nanotubes, polyphosphazenes, and polyacetylenes.

The metal and metalloid-containing macromolecules that are covered in this series will be essential materials for the twenty-first century. The first volume is an overview of the discovery and development of these substances. Succeeding volumes will focus on thematic reviews of areas included within the scope of metallic and metalloid-containing macromolecules.

Alaa S. Abd-El-Aziz
Charles E. Carraher Jr.
Charles U. Pittman Jr.
John E. Sheats
Martel Zeldin

CHAPTER 1

Overview of Organoiron Polymers

Alaa S. Abd-El-Aziz

Department of Chemistry, The University of Winnipeg, Winnipeg, Manitoba, Canada

CONTENTS

I. INTRODUCTION

Iron is the second most abundant metal and the fourth most abundant element found in Earth's crust. In 1951, Kealy and Pauson made the extraordinary discovery of ferrocene.[1] Prior to that time, complexes containing transition metal–carbon bonds were rare, and it was thought that these bonds must be unstable. The high thermal stability of ferrocene changed many of these ideas, and organoiron chemistry

Macromolecules Containing Metal and Metal-like Elements, Volume 2: Organoiron Polymers, Edited by Alaa S. Abd-El-Aziz, Charles E. Carraher, Jr., Charles U. Pittman, Jr., John E. Sheats, and Martel Zeldin
ISBN 0-471-45078-2

became the focus of numerous investigations. From the initial reports on the synthesis and structure of ferrocene, there have been countless studies examining the chemistry of organoiron complexes.[1–3]

The rich chemistry of ferrocene stems from the nucleophilicity of the cyclopentadienyl rings, which allows for their reactions with numerous electrophiles. Within a few years of its discovery, a number of functionalized ferrocene molecules had been prepared, and in 1955, the first polymer containing ferrocene in its structure was reported by Arimoto and Haven.[4] In the years to follow, the fascinating chemistry associated with ferrocene led to research in the synthesis of ferrocene-based polymers in which the organometallic group exists in sidechains, the mainchain, or discrete locations within the polymer.[5–7] Ferrocene-based polymers are the most well-examined class of organometallic polymer, and their methods of synthesis and their properties cover a wide spectrum. These types of polymers have been shown to exhibit interesting electrochemical, optical, thermal, morphological, pharmacological, and magnetic properties.[5,6]

The displacement of one of the cyclopentadienyl rings of ferrocene by an arene allows for the isolation of cationic η^6-arene-η^5-cyclopentadienyliron complexes.[8] While Coffield and coworkers reported the first cyclopentadienyliron coordinated arene in 1957 by refluxing mesitylene with cyclopentadienyliron dicarbonyl chloride,[9] it was 6 years later when Nesmeyanov and coworkers prepared these complexes using ferrocene.[10,11] These cationic organoiron complexes had properties very different from those exhibited by ferrocene. For example, the complexed benzene rings were found to be susceptible to attack by nucleophiles, and did not show the same reactivity as did uncomplexed benzenes. Also, while the iron centers in ferrocene undergo stable electrochemical oxidation, arene cyclopentadienyliron complexes are reduced electrochemically.[12] It is also important to note that the arene iron bond does not show the same thermal stability, and is readily cleaved by pyrolysis, photolysis, and electrolysis. While arene complexes of cyclopentadienyliron have been known since the 1950s, it was not until the 1990s that polymers containing these organometallic groups in their structures were reported.

While many studies have reported the interesting chemistry associated with the cyclopentadienyl and benzene complexes of iron, a number of other studies have reported the synthesis of other classes of organoiron polymers. For example, iron carbonyl moieties π-coordinated to dienes and cyclopentadienyl compounds have been investigated, and each new class of polymer relates new information about organoiron polymers and the chemistry of organoiron complexes. Polymers possessing iron–carbon σ and π bonds or only iron–carbon σ bonds within the polymer's backbones are classes of polymers that have not received a great deal of attention. Polymers containing iron–iron bonds within, or pendent to their backbones have also been synthesized using a number of different strategies, and have exhibited interesting properties.

This chapter presents an overview of all classes of macromolecules containing iron–carbon bonds and highlights some examples of these materials. The methods utilized to synthesize and characterize these polymers are described and the properties of some of the organoiron-based polymers are noted. This chapter focuses on the diversity found in the area of organoiron polymer chemistry and briefly introduces the materials covered in the remaining chapters in this volume.

II. FERROCENE-BASED POLYMERS

Soon after the monumental discovery and elucidation of the structure of ferrocene, the homo- and copolymerization of vinylferrocene was reported using a number of different catalysts.[4] The solution and bulk synthesis of polyvinylferrocene (**1**) has been studied in detail, as have the properties of polyvinylferrocene.[13–15] While many of these studies were undertaken in the 1960s and 1970s, the polymerization of vinylferrocene continues to be an active area of research. The copolymerization of vinylferrocene with styrene using a "living" radical initiator (viz., TEMPO) was also reported.[16]

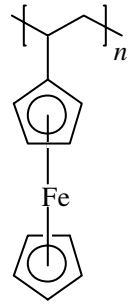

1

The properties that the ferrocenyl groups introduce into polymers have been the focus of numerous investigations. Kuramoto and coworkers have shown that copolymers (**2**) prepared from *N,N*-diethylacrylamide and vinyl ferrocene had decreasing low critical solution temperature (LCST) values with increasing ferrocene incorporation because of their reduced solubility in aqueous solution.[17] Oxidation of the ferrocene units increased their hydrophilicity and resulted in increased LCST values for these materials. The same observations were observed for copolymers prepared with ferrocenylethylacrylamide and isopropylacrylamide.[18] These organoiron polymers had lower LCST values than did poly(*N*-isopropylacrylamide). In both of these studies, there was only a low incorporation of the organometallic monomer into these materials.

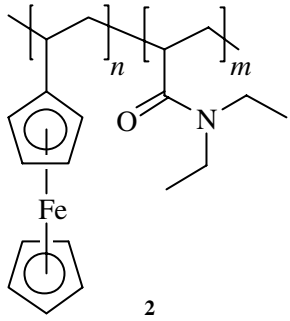

2

It has also been reported that polymers containing ferrocene units in the mainchain or sidechains may possess liquid crystalline characteristics.[19–23] Ferrocene-based liquid crystalline polyesters (**3**) containing phosphorous groups in their backbones have been reported by Senthil and Kannan.[23]

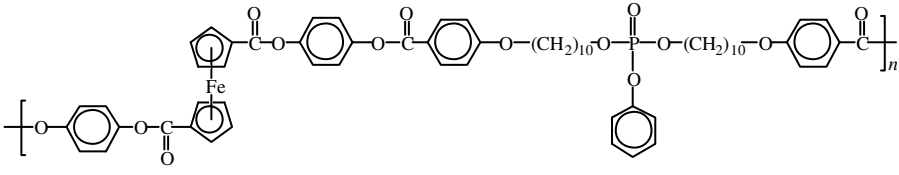

3

Polymers containing sidechain and mainchain ferrocenyl moieties have also been reported to possess nonlinear optical (NLO) properties.[24–26] By incorporating 5 mol% of the organometallic monomer into the polymethacrylate (**4**), it was possible to generate NLO properties.[26]

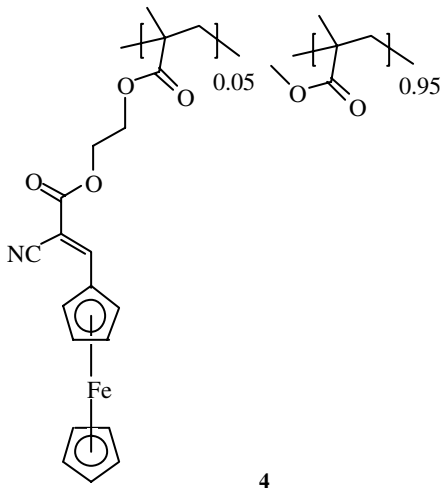

4

Similarly, Neuse and coworkers have reported that the incorporation of a small amount of a ferrocene-containing sidechain into polyaspartamide introduces antiproliferative properties into these materials.[27–29] Polymer **5** is an example of an organoiron-functionalized polymer prepared from reaction of the preformed organic polymer with 4-ferrocenylbutanoic acid.[29]

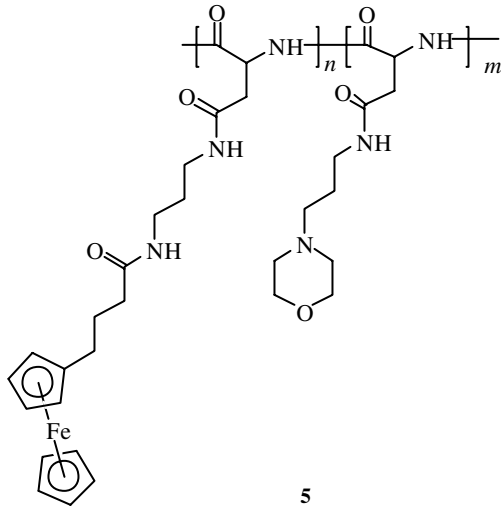

5

The redox stability of the ferrocenyl group has led to the incorporation of this organoiron unit into a number of different classes of macromolecules.[30–32] An amperometric glucose sensing electrode has been prepared utilizing a polymethylsiloxane with ferrocene groups in its sidechain.[30] Peptides functionalized with ferrocene units interact with each other through hydrogen bonds resulting in supramolecular assemblies.[31] Schrock and Wrighton have reported the synthesis of polynorbornenes with ferrocenyl moieties pendent to the norbornene unit (**6**).[32]

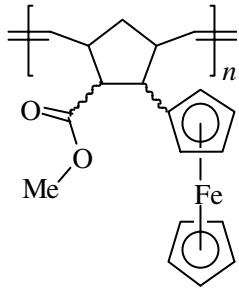

6

The synthesis of metallocenes functionalized with alkyne groups has been reported using a molybdenum catalyst to produce polyacetylenes with ferrocene groups in their sidechains (**7**).[33,34] The living polymerization reactions produced head-to-tail polymers with *trans* double bonds. The living polyacetylene could be surface grafted to a norbornene-functionalized silica support and used in anion exchange chromatography following oxidation of the iron centers.[34]

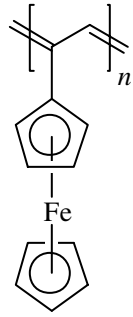

7

Allcock and coworkers have reported the ring-opening polymerization of cyclic phosphazenes functionalized with ferrocenyl groups.[35,36] The polymers were attached to the metallocenes by the phosphorous atoms to either one or both of the cyclopentadienyl rings (**8**).[36]

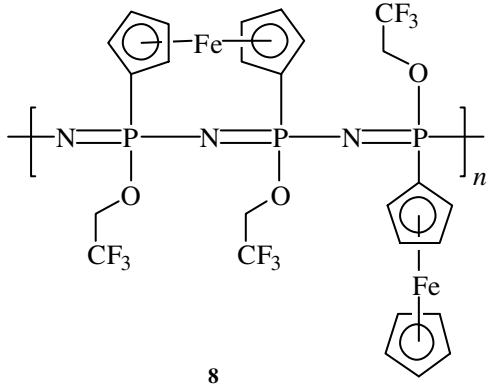

8

Polycondensation reactions have produced mainchain ferrocene polymers since 1961, and since that time, there have countless studies outlining the preparation of this class of material.[37] The functional groups and reaction conditions utilized to prepare these materials are varied, as are the properties of the resulting materials. In the 1970s, Pittman and coworkers reported the synthesis of a thermally stable, high molecular weight polymer (**9**) via polycondensation of disilanols with *bis*-dimethylaminodimethylsilylferrocene.[38]

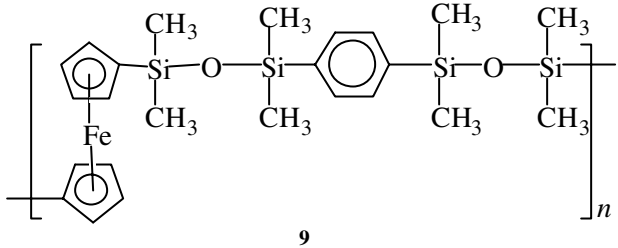

9

Polyamides and polyureas (**10**) have also been synthesized by polycondensation reactions of 1,1′-*bis*(β-aminoethyl)ferrocene with diisocyanates or diacid chlorides, respectively.[39]

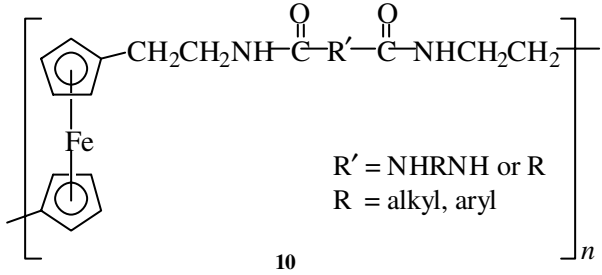

10

The polymerization of 1,2,3-substituted ferrocenes containing one iodo and one acetlyene group using Sonogashira coupling resulted in the production of polymers with functionalized sidechains (**11**).[40] The reaction of 1,1′-diiodoferrocene with diethynyl monomers has also been used in the production of polymetallocenes with semiconducting properties (**12**).[41]

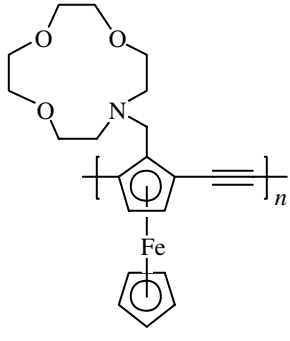

11

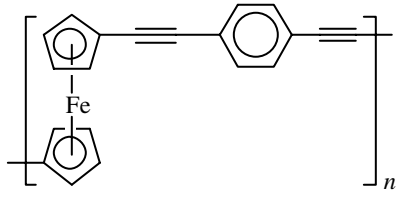

12

Mainchain ferrocene-based polymers have also been synthesized by polyaddition reactions.[42] For example, the reaction of 1,1′-dimercaptoferrocene with 1,4-butandiyl dimethacrylate resulted in the isolation of polymer **13**.

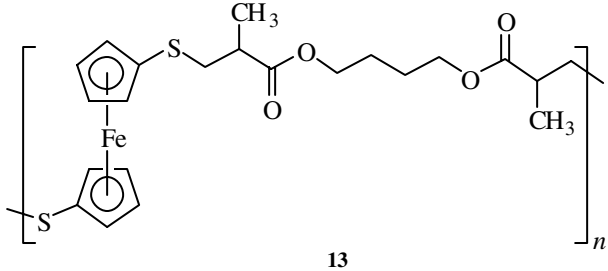

13

A polyferrocenylsilane (**14**) has been prepared via the reaction of the dilithium salt of dicyclopentadienyldimethylsilane with ferrous chloride.[43] Polyferrocenylene substituted with hexyl groups (**15**) has been reported by reaction of the dihexylfulvalene dianion with $[FeCl_2(THF)_2]$.[44] The hexyl groups attached to the cyclopentadienyl rings resulted in an enhanced solubility of these materials, and electrochemical studies showed that the iron centers were interacting. Southard and Curtis have used a similar strategy to prepare soluble conjugated polymetallocenes (**16**) by reaction of an isomeric mixture of *bis*(alkylcyclopentadienide arenes) with ferrous iodide.[45]

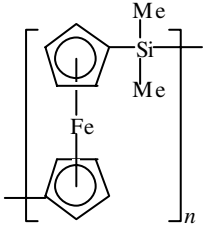

14

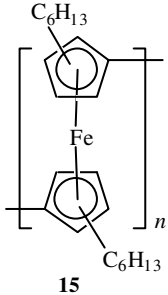

15

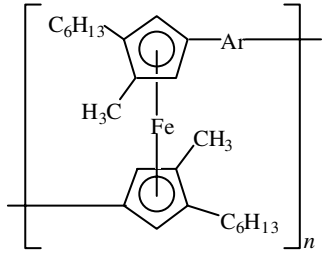

16

High molecular weight face-to-face polymetallocenes (**17**) have been prepared by Rosenblum and coworkers.[46] These polyferrocenes were found to be electrically conducting on doping with I_2.

The ring-opening metathesis polymerization of ferrocenophanes containing bridging vinyl groups has also been reported.[47–49] The incorporation of alkyl groups pendent to their backbones increased the solubility of these polymers (**18**). An enhancement of solubility could also be achieved by copolymerization reactions. Some of these polymers exhibited electrical conductivity.

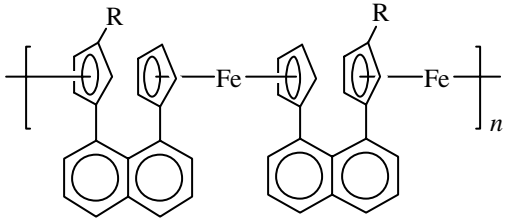

17

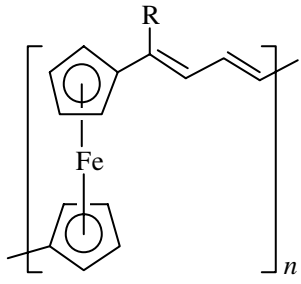

18

Rauchfuss and coworkers have reported the ring-opening polymerization of [3]trithiaferrocenes and [3]triselenaferrocenes with PBu_3.[50,51] The ring-opening-induced desulfurization and deselenization reactions resulted in the formation of high molecular weight polymers. The polyferrocenylene persulfides (**19**) can be reductively decomposed with $LiBHEt_3$ and regenerated on oxidation. The thermal and anionic ROP of [1]thia- and [1]selenaferrocenophanes has also been reported by Manners.[52] The presence of two reversible oxidation processes in the cyclic voltammograms of the polyferrocenyl sulfides indicates that these polymers possess strong metal–metal interactions.

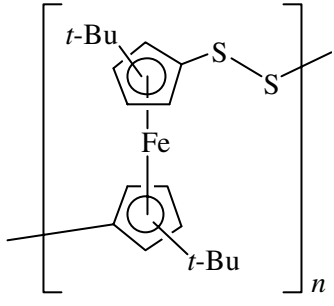

19

Thermal ring-opening polymerization of [2]ferrocenophanes has also been reported by Manners and coworkers (**20**).[53,54] Oxidation of the polyferrocenylethylene with tetracyanoethylene resulted in antiferromagnetic interactions.[53] Unsymmetric [2]ferrocenophanes (R=S, P) have also been synthesized and ring-opened; however, a ferrocenophane containing a C–Si bridge was resistant to thermal, anionic, and transition-metal-catalyzed ROP.[54] The [2]carbathioferrocenophane could also be polymerized in the presence of cationic initiators.

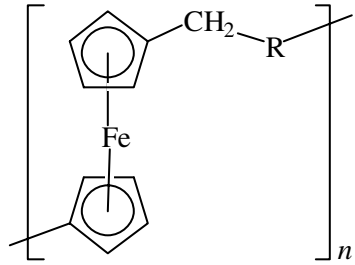

20 R = CH_2, S, P

Polyferrocenylphosphines have been synthesized by the ring-opening polymerization of [1]ferrocenophanes.[55–57] These polymers can be further reacted with elemental sulfur to produce the corresponding polyferrocenylphosphine sulfides (**21**).[55] Borane adducts of polyferrocenylphosphines have been isolated via thermal ROP of the functionalized ferrocenophane, or by addition of the borane to the preformed polyferrocenylphosphine.[56] Manganese and tungsten complexes have also been reacted with a [1]ferrocenophane bearing a bridging phosphine ligand.[57] [1]Ferrocenophanes containing boron bridges have been found to possess large ring tilts, and have been ring-opened thermally to produce the corresponding polymers (**22**).[58] [1]Germaferrocenophanes undergo facile ROP to yield high molecular weight poly(ferrocenyl germanes) (**23**) thermally and with transition metal catalysts.[59,60] The ROP of ferrocenophanes with tin bridges has also been described by the research groups of Manners and Pannell.[61,62] High molecular weight tin polymers (**24**) have been produced by thermal ring-opening polymerization, or at room temperature in solution. It was reported that the ring opening of tin- and germanium-bridged [1]ferrocenophanes is facilitated by the addition of amines.[61]

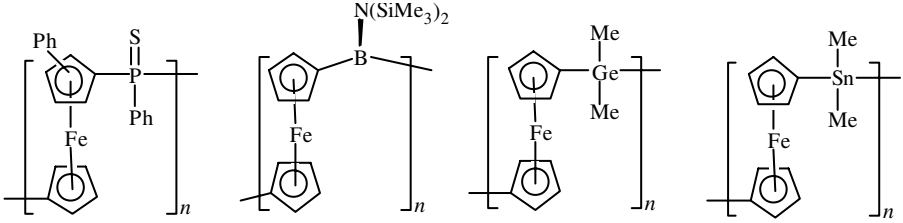

21 **22** **23** **24**

Since the first report on the ring-opening polymerization of [1]silaferrocenophanes in 1992, there have been many developments in this area of research.[63–65] Polymerization of [1]silaferrocenophanes has now been achieved thermally, anionically and with transition metal catalysts. The solid-state polymerization of $Fe(\eta\text{-}C_5H_4)_2SiMeR$ (R=Me, Ph) has also been accomplished using a ^{60}C γ-ray source.[66] It was determined that irradiation of the unsymmetric ferrocenophane (R=Ph) resulted in a stereoregular polymer.

A number of copolymers have been prepared by anionic polymerization of silicon-bridged [1]ferrocenophanes.[67–69] For example, the copolymerization of dimethylsilaferrocenophane with living polystyrene produced a polymer to which 12-crown-4 and $[Me_2SiO]_3$ was added. The living polymer ends of the resulting triblock copolymer were subsequently coupled with Me_2SiCl_2 to produce polymer **25**.[67]

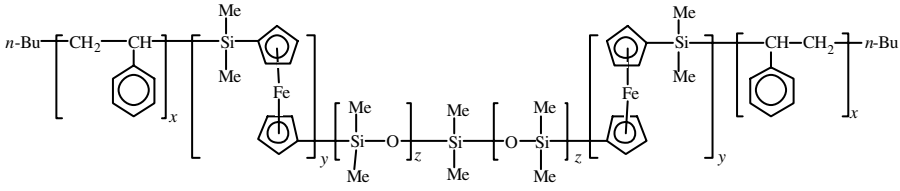

25

Copolymerization reactions with ferrocenophanes using transition metal catalysts have also been accomplished.[70,71] The self-assembly of block copolymers has been examined, and polymers with dimethylsiloxane or ethyleneoxide blocks have been found to be soluble in aqueous solution.[72,73] These ferrocene-based polymers have been found to self-assemble in solution, and their morphologies have been investigated.[70–73] A number of water-soluble anionic (**26**)[74] and cationic (**27**)[75] polyelectrolytes have also been produced by sidechain functionalization.

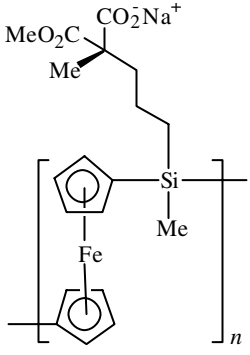

26

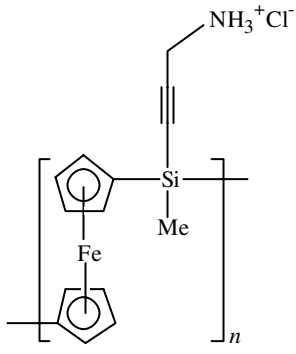

27

Tang and coworkers have reported that pyrolyzed hyperbranched polyferrocenylsilanes have greater ceramic yields than their linear polymeric counterparts.[76] Manners has reported that thermally crosslinked polyferrocenylsilanes (**28**) possessed greater thermal stability than their linear analogs.[77] The swelling properties of these crosslinked polymers were examined, and the solubility parameter of the corresponding linear homopolymer was determined. The pyrolysis of linear, hyperbranched, and crosslinked polyferrocenylsilanes has resulted in the production of ceramics that possess magnetic properties.[76–78]

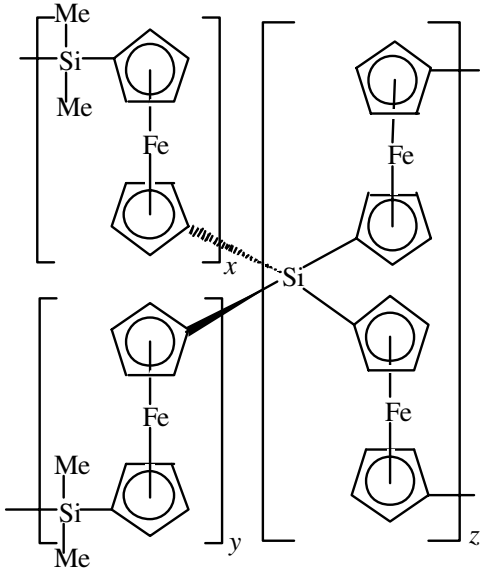

28

The synthesis and properties of star polymers and dendrimers functionalized with ferrocene units has attracted a great deal of attention. The synthesis of high-generation dendrimers functionalized with chiral ferrocenyl units in their structures has been reported.[79] The chiroptical properties of this class of dendrimer was dependent on the number of ferrocenyl groups and their chemical environment, but not on their position within the dendrimer. Deschenaux has reported the synthesis of liquid crystalline ferrocene-based polymers prossessing an enantiotropic smectic A phase.[80] Ferrocene-functionalized cyclic siloxane (**29**) and silsesquioxane branched polymers have also been reported.[81] A hyperbranched polymer with a cubic silsesquioxane core was used to mediate the electrocatalytic oxidation of ascorbic acid.

The guest-host relationship of dendrimers containing 4, 6, and 8 ferrocene groups with cyclodextrins has been examined by Cuadrado and coworkers.[82] It was found that the low-generation dendrimers formed reversible complexes with β-cyclodextrin, while the dendrimer with 16 peripheral ferrocene groups underwent incomplete complexation reactions. The synthesis of a dendrimer containing nine

peripheral organoiron groups (**30**) was prepared by reaction of an amine-functionalized dendrimer with the acid chlorides of ferrocene.[83] These polymers were utilized as supramolecular redox sensors for the recognition of small inorganic anions. Ferrocenylsililation reactions were also used by Astruc and coworkers to prepare dendrimers with up to 243 ferrocenyl units at the periphery.[84]

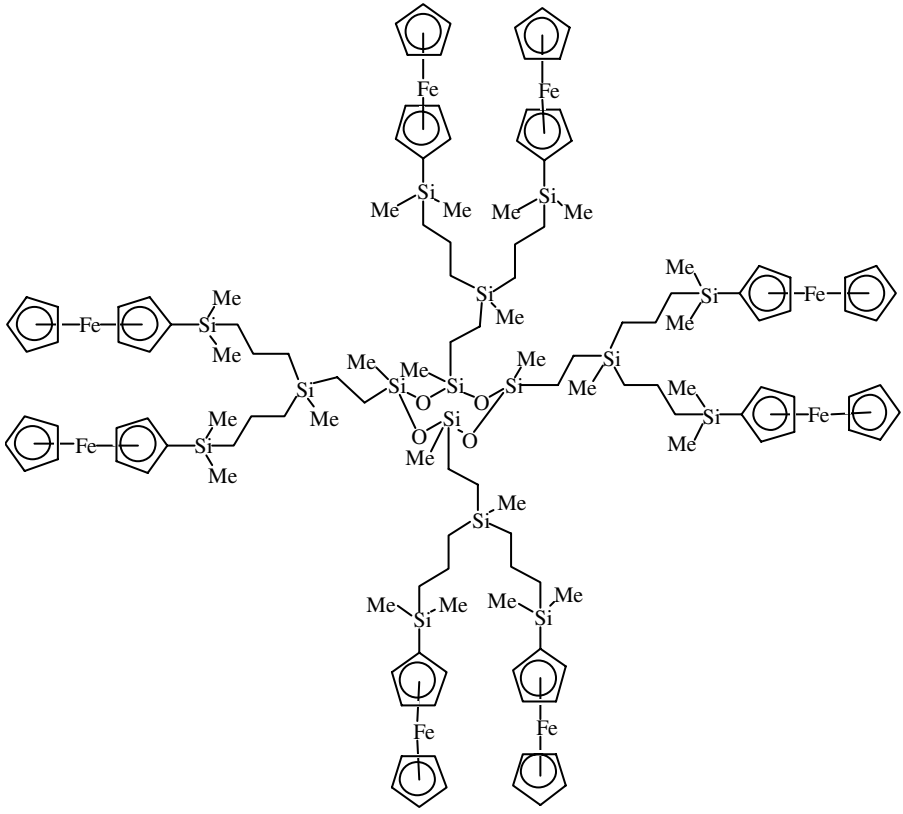

29

III. POLYMERS CONTAINING CYCLOPENTADIENYLIRON–COMPLEXED ARENES

We have reported the synthesis of polymethacrylates (**31**) and polystyrenes with cationic cyclopentadienyliron moieties coordinated to their sidechains using AIBN.[85,86] Photolysis of these organoiron polymethacrylates allowed for the isolation of the corresponding organic polymethacrylates. The weight-average molecular weights (M_w) of these organic polymers ranged from 48,000 to 68,000. Electrochemical studies of the metallated polymethacrylates showed reductions of the iron centers occurring between $E_{1/2} = -1.1$ and -1.3 V.

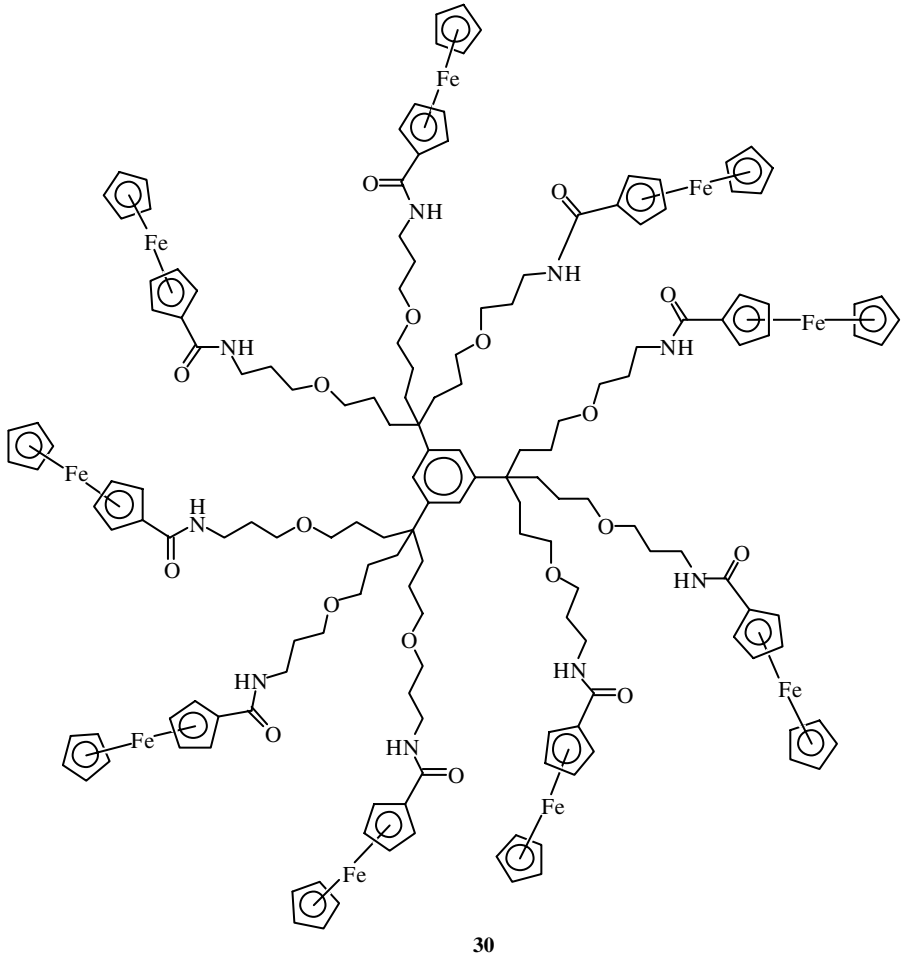
Fe
O
NH
O
O
O
NH
O
Fe
Fe
O
NH
O
O
O
NH
O
Fe
Fe
H
N
O
O
O
O
O
O
HN
O
Fe
O
HN
O
Fe
O
HN
O
Fe
Fe

30

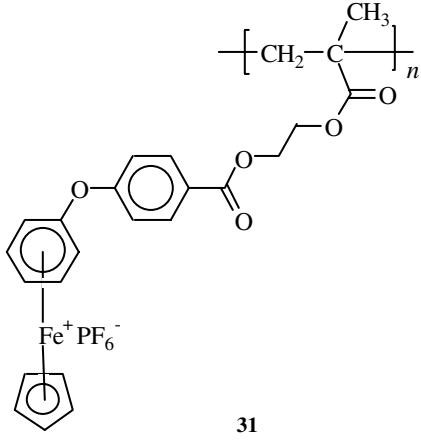
CH3
CH2
C
n
O
O
O
O
O
O
Fe+ PF6-

31

The ring-opening metathesis polymerization of norbornene monomers functionalized with arene complexes of cyclopentadienyliron has been reported using Grubbs' catalyst.[87] These polymerization reactions proceeded rapidly to produce the corresponding polynorbornenes (**32** and **33**). It was found that the incorporation of bulkier aromatic groups in the sidechains of these materials increased their glass transition temperatures and thermal stability.

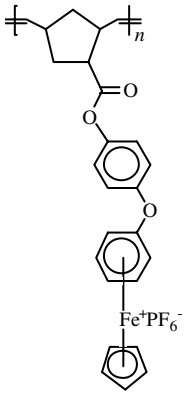

32

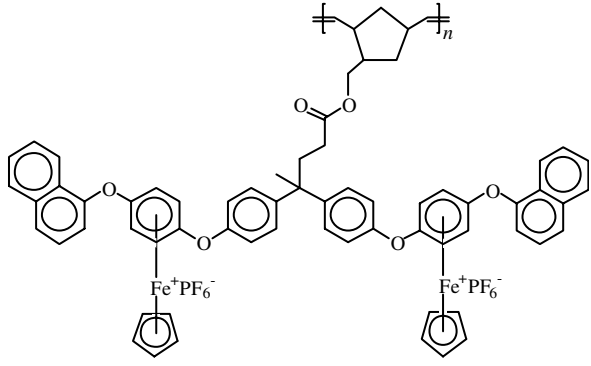

33

The synthesis of cyclopentadienyliron-coordinated polyaromatic ethers and thioethers has been achieved by reaction of dichlorobenzene complexes with various oxygen and sulfur dinucleophiles.[88] These polymers exhibited good solubility in polar organic solvents such as acetone, acetonitrile, DMF, and DMSO. Photolysis of these polymers allowed for the isolation of the corresponding organic polymers; however, the solubilities of these polymers were much lower than those of their metallated analogues. Thermogravimetric analysis of the organoiron polymers indicated that the metallic moieties were cleaved from the polymers at approximately 200°C, while degradation of the polymer backbones occurred around 500°C. By designing diiron complexes containing terminal chloroarenes, polymers with alternating ether– thioether or amine–thioether spacers were also synthesized.[88] Differential scanning calorimetry (DSC) showed that the organic polyethers had the highest glass transition temperatures and polymers with thioether bridges had the lowest. Cyclic voltammetric studies of the cyclopentadienyliron-coordinated polyethers and thioethers (**34**–**36**) showed that these polymers underwent reversible reduction processes. Polymers containing $CpFe^+$ and Cp^*Ru^+ moieties pendent to their backbones have also been synthesized.[89]

The synthesis of polyaromatic ethers (**37**) and thioethers containing azobenzene dyes in their sidechains has been achieved.[90] These polymers were prepared by reaction of cyclopentadienyliron-complexed azobenzene monomers with various dinucleophiles. These organoiron polymers were bright orange or red, and could be bleached by irradiating the polymer in a solution containing hydrogen peroxide.

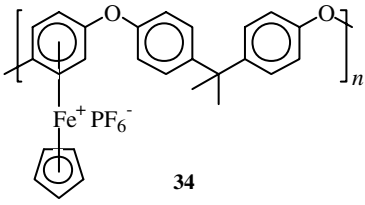

34

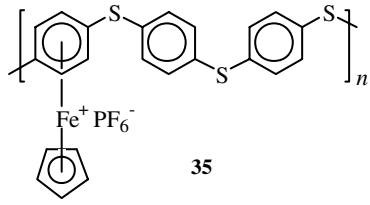

35

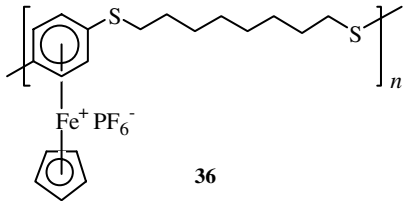

36

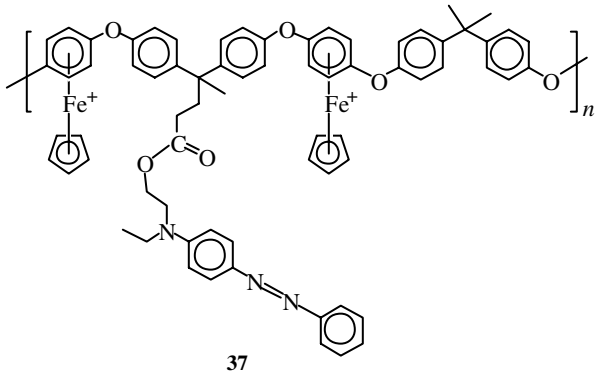

37

The synthesis of polymers containing cyclopentadienyliron moieties within and pendent to their backbones (**38**) was reported by Abd-El-Aziz and coworkers.[91] The cationic cyclopentadienyliron moieties were pendent to the polymer backbones, while the neutral ferrocene units were incorporated into the polymer backbones. The cationic iron centers underwent reversible reduction processes, while the neutral iron centers underwent reversible oxidation processes. The cationic cyclopentadienyliron moieties were cleaved from the polymer backbones by photolysis; however, the ferrocene units in the polymer backbones were not degraded.

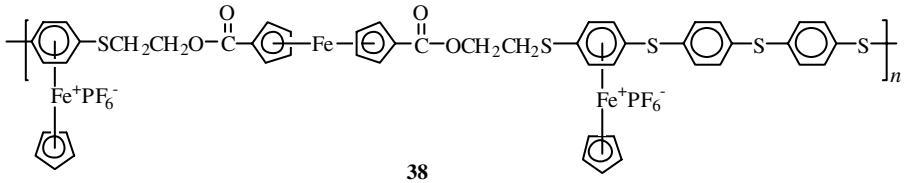

38

The design of polyether/imines coordinated to cyclopentadienyliron moieties (**39**) has been achieved via the reaction of a dialdehyde complex of cyclopentadienyliron with a number of aliphatic and aromatic diamines.[92] The polycondensation reactions resulted in the isolation of the polyether/imines in good yields.

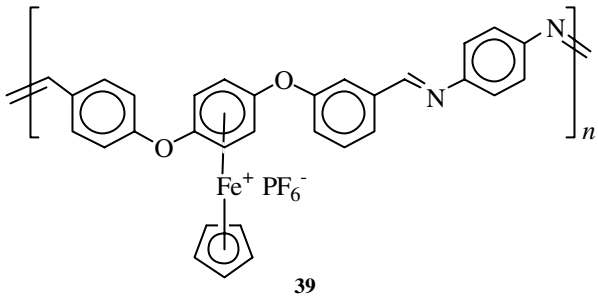

39

Nishihara has reported the complexation of poly(hexyl phenylene) with cyclopentadienyliron, where approximately 1 in every 1.6 aromatic rings was coordinated to the metallic moiety.[93] Spectroelectrochemical analysis of this organoiron polymer (**40**) suggested that a network was formed between the aromatic rings of neighboring polymer chains following reduction of the cationic iron centers to the neutral radicals.

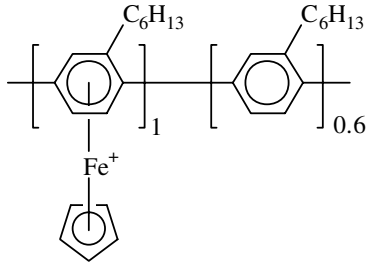

40

Star polymers and dendrimers have been synthesized by Astruc using cyclopentadienyliron-mediated peralkylation, benzylation, and allylation reactions of cationic tri-, *tetra*-, and *hexa*-methylbenzene cyclopentadienyliron complexes.[94–96] These star and dendritic polymers contained cationic cyclopentadienyliron moieties at the core and/or the periphery. The cathodic reduction of nitrates and nitrites to ammonia has been achieved using a water-soluble dendrimer containing six cationic cyclopentadienyliron moieties as a redox catalyst.[94] The octametallic star (**41**) was prepared by deprotonation of permethylated iron complexes.[96]

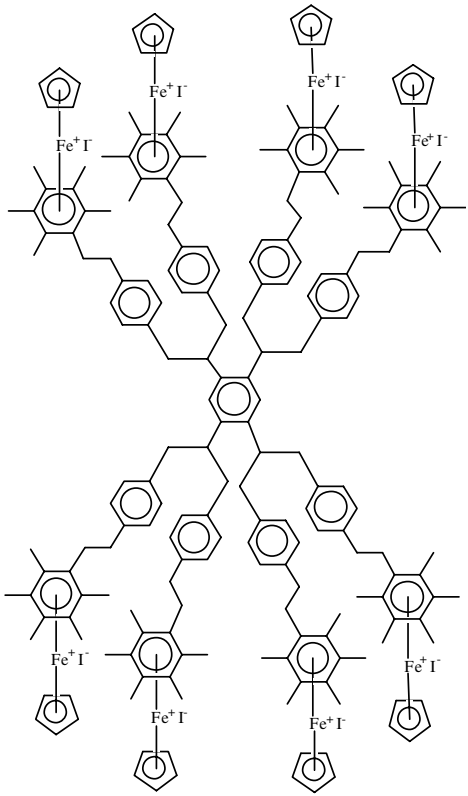

41

Abd-El-Aziz and coworkers have reported the synthesis of star-shaped polyaromatic ethers containing up to 15 cyclopentadienyliron cations pendent to aromatic rings.[97] Polymer **42** is an example of a water-soluble *hexa*-metallic star complex. Electrochemical studies showed that reduction processes for the inner and outer iron complexes could be distinguished for the *hexa*- and nonametallic stars.

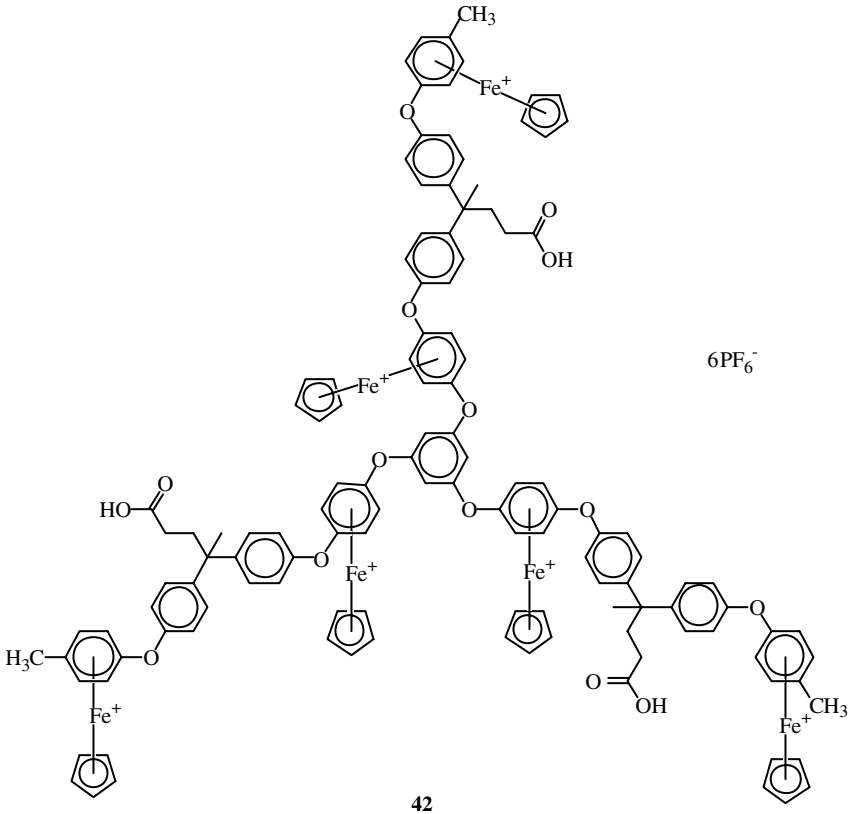

42

IV. POLYMERS CONTAINING IRON CARBONYL COMPLEXES

Polymers containing metal–carbon σ and π bonds were reported by Mapolie and coworkers.[98] Homo- and copolymerization reactions of organoiron monomers containing olefins with AIBN yielded the corresponding organometallic polymers (**43**). Bifunctional hydroxyl monomers functionalized with iron complexes were subjected to polycondensation with terephthaloyl chloride to produce low molecular weight polyesters (**44**).[99]

Martin and Hanks have reported the oxidative polymerization of dicarbonyl (η^5-cyclopentadienyl)(η^1-pyrrolyl)iron(II).[100,101] The resulting polymer (**45**) yielded an azaferrocene polymer (**46**) on refluxing. The electrical conductivities of polymers **45** and **46** were found to be 7×10^{-3} and 1.5×10^{-4} S/cm, respectively.

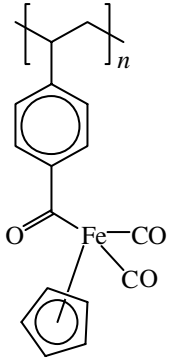

43

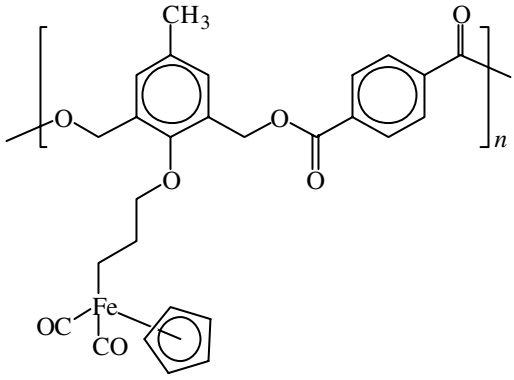

44

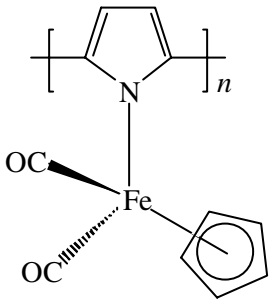

45

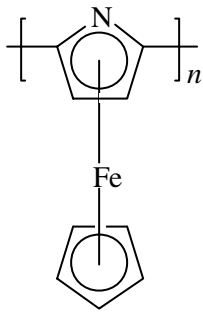

46

In 1973, the homo- and copolymerization of π-(2,4-*hexa*-dienyl acrylate)tricarbonyliron with styrene, methyl acrylate, acrylonitrile, and vinyl acetate was reported by Pittman and coworkers.[102,103] It was reported that these polymers (**47**) could be protonated to produce the π-allyliron derivatives.[103] Nakamura and coworkers have also reported the synthesis and electrochemical properties of polymers containing dienes coordinated to iron tricarbonyl moieties in the polymer sidechains.[104]

UV irradiation of polymers containing silole units in their backbones in the presence of iron pentacarbonyl resulted in the coordination of iron tricarbonyl units to one of every two silole rings in the polymer backbone.[105] On doping, these organoiron polymers (**48**) become electrically conducting and their UV absorption bands are red shifted relative to the uncoordinated polymers.

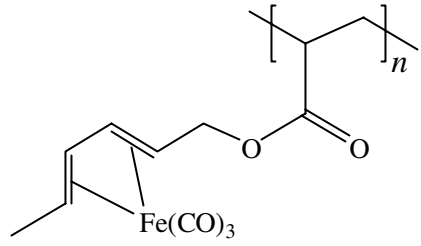

47

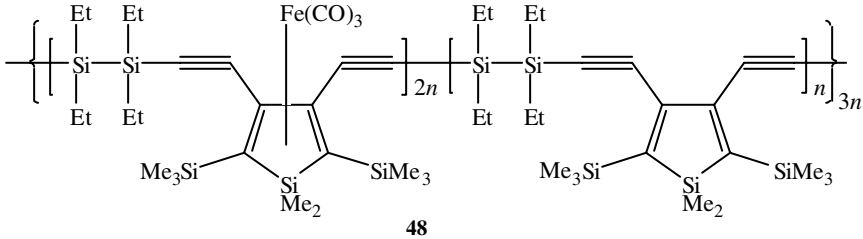

48

V. IRON POLYYNES

Since the late 1970s, poly(metal acetylide)s have been examined for group 9 and 10 transition metals. Lewis and coworkers have also demonstrated that group 8 metals, including iron, can form σ bonds with alkynes via reaction of an iron-chelating phosphine dichloro complex with *bis*-trimethylstannylalkynes to form high molecular weight polymers in the presence of a catalytic amount of CuI.[106,107] The weight-average molecular weight of polymer **49** was determined to be 173,000 by GPC.

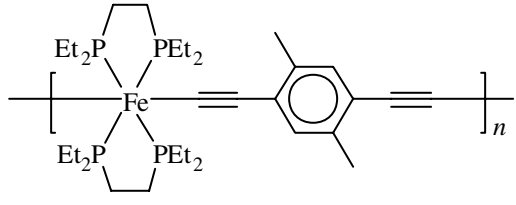

49

Oligomeric complexes containing iron acetylide units in units in their structures (**50**) were also examined by Lo Sterzo and coworkers.[108]

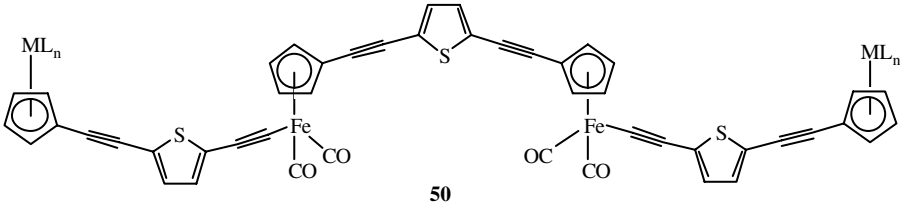

50

VI. POLYMERS WITH IRON-IRON BONDS

In the early 1990s, Tyler and coworkers described the synthesis of oligomeric urethanes and ether urethanes containing photodegradable iron–iron bonds in their backbones.[109–112] The solid-state photochemical degradation of low molecular weight polyurethanes such as **51** was also examined in the presence of light and oxygen.

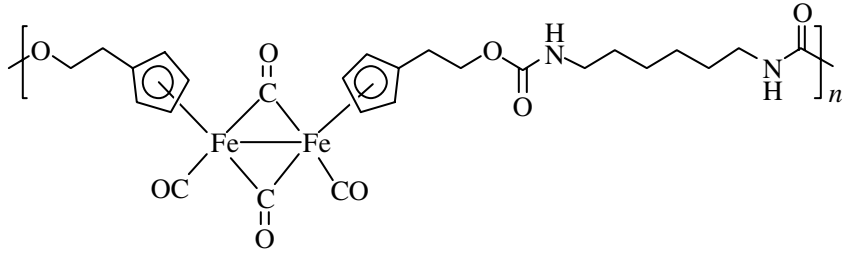

51

Vinyl monomers were also homo- and copolymerized in the presence of AIBN to produce polymers (**52**) with Fe–Fe bonds in their backbones.

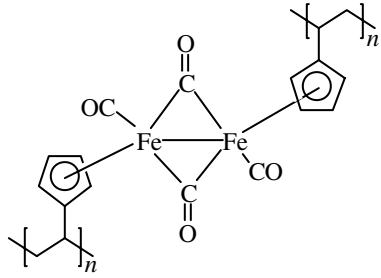

52

Cuadrado and coworkers have reported the synthesis of polysiloxanes with Fe–Fe bonds using two different methodologies.[113] Polymers with the metal–metal bonds within their backbones (**53**) were synthesized by polycondensation reactions of disilanols with a dinuclear iron–iron bonded complex, while reaction of a polysiloxane with $Fe(CO)_5$ resulted in polymer **54**. Polymer **54** possessed good thermal stability and poor solubility, which indicates that crosslinking between polymer chains may have occurred. Molecular weight analysis of polymers prepared by polycondensation reactions shows that these polymers have degrees of polymerization between 5 and 10.

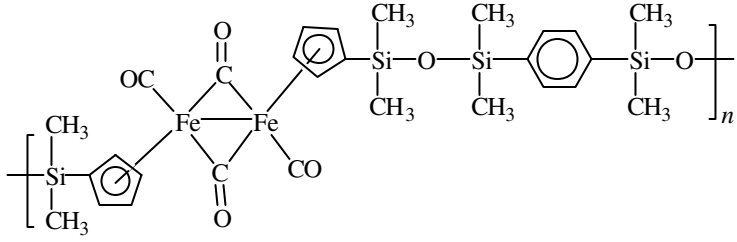

53

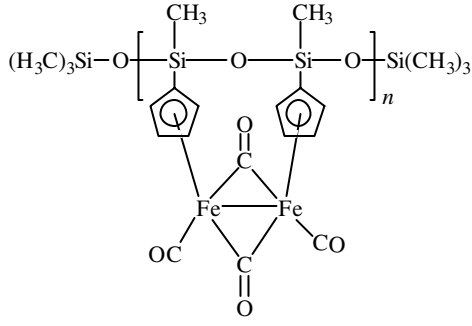

54

VII. OUTLOOK

The history of organoiron polymers can be traced to the 1950s, and much of the fundamental knowledge we possess of these materials, and organometallic polymers in general, stems from work done in and prior to the 1970s. However, there have been significant advances in organoiron polymers since the early 1990s. Within this time, we have seen a huge variety of organoiron polymers emerge. The discovery that the ring opening of ferrocenophanes produces high molecular weight

polymers, and that these polymers possess a wide range of properties, has changed the perceptions of organometallic polymers. Many of the difficulties that early researchers in this area had in producing well-defined, high molecular weight polymers have since been overcome. New classes of polymers containing organoiron groups continue to emerge, leading to new properties and applications.

This chapter was intended to briefly introduce the types of organoiron polymers that have been developed since the early 1950s. Subsequent chapters in this volume will detail some of the advances that have taken place in recent years. The synthesis and properties of ferrocene-based polymers and polymers containing arene complexes of cyclopentadienyliron will be described. The properties and applications of some of these materials will be described, and the reader will hopefully gain an appreciation of organoiron polymers.

VIII. REFERENCES

1. T. J. Kealy, P. L. Pauson, *Nature* **168,** 1039 (1951).
2. G. Wilkinson, M. Rosenblum, H. C. Whiting, R. B. Woodward, *J. Am. Chem. Soc.* **74,** 2125 (1952).
3. R. B. Woodward, M. Rosenblum, H. C. Whiting, *J. Am. Chem. Soc.* **74,** 3458 (1952).
4. F. S. Arimoto, A. C. Haven, Jr., *J. Am. Chem. Soc.* **77,** 6295 (1955).
5. P. Nguyen, P. Gomez-Elipe, I. Manners, *Chem. Rev.* **99,** 1515 (1999).
6. A. S. Abd-El-Aziz, "Metal-Containing Polymers," in *Encyclopedia of Polymer Science and Technology, 3rd ed.,* J. I. Kroschwitz, ed., Wiley, New York, in Press.
7. C. U. Pittman, Jr., C. E. Carraher, Jr., M. Zeldin, J. E. Sheats, B. M. Culbertson, eds., *Metal-Containing Polymeric Materials*, Plenum Press, New York, 1996.
8. A. S. Abd-El-Aziz, *Coord. Chem. Rev.* **233–234,** 177 (2002).
9. T. H. Coffield, V. Sandel, R. D. Closson, *J. Am. Chem. Soc.* **79,** 5826 (1957).
10. A. N. Nesmeyanov, N. A. Vol'kenau, I. N. Bolesova, *Dokl. Akad. Nauk SSSR* **149,** 615 (1963).
11. A. N. Nesmeyanov, N. A. Vol'kenau, I. N. Bolesova, *Tetrahedron Lett.* **25,** 1725 (1963).
12. D. Astruc, *Electron Transfer and Radical Processes in Transition-Metal Chemistry,* VCH Publishers, New York, 1995.
13. C. U. Pittman, Jr., P. Grube, *J. Polym. Sci., A1* **9,** 3175 (1971).
14. D. O. Cowan, J. Park, C. U. Pittman Jr., Y. Sasaki, T. K. Mukherjee, N. A. Diamond, *J. Am. Chem. Soc.* **94,** 5110 (1972).
15. C. U. Pittman Jr., B. Surynarayanan, *J. Am. Chem. Soc.* **96,** 7916 (1974).
16. M. Baumert, J. Frohlich, M. Stieger, H. Frey, R. Mulhaupt, H. Plenio, *Macromol. Rapid Commun.* **20,** 203 (1999).
17. N. Kuramoto, Y. Shishido, K. Nagai, *J. Polym. Sci., Part A, Polym. Chem.* **35,** 1967 (1997).
18. Y. Yang, Z. Xie, C. Wu, *Macromolecules* **35,** 3426 (2002).
19. R. Deschenaux, F. Turpin, D. Guillon, *Macromolecules* **30,** 3759 (1997).
20. R. Deschenaux, I. Jauslin, U. Scholten, F. Turpin, D. Guillon, B. Heinrich, *Macromolecules* **31,** 5647 (1998).
21. G. Wilbert, A. Wiesemann, R. Zentel, *Macromol. Chem. Phys.* **196,** 3771 (1995).
22. A. Wiesemann, R. Zentel, G. Lieser, *Acta Polym.* **46,** 25 (1995).
23. S. Senthil, P. Kannan, *J. Appl. Polym. Sci.* **85,** 831 (2002).

24. M. E. Wright, M. S. Sigman, *Macromolecules* **25,** 6055 (1992).
25. M. E. Wright, B. B. Cochran, E. G. Toplikar, H. S. Lackritz, J. T. Kerney, *Inorganic and Organometallic Polymers II*, P. Wisian-Neilson, H. R. Allcock, K. J. Wynne, eds., ACS Symp. Series Vol. 572, American Chemical Society, Washington, DC, 1994.
26. M. E. Wright, E. G. Toplikar, *Macromolecules* **27,** 3016 (1994).
27. E. W. Neuse, M. C. Meirim, D. D. N"Da, G. Caldwell, *J. Inorg. Organomet. Polym.* **9,** 221 (1999).
28. B. Schechter, G. Caldwell, E. W. Neuse, *J. Inorg. Organomet. Polym.* **10,** 177 (2000).
29. G. Caldwell, M. C. Meirim, E. W. Neuse, K. Beloussow, W.-C. Shen, *J. Inorg. Organomet. Polym.* **10,** 93 (2000).
30. C. M. Casado, M. Moran, J. Losada, I. Cuadrado, *Inorg. Chem.* **34,** 1668 (1995).
31. P. Saweczko, G. D. Enright, H.-B. Kraatz, *Inorg. Chem.* **40,** 4409 (2001).
32. D. Albagli, G. Bazan, M. S. Wrighton, R. R. Schrock, *J. Am. Chem. Soc.* **114,** 4150 (1992).
33. M. Buchmeiser, R. R. Schrock, *Macromolecules* **28,** 6642 (1995).
34. K. Eder, E. Reichel, H. Scottenberger, C. G. Huber, M. R. Buchmeiser, *Macromolecules* **34,** 4334 (2001).
35. I. Manners, G. H. Riding, J. A. Dodge, H. R. Allcock, *J. Am. Chem. Soc.* **111,** 3067 (1989).
36. H. R. Allcock, G. H. Riding, K. D. Lavin, *Macromolecules* **20,** 6 (1987).
37. F. W. Knobloch, W. H. Rauscher, *J. Polym. Sci.* **54,** 651 (1961).
38. W. J. Patterson, S. P. McManus, C. U. Pittman, Jr., *J. Polym. Sci., Polym. Chem.* **12,** 837 (1974).
39. K. Gonzalves, L. Zhan-ru, M. D. Rausch, *J. Am. Chem. Soc.* **106,** 3862 (1984).
40. H. Plenio, J. Hermann, J. Leukel, *Eur. J. Inorg. Chem.* **12,** 2063 (1998).
41. T. Morikita, T. Mauyama, T. Yamamoto, K. Kubota, M. Katada, *Inorg. Chim. Acta* **269,** 310 (1998).
42. O. Nuyken, T. Pohlmann, M. Herberhold, *Macromol. Chem. Phys.* **197**, 3343 (1996).
43. J. Park, Y. Seo, S. Cho, D. Whang, K. Kim, T. Chang, *J. Organomet. Chem.* **489,** 23 (1995).
44. T. Hirao, M. Kurashina, K. Aramaki, H. Nishihara, *J. Chem. Soc., Dalton Trans.* 2929 (1996).
45. G. E. Southard, M. D. Curtis, *Synthesis* **9,** 1177 (2002).
46. R. D. A. Hudson, B. M. Foxman, M. Rosenblum, *Organometallics* **18,** 4098 (1999).
47. M. A. Buretea, T. D. Tilley, *Organometallics* **16,** 1507 (1997).
48. C. E. Stanton, T. R. Lee, H. R. Grubbs, N. S. Lewis, J. K. Pudelski, M. R. Callstrom, M. S. Erickson, M. L. McLaughlin, *Macromolecules* **28,** 8713 (1995).
49. R. W. Heo, F. B. Somoza, T. R. Lee, *J. Am. Chem. Soc.* **120,** 1621 (1998).
50. D. L. Compton, T. B. Rauchfuss, *Organometallics* **13,** 4367 (1994).
51. D. L. Compton, P. F. Brandt, T. B. Rauchfuss, D. F. Rosenbaum, C. F. Zukoski, *Chem. Mater.* **7,** 2342 (1995).
52. R. Rulkens, D. P. Gates, D. Balaishis, J. K. Pudelski, D. F. McIntosh, A. J. Lough, I. Manners, *J. Am. Chem. Soc.* **119,** 10976 (1997).
53. J. M. Nelson, P. Nguyen, R. Petersen, H. Rengel, P. M. Macdonald, A. J. Lough, I. Manners, N. P. Raju, J. E. Greedan, S. Barlow, D. O'Hare, *Chem. Eur. J.* **3,** 573 (1997).
54. R. Resendes, J. M. Nelson, A. Fischer, F. Jakle, A. Bartole, A. J. Lough, I. Manners, *J. Am. Chem. Soc.* **123,** 2116 (2001).
55. C. H. Honeyman, D. A. Foucher, F. Y. Dahmen, R. Rulkens, A. J. Lough, I. Manners, *Organometallics* **14,** 5503 (1995).
56. C. E. B. Evans, A. J. Lough, H. Grondey, I. Manners, *New J. Chem.* **24,** 447 (2000).
57. T. Mizuta, M. Onishi, K. Miyoshi, *Organometallics* **19,** 5005 (2000).
58. A. Berenbaum, H. Braunschweig, R. Dirk, U. Englert, J. C. Green, F. Jakle, A. J. Lough, I. Manners, *J. Am. Chem. Soc.* **122,** 5765 (2000).

59. T. J. Peckham, J. A. Massey, M. Edwards, I. Manners, D. A. Foucher, *Macromolecules* **29,** 2396 (1996).
60. R. N. Kapoor, G. M. Crawford, J. Mahmoud, V. V. Dementiev, M. T. Nguyen, A. F. Diaz, K. H. Pannell, *Organometallics* **14,** 4944 (1995).
61. F. Jakle, R. Rulkens, G. Zech, J. A. Massey, I. Manners, *J. Am. Chem. Soc.* **122,** 4231 (2000).
62. H. K. Sharma, F. Cervantes-Lee, J. S. Mahmoud, K. H. Pannell, *Organometallics* **18,** 399 (1999).
63. D. A. Foucher, B. Z. Tang, I. Manners, *J. Am. Chem. Soc.* **114,** 6246 (1992).
64. I. Manners, *Can. J. Chem.* **76,** 371 (1998).
65. I. Manners, *Chem. Commun.* 857 (1999).
66. J. Rasburn, D. A. Foucher, W. F. Reynolds, I. Manners, G. J. Vancso, *Chem. Commun.* 843 (1998).
67. Y. Ni, R. Rulkens, I. Manners, *J. Am. Chem. Soc.* **118,** 4102 (1996).
68. J. Massey, K. N. Power, I. Manners, M. A. Winnik, *J. Am. Chem. Soc.* **120,** 9533 (1998).
69. R. G. H. Lammertink, M. A. Hempenius, G. J. Vancso, K. Shin, M. H. Rafailovich, J. Sokolov, *Macromolecules* **34,** 942 (2000).
70. K. N. Power-Billard, I. Manners, *Macromol. Rapid Commun.* **23,** 607 (2002).
71. J. A. Massey, K. Temple, L. Cao, Y. Rharbi, J. Raez, M. A. Winnik, I. Manners, *J. Am. Chem. Soc.* **122,** 11577 (2000).
72. X. -S. Wang, M. A. Winnik, I. Manners, *Macromol. Rapid Commun.* **23,** 210 (2002).
73. R. Resendes, J. A. Massey, K. Temple, L. Cao, K. N. Power-Billard, M. A. Winnik, I. Manners, *Chem. Eur. J.* **7,** 2414 (2001).
74. M. A. Hempenius, G. J. Vancso, *Macromolecules* **35,** 2445 (2002).
75. Z. Wang, A. Lough, I. Manners, *Macromolecules* **35,** 7669 (2002).
76. Q. Sun, J. W. Y. Lam, K. Xu, H. Xu, J. A. K. Cha, P .C. L. Wong, G. Wen, X. Zhang, X. Jing, F. Wang, B. Z. Tang, *Chem. Mater.* **12,** 2617 (2000).
77. K. Kulbaba, M. J. MacLachlan, C.E.B. Evans, I. Manners, *Macromol. Chem. Phys.* **202,** 1768 (2001).
78. J. Galloro, M. Ginzburg, H. Miguez, S. M. Yang, N. Coombs, A. Safa-Sefat, J.E. Greedan, I. Manners, G.A. Ozin, *Adv. Funct. Mater.* **12,** 382 (2002).
79. C. -O. Turrin, J. Chiffre, D. de Montauzon, G. Balavoine, E. Manoury, A. -M. Caminade, J. -P. Majoral, *Organometallics* **21,** 1891 (2002).
80. R. Deschenaux, E. Serrano, A.-M. Levelut, *Chem. Commun.* 1577 (1997).
81. C. M. Casado, I. Cuadrado, M. Moran, B. Alonso, M. Barranco, J. Losada, *Appl. Organometal. Chem.* **13,** 245 (1999).
82. R. Castro, I. Cuadrado, B. Alonso, C. M. Casado, M. Moran, A. E. Kaifer, *J. Am. Chem. Soc.,* **119,** 5760 (1997).
83. C. Valerio, J.-L. Fillaut, J. Ruiz, J. Guittard, J.-C. Blais, D. Astruc, *J. Am. Chem. Soc.* **119,** 2588 (1997).
84. S. Nlate, J. Ruiz, V. Sartor, R. Navarro, J.-C. Blais, D. Astruc, *Chem. Eur. J.* **6,** 2544 (2000).
85. A. S. Abd-El-Aziz, E. K. Todd, G. Z. Ma, J. DiMartino, *J. Inorg. Organomet. Polym.* **10,** 265 (2000).
86. A. S. Abd-El-Aziz, E. K. Todd, *Polym. Mater. Sci. Eng.* **86**(1), 103 (2002).
87. A. S. Abd-El-Aziz, L. J. May, J. A., R. M. Okasha, *J. Polym. Sci. Part A, Polym. Chem.* **39,** 2716 (2001).
88. A. S. Abd-El-Aziz, E. K. Todd, G. Z. Ma, *J. Polym. Sci. Part A, Polym. Chem.* **39,** 1216 (2001).
89. C. R. de Denus, L. M. Hoffa, E. K. Todd, A. S. Abd-El-Aziz, *J. Inorg. Organomet. Polym.* **10,** 189 (2000).
90. A. S. Abd-El-Aziz, T. H. Afifi. W. R. Budakowski, K. J. Friesen, E. K. Todd, *Macromolecules* **35,** 8929 (2002).

91. A. S. Abd-El-Aziz, E. K. Todd, R. M. Okasha, T. E. Wood, *Macromol. Rapid Commun.* **23,** 743 (2002).
92. A. S. Abd-El-Aziz, T. H. Afifi, E. K. Todd, G. Z. Ma, *Polym. Prepr.* (*Am. Chem. Soc., Div. Polym. Chem.*) **42**(2), 450 (2001).
93. H. Funaki, K. Aramaki, H. Nishihara, *Synth. Met.* **74,** 59 (1995).
94. S. Rigaut, M. -H. Delville, D. Astruc, *J. Am. Chem. Soc.* **119,** 11132 (1997).
95. J. -L. Fillaut and D. Astruc, *New J. Chem.* 20, 945 (1996).
96. C. Valério, F. Moulines, J. Ruiz, J.-C. Blais, D. Astruc, *J. Org. Chem.* **65,** 1996 (2000).
97. A. S. Abd-El-Aziz, E. K. Todd and T. H. Afifi, *Macromol. Rapid Commun.* **23,** 113 (2002).
98. S. F. Mapolie, J. R. Moss, G. S. Smith, *J. Inorg. Organomet. Polym.* **7,** 233 (1997).
99. S. F. Mapolie, I. J. Mavunkal, J. R. Moss, G. S. Smith, *Appl. Organomet. Chem.* **16,** 307 (2002).
100. K. Martin, M. Dotson, M. Litterer, T. W. Hanks, C. Veas, *Synth. Met.* **78,** 161 (1996).
101. K. F. Martin, T. W. Hanks, *Organometallics* **16,** 4857 (1997).
102. C. U. Pittman, Jr., O. E. Ayers, S. P. McManus, *J. Macromol. Sci.-Chem.* **A7**(8), 1563 (1973).
103. C. U. Pittman, Jr., *Macromolecules* **7,** 396 (1974).
104. H. Yasuda, I. Noda, S. Miyanaga, A. Nakamura, *Macromolecules* **17,** 2453 (1984).
105. J. Ohshita, T. Hamaguchi, E. Toyoda, A. Kunai, K. Komaguchi, M. Shiotani, M. Ishikawa, A. Naka, *Organometallics* **18,** 1717 (1999).
106. B. F. G. Johnson, A. K. Kakkar, M. S. Khan, J. Lewis, *J. Organomet. Chem.* **409,** C12 (1991).
107. Z. Atherton, C. W. Faulkner, S. L. Ingham, A. K. Kakkar, M. S. Khan, J. Lewis, N. J. Long, P. R. Raithby, *J. Organomet. Chem.* **462,** 265 (1993).
108. A. Buttinelli, E. Viola, E. Antonelli, C. Lo Sterzo, *Organometallics* **17,** 2574 (1998).
109. S. C. Tenhaeff, D. R. Tyler, *Organometallics* **10,** 1116 (1991).
110. S. C. Tenhaeff, D. R. Tyler, *Organometallics* **10,** 473 (1991).
111. D. R. Tyler, J. J. Wolcott, G. W. Nieckarz, S. C. Tenhaeff, in *Inorganic and Organometallic Polymers II*, P. Wisian-Neilson, H. R. Allcock, K. J. Wynne, eds., ACS Symp. Series Vol. 572, American Chemical Society, Washington, DC, 1994; Chap. 36, pp. 481–496.
112. S. C. Tenhaeff, D. R. Tyler, *Organometallics* **11,** 1466 (1992).
113. M. Moran, M. C. Pascual, I. Cuadrado, J. Losada, *Organometallics* **12,** 811 (1993).

CHAPTER 2

Synthesis and Properties of Hyperbranched Polyferrocenylenesilynes

Qunhui Sun, Han Peng, Kaitian Xu, and Ben Zhong Tang

Department of Chemistry, Institute of Nano Science and Technology and Open Laboratory of Chirotechnology of the Institute of Molecular Technology for Drug Discovery and Synthesis, Hong Kong University of Science and Technology, Kowloon, Hong Kong, China

CONTENTS

Macromolecules Containing Metal and Metal-like Elements, Volume 2: Organoiron Polymers, Edited By Alaa S. Abd-El-Aziz, Charles E. Carraher, Jr., Charles U. Pittman, Jr., John E. Sheats, and Martel Zeldin
ISBN 0-471-45078-2

I. INTRODUCTION

Organometallic macromolecules are hybrids of organic and metallic species. The hybrid vigor enables the molecular offspring to inherit specific characteristics of its parents and meanwhile to develop new features that are difficult or impossible to access by either of its parents alone. The creation of new organometallic polymers and the exploration of their unique properties have been under enthusiastic pursuit; during the course, many advanced materials with high potentials for technological applications have been generated.

Polyalkynes, with polyacetylene as their representative example, are the best-known conjugated macromolecules, whose studies have attracted much interest among scientists and technologists. A rich variety of polyalkynes has been prepared, thanks to the relentless synthetic efforts of polymer chemists.[1–13] The conjugated polymers exhibit an array of exotic properties, examples of which include photoconductivity,[14,15] chromism,[16–18] photo- and electroluminescence,[19–21] radiolysis,[22,23] optical nonlinearity,[24] liquid crystallinity,[25–28] helical chirality,[29–31] biomimetic environmental adaptability,[32] and cell growth-stimulating capability.[33–35] Polysilynes, a group of inorganic congeners of the organic polyalkynes, have also been created in the hot pursuit of new polymers with new *molecular structures*.[36–38] Indeed, although the polysilynes resemble the polyalkynes in *stoichiometry* [−$(RSi)_n$− vs. −$(RC)_n$−], their molecular *structures* are distinctly different: the backbone of the former comprises three-dimensionally continuous silicon–silicon single bonds, while that of the latter consists of linear alternating carbon–carbon double bonds. The polysilynes have a random network structure analogous to that postulated for bulk amorphous silicon[39,40] and this structural feature endows the polymers with a host of intriguing properties. For example, the polymers possess extensive Si−Si σ conjugation, whose absorption extends well into the visible spectral region.[36–38,41–44]

In the polysilyne backbone, each silicon atom is tetrahedrally hybridized and bound via single bonds to three other silicon atoms. The resulting silicon cages are thus tight inorganic networks knitted up by the short σ bonds. Insertion of bulky organometallic moieties such as ferrocene rings into the polysilyne structures may expand the caged networks into hyperbranched spheres divergently emanating in the three-dimensional space, thus improving the solubility (and processibility) of the

inorganic polymers.[45–62] The mixing between the σ orbitals of the silicon atoms and the π orbitals of the ferrocene rings may confer unique electronic properties on the polymers.[63–66] The introduction of another kind of inorganic atom, namely, iron, into the silicon polymers may add new functionalities to the materials; for example, the polymers may show electrochemical redox activity[67–68] and serve as precursors to magnetoceramics.[69–73] An outstanding example in this regard is the creation of polyferrocenylenesilenes by the incorporation of ferrocene rings into linear polysilene chains at the molecular level.[74–84] The molecular melds have been found to exhibit an impressive array of novel materials properties.[85–87] Hybridization of the organometallic ferrocene rings with the nonlinear inorganic silicon networks has, however, not been attempted.[88–95]

The use of chemical approaches to generate nanostructured morphologies and to tune the properties of ceramic materials is a rapidly growing area of research. The vigorous research activity in the synthesis of organometallic polymer precursors and their controlled pyrolysis to ceramic materials has opened up a new branch of macromolecular science—preceramic polymer chemistry. The polymer precursor route offers the following, among other, noteworthy advantages: (1) the diversity in chemical compositions of organometallic macromolecules provides a large palette for manipulating the structure and properties of the ceramic products; (2) the inorganic metal atoms distributed along the macromolecular chains and segregated by the organic moieties can, on pyrolysis, form nanoclusters, interconnection of which may generate mesoporous morphologies; and (3) the unique processing characteristics of the precursor polymers may enable the fabrication of bulk ceramic bodies of complex shapes. Not all these advantages have, however, been realized or utilized, and indeed, most studies in preceramic polymer chemistry have thus far focused on the fabrication of structural ceramics with outstanding mechanical properties, examples of which include silicon carbide (SiC) and silicon nitride (Si_3N_4). Incorporation of nanoclusters of transition metals into ceramics may lead to the development of novel nanostructured materials with unique magnetic, electrical, and optical properties. Such possibility, intriguing notwithstanding, has not been well explored.

Hyperbranched polymers are different from their linear counterparts in architectural dimensionality; the former are three-dimensional spheres, whereas the latter are one-dimensional chains. Compared to the chains, the spheres should in principle better retain the constituent elements during the pyrolysis process, leading to the formation of ceramic materials in higher yields. Hyperbranched polymers are also different from crosslinked networks—the former are often soluble, whereas the latter are inherently insoluble. Processibility or tractability is one of the most important advantages of preceramic polymer processes, and the hyperbranched polymers are thus promising precursor candidates for the fabrication of advanced ceramic materials.

In this work, we utilized a coupling reaction of difunctional ferrocene with trifunctional silane and synthesized hyperbranched polyferrocenylenesilynes with different organic substituents (**1**; Scheme 1). In comparison to the parent inorganic polysilyne networks, the hyperbranched organometallic polyferrocenylenesilynes showed improved solubility, better stability, and more extended conjugation. Pyrolysis

of the polymers with small R substituents produced in high yields ceramic materials consisting of metallic nanoclusters, all of which were magnetizable and one of which showed excellent soft ferromagnetism.

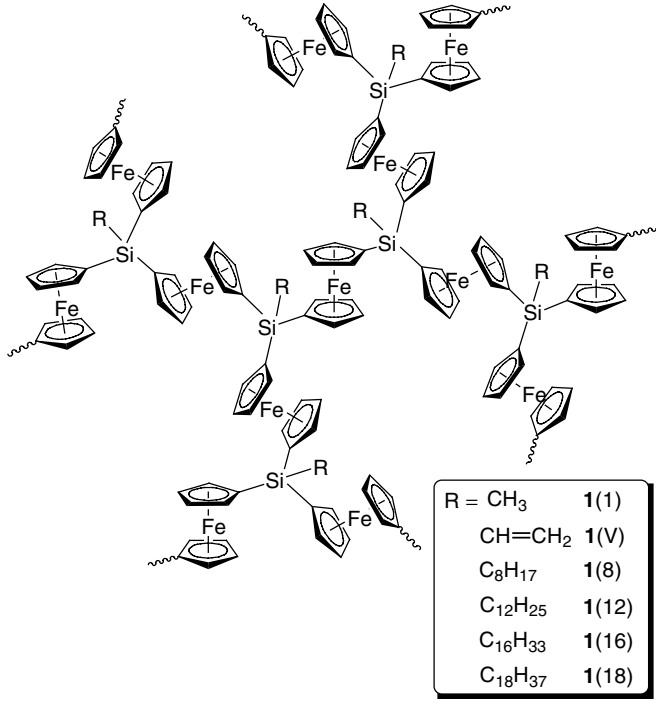

Scheme 1 Molecular structure of polyferrocenylenesilynes (**1**).

II. POLYMER SYNTHESIS

To prepare the hyperbranched polyferrocenylenesilynes, dilithioferrocene [$(\eta^5\text{-}C_5H_4Li)_2Fe$ or $FcLi_2$] and trichlorosilanes (Cl_3SiR) were made to react under vigorously dried and strictly controlled polymerization conditions (Scheme 2). The coupling of $FcLi_2 \cdot$TMEDA complex with Cl_3SiCH_3 readily produced hyperbranched poly[1,1′-ferrocenylene(methyl)silyne] [**1**(1)] in a high isolation yield (~71%; Table 1, no. 1). Poly(methylsilyne) network was completely insoluble[13] but **1**(1) was partially soluble in common organic solvents; that is, the hyperbranched polymer had a better solubility. The polymerization of $FcLi_2$ with $Cl_3SiHC{=}CH_2$ also produced a partially soluble polymer [**1**(V)], although the isolation yield of the polymer was low.

Many (partially) insoluble conjugated polymers can be made soluble by introducing long alkyl chains into their molecular structures.[96–112] Borrowing this "solvating flexible chain" concept, we incorporated long alkyl groups into the polyferrocenylenesilyne structures. This strategy worked well: the polymer with

flexible *n*-octyl substituents [**1**(8)] was completely soluble in common organic solvents (Table 1, no. 3). Increasing the length of the alkyl chain to 12 carbon atoms resulted in the formation of a high molecular weight polymer [**1**(12)] in a high yield (77%). Different from the polymers with short R groups, this polymer was a brown elastomer, due to a large decrease in its glass transition temperature (T_g) induced by the internal plasticizing effect of the long *n*-dodecyl group. The elastomeric polymer easily formed shaped objects during the isolation process. When the thick films or bars of the polymer were broken, their cross sections exhibited shinny metallic luster.

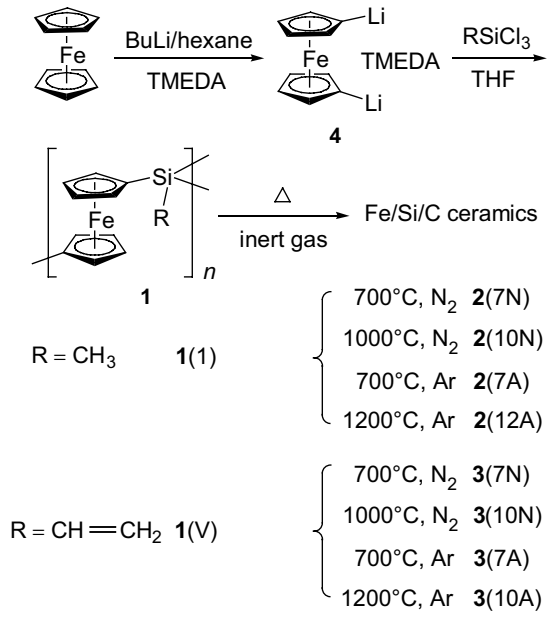

Scheme 2 Polymer synthesis and pyrolytic ceramization.

Table 1 Synthesis of Hyperbranched Polyferrocenylenesilynes (**1**)[a]

No.	*R* in **1**	Yield (wt%)	Solubility[b]	M_w (Da)[c]	M_w/M_n[c]	Appearance
1	CH_3	71.1	×	2,000	2.0[d]	Golden powder
2	$CH{=}CH_2$	32.0	×	1,300	1.6[d]	Golden powder
3	C_8H_{17}	67.5	√	2,600	1.5	Amber powder
4	$C_{12}H_{25}$	77.0	√	6,300	3.8	Brown elastomer
5	$C_{16}H_{33}$	52.0	√	9,800	4.3	Brown elastomer
6	$C_{18}H_{37}$	72.3	√	11,900	7.3	Golden powder

[a] Carried out under nitrogen in THF at −78°C for 24 h.
[b] Tested in common organic solvents (chloroform, dichloromethane, toluene, hexane, dioxane, acetone, THF, DMF, DMSO, etc.); symbols: ×=partially soluble, √=completely soluble.
[c] Estimated by SEC in THF on the basis of a polystyrene calibration.
[d] For the THF-soluble fraction.

We further increased the length of the alkyl chain and found that the molecular weight of the polymer monotonically increased with the alkyl chain lengthening. When the alkyl length was increased to 18, the M_w of the polymer [**1**(18)] reached a high value of ~12,000 Da [noting that this is an SEC (size-exclusion chromatography)-estimated relative value; the absolute value is much higher]. Interestingly, while polymer **1**(16) was elastomeric, **1**(18) was powdery in appearance. As will be discussed later, this is probably due to the self-crystallization of the long *n*-octadecyl chains, a phenomenon often observed in sidechain liquid crystalline polymer systems.[25–28,112–117]

The excellent solubility of the high molecular weight polymer **1**(18) was a particularly exciting result. It has been reported that the solubility of some polysilynes decreases with time,[13b] and we thus checked whether **1**(18) would undergo a similar solubility change. We took two approaches: one accelerated test in which a high temperature was applied and another, slow test that involved a long period of time. In the accelerated test, we added ~150 mg of the polymer to a Pyrex vacuum tube, which was sealed under vacuum and was then heated at 150°C for 2 h. This thermal treatment resulted in little change in the solubility of the polymer. To test this quantitatively, we used a DSC apparatus to check the heat flow in situ at 150°C isothermally. Nothing except a horizontal straight line was recorded, proving that the polymer has not undergone any chemical reactions during the heating process. For the slow test, we put a sample of **1**(18) on a shelf in our laboratory under ambient conditions. After ~4 years, the sample was still completely soluble. The polymer thus passed both the short- and long-term tests; it maintained soluble after the thermal treatment and the shelf storage.

It is well known that SEC, when calibrated with standards of linear polymers (normally polystyrene), often underestimates the molecular weights of hyperbranched polymers.[45–59,96,97,118–120] Bianconi et al., for example, found that the molecular weights of their polysilynes estimated by SEC were ~4-fold smaller than the actual (or absolute) values.[37] More recent research in the area has revealed that the underestimation can be as high as ~30 fold for some hyperbranched polymers.[119] We thus determined the absolute molecular weights of **1**(18) by an SEC system equipped with light-scattering and viscometer detectors.[96] The absolute M_w value given by the light-scattering detector was 5×10^5 Da, much higher than the relative M_w value calibrated against the linear polystyrene standards. The intrinsic viscosity ([η]) given by the viscometer was, however, as low as 0.02 dL/g. A hyperbranched polymer with a high molecular weight often shows a low intrinsic viscosity;[96,97,118–120] polymer **1**(18) exhibited this characteristic property of a hyperbranched polymer.

III. STRUCTURAL CHARACTERIZATION

We used spectroscopic methods to analyze the molecular structures of the polyferrocenylenesilynes. Figure 1 shows their Fourier transform infrared (FTIR) spectra. All the polymers exhibited similar spectral profiles. Taking **1**(1) as an example, it

exhibited ferrocene-associated vibration bands at 1690, 1421, and 1036 cm^{-1} and silicon bands at (1421), 1166, and 732 cm^{-1},[121–123] spectroscopically proving that the polymer is consisted of ferrocene ring and silicon atom. The vinylsilyl (CH_2=CH−Si) moiety of **1**(V) vibrated at 1592, 1404, and 958 cm^{-1} (Fig. 1, curve *B*). Silane (Si−H) and siloxane (Si−O−Si) bonds are known to show very intense and broad absorption bands at ~2200 and ~1100 cm^{-1}.[36–38,121–123] No such bands were, however, observed at the wavenumbers in the spectra of the hyperbranched polymers.

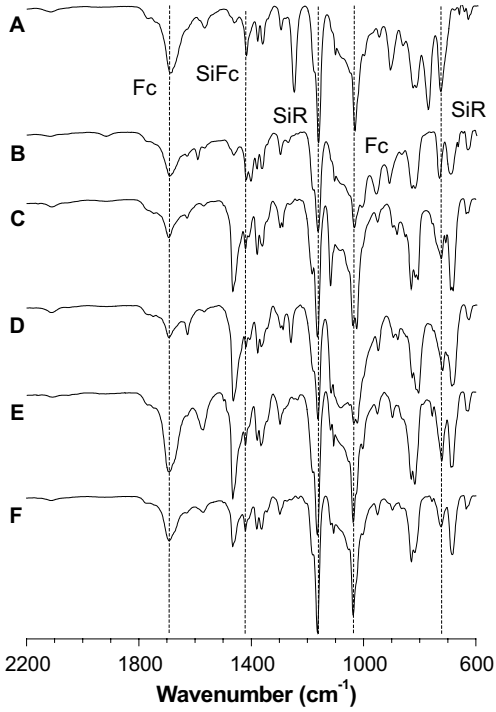

Figure 1 FTIR spectra of hyperbranched polyferrocenylenesilynes (**1**) with R = CH_3 [**1**(1)] (*A*), CH=CH_2 [**1**(V)] (*B*), *n*-C_8H_{17} [**1**(8)] (*C*), *n*-$C_{12}H_{25}$ [**1**(12)] (*D*), *n*-$C_{16}H_{33}$ [**1**(16)] (*E*), and *n*-$C_{18}H_{37}$ [**1**(18)] (*F*).

Two broad resonance peaks at δ 4.12 and 0.55 were observed in the ^1H NMR (nuclear magnetic resonance) spectrum of polymer **1**(1) (Fig. 2), which can be readily assigned to the absorptions of the protons of the cyclopentadienyl (Cp) and methyl (Me) groups, respectively.[78–84,124] The repeat unit of polymer **1**(1) comprises 1.5 ferrocenylene {$[(\eta^5\text{-}C_5H_4)_2Fe]_{3/2}$ or $(Cp_2Fe)_{3/2}$] and 1 methyl (CH_3) groups or 12 Cp and 3 Me protons. The ratio of the integrated areas of the resonance peaks of the Cp and Me protons was 1 : 0.26, identical (within experimental error) to the theoretical value of 12 : 3 (or 1 : 0.25). For comparison, we prepared a linear polysilene of similar structure, poly[1,1′-ferrocenylene(dimethyl)silene] [**5**(1)], according to a published

procedure.[24] The linear polymer showed two resonance peaks in the Cp and Me spectral regions with a Cp/Me ratio of 1:0.76 (the theoretical ratio was 4 : 3 or 1 : 0.75). The spectral profile of the linear polymer was similar to that of its hyperbranched counterpart but the peaks of the former were better resolved than those of the latter. The absorption of the Cp protons of **5**(1), for example, were resolved into a partially overlapping bimodal envelope with two peaks clearly discernible at δ ~4.2 and ~4.1. These two peaks were almost completely merged into one broad one in the case of **1**(1). The broadness of the absorption peak is indicative of the structural complexity of the three-dimensional hyperbranched polymer arising from the variations in the chemical environments where the protons are located.

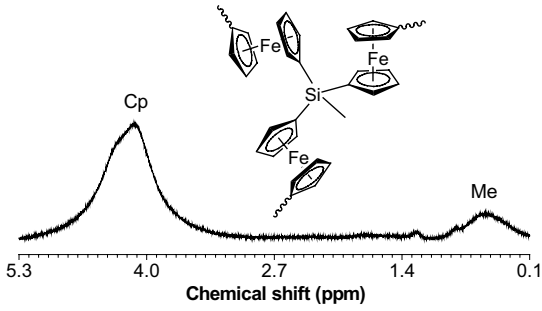

Figure 2 ^{1}H NMR spectrum of a chloroform-*d* solution of hyperbranched poly[1,1′-ferrocenylene(methyl)silyne] [**1**(1)] (soluble fraction).

The poor solubility of the hyperbranched polymers with small R groups made it difficult to measure their ^{13}C NMR spectra. The excellent solubility of the polymers with long alkyl groups made the job easier and enabled us to obtain ^{13}C NMR spectra of good quality, an example of which is shown in Figure 3. The *ipso* carbon atoms of the Cp ring gave three resonance peaks: two small but clearly observable ones at δ 73.15 and 70.93, and another partially observable one underneath the big peak of the other carbon atoms of the Cp ring. These three peaks may be associated with the absorptions of the ipso carbon atoms in the dendritic, linear, and terminal units,[28] each of which experiences a different microstructural environment, although we do not know the exact assignments of the peaks at present. The carbon atoms of the alkyl group resonated in the upfield (δ ~35–10). Close inspection of the carbon resonance structures revealed that the carbon atoms located closer to the silicon core gave weaker, broader "peaks," in comparison to those located far apart from the core. Similar phenomenon was observed in the polysilyne system, in which the resonance signal of the carbon atom directly attached to the silicon atom (C1) was completely missing or totally unobservable.[37] This suggests that, similar to the polysilynes, our hyperbranched polyferrocenylenesilynes also possess a rigid molecular structure.

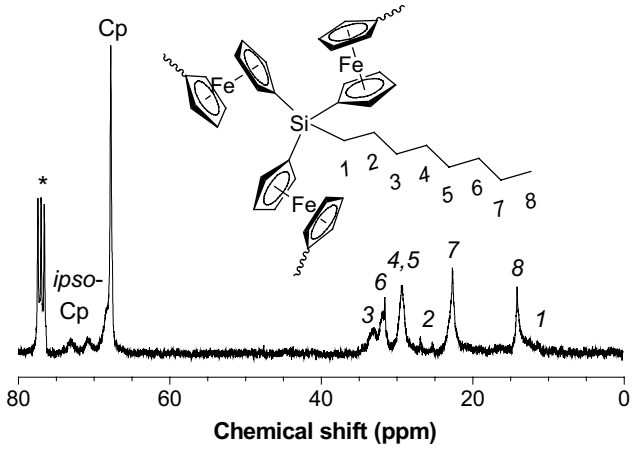

Figure 3 ^{13}C NMR spectrum of hyperbranched poly[1,1′-ferrocenylene(*n*-octyl)silyne] [**1**(8)] in chloroform-*d*. The solvent peaks are marked with an asterisk (*).

IV. ELECTRONIC AND THERMAL TRANSITIONS

All the soluble hyperbranched polyferrocenylenesilynes, namely, **1**(8)–**1**(18), exhibited absorption peaks in the UV region, and the maximum molar absorptivity (ε_{max}) increased with an increase in the length of the alkyl chain (Fig. 4). The absorption spectra of the polymers tailed into the infrared spectral region (>700 nm). On the other hand, **5**(1), a linear congener of **1**, had a lower ε_{max} in the UV region and a shorter-wavelength band edge in the visible. The higher molar absorptivities and longer-wavelength band edges of the hyperbranched polymers indicate that they possess more extended conjugations than their linear counterparts.

The absorption band edges of linear polydiorganosilenes {−[(RR′)Si]$_n$−; R, R′=alkyl and/or aryl} normally do not enter the visible region irrespective of whether they are symmetrically (R=R′) or asymmetrically substituted (R ≠ R′).[36–38,125–127] The band edge of poly(di-*n*-hexylsilene) {−[(*n*-$C_6H_{13})_2$Si]$_n$−}, for example, is located in the UV region (~350 nm).[36,37] The absorption spectra of the three-dimensional polysilyne networks were, however, tailing into the visible spectral region; for instance, the band edge of poly[(*n*-hexyl)silyne] {−[(*n*-C_6H_{13})Si]$_n$−} was at ~450 nm, which was about 100 nm redshift from that of its linear congener.[36,37] This bathochromic shift was attributed to the extended Si−Si σ conjugation across the three-dimensional polysilyne networks.[36–38,41–44] Linear poly[1,1′-ferrocenylene(methyl)silene] **5**(1) had a band edge in the visible (~600 nm), due possibly to the σ–π conjugation[63–66,128–130] between the silene moiety and the Cp ring. The band edge of the hyperbranched polyferrocenylenesilynes further extended into the infrared with even larger extents of bathochromic shifts, probably due to the more extended σ–π conjugations in the three-dimensional hyperbranched macromolecular spheres.

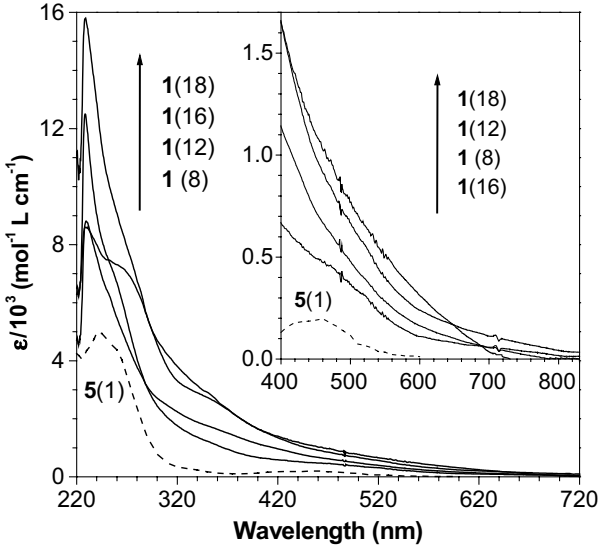

Figure 4 Absorption spectra of hyperbranched polyferrocenylenesilynes −[$Fc_{3/2}$(n-C_mH_{2m+1})Si]$_n$− [1(m); m=8–18] in dichloromethane. The spectra of the partially soluble polymers **1**(1) and **1**(V) are not given because it was difficult to accurately determine their solution concentrations and molar absorptivities. The spectral data for a THF solution of linear poly[1,1′-ferrocenylene(dimethyl)silene] [**5**(1)] is shown for comparison.

The polyorganosilynes {−[(R)Si]$_n$−} were photoluminescent, emitting blue and green lights with luminescence maximums in the wavelength region of ~440–520 nm.[41] In contrast, the hyperbranched polyferrocenylenesilynes were nearly nonemissive, although they were more conjugated than their polyorganosilene congeners. This seemed to be odd at first glance but may not be difficult to understand if we think about it twice. The better conjugation can confer high charge mobility and fast charge transport on the polymers on the positive side, but on the negative side, it may generate many defective traps that quench the emission of the polymers. This is not an uncommon phenomenon in conjugated polymer systems. We have, for example, synthesized many chromophorically substituted polyacetylenes [−(RC=CR′)$_n$−] that have shorter effective conjugation lengths but are highly photo- and electroluminescent.[19–21,131–138] Their parent form, i.e., the unsubstituted polyacetylene [−(HC=CH)$_n$−], is highly conjugated but is practically nonluminescent.[139,140]

As shown in Table 1, the physical appearance of the hyperbranched polyferrocenylenesilynes changed with their R groups (from powdery to elastomeric and then back to powdery). To know the cause for this change in physical state, we investigated the thermal transitions of the polymers by differential scanning calorimetry (DSC) analyses. The polymer samples were pretreated by heating them to, and annealed at, a high temperature of 150°C. The DSC thermograms of the polymers were recorded during the second heating scans, as a precaution against recording

false signals in the heat changes associated with such events as evaporation of volatile impurities, such as the solvents trapped inside the hyperbranched polymers. An example of the DSC curves so recorded is shown in Figure 5. The thermogram is clearly artifact-free, from which, the glass transition temperature (T_g) and the melting point (T_m) of the polymer can be readily determined.

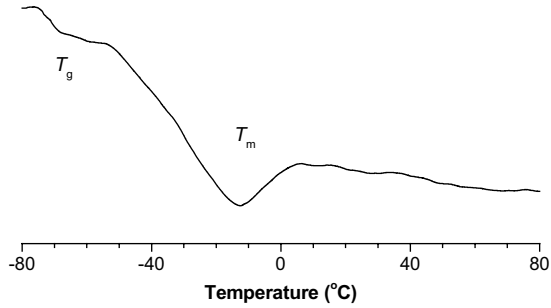

Figure 5 DSC thermogram of poly[1,1′-ferrocenylene(*n-hexa*-decyl)silyne] [**1**(16)] measured under nitrogen at a heating rate of 10°C/min during the second heating scan after the sample had been annealed at 150°C for 10 min.

The thermal transition parameters obtained from the DSC analyses are summarized in Table 2. The polymer with a methyl group [**1**(1)] underwent no melting transition but a glass transition at ~53°C. When the R substituent changed to a "big" vinyl group, T_g decreased to 40°C. When the number of the carbon atoms in the alkyl chains (m) increased from 8 to 18, T_g monotonically decreased from 0 to approximately −70°C. Compared to their linear poly[1,1′-ferrocenylene(di-*n*-alkyl)silene] counterparts [**5**(m)], the hyperbranched poly[1,1′-ferrocenylene(*n*-alkyl)silyne]s [**1**(m)] exhibited higher T_g values ($\Delta T > 20$°C; Fig. 6). This is a reflection of the rigid molecular structure of **1**; the hyperbranched polymers possess three rigid Cp rings in one of their constitutional repeat units, while the linear polymers have only two Cp rings in one of their monomer units. The T_g of **1**(m) sharply decreased with an increase in m when m was small, but the extent of change (or the slope of the T_g–m plot) became smaller when m became larger. This is probably caused by the antagonistic effect of the partial crystallization of the long alkyl chains, as discussed below, which hampered the segmental movements of the macromolecular branches.

From R=*n*-$C_{12}H_{25}$ (or m=12) onward, the hyperbranched polymers [**1**(m)] started to undergo crystallization/melting transitions (Table 2, nos. 4–6). It has been observed in many liquid crystalline polymer systems that the long alkyl spacers and tails of their mesogenic units tend to order and eventually to crystallize, when the alkyl chain lengths become long enough.[112,141] The melting transitions observed in our hyperbranched polymers thus may be associated with the disassembling of the partially aligned or crystallized long alkyl chains. It has been noted that the polyalkylsilyne with

short methyl groups is apt to form irregular cagelike networks, whereas the polymers with long alkyl groups favor the formation of sheetlike structures,[36–38] which allow better steric packing. Similarly, our hyperbranched polyferrocenylenesilynes with small R groups were amorphous, while those with long alkyl chains were semicrystalline. To further verify this point, we measured the X-ray diffraction (XRD) patterns of the polymers.

Table 2 Thermal Properties of Polyferrocenylenesilynes (1)[a]

No.	*R* in −[$Fc_{3/2}$(*R*)Si]$_n$− (**1**)	T_g (°C)	T_m (°C)	ΔH (kcal/mol)[b]	Ceramic Yield (wt%)[c]
1	CH_3 [**1**(1)]	53.1	—	—	62.5
2	CH=CH_2 [**1**(V)]	40.0	—	—	61.3
3	*n*-C_8H_{17} [**1**(8)]	0	—	—	33.1
4	*n*-$C_{12}H_{25}$ [**1**(12)]	−54.5	−20.5	0.91	29.9
5	*n*-$C_{16}H_{33}$ [**1**(16)]	−67.7	−13.8	1.15	28.5
6	*n*-$C_{18}H_{37}$ [**1**(18)]	−69.7	−36.7	7.76	23.6

[a] Measured under nitrogen by DSC (T_g, T_m, and ΔH) and thermogravimetric analysis (TGA) (ceramic yield) at heating rates of 10 and 20°C/min respectively. *Abbreviation*: Fc=1,1′-ferrocenylene.
[b] Enthalpy of melting transition.
[c] In the temperature region of 678–687°C.

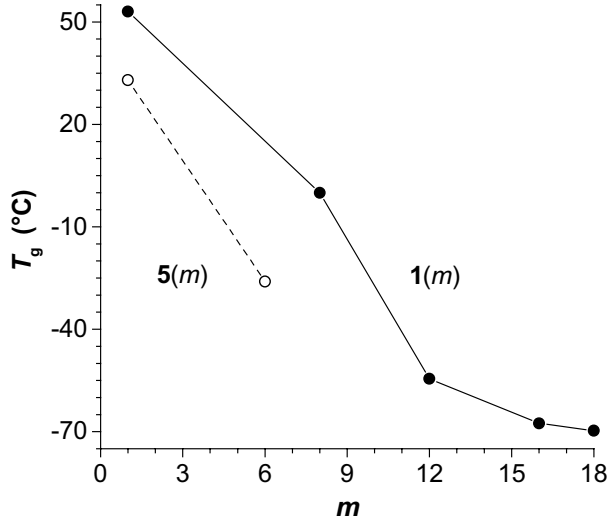

Figure 6 Change of glass transition temperature (T_g) with number of carbon atoms of alkyl chains (*m*) in the hyperbranched poly[1,1′-ferrocenylene(*n*-alkyl)silyne]s [**1**(*m*)]. Data for the linear poly[1,1′-ferrocenylene(di-*n*-alkyl)silene]s [**5**(*m*)] are shown for comparison (data taken from Refs. 72, 73, and 78–84).

As can be seen from Figure 7, polymer **1**(1) exhibited no sharp reflection signals but a diffuse halo peak at a 2θ angle of 15°. Polymer **5**(1), an amorphous polymer and the linear congener of **1**(1), was found to show a diffuse halo at a similar 2θ angle (~14°).[145] Thus, like **5**(1), **1**(1) is also an amorphous glass at room temperature. A narrow reflection peak was, however, observed at a 2θ angle of 21.6° in the XRD diffratogram of **1**(18). The reflection peak was not sharp because of the imperfect packing of the alkyl chains in the crystallites. Using the Scherrer equation,[88,146] it was calculated from the line broadening that the crystallite was of nanodimension, as it was ~15 nm in size. Obviously, the rigid skeleton structure of the hyperbranched polymer impeded the nanocrystallites from growing into big crystals of macroscopic sizes.

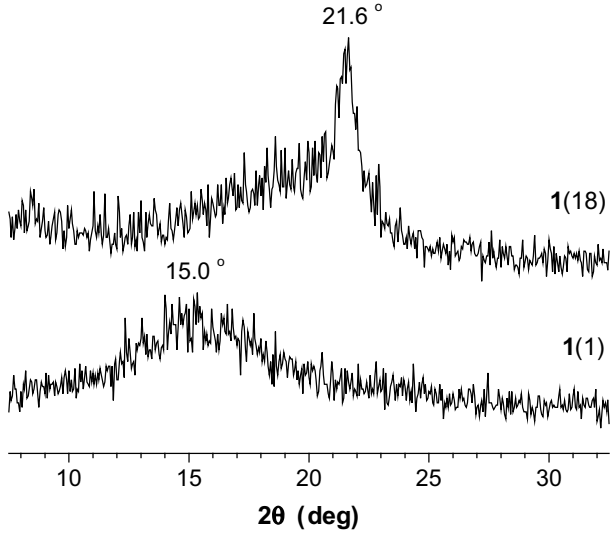

Figure 7 XRD diagrams of poly[1,1′-ferrocenylene(methyl)silyne] [**1**(1)] and poly[1,1′-ferrocenylene(*n*-octadecyl)silyne] [**1**(18)] measured at room temperature at a scan rate of 2θ = 0.02°/s.

V. PYROLYTIC CERAMIZATION

The linear polyferrocenylenesilenes have been utilized as organometallic polymer precursors to ceramics,[72,73,85–87,147–150] and we also explored the possibility of using our hyperbranched polyferrocenylenesilynes as the precursor materials.[88–90] We investigated the thermolysis behaviors of our polymers by TGA analyses. The polymer with methyl groups [**1**(1)] was thermally stable, losing little of its weight when heated to ~400°C (Fig. 8). The polymer underwent a rapid thermolytic degradation in the temperature region of ~400–500°C, after which the TGA curve almost

leveled off. Little further weight loss was recorded when the sample was further heated to ~680°C, indicating that the polymer had been ceramized by the high-temperature pyrolysis. The ceramization yield of the polymer at this temperature was ~63 wt%, much higher than that of its linear cousin **5**(1) under comparable pyrolysis conditions (36 wt%).[73] It is worth pointing out that **5**(1) dropped to ~50% of its original weight when heated to 500°C,[73] while at this temperature, **1**(1) still held more than 72% of its weight. This difference is obviously associated with the difference in their molecular structures. It was found that the three-dimensional polyorganosilyne networks were more stable than their linear polydiorganosilene congeners;[13a] for example, to achieve the same extent of photolysis, the network polymers require larger doses of photoirradiation.[74] The higher ceramization yield of hyperbranched polyferrocenylenesilyne **1**(1), in comparison to that of its linear counterpart **5**(1), may thus be attributed to the higher stability of the hyperbranched polymer and to the better retention of the pyrolysis-generated ceramic species inside the three-dimensional macromolecular spheres, melding of which within the cages afforded the desired ceramic product in a higher yield.

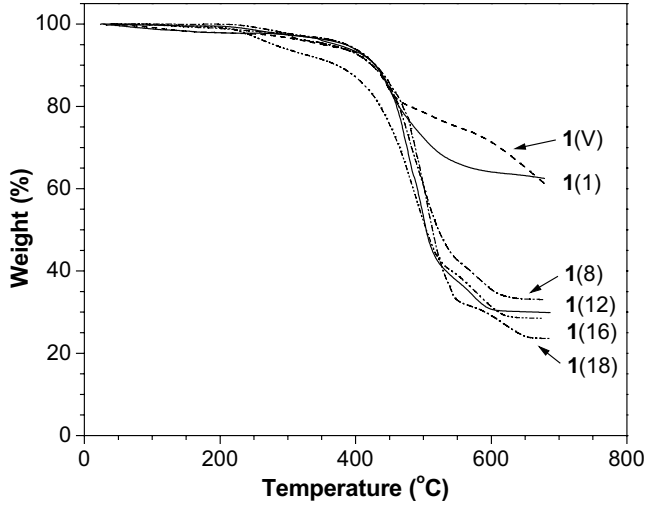

Figure 8 TGA thermograms of hyperbranched polyferrocenylenesilynes measured under nitrogen at a heating rate of 20°C/min.

The pyrolysis behavior of the hyperbranched polymer with short, reactive vinyl groups [**1**(V)] was similar to that of **1**(1). Its ceramization yield at the high temperature was also quite high (~61 wt%). Although the polymer with the long *n*-octyl chains [**1**(8)] commenced to lose its weight at a temperature similar to that of **1**(1) or **1**(V), its ceramization yield was much lower: only ~33 wt% at ~680°C. A further increase in the alkyl chain length led to a further decrease in the ceramization yield. From the pyrolysis of **1**(18) at ~690°C, a ceramic product was obtained in a

yield as low as ~24 wt%. Clearly, the long alkyl chains are detrimental to the ceramization of the hyperbranched polymers.

Since the TGA analyses showed that the polymers with small methyl [**1**(1)] and vinyl groups [**1**(V)] were promising precursor candidates for ceramics, we further studied their ceramization processes. We heated the polymers to high temperatures (700–1200°C) and isothermally sintered the samples at high temperatures under inert-gas atmosphere (see Scheme 2), which afforded ceramic products in ~50 wt% yields. As shown in Figure 9, the ceramic produced by the calcination of polymer **1**(1) at 1200°C under argon [**2**(12A)] was mesoporous in morphology, composed of many three-dimensionally tortuously interconnected clusters with sizes of a few hundred nanometers. This morphological structure suggests such a process of ceramization; the pyrolytic decomposition strips off some of the organic moieties from the skeletons of the hyperbranched polymer spheres, and the fast evaporation of the volatile fragments at the high temperature leaves behind the mesoscopic pores. In the meantime, the naked reactive inorganic residues undergo heavy crosslinking reactions to aggregate into the nanoscopic clusters, forming the basic components of the ceramic product.

Figure 9 SEM photomicrograph of ceramic **2**(12A) prepared by pyrolysis of hyperbranched poly[1,1′-ferrocenylene(methyl)silyne] **1**(1) at 1200°C in an atmosphere of argon.

VI. CERAMIC COMPOSITION

We used X-ray photoelectron spectroscopy (XPS) and energy-dispersion X-ray (EDX) techniques to analyze the ceramic products in an effort to learn their chemical compositions. Similar to the ceramics prepared from the pyrolyses of the linear polyferrocenylenesilenes,[72–73,85–87] the ceramics from our hyperbranched polyferrocenylenesilynes all contained iron, silicon, carbon, and oxygen species. The combined XPS and energy-dispersive X-ray (EDX) analyses revealed that the

oxygen contents of the ceramics decreased from the surfaces to the bulk, suggesting that the oxygenic species were formed by the reactions of the oxygen and moisture absorbed on the surfaces of the polymer precursors during the ceramization processes and/or by the postreactions of oxygen and moisture with the surfaces of the ceramic products during the handling and storage processes. The latter possibility is supported by the observations that many metallic nanoclusters can be readily oxidized in a split second.[151–154] Moving inward from the surfaces to the bulk, the iron contents of the ceramics increased, while their carbon contents decreased. For example, the atomic composition of iron of **2**(12A) increased from a low surface value of ~4% (measured by XPS) to a high bulk value of ~43% (by EDX). On the contrary, its atomic composition of carbon decreased from ~87% (on the surface) to ~22% (in the bulk). This suggests that the ceramization process started from the formation of the iron nanocluster inner cores, onto which other ceramic species were depositing along with the progress of the pyrolytic crosslinking reaction.

The surface and bulk iron contents of the ceramics prepared under different conditions varied in the ranges of ~4–17% (XPS) and ~15–43% (EDX), respectively, both of which are much higher than those (1% by XPS and 11% by EDX) of the ceramic prepared from the pyrolysis of linear **5**(1) at a similarly high temperature (1000°C) under inert-gas atmosphere.[72,73] For the linear polymer, cutting a few bonds will significantly decrease its molecular weight and generate volatile ferrocenyl fragments, evaporation of which at the high temperature results in the loss of the iron species. On the other hand, the molecular weight of our hyperbranched polymers would not change much by cleaving a few bonds because of their three-dimensional topological structures. The retention of the high molecular weight branches and the confinement of the ferrocenylene moieties in the hyperbranched spheres allow the iron species to have more time to take part in the crosslinking reactions, hence enhancing their chances to transform into the nonvolatile inorganic agglomerates.

To gain insights into the chemical structures of the iron species in the ceramic products, we inspected their Fe 2*p* core level photoelectron spectra. Examples of the Fe 2*p* photoelectron spectra of ceramics **2** and **3** are given in Figure 10. The ceramic produced by the pyrolysis of polymer **1**(1) at 1200°C [**2**(12A)] exhibited, in addition to the noisy tails in the high-binding-energy region, three major peaks at 720.2, 710.8, and 707.4 eV, which are the Fe $2p_{1/2}$ peak of iron atom and the Fe $2p_{3/2}$ peaks of Fe_3O_4 and Fe_3Si species, respectively.[88–90,155–157] On the other hand, the ceramic obtained from the pyrolysis of polymer **1**(V) at 1000°C, namely, **3**(10A), displayed two main peaks at 724.8 and 711.2 eV, which are associated with the Fe $2p_{1/2}$ and Fe $2p_{3/2}$ core-level binding energies of Fe_3O_4 and Fe_2O_3, respectively.[88–90,155–157] Thus the ceramics prepared from different precursor polymers under different sintering conditions can have quite different chemical compositions.

To collect more information on the bulk compositions of the ceramic materials, we measured their XRD patterns. While the precursor polymers **1**(1) and **1**(V) were amorphous (see Table 2 and Fig. 7), their ceramic products exhibited XRD diagrams with many Bragg reflection peaks, suggesting that they contain different

crystalline species. We used the data files in the databases of the Joint Committee on Powder Diffraction Standards of the International Center for Diffraction Data (JCPDS–ICDD) to identify the reflections; for instance, the peaks at 2θ angles of 14.15° and 35.60° in the diffractogram of **2**(7A) (Fig. 11, curve *A*) are associated with the reflections of γ-$Fe_2O_3 \cdot H_2O$ and γ-Fe_2O_3 crystals, according to ICDD data files 02-0127 and 25-1402, respectively. The reflection peaks were, however, broad, suggesting that the crystallites are imperfect in packing and small in size. Using the full widths at half-maxima (FWHMs) of the reflection peaks, it was calculated from the Scherrer equation that the sizes of the γ-$Fe_2O_3 \cdot H_2O$ and γ-Fe_2O_3 crystallites were ∼9 and ∼7 nm, respectively, similar to those (∼2–20 nm) of the iron oxide nanoparticles in the ceramics prepared from the pyrolyses of the linear polyferrocenylenesilenes.[72,73,78–84,147–150]

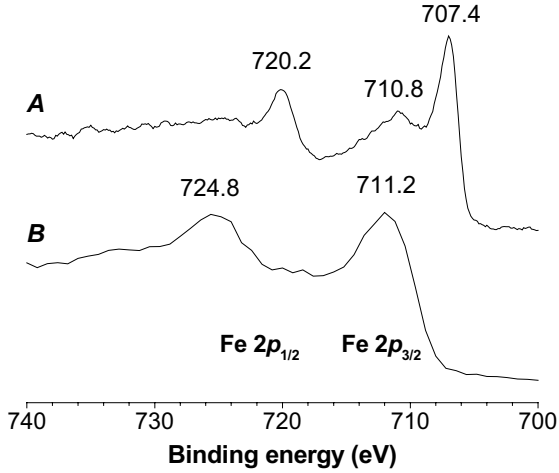

Figure 10 Fe 2*p* photoelectron spectra of ceramics (curve *A*) **2**(12A) and (curve *B*) **3**(10A) prepared by pyrolytic ceramizations of hyperbranched (curve *A*) poly[1,1′-ferrocenylene(methyl)silyne] [**1**(1)] at 1200°C and (curve *B*) poly[1,1′-ferrocenylene(vinyl)silyne] [**1**(V)] at 1000°C under argon.

The reflection peaks of the ceramic prepared at a higher temperature of 1200°C, specifically, **2**(12A), were much sharper, indicating that the ceramic contains bigger crystals. Among the many peaks in the XRD diagram, the most outstanding one was the intense peak of iron silicide (Fe_3Si) crystal at a 2θ angle of 45.4° (ICDD data file 45-1207). Its size calculated from the Scherrer equation was as big as ∼37 nm. This ceramic also contained γ-Fe_2O_3 crystal (2θ=35.5°), whose reflection was, however, better defined and whose size was much bigger (∼60 nm). Thus the calcination at the higher temperature facilitated the crystallites to increase in size, in agreement with the early observations of Manners and Ozin's groups.[72,73,78–84,147–150]

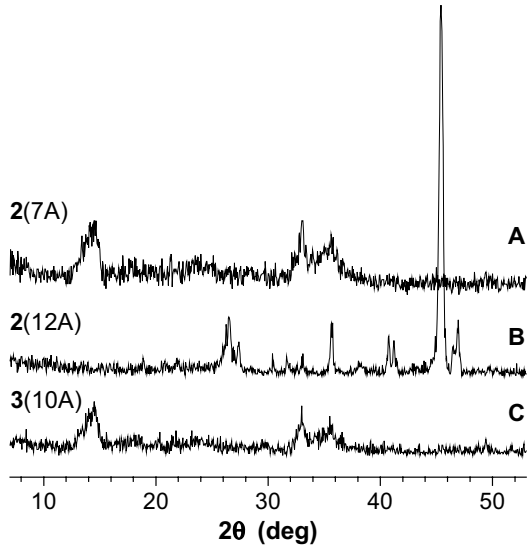

Figure 11 XRD diffractograms of ceramics (tracing *A*) **2**(7A), (tracing *B*) **2**(12A), and (tracing *C*) **3**(10A).

The diffractogram of **3**(10A) was similar to that of **2**(7A); thus, although **3**(10A) was prepared at a higher temperature (1000°C), it contained small nanocrystallites. The high reactivity or polymerizability of the vinyl groups may have enabled **1**(V) to undergo crosslinking reactions at lower temperatures and this early formation of carbonaceous network structures may have prevented the metallic species from entering the crystalline lattices in the latter ceramization stage at high temperatures, hence hampering them from growing into bigger crystals.

VII. MAGNETIC SUSCEPTIBILITY

It has now become clear that all the ceramic materials contain nanoscopic iron species, which are thus expected to be magnetically active. This was indeed the case: the ceramics were attracted to a bar magnet at room temperature; that is, they were readily magnetizable. We thus used the SQUID (superconducting quantum interference device) technique to investigate their magnetization behaviors in externally applied magnetic fields (with field strength up to 20 kOe) at different temperatures (300 and 5 K). The magnetization curves for ceramic **2**(12A) are shown in Figure 12 as an example and the magnetic properties of all the ceramic materials are summarized in Table 3.

When placed in an external magnetic field at a temperature close to room temperature (300 K), **2**(12A) was swiftly magnetized, as evidenced by an immediate raise in its magnetization curve (Fig. 12). The magnetization rapidly increased with an increase in the strength of the applied field and leveled off at a field strength of ~5 kOe.

When the temperature was decreased to 5 K, the magnetization was enhanced, and the saturation magnetization (M_s) rose to ~51 emu/g, close to the value for bulk γ-Fe_2O_3 maghemite (74 emu/g).[158] To see whether there exists any hysteresis in the magnetization process of **2**(12A), we enlarged its magnetization curves in the low-field region. As can be seen from the inset of Figure 12, even at the high magnification, no hysteresis loops can be identified; its magnetization curves cross directly through the zero point, when the magnetization experiments were carried out at either 300 or 5 K. Clearly, no remanence and coercivity were observable in the magnetization of **2**(12A).

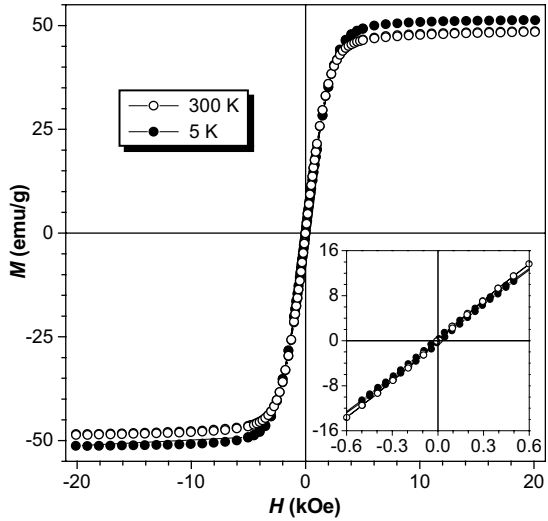

Figure 12 Plots of magnetization (M) versus applied magnetic field (H) at 300 and 5 K for ceramic **2**(12A). Inset (lower right panel): enlarged portion of the magnetization curves in the low magnetic field region.

Table 3 Magnetic Properties of Ceramics **2** and **3**[a]

		300 K[b]			5 K[b]		
No.	Ceramic	M_s	M_r	H_c	M_s	M_r	H_c
1	**2**(7N)	7.3	0.9	0.19	8.9	3.4	0.61
2	**2**(10N)	15.9	2.6	0.65	21.3	6.4	0.18
3	**2**(7A)	5.0	0.3	0.50	7.3	1.6	0.43
4	**2**(12A)	48.6	~0	~0	51.3	~0	~0
5	**3**(7N)	9.6	~0	~0	13.0	3.1	0.54
6	**3**(10N)	12.1	1.3	0.11	14.8	5.1	0.60
7	**3**(7A)	9.7	~0	~0	13.1	2.6	0.59
8	**3**(10A)	10.8	2.0	0.27	13.2	4.6	0.67

[a] Fabricated by pyrolysis at a high temperature (700, 1000, or 1200°C) in an inert-gas atmosphere (nitrogen or argon).

[b] *Abbreviations:* M_s (emu/g)=saturation magnetization (in an external field of 20 kOe), M_r (emu/g)=magnetic remanence (at zero external field); H_c (kOe)=coercivity (at zero magnetization).

Not all the ceramics, however, behaved like **2**(12A). The ceramics fabricated from different precursor polymers under different pyrolysis conditions performed magnetically differently. The ceramic prepared from the pyrolysis of precursor **1**(1) at 700°C under nitrogen [**2**(7N)] exhibited a low M_s of ~7 emu/g in a magnetic field of 20 kOe at 300 K (Table 3, no. 1). Hysteresis loop was observed in the magnetization process, although both remanence M_r (<1 emu/g) and coercivity H_c (~0.2 kOe) were low. When the magnetization temperature decreased to 5 K, all the magnetization parameters increased. The ceramic prepared from **1**(1) at a higher temperature [1000°C; **2**(10N)] performed better magnetically than did its counterpart prepared at the low temperature [**2**(7N)]; the M_s values of the former were more than 2-fold higher than those of the latter at both 300 and 5 K.

Similar but more profound effect of pyrolysis temperature was observed when the ceramics prepared under argon was magnetized. Similar to **2**(7N), **2**(7A) was also poorly magnetic, whose M_s values were in the range of ~5–7 emu/g. The ceramic prepared at the high temperature of 1200°C [**2**(12A)] was, however, a much stronger magnet, whose M_s values were ~10- and ~7-fold higher than those of **2**(7A) at 300 and 5 K, respectively. The superior magnetic performance of the ceramics fabricated at the higher temperatures may be associated with their greater crystal sizes. A small crystal possesses a large area of surface, on which the discontinuity of the superexchange bonds between the iron species leads to the formation of canted spins.[159–171] The noncollinear spin structures due to the pinning of the surface spins at the interfaces of the magnetic nanoclusters and the nonmagnetic ceramic surroundings reduce the total magnetic moments of the nanoclusters, resulting in a decrease in their magnetizability.[159–171] The bigger crystals have smaller surface areas and hence higher magnetic susceptibilities.

The magnetization behaviors of the ceramics fabricated from polymer **1**(V), namely, **3**, were similar to those of **2** in one aspect but different in the other. Similarly, higher pyrolysis temperature again favored the formation of ceramics with higher magnetizabilities; the M_s values of the ceramics prepared at 1000°C were always higher than did those prepared at 700°C. However, different from **2**, none of ceramics **3** exhibited a really high magnetizability. The M_s values of the ceramics prepared at the high pyrolysis temperature (1000°C) [i.e., **3**(10N) and **3**(10A)] were moderate at the low magnetization temperature (5 K), in the range of ~13–15 emu/g. These values are, however, still much higher than those of the ceramics prepared from the pyrolyses of linear polymer **5**(1), which were in the range of 0.52–3.5 emu/g.[72,73,78–84,147–150] This difference in magnetizability may be caused by the difference in their iron contents: the atomic compositions of iron in **3** were ~28–31% (by EDX), while those in the ceramic prepared from the linear polymer precursor was only 11% (also by EDX).[72,73]

Ceramics **3**(7N) and **3**(7A) exhibited typical superparamagnetic behavior;[172–176] there were practically no hysteresis loops in their magnetization curves at 300 K but well-defined loops were observed when the magnetization was carried out at 5 K (Table 3, nos. 5 and 7). Remarkably, however, **2**(12A) did not show any hysteresis loops even when it was magnetized at 5 K (Table 3, no. 4). In other words, this ceramic does not suffer any magnetic hysteresis loss at either high or low temperature. Silicon

steel (Si–Fe) is widely used in the electromagnetic systems (generators, motors, transformers, solenoids, etc.) because of its very low magnetic hysteresis loss.[177–180] XRD analysis has revealed that the major component of iron nanoclusters in **2**(12A) is the iron silicide (Fe_3Si) species (see curve *B* in Fig. 11), which may be the cause for its near-zero M_r and H_c values. This ceramic is thus an excellent soft ferromagnetic material with a high magnetic susceptibility (M_s ~51 emu/g) and low hysteresis loss (M_r and H_c: practically nil).

VIII. SUMMARY AND PERSPECTIVES

In summary, in this work, we generated a group of new hyperbranched organometallic polymers by molecularly fusing the ferrocenylene and silyne moieties into a three-dimensional macromolecular structure. The polyferrocenylenesilynes were readily synthesized by a one-pot experimental procedure in good isolation yields. The properties of the polymers changed with the alkyl substituents on the silicon atom; with an increase in the length of the alkyl chain, the solubility of the polymer increased, while its T_g and ceramization yield decreased. The pyrolysis temperature affected the structure and properties of the resultant ceramic materials: sintering polymers **1**(1) and **1**(V) at higher temperatures produced ceramic materials with bigger iron nanoclusters and higher magnetic susceptibilities. Pyrolyzing **1**(1) at 1200°C under argon resulted in the formation of an outstanding soft ferromagnetic ceramic, **2**(12A), which was magnetically highly susceptible but practically hysteresis-free in its magnetization processes.

In comparison to the polyalkylsilyne networks, our hyperbranched polyferrocenylenesilynes were electronically more conjugated, with their absorption band edges entered the infrared spectral region, due probably to the extended σ–π conjugation in the three-dimensional macromolecular spheres. Compared to their linear polyferrocenylenesilene cousin **5**(1), hyperbranched polymers **1**(1) and **1**(V) produced, on sintering at high temperatures, ceramics with higher iron contents and bigger nanocrystals in higher ceramization yields, due to the better retention of the pyrolysis-generated ceramizing species inside the macromolecular cages. Our hyperbranched polymers are thus a group of better precursor polymers for the fabrication of nanostructured magnetoceramics.

The information gained in this work is useful in terms of guiding molecular engineering endeavors in the design of molecular structures of precursor polymers. Our study suggests such an "ideal" molecular structure for an organometallic polysilyne precursor: "high branching density + small substituents on silicon." Thus, replacing the methyl group in **1** with a hydrogen atom, which is small yet reactive, should lead to high-yield production of a ceramic material with high iron content.

The pyrolysis process provides a fast and simple route for the preparation of mesoporous ceramic materials. While the spatial distribution of the nanoclusters in **2** is random, we are extending our research efforts to the design and synthesis of amphiphilic copolyferrocenylenesilynes, in the hope of converting self-assembled

nanostructures of the copolymers to well-ordered mesoporous morphologies by controlled pyrolysis.

The mesoporous structure, coupled with other properties inherent with ceramic materials (thermal stability, mechanical strength, solvent resistance, etc.), makes ceramic **2** a promising candidate for many practical applications. For example, this ceramic may be used as high-temperature filters or separation membranes, whose three-dimensionally tortuously interconnected pathways offer the advantage of decreasing the likelihood of the mesopores being clogged by filtrates. The high surface areas associated with the mesoporous structures may be utilized in the supported catalysis; that is, **2** may be used as matrix nanomaterials for embedding catalytic species in the preparation of efficient and reusable catalysts.

The soft ferromagnetism of **2**(12A) may also find technological applications in many areas such as information storage and magnetic refrigeration. The nanostructured magnetoceramic materials are electrically highly conductive, further investigation of which may lead to the development of novel electromagnetic devices of nanodimensions, for example, nanomotors[24,181] and nanoswitches.

IX. EXPERIMENTATION

A. Materials

Ferrocene was purchased from Aldrich and was further purified by recrystallization from ethanol in our laboratory before use. The R-substituted trichlorosilanes R−$SiCl_3$, i.e., methyl- (Aldrich), vinyl-, *n*-octyl-, *n*-octyldecyl- (all Lancaster), *n*-dodecyl-, and *n*-hexadecylltrichlorosilanes (both UCT) were all distilled over calcium hydride. Diethyl ether, hexane, THF (all Lab-Scan), dichloromethane (DCM; Aldrich), and *N,N,N′,N′*-tetramethylethylenediamine (TMEDA; Acros) were distilled from either calcium hydride or sodium benzophenone ketyl. *n*-Butyllithium (1.7 M in heptane) and all other solvents and reagents were from Aldrich and were used as received. Dilithioferrocene·TMEDA (**4**; Scheme 2) and poly[1,1′-ferrocenylene(methyl)silene] **5**(1) were prepared according to published experimental procedures.[78–84]

B. Instrumentation

The IR spectra of the polymers were measured on a Perkin Elmer 16 PC FTIR spectrophotometer. The NMR analyses were performed on a Bruker ARX 300 NMR spectrometer in deuterated chloroform using TMS as internal standard. The UV spectra were recorded on a Milton Roy Spectronic 300 Array spectrophotometer and the molar absorptivity (ε_{max}) was calculated on the basis of the repeat unit of the polymer. The relative molecular weights of the polymers were estimated using a size-exclusion chromatograph (SEC) system equipped with a Waters 510 HPLC pump, ultrastyragel

columns (HT3, HT4, and HT6), a column temperature controller, a Waters 486 wavelength-tunable UV–vis detector, and a Waters 410 differential refractometer (RI). THF was used as eluent at a flow rate of 1.0 mL/min. A set of monodisperse polystyrene standards covering molecular weight range of 10^2–10^7 Da was used as calibration references. The absolute molecular weights and the intrinsic viscosities of the polymers were determined in THF by another SEC system (Waters 590) equipped with a set of parallel-series detectors, where a RI detector is connected in parallel with two series detectors: a right-angle laser light-scattering (RALLS) detector and a differential viscometer (DV) detector.[96–99]

The differential scanning calorimetry (DSC) analysis was performed on a Setaram DSC 92 calorimeter at a heating rate of 10°C/min under nitrogen. Thermogravimetric analysis (TGA) was performed at a heating rate of 20°C/min under nitrogen using a Perkin-Elmer TGA 7 analyzer. The morphologies of the ceramization products of the polymers were imaged on a JEOL 6300 scanning electron microscope (SEM) operating at an accelerating voltage of 5 kV. The X-ray photoelectron spectroscopy (XPS) experiments were conducted on a PHI 5600 spectrometer (Physical Electronics), and core level spectra were measured using a monochromatic Al K_α X-ray source ($h\nu = 1486.6$ eV). The analyzer was operated at 23.5 eV pass energy and the analyzed area was 800 μm in diameter. The binding energies were referenced to the adventitious hydrocarbon C 1*s* line at 285.0 eV, and curve fitting of the XPS spectra was performed using the least-square method. Energy-dispersion X-ray (EDX) analyses were performed on a Philips XL30 SEM system with quantitative elemental mapping and linescan capacities operating at an accelerating voltage of 15 kV. The X-ray diffraction (XRD) diagrams were recorded on a Philips PW 1830 powder diffractometer using the monochromatized X-ray beam from a nickel-filtered Cu K_α radiation ($\lambda = 1.5406$ Å). The magnetization measurements were carried out using a SQUID magnetometer (Quantum Design MPMS-5S) at fields ranging from 0 to 20 kOe and at temperatures of 5 and 300 K.

C. Polymerization

All the polymerization reactions were carried out in an atmosphere of vigorously dried nitrogen using the Schlenk technique. A typical experimental procedure for the preparation of poly[1,1′-ferrocenylene(*n*-hexadecyl)silyne] **1**(16) is given below as an example. Ferrocene (0.622 g), 0.6 mL of TMEDA, and 15 mL anhydrous hexane were added into a baked 100 mL two-necked round-bottomed flask at room temperature (~22°C), into which a 2.5 M hexane solution of *n*-BuLi (2.7 mL) was carefully injected using a syringe under nitrogen with magnetic stirring. An orange slurry solution was obtained gradually. The solution was stirred for 8 h at room temperature and was then cooled to −78°C using a dry ice/acetone bath, after which, 0.8 mL *n*-hexadecyltrichlorosilane in 50 mL THF was added. The temperature was gradually raised from −78°C to room temperature in 4 h. The mixture was stirred for another 20 h at room temperature and the reaction was then terminated by adding 0.2 mL methanol. The mixture was passed through a Pyrex filter to remove the fine

white particles of LiCl. The filtrate was slightly concentrated and then passed through a cotton filter into a large volume of methanol (~1000 mL) in a glass beaker under vigorous stirring. A brown thin film formed at the bottom of the beaker on standing. After standing overnight, the methanol solvent was decanted and the film became transparent. The film was put into an oven and dried under vacuum to a constant weight.

Characterization Data of the Polymers. Poly[*1,1′-ferrocenylene*(*methyl*)*silyne*] [*1*(*1*)]. Golden yellow powder. IR: ν (cm^{-1}) 3088, 2958, 2930, 2115, 1690, 1570, 1421, 1252, 1166, 1036, 776, 732. (Soluble fraction used for NMR analysis) ^{1}H NMR (300MHz, CDCl3), δ (TMS, ppm): 4.12 (Cp), 0.55 (Me).

Poly[*1,1′-ferrocenylene*(*vinyl*)*silyne*] [***1***(*V*)]. Golden yellow powder. IR: ν (cm^{-1}) 3090, 2943, 1694, 1592, 1420, 1404, 1164, 1105, 1036, 958, 830, 819, 732, 693. (Soluble fraction used for NMR analysis) ^{1}H NMR (300 MHz, $CDCl_3$), δ (TMS, ppm): 5.5–6.2 (vinyl), 4.19 (Cp).

Poly[*1,1′-ferrocenylene*(n-*octyl*)*silyne*] [***1***(*8*)]. Amber powder. IR: ν (cm^{-1}) 3090, 2955, 2924, 2854, 1693, 1466, 1164, 1108, 1036, 830, 724, 684. ^{1}H NMR (300 MHz, $CDCl_3$), δ (TMS, ppm): 4.31 (Cp), 1.45, 1.06 (alkyl). ^{13}C NMR (75 MHz, $CDCl_3$), δ (TMS, ppm): 73.15, 70.93 (*ipso*-Cp), 67.73 (Cp), 34.88, 31.53, 29.31, 26.90, 25.32, 22.80, 14.22, 12.30, 11.51 (alkyl). UV (DCM), λ_{max} 229 nm, ε_{max} 8.88×10^3 mol^{-1} L cm^{-1}.

Poly[*1,1′-ferrocenylene*(n-*dodecyl*)*silyne*] [***1***(*12*)]. Brown elastomer. IR: ν (cm^{-1}) 3088, 2954, 2922, 2855, 1694, 1466, 1360, 1164, 1037, 1024, 829, 688. ^{1}H NMR (300 MHz, $CDCl_3$), δ (TMS, ppm): 4.52, 4.21 (Cp), 1.30, 0.90 (alkyl). ^{13}C NMR (75 MHz, $CDCl_3$), δ (TMS, ppm): 73.10, 70.81 (*ipso*-Cp), 67.91 (Cp), 31.93, 22.68, 14.09, 13.38, 2.34 (alkyl). UV (DCM), λ_{max} 229 nm, ε_{max} 8.98×10^3 mol^{-1} L cm^{-1}.

Poly[*1,1′-ferrocenylene*(n-*hexa-decyl*)*silynes*] [***1***(*16*)]. Brown elastomer. IR: ν (cm^{-1}) 3090, 2922, 2852, 2112, 1696, 1629, 1466, 1379, 1165, 1036, 807, 722, 688. ^{1}H NMR (300 MHz, $CDCl_3$), δ (TMS, ppm): 4.12 (Cp), 1.26 (alkyl). UV (DCM), λ_{max} 229 nm, ε_{max} 12.49×10^3 mol^{-1} L cm^{-1}.

Poly[*1,1′-ferrocenylene*(n-*octyldecyl*)*silyne*] [***1***(*18*)]. Golden yellow powder. IR: ν (cm^{-1}) 3091, 2923, 2853, 1692, 1672, 1467, 1379, 1165, 1037, 830, 817, 721, 688. ^{1}H NMR (300 MHz, $CDCl_3$), δ (TMS, ppm): 4.52, 4.22 (Cp), 1.28, 0.89 (alkyl). ^{13}C NMR (75 MHz, $CDCl_3$), δ (TMS, ppm): 73.30, 71.60 (*ipso*-Cp), 68.40 (Cp), 33.81, 31.88, 30.43, 30.07, 29.74, 22.63, 14.82, 13.44 (alkyl). UV (DCM), λ_{max} 229 nm, ε_{max} 15.80×10^3 mol^{-1} L cm^{-1}.

D. Ceramization

The ceramics were prepared by high-temperature pyrolyses of the polymers under nitrogen or argon (see Scheme 2). In one typical ceramization experiment conducted under nitrogen, poly[1,1′-ferrocenylene(methyl)silyne] [**1**(1); 28 mg] was placed in a sample cell of Perkin-Elmer TGA 7 analyzer. The sample was heated to 1000°C at a rate of 10°C/min and calcinated at the highest temperature for 1 h.

A ball-shaped ceramic product **2**(10N) was obtained in ~50% yield. In another typical pyrolysis experiment carried out under argon, ~40 mg of **1**(1) was placed in a quartz tube in a Winston-Salem Thermcraft furnace, which was heated to 1200°C at a rate of 10°C/min in a stream of argon (flow rate ~200 cm^3/min). The sample was sintered at the highest temperature for 1 h, which gave a ceramic product **2**(12A) in ~50% yield.

Characterization data of the ceramics are as follows:

2(*7N*). XPS, atomic composition (%): Fe 10.3, Si 21.7, C 6.4, O 61.6; binding energy (eV): Fe $2p_{3/2}$: 711.7; Fe $2p_{1/2}$: 720.0, 725.1; Si 2*p*: 104.1. EDX, atomic composition (%): Fe 24.0, Si 19.8, C 7.4, O 48.9. XRD, 2θ (degree)/*d* spacing (Å): 25.25/3.52, 33.2/2.70, 35.7/2.51, 40.9/2.21, 49.5/1.84, 54.25/1.69, 62.6/1.48, 64.05/1.45, 72.05/1.31, 75.5/1.26.

2(*10N*). XPS, atomic composition (%): Fe 6.1, Si 0.7, C 78.0, O 15.2; binding energy (eV): Fe $2p_{3/2}$: 707.4, 712.3; Fe $2p_{1/2}$: 720.2, 725.8; Si 2*p*: 104.0. EDX, atomic composition (%): Fe 36.0, Si 24.4, C 30.2, O 9.4. XRD, 2θ (degree)/*d* spacing (Å): 19.00/4.68, 26.90/3.31, 28.45/3.13, 32.35/2.76, 33.00/2.71, 35.65/2.52, 38.45/2.34, 43.65/2.07, 44.55/2.03, 49.50/1.84, 51.00/1.79, 51.60/1.77, 54.75/1.68, 57.50/1.60, 59.85/1.54, 66.30/1.41, 67.40/1.39.

2(*7A*). XPS, atomic composition (%): Fe 12.9, Si 19.7, C 6.7, O 60.7; binding energy (eV): Fe $2p_{3/2}$: 711.2; Fe $2p_{1/2}$: 719.4, 724.9; Si 2*p*: 103.2. EDX, atomic composition (%): Fe 15.5, Si 20.3, C 6.6, O 57.8. XRD, 2θ (degree)/*d* spacing (Å): 14.15/6.25, 33.05/2.71, 35.6/2.52.

2(*12A*). XPS, atomic composition (%): Fe 3.8, Si 0.6, C 86.7, O 8.9; binding energy (eV): Fe $2p_{3/2}$: 707.4, 710.8; Fe $2p_{1/2}$: 720.2, 724.8; Si 2*p*: 99.9, 101.5, 104.0. EDX, atomic composition (%): Fe 43.2, Si: 29.1, C 22.4, O 5.3. XRD, 2θ (degree)/*d* spacing (Å): 26.50/3.36, 27.40/3.24, 30.40/2.94, 33.00/2.71, 35.48/2.53, 38.05/2.36, 40.75/2.21, 41.20/2.19, 45.40/2.00, 46.50/1.95, 59.95/1.54, 66.35/1.41, 69.00/1.36, 84.15/1.15.

3(*7N*). XPS, atomic composition (%): Fe 14.9, Si 15.7, C 14.3, O 55.2; binding energy (eV): Fe $2p_{3/2}$: 711.4; Fe $2p_{1/2}$: 719.3, 725.1; Si 2*p*: 103.1. EDX, atomic composition (%): Fe 29.1, Si 15.8, C 5.2, O 50.0. XRD, 2θ (degree)/*d* spacing (Å): 14.5/6.10, 35.55/2.52, 40.65/2.22, 49.5/1.84, 54.1/1.69, 57.5/1.60.

3(*10N*). XPS, atomic composition (%): Fe 9.1, Si 21.0, C 14.9, O 55.0; binding energy (eV): Fe $2p_{3/2}$: 711.1; Fe $2p_{1/2}$: 719.4, 724.8; Si 2*p*: 103.3. EDX, atomic composition (%): Fe 27.7, Si 18.1, C 3.1, O 51.2. XRD, 2θ (degree)/*d* spacing (Å): 24.15/3.68, 33.2/2.70, 35.7/2.51, 40.9/2.21, 49.5/1.84, 54.25/1.69, 62.6/1.48, 64.05/1.45, 72.05/1.31, 75.5/1.26.

3(*7A*). XPS, atomic composition (%): Fe 17.1, Si 16.7, C 8.0, O 57.8; binding energy (eV): Fe $2p_{3/2}$: 711.4; Fe $2p_{1/2}$: 720.0, 725.0; Si 2*p*: 103.0. EDX, atomic composition (%): Fe 28.1, Si 13.0, C 3.6, O 55.3. XRD, 2θ (degree)/*d* spacing (Å): 32.70/2.74, 34.95/2.57.

3(*10A*). XPS, atomic composition (%): Fe 14.7, Si 18.4, C 8.7, O 58.2; binding energy (eV): Fe $2p_{3/2}$: 711.2; Fe $2p_{1/2}$: 719.6, 724.8; Si 2*p*: 103.2. EDX, atomic composition (%): Fe 30.9, Si 16.7, C 5.6, O 46.9. XRD, 2θ (degree)/*d* spacing (Å): 14.50/6.10, 33.00/2.71, 34.95/2.57, 35.60/2.52.

X. ACKNOWLEDGMENTS

This work was partially supported by the Research Grants Council of the Hong Kong Administrative Region, China (Projects HKUST 6187/99P, 6121/01P, and 6085/02P) and by the University Grants Committee of Hong Kong through an Area of Excellence scheme (Project AoE/P-10/01-1-A). We are grateful to the experimental assistance of the technical staffs in the Materials Characterization & Preparation Facility of our university. We thank Drs. Yuping Dong, Fouad Salhi, Jacky W. Y. Lam, and Kevin K. L. Cheuk of our research group for their helpful discussions.

XI. REFERENCES AND NOTES

1. H. Shirakawa, *Angew. Chem. Int. Ed*. **40,** 2575 (2001).
2. A. G. MacDiarmid, *Angew. Chem. Int. Ed*. **40,** 2581 (2001).
3. A. J. Heeger, *Angew. Chem. Int. Ed*. **40,** 2591 (2001).
4. T. Masuda, T. Higashimura, *Adv. Polym. Sci*. **81,** 121 (1987).
5. B. M. Novak, W. Risse, R. H. Grubbs, *Adv. Polym. Sci*. **102**, 47 (1992).
6. E. J. Ginsburg, C. B. Gorman, R. H. Grubbs, in *Modern Acetylene Chemistry,* P. J. Stang, F. Diederich, eds. VCH, New York, 1995, p. 353.
7. M. Tabata, T. Sone, Y. Sadahiro, *Macromol. Chem. Phys.* **200,** 265 (1999).
8. J. L. Reddinger, J. R. Reynolds, *Adv. Polym. Sci*. **145,** 57 (1999).
9. S. K. Choi, Y. S. Gal, S. H. Jin, H. K. Kim, *Chem. Rev*. **100,** 1645 (2000).
10. E. Yashima,. *Anal. Sci*. **18,** 3 (2002).
11. B. Z. Tang, K. Xu, Q. Sun, P. P. S. Lee, H. Peng, F. Salhi, Y. Dong, *ACS Symp. Ser.* **760,** 146 (2000).
12. B. Z. Tang, K. K. L. Cheuk, F. Salhi, B. Li, J. W. Y. Lam, J. A. K. Cha, X. Xiao, *ACS Symp. Ser*. **812,** 133 (2001).
13. K. K. L. Cheuk, B. Li, B. Z. Tang, *Curr. Trends Polym. Sci*. **7,** 41 (2002).
14. B. Z. Tang, H. Chen, R. Xu, J. W. Y. Lam, K. K. L. Cheuk, H. N. C. Wong, M. Wang, *Chem. Mater.* **12,** 213 (2000).
15. J. Sun, H. Chen, R. Xu, M. Wang, J. W. Y. Lam, B. Z. Tang, *Chem. Commun.* 1222 (2002).
16. B. Z. Tang, W. H. Poon, H. Peng, H. N. C. Wong, X. Ye, T. Monde, *Chin. J. Polym. Sci.* **17,** 81 (1999).
17. B. Z. Tang, *Polym. News* **26,** 262 (2001).
18. J. Chen, Z. Xie, J. W. Y. Lam, C. C. W. Law, B. Z. Tang, *Macromolecules* **36,** 1108 (2003).
19. Y. Huang, W. Ge, J. W. Y. Lam, B. Z. Tang, *Appl. Phys. Lett.* **78,** 1652 (2001).
20. Y. M. Huang, J. W. Y. Lam, K. K. L. Cheuk, W. Ge, B. Z. Tang, *Macromolecules* **32,** 5976 (1999).
21. B. Z. Tang, H. Xu, J. W. Y. Lam, P. P. S. Lee, K. Xu, Q. Sun, K. K. L. Cheuk, *Chem. Mater.* **12,** 1446 (2000).
22. B. Z. Tang, T. Masuda, T. Higashimura, H. Yamaoka, *J. Polym. Sci. Polym. Phys. Ed.* **28,** 281 (1990).
23. B. Z. Tang, T. Masuda, T. Higashimura, H. Yamaoka, *J. Polym. Sci. Polym. Chem. Ed.* **27,** 1197 (1989).
24. B. Z. Tang, H. Xu, *Macromolecules* **32,** 2569 (1999).
25. J. W. Y. Lam, Y. Dong, K. K. L. Cheuk, J. Luo, Z. Xie, H. S. Kwok, Z. Mo, B. Z. Tang, *Macromolecules* **35,** 1229 (2002).

26. B. Z. Tang, J. W. Y. Lam, J. Luo, Y. Dong, K. K. L. Cheuk, Z. Xie, H. S. Kwok, *Proc. SPIE* **4463,** 132 (2001).
27. J. W. Y. Lam, X. Kong, Y. Dong, K. K. L. Cheuk, K. Xu, B. Z. Tang, *Macromolecules* **33,** 5027 (2000).
28. J. W. Y. Lam, J. Luo, D. Dong, K. K. L. Cheuk, K. K. L. Tang, *Macromolecules* **35,** 8288 (2002).
29. B. Z. Tang, N. Kotera, *Macromolecules* **22,** 4388 (1989).
30. K. Xu, H. Peng, J. W. Y. Lam, T. W. H. Poon, Y. Dong, H. Xu, Q. Sun, K. K. L. Cheuk, F. Salhi, P. P. S. Lee, B. Z. Tang, *Macromolecules* **33,** 6918 (2000).
31. F. Salhi, , K. K. L. Cheuk, Q. Sun, J. W. Y. Lam, J. A. K. Cha, G. Li, B. Li, J. Luo, J. Chen, B. Z. Tang, *J. Nanosci. Nanotechnol.* **1,** 137 (2001).
32. B. Li, K. K. L. Cheuk, F. Salhi, J. W. Y. Lam, J. A. K. Cha, X. Xiao, C. Bai, B. Z. Tang, *Nano Lett*. **1,** 323 (2001).
33. B. Z. Tang, *Polym. Prepr*. **43**(1), 48 (2002).
34. B. S. Li, K. K. L. Cheuk, J. Zhou, Y. Xie, B. Z. Tang, *Polym. Mater. Sci. Eng.* **85,** 401 (2001).
35. B. S. Li, K. K. L. Cheuk, J. Zhou, J. Xie, J. A. K. Cha, X. Xiao, B. Z. Tang, *Polym. Prepr.* **42** (1), 543 (2001).
36. P. A. Bianconi, T. W. Weidman, *J. Am. Chem. Soc.* **110,** 2342 (1988).
37. P. A. Bianconi, F. C. Schilling, T. W. Weidman, *Macromolecules* **22,** 1697 (1989).
38. D. A. Smith, C. A. Freed, P. A. Bianconi, *Chem. Mater*. **5,** 245 (1993).
39. R. A. Street, *Technology and Applications of Amorphous Silicon,* Springer, Hong Kong, 2000.
40. H. Fritzsche, *Amorphous Silicon and Related Materials,* World Scientific, Hong Kong, 1989.
41. K. Furukawa, M. Fujino, N. Matsumoto, *Macromolecules* **23,** 3423 (1990).
42. A. Watanabe, T. Komatsubara, M. Matsuda, Y. Yoshida, S. Tagawa, *Macromol. Chem. Phys.* **196,** 1229 (1995).
43. A. Watanabe, Y. Tsutsumi, M. Matsuda, *Synth. Met*. **74,** 191 (1995).
44. A. Watanabe, T. Sato, M. Matsuda, *Jpn. J. Appl. Phys.* **40,** 6457 (2001).
45. S. Hecht, J. M. J. Frechet, *Angew. Chem. Int. Ed*. **40,** 74 (2001).
46. B. Voit, *J. Polym. Sci. Polym. Chem*. **38,** 2505 (2000).
47. C. J. Hawker, *Adv. Polym. Sci*. **147,** 113 (1990).
48. A. Hult, M. Johansson, E. Malmstrom, *Adv. Polym. Sci*. **143,** 1 (1999).
49. W. Burchard, *Adv. Polym. Sci*. **143,** 113 (1999).
50. O. A. Matthews, A. N. Shipway, J. F. Stoddart, *Prog. Polym. Sci*. **23,** 1 (1998).
51. D. A. Tomalia, H. D. Durst, *Top. Curr. Chem*. **165,** 193 (1993).
52. R. M. Crooks, *Chem. Phys. Chem.* **2,** 644 (2001).
53. H. Frey, C. Schlenk, *Top. Curr. Chem*. **210,** 69 (2000).
54. R. Bischoff, S. E. Cray, *Prog. Polym. Sci*. **24,** 185 (1998).
55. I. Cuadrado, M. Moran, C. M. Casado, B. Alonso, J. Losada, *Coord. Chem. Rev*. **195,** 395 (1999).
56. H. Frey, C. Lach, K. Lorenz, *Adv. Mater*. **10,** 279 (1998).
57. N. Ardoin, D. Astruc, *Bull. Soc. Chim. Fr*. **132,** 875 (1995).
58. R. West, K. Oka, H. Takahashi, M. Miller, T. Gunji, *ACS Symp. Ser.* **572,** 92 (1994).
59. H. Sakurai, K. Sakamoto, Y. Funada, M. Yoshida, *ACS Symp. Ser*. **572,** 8 (1994).
60. C. W. Whitmarsh, L. V. Interrante, *Organometallics* **10,** 1336 (1991).
61. I. L. Rushkin, Q. Shen, S. E. Lehman, L. V. Interrante, *Macromolecules* **30,** 3141 (1997).
62. G. D. Sorarù, Q. Liu, L. V. Interrante, T. Apple, *Chem. Mater*. **10,** 4047 (1998).
63. J. Ohshita, *Synth. Org. Chem. Jpn*. **59,** 11 (2001).
64. Y. Yamaguchi, *Synth. Met*. **82,** 149 (1996).

65. S. Yamaguchi, K. Tamao, *Bull. Chem. Soc. Jpn*. **69,** 2327 (1996).
66. R. D. Miller, R. Sooriyakumaran, *J. Polym. Sci. Part C, Polym. Lett.* **25,** 321 (1987).
67. R. D. Adams, *50th Anniversary of the Discovery of Ferrocene,* Elsevier, Amsterdam, 2001.
68. H. Hoffmann, M. Schwoerer, T. Vogtmann, *Macromolecular Systems: Microscopic Interactions and Macroscopic Properties,* Wiley-VCH, Weinheim, 2000.
69. D. Seyferth, J. M. Zeigler, in *Silicon-Based Polymer Science: A Comprehensive Resource,* F. W. G. Fearon, American Chemical Society, Washington, DC, 1990, p. 565.
70. W. G. J. Bunk, *Advanced Structural and Functional Materials,* Springer-Verlag, Hong Kong, 1991.
71. C. U. Jr. Pittman, *Metal-Containing Polymeric Materials,* Plenum, New York, 1996.
72. B. Z. Tang, R. Petersen, D. A. Foucher, A. Lough, N. Coombs, R. Sodhi, I. Manners, *J. Chem. Soc. Chem. Commun*. 523 (1993).
73. R. Petersen, D. A. Foucher, B. Z. Tang, A. Lough, N. P. Raju, J. E. Greedan, I. Manners, *Chem. Mater*. **7,** 2045 (1995).
74. "Polysilene" is a structure-based name according to the systematic nomenclature rules of IUPAC [e.g., K. Kabeta, K. Shuto, S.-I. Sugi, T. Imai, *Polymer* **37,** 4327 (1996)].
75. K. Matyjaszewski, P. J. Miller, E. Fossum, Y. Nakagawa, *Appl. Organomet. Chem*. **12,** 667 (1998).
76. K. H. Pannell, H. K. Sharma, *Organometallics* **16,** 3077 (1997).
77. J. M. Nelson, P. Nguyen, R. Petersen, H. Rengel, P. M. Macdonald, A. J. Lough, I. Manners, N. P. Raju, J. E. Greedan, S. Barlow, D. O'Hare, *Chem. Eur. J.* **3,** 573 (1997).
78. D. A. Foucher, B. Z. Tang, I. Manners, *J. Am. Chem. Soc*. **114,** 6246 (1992).
79. D. A. Foucher, C. H. Honeyman, J. M. Nelson, B. Z. Tang, I. Manners, *Angew. Chem. Int. Ed*. **32,** 1709 (1993).
80. D. A. Foucher, R.. Ziembinski, B. Z. Tang, P. M. Macdonald, J. Massey, C. R. Jaeger, G. J. Vancso, I. Manners, *Macromolecules* **26,** 2878 (1993).
81. W. Finckh, B. Z. Tang, D. A. Foucher, D. B. Zamble, R. Ziembinski, A. Lough, I. Manners, *Organometallics* **12,** 823 (1993).
82. J. Rasburn, F. Seker, K. Kulbaba, P. G. Klein, I. Manners, G. J. Vancso, P. M. Macdonald, *Macromolecules* **34,** 2884 (2001).
83. R. G. H. Lammertink, M. A. Hempenius, G. J. Vancso, K. Shin, M. H. Rafailovich, J. Sokolov, *Macromolecules* **34,** 942 (2001).
84. M. A. Hempenius, G. J. Vancso, *Macromolecules* **35,** 2445 (2002).
85. P. Nguyen, P. Gomez-Elipe, I. Manners, *Chem. Rev*. **99,** 1515 (1999).
86. I. Manners, *Angew. Chem. Int. Ed*. **35,** 1603 (1996).
87. I. Manners, *Adv. Organomet. Chem*. **37,** 131 (1995).
88. Q. Sun, J. W. Y. Lam, K. Xu, H. Xu, J. A. P. Cha, P. C. L. Wong, G. Wen, X. Zhang, X. Jing, F. Wang, B. Z. Tang, *Chem. Mater.* **12,** 2617 (2000).
89. Q. Sun, K. Xu, J. W. Y. Lam, J. A. P. Cha, X. Zhang, B. Z. Tang, *Mater. Sci. Eng. C* **16,** 107 (2001).
90. B. Z. Tang, Q. Sun, K. Xu, H. Peng, J. W. Y. Lam, J. A. K. Cha, J. Luo, X. Zhang, U.S. Patent 10,106,752 (2002).
91. Q. Sun, B. Z. Tang, *Polym. Prepr*. **40**(2), 657 (1999).
92. Q. Sun, B. Z. Tang, *Polym. Mater. Sci. Eng.* **82,** 105 (2000).
93. Q. Sun, W. G. Wen, X. Zhang, B. Z. Tang, *Polym. Mater. Sci. Eng.* **82,** 107 (2000).
94. Q. Sun, B. Z. Tang, *Polym. Mater. Sci. Eng.* **82,** 109 (2000).
95. Q. Sun, K. Xu, H. Peng, B. Z. Tang, *Polym. Mater. Sci. Eng.* **86,** 89 (2002).
96. K. Xu, H. Peng, Q. Sun, Y. Dong, F. Salhi, J. Luo, J. Chen, Y. Huang, D. Zhang, Z. Xu, B. Z. Tang, *Macromolecules* **35,** 5821 (2002).
97. H. Peng, L. Cheng, J. Luo, K. Xu, Q. Sun, Y. Dong, F. Salhi, P. P. S. Lee, J. Chen, B. Z. Tang, *Macromolecules* **35,** 5349 (2002).

98. K. Xu, B. Z. Tang, *Chin. J. Polym. Sci.* **17,** 397 (1999); B. Z. Tang, *Polym. Prepr.* **43** (1), 48 (2002).
99. B. Z. Tang, *Polym. Prepr.* **43**(1), 48 (2002).
100. H. Peng, J. Luo, L. Cheng, J. W. Y. Lam, K. Xu, Y. Dong, D, Zhang, Y. Huang, Z. Xu, B. Z. Tang, *Opt. Mater.* **21,** 315 (2002).
101. J. W. Y. Lam., J. Luo, H. Peng, Z. Xie, K. Xu, Y. Dong, L. Cheng, C. Qiu, H. S. Kwok, B. Z. Tang, *Chin. J. Polym. Sci.* **19,** 585 (2001).
102. B. Z. Tang, K. Xu, H. Peng, Q. Sun, J. Luo, U.S. Patent 10,109,316 (2002).
103. J. L. Reddinger, J. R. Reynolds, *Adv. Polym. Sci*. **145,** 57 (1999).
104. J. L. Segura, *Acta Polym*. **49,** 319 (1998).
105. F. E. Goodson, T. I. Wallow, B. M. Novak, *Macromolecules* **31,** 2047 (1998).
106. U. Scherf, K. Mullen, *ACS Symp. Ser.* **672,** 358 (1997).
107. R. M. Tarkka, X. L. Chen, S. A. Jenekhe, *ACS Symp.* **672,** 475 (1997).
108. S. J. Higgins, *Chem. Soc. Rev*. **26,** 247 (1997).
109. H. Nishide, *ACS Symp.* **644,** 247 (1996).
110. A. D. Schluter, G. Wegner, *Acta Polym*. **44,** 59 (1993).
111. J. Roncali, *Chem. Rev*. **92,** 711 (1992).
112. J. M. G. Cowie, *Polymers: Chemistry & Physics of Modern Materials,* 2nd ed., Blackie Academic and Professional, London, 1991, Chap. 16, pp. 362–398.
113. X. Kong, J. W. Y. Lam, B. Z. Tang, *Macromolecules* **32,** 1722 (1999).
114. X. Kong, B. Z. Tang, *Chem. Mater.* **10,** 3352 (1998).
115. B. Z. Tang, X. Kong, X. Wan, H. Peng, J. W. Y. Lam, X. Feng, H. S. Kwok, *Macromolecules* **31,** 2419 (1998).
116. B. Z. Tang, X. Kong, X.-D. Feng, *Chin. J. Polym. Sci.* **17,** 289 (1999).
117. X. Kong, X. Wan, H. S. Kwok, X.-D. Feng, B. Z. Tang, *Chin. J. Polym. Sci.* **16,** 185 (1998).
118. S. M. Grayson, J. M. J. Frechet, *Macromolecules* **34,** 6542 (2001).
119. Z. Muchtar, M. Schappacher, A. Deffieux, *Macromolecules* **34,** 7595 (2001).
120. K. E. Uhrich, C. J. Hawker, J. M. J. Frechet, S. R. Turner, *Macromolecules* **25,** 4583 (1992).
121. R. M. Silverstern, F. X. Webster, *Spectrometric Identification of Organic Compounds,* 6th ed., Wiley, 1998, Chap. 3, pp. 71–143.
122. E. Pretsch, P. Buhlmann, C. Affolter, *Structure Determination of Organic Compounds: Table of Spectral Data,* 3rd ed., Springer, Hong Kong, 2000, Chap. 6, pp. 243–312.
123. J. B. Lambert, H. F. Shurvell, D. A. Lightner, R. G. Cooks, *Organic Structural Spectroscopy,* Prentice-Hall, Englewood Cliffs, NJ, 1998, Part II, pp. 152–251.
124. C. Konstantinovic, S. Simova, A. Rufinska, Z. Ratkovic, J. Predojevic, A. Rufinska, S. Gojkovic, *Ind. J. Chem. B* **35,** 960 (1996).
125. S. Aihara, N. Kamata, M. Umeda, S. I. Kanezaki, K. Nagumo, D. Terunuma, K. Yamada, *Opt. Rev.* **6,** 393 (1999).
126. N. Matsumoto, *Jpn. J. Appl. Phys*. **37,** 5425 (1998).
127. M. G. Steinmetz, *Chem. Rev*. **95,** 1527 (1995).
128. H. Chen, J. W. Y. Lam, J. Luo, Y. Ho, B. Z. Tang, D. Zhu, M. Wong, H. S. Kwok, *Appl. Phys. Lett.* **81,** 574 (2002).
129. J. Luo, Z. Xie, J. W. Y. Lam, L. Cheng, H. Chen, C. Qiu, H. S. Kwok, X. Zhan, Y. Liu, D. Zhu, B. Z. Tang, *Chem. Commun.* 1740 (2001).
130. B. Z. Tang, X. Zhan, G. Yu, P. P. S. Lee, Y. Liu, D. Zhu, *J. Mater. Chem.* **11,** 2874 (2001).
131. Y. Huang, C. Law, W. Ge, J. W. Y. Lam, B. Z. Tang, *J. Lumin*. **99,** 161 (2002).
132. J. W. Y. Lam; J. Luo, H. Peng, Z. Xie, K. Xu, Y. Dong, L. Cheng, C. Qiu, H. S. Kwok, B. Z. Tang, *Chin. J. Polym. Sci*. **19,** 585 (2001).
133. Y. Huang, W. Ge, J. W. Y. Lam, K. K. L. Cheuk, B. Z. Tang, *Mater. Sci. Eng. B* **85,** 242 (2001).

134. Y. Huang, W. Ge, J. W. Y. Lam, K. K. L. Cheuk, B. Z. Tang, *Mater. Sci. Eng. B* **85,** 122 (2001).
135. Y. Huang, W. Ge, J. W. Y. Lam, K. K. L. Cheuk, B. Z. Tang, *Mater. Sci. Eng. B* **85,** 118 (2001).
136. P. P. S. Lee, Y. Geng, H. S. Kwok, B. Z. Tang, *Thin Solid Films* **363,** 149 (2000).
137. Y. Huang, J. W. Y. Lam, K. K. L. Cheuk, W. Ge, B. Z. Tang, *Thin Solid Films* **363,** 146 (2000).
138. H. Xu, Q. Sun, P. P. S. Lee, H. S. Kwok, B. Z. Tang, *Thin Solid Films* **363,** 143 (2000).
139. R. H. Friend, R. W. Gymer, A. B. Holmes, J. H. Burroughes, R. N. Marks, C. Taliani, D. D. C. Bradley, D. A. Dos Santos, J. L. Bredas, M. Logdlund, W. R. Salaneck, *Nature* **397,** 121 (1999).
140. X. C. Li, S. C. Moratti, in *Photonic Polymer Systems,* D. L. Wise, G. E. Wnek, D. J. Trantolo, T. M. Cooper, Gresser, eds., Marcel Dekker, Hong Kong, 1998, pp. 335–371.
141. C. Pugh, A. L. Kiste, *Prog. Polym. Sci*. **22,** 601 (1997).
142. A. Shiota, C. K. Ober, *Prog. Polym. Sci*. **22,** 975 (1997).
143. V. Percec, D. Tomazos, *Adv. Mater*. **4,** 548 (1992).
144. W. H. Daly, I. I. Negulescu, P. S. Russo, D. S. Poche, *ACS Symp. Ser.* **493,** 292 (1992).
145. J. Rasburn, R. Petersen, T. Jahr, R. Rulkens, I. Manners, G. J. Vancso, *Chem. Mater*. **7,** 871 (1995).
146. B. Z. Tang, Y. Geng, J. W. Y. Lam, B. Li, X. Jing, X. Wang, F. Wang, A. B. Pakhomov, X. X. Zhang, *Chem. Mater.* **11,** 1581 (1999).
147. M. Ginzburg, M. J. MacLachlan, S. M. Yang, N. Coombs, T. W. Coyle, N. P. Raju, J. E. Greedan, R. H. Herber, G. A. Ozin, I. Manners, *J. Am. Chem. Soc*. **124,** 2625 (2002).
148. J. A. Massey, M. A. Winnik, I. Manners, V. Z. H. Chan, J. M. Ostermann, R. Enchelmaier, J. P. Spatz, M. Moller, *J. Am. Chem. Soc*. **123,** 3147 (2001).
149. M. J. MacLachlan, M. Ginzburg, N. Coombs, N. P. Raju, J. E. Greedan, G. A. Ozin, I. Manners, *J. Am. Chem. Soc*. **122,** 3878 (2000).
150. M. J. MacLachlan, M. Ginzburg, N. Coombs, T. W Coyle, N. P. Raju, J. E. Greedan, G. A. Ozin, I. Manners, *Science* **287,** 1460 (2000).
151. R. M. Crooks, M. Q. Zhao, L. Sun, V. Chechik, L. K. Yeung, *Acc. Chem. Res*. **34,** 181 (2001).
152. R. M. Penner, *Acc. Chem. Res*. **33,** 78 (2000).
153. C. N. R. Rao, G. U. Kulkarni, P. J. Thomas, P. P. Edwards, *Chem. Soc. Rev*. **29,** 27 (2000).
154. M. Joseyacaman, M. Avalosborja, *Cat. Rev*. **34,** 55 (1992).
155. J. Chastain, *Handbook of X-ray Photoelectron Spectroscopy: A Reference Book of Standard Spectra for Identification and Interpretation of XPS Data,* Physical Electronics Division, Perkin-Elmer Corp., Eden Prairie, MN, 1992.
156. D. Briggs, M. P. Seah, *Practical Surface Analysis,* Wiley, Chichester, UK, 1990.
157. V. I. Nefedov, *X-Ray Photoelectron Spectroscopy of Solid Surfaces,* VSP, Utrecht, The Netherlands, 1988.
158. K. -K. Hellwege, A. M. Hellwege, *Landolt-Börnstern: Numerical Data and Functional Relationships in Science and Technology,* Springer-Verlag, New York, 1970, New Series, Group III, Vol. 4, Part a, Fig. 59.
159. X. H. Yan, G. J. Liu, F. T. Liu, B. Z. Tang, H. Peng, A. B. Pakhomov, C. Y. Wong, *Angew. Chem. Int. Ed.* **40,** 3593 (2001).
160. D. Lopez, I. Cendoya, C. Mijangos, A. Julia, R. F. Ziolo, J. Tejada, *Macromol. Symp*. **166,** 173 (2001).
161. G. J. Liu, J. F. Ding, T. Hashimoto, K. Kimishima, F. M. Winnik, S. Nigam, *Chem. Mater*. **11,** 2233 (1999).
162. F. M. Winnik, A. Morneau, A. M. Mika, R. F. Childs, A. Roig, E. Molins, R. F. Ziolo, *Can. J. Chem*. **76,** 10 (1998).
163. L. Zhang, G. C. Papaefthymiou, J. Y. Ying, *J. Appl. Phys.* **81,** 6892 (1997).
164. L. Zhang, G. C. Papaefthymiou, R. F. Ziolo, J. Y. Ying, *Nanostruct. Mater.* **9,** 185 (1997).
165. A. Douy, *Int. J. Inorg. Mater*. **3,** 699 (2001).
166. P. F. W. Simon, R. Ulrich, H. W. Spiess, U. Wiesner, *Chem. Mater.* **13,** 3464 (2001).
167. J. M. Nedeljkovic, *Mater. Sci. Forum* **352,** 79 (2000).

168. E. Kroke, Y. L. Li, C. Konetschny, E. Lecomte, C. Fasel, R. Riedel, *Mater. Sci. Eng. R* **26,** 97 (2000)
169. M. Breulmann, S. A. Davis, S. Mann, H. P. Hentze, M. Antonietti, *Adv. Mater*. **12,** 502 (2000).
170. D. Vollath, D. V. Szabo, J. Fuchs, *Nanostruct. Mater*. **12,** 433 (1999).
171. C. Suryanarayana, *Int*. *Mater*. *Rev*. **40,** 41 (1995).
172. I. Safarik, M. Safarikova, *Monatsh. Chem*. **133,** 737 (2002).
173. J. J. Schneider, N. Czap, J. Hagen, J. Engstler, J. Ensling, P. Gutlich, U. Reinoehl, H. Bertagnolli, F. Luis, L. J. Jongh, M. Wark, G. Grubert, G. L. Hornyak, R. Zanoni, *Chem. Eur. J.* **6,** 4305 (2000).
174. S. A. Majetich, Y. Jin, *Science* **284,** 470 (1999).
175. J. Shi, S. Gider, K. Babcock, D. D. Awschalom, *Science* **271,** 937 (1996).
176. K. L Taft, G. C. Papaefthymiou, S. J. Lippard, *Science* **259,** 1302 (1993).
177. *Power Electronics in Transportation; Power,* Electronics Society, Piscataway, NJ, 1998.
178. C.-W. Chen, *Magnetism and Metallurgy of Soft Magnetic Materials,* Dover, New York, 1986.
179. T. Kemeny, D. Kaptas, L. F. Kiss, J. Balogh, I. Vincze, S. Szabo, D. L. Beke, *Hyperfine Interact*. **130,** 181.
180. M. E. McHenry, M. A. Willard, D. E. Laughlin, *Prog. Mater. Sci*. **44,** 291 (1999).
181. B. Z. Tang, H. Xu, in *Physics and Chemistry of Nanostructured Materials,* S. Yang, P. Sheng, eds., Taylor & Francis, London, 2000, pp. 121–139.

CHAPTER 3

Ring-Opened Polyferrocenes: Metal-Containing Polymers for Materials Science, Self-Assembly, and Nanostructure Applications

Paul Cyr, David Rider, and Ian Manners

Department of Chemistry, University of Toronto, Toronto, Ontario, Canada

CONTENTS

Macromolecules Containing Metal and Metal-like Elements, Volume 2: Organoiron Polymers, Edited By Alaa S. Abd-El-Aziz, Charles E. Carraher, Jr., Charles U. Pittman, Jr., John E. Sheats, and Martel Zeldin
ISBN 0-471-45078-2

I. INTRODUCTION

Metal-containing polymers[1–3] exhibit rich potential, and much of the early work in the area in the 1950s and 1960s targeted polymetallocenes.[1–6] However, most of the attempted polymer syntheses utilized polycondensation reactions involving inefficient coupling methodologies or impure difunctional monomers.[1–3] In the vast majority of cases, such step-growth processes led to the generation of poorly defined, low molecular weight oligomeric materials ($M_n < \sim 3000$) of correspondingly low processability, which were often also insoluble and poorly characterized, although important recent advances have been made.[4–6]

Our group has developed ring-opening polymerization (ROP) routes to a variety of polyferrocenes since the early 1990s. Among the species studied were silicon-bridged [1]ferrocenophanes **1** ([1]silaferrocenophanes), which undergo thermal ROP at 120–150°C to afford high molecular weight ($M_n > 10^5$) polyferrocenylsilanes (PFSs) (Scheme 1).[7] A large variety of monomers **1** are readily accessible via reaction of dilithioferrocene-TMEDA adduct with the appropriate dichlorosilane $RR'SiCl_2$.

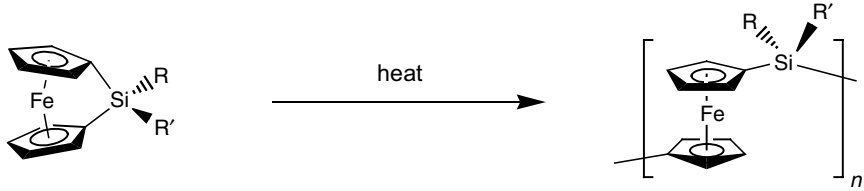

1

Scheme 1 Preparation of polyferrocenylsilanes via ROP of [1]ferrocenophanes.

Copolymerization of silicon-bridged [1]ferrocenophanes with other monomers has also been achieved, and we have expanded this ROP methodology to a range of analogous strained monomers that contain other single-atom bridges (Ge, P, Sn, S, etc.), 2-atom bridges (C–C, C–P, C–S, etc.), and transition metals (e.g., Ru, Cr) and/or different π-hydrocarbon rings (arenes).[8,9] Thus an extensive array of polyferrocene materials are accessible, opening an interesting and broad area of potential applications. This chapter surveys some of the most recent developments.

II. PROPERTIES OF POLYFERROCENYLSILANES

Polyferrocenylsilanes (PFSs) have attracted growing interest since the early 1990s.[10–18] These materials exemplify the types of polymers accessible by the use of the novel ring-opening polymerization (ROP) approach. PFS materials can be easily fabricated and processed as films, gels, and monoliths, and have even been

electrospun into nanofibers.[10] Thermotropic, liquid crystalline PFSs have also been synthesized and studied.[10,19] A *trans*-planar zigzag conformation for the protypical PFS, polyferrocenyldimethylsilane appears favored in the solid state according to studies of model oligomers, molecular mechanics calculations, and X-ray diffraction studies of crystalline films and fibers (see Fig. 1).[10,14,20]

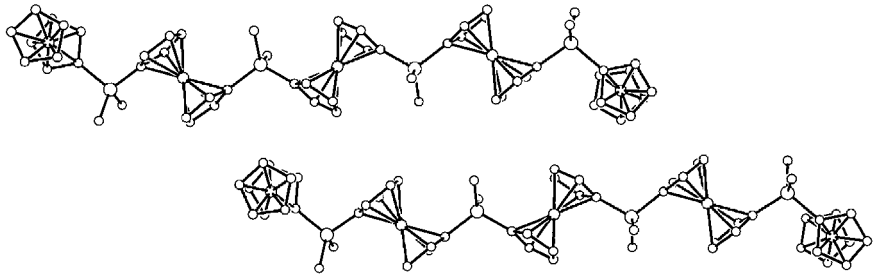

Figure 1 View of the crystal packing arrangement of the pentamer analog of polyferrocenylsimethylsilane showing one pair of molecules. The terminal ferrocenyl groups are twisted in opposite directions perpendicular to the interior, planar, all-*trans*, zigzag units.

Cyclic voltammetric studies of PFSs show clear evidence for the existence of interactions between the iron atoms.[10] Comparisons of the behavior of PFSs with other polyferrocenes indicate that the metal–metal interactions are influenced by the silicon spacer.[9,10] PFSs have been found to possess interesting hole transport properties, and partial oxidation causes up to a 10^{10} increase in electrical conductivity with values in to the semiconductor range.[10,21–23]

Controlled crosslinking of PFSs has also been achieved to yield solvent-swellable, redox-active gels.[24] The degree of crosslinking can be varied by using specific amounts of a spirocyclic [1]ferrocenophane **2** in the polymerization mixtures (see Scheme 2). On oxidation of the gels a broad absorption assigned to an intervalence (charge) transfer (IT) band is detected, consistent with the presence of hole-hopping processes.[10,24]

In collaboration with G. A. Ozin and others, we have reported the formation of shaped, magnetic ceramics (including films) from the pyrolysis of highly crosslinked PFS networks.[11] The magnetic properties arise from the presence of iron nanoparticles (Fe_n) formed within the ceramic matrix. Their size is dependent on the pyrolysis temperature, which allows the magnetic properties to be controlled. Magnetization measurements for ceramics formed at 650 and 850°C show evidence for smaller, superparamagnetic Fe_n clusters, while at higher temperatures (1000°C) the size of the Fe_n clusters is large enough to display ferromagnetic behavior. Ordered micrometer-scale patterns of the magnetic ceramic can also be fashioned by the pyrolysis of the patterned crosslinked PFS precursors created using soft lithography techniques (see Fig. 2).[25]

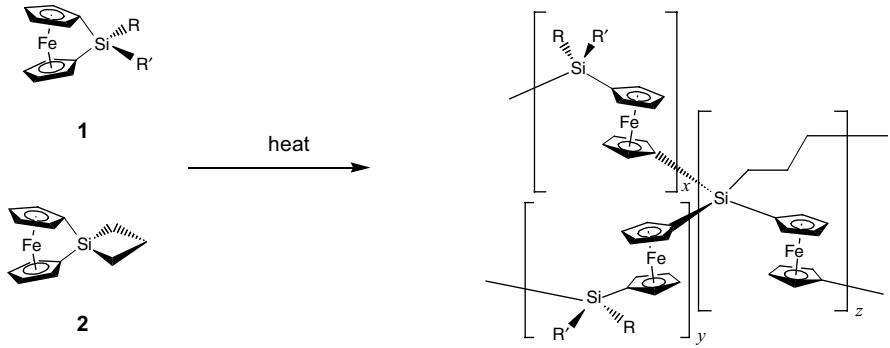

Scheme 2 Preparation of crosslinked PFSs.

PFSs have been synthesized in the form of microspheres by the use of a precipitation polymerization methodology developed by Stöver.[12,26] Chemical oxidation of the microspheres with iodine leads to positively charged particles, which then can electrostatically self-assemble into superstructures with smaller, negatively charged silica particles (see Fig. 3a). The crosslinked PFS microspheres act as precursors to spherical magnetic ceramic particles on pyrolysis. As a result of their magnetic properties, assembly into well-ordered 1D and 2D arrays by interaction with an applied magnetic field is possible (Fig. 3b).[12,26] PFSs can also be formed via ROP within the 3-nm channels of mesoporous silica (MCM-41). As a result of the constrained environment, subsequent pyrolysis yields nanostructured magnetic ceramic composite materials with smaller Fe_n nanoparticles compared to those obtained from pyrolysis of the bulk polymeric material.[10,25]

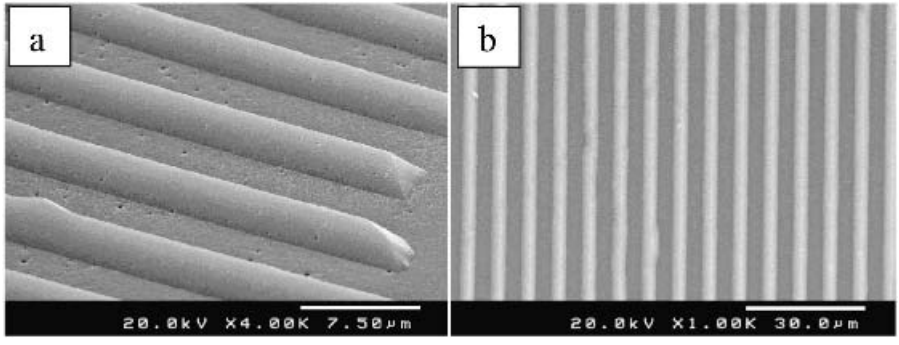

Figure 2 SEM micrographs showing (a) surface relief pattern and (b) top view of ceramic film obtained by micromolding spirocyclic [1]ferrocenophane **2** into anisotropically etched channels housed inside silicon wafers (periodic spacing is ~8 µm), crosslinking via thermal ROP and pyrolyzing at 600°C under N_2. (Adapted from Ref. 25.)

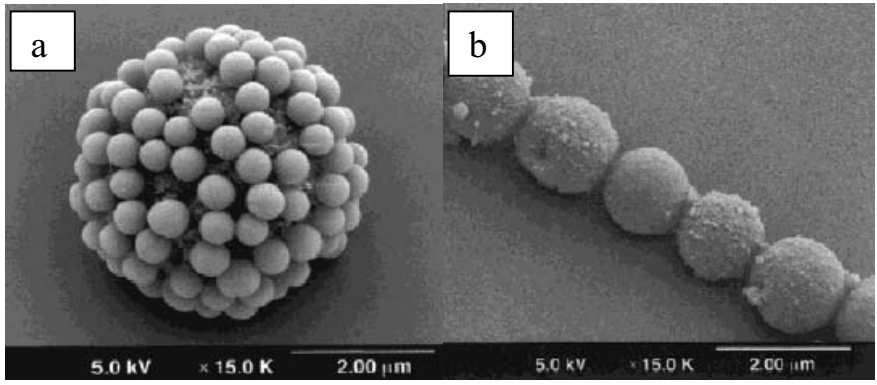

Figure 3 SEM micrographs of (a) negatively charged silica microspheres electrostatically bound to the surface of oxidized polyferrocenylsilane microspheres and (b) aligned strand of spherical magnetic ceramic particles obtained from pyrolysis of polyferrocenylsilane microspheres at 900°C displaying magnetic ordering in an external magnetic field. (Adapted from Ref. 26.)

Thin films of PFS homopolymers have also attracted attention as potential protective charge dissipation coatings for dielectrics, as electrochromic materials, as sensors, and as electrode mediators.[10] In addition, the relatively high refractive indices of PFS derivatives make these materials of interest for applications in photonics—for example, in photonic crystals where periodic variations in refractive index are necessary.[27]

Although much less studied than PFSs, significant information has been gathered on other ring-opened polyferrocene systems.[8] For example, polyferrocenylgermanes appear to possess properties that are generally similar to those of their silicon analogs. However, polyferrocenylethylenes with a CH_2–CH_2 spacer (and other polymers derived from the ROP of [2]ferrocenophanes) possess much weaker metal–metal interactions than for PFSs, whereas for polyferrocenylsulfides the interaction is stronger.[8,9] Polyferrocenylphosphines offer additional possibilities as facile coordination of transition metals to phosphorus is possible.[8]

III. WATER-SOLUBLE PFS DERIVATIVES FOR LAYER-BY-LAYER SELF-ASSEMBLY APPLICATIONS

Water-soluble polymers are of great industrial and commercial importance. While water-soluble organic polymers have been widely studied, their inorganic counterparts have been largely left unexplored. Modification of the polymer side groups at silicon has been shown to allow access to water-soluble PFSs.[28] For

example, ROP of **1a** (R=Me, R=Cl) to give poly(ferrocenylchloromethylsilane) (**3**), followed by substitution of the Si–Cl bonds with functionalized alcohols permits access to hydrophilic and water-soluble PFSs.[28]

Convenient and general routes have been established for the preparation of a range of water-soluble PFS polyelectrolytes from the substitutionally labile silicon-bridged [1]ferrocenophane fcSiMeCl (**1a**) (fc=$Fe(\eta^5\text{-}C_5H_4)_2$) and polymer **3** via reaction of the Si–Cl bonds with lithium reagents.[29,30] Scheme 3 highlights the preparation of both cationic and anionic water-soluble PFSs.[30] For example, reaction of **3** with the amino-protected, propargyl lithium salt $Li(C{\equiv}CCH_2NR_2)$ [$R_2=(SiMe_2CH_2)_2$] yields $[fcSiMeC{\equiv}CCH_2N(SiMe_2CH_2)_2]_n$ (**4**). Deprotection of **4** is readily achieved using THF/MeOH, to yield the aminopropynyl-functionalized polymer $[fcSiMe(C{\equiv}CCH_2NH_2)]_n$ (**5**), which is then conveniently reduced with hydrazine in THF to the analogous aminopropyl polymer $[fcSiMe(CH_2CH_2CH_2NH_2)]_n$ (**6**). Treatment of PFSs **5** and **6** with HCl generates the water-soluble cationic polyelectrolytes $[fcSiMe(C{\equiv}CCH_2NH_3Cl)]_n$ (**7**) and $[fcSiMe(CH_2CH_2CH_2NH_3Cl)]_n$ (**8**), respectively. Treatment of polymer **4** with 1,3-propanesultone affords the anionic polyelectrolyte $[fcSiMe\{C{\equiv}CCH_2N(CH_2CH_2CH_2SO_3Na)_2\}]_n$ (**9**) and reduction of the propynyl unit with hydrazine gives $[fcSiMe\{CH_2CH_2CH_2N(CH_2CH_2CH_2SO_3Na)_2\}]_n$ (**10**). The PFS polyelectrolytes **7–10** are readily soluble in water, making them potentially useful materials for a range of applications.

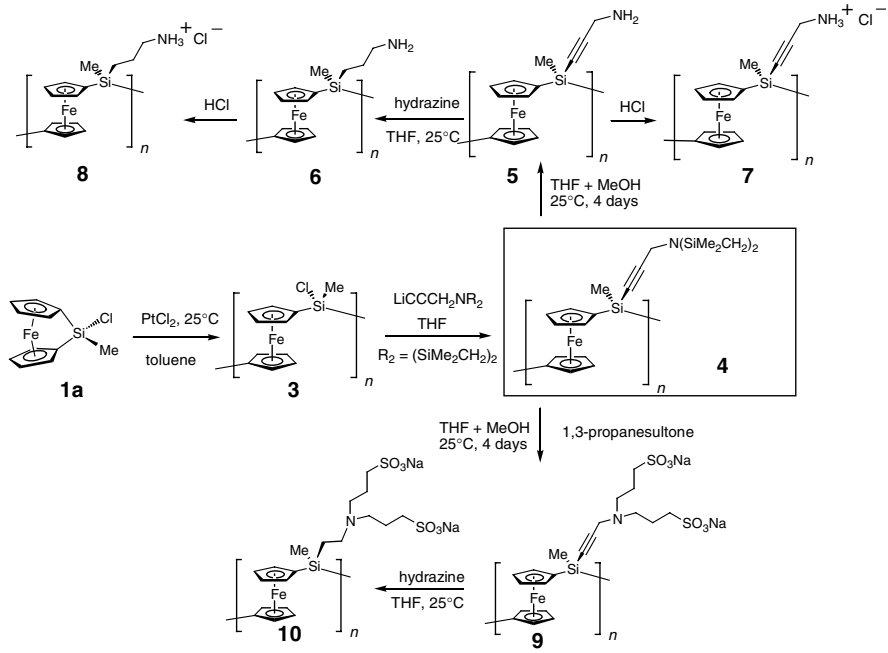

Scheme 3 Synthetic routes to anionic and cationic PFS polyelectrolytes.

These water-soluble PFS derivatives are of potential interest as electrode materials and as redox-active polymeric electrolytes for which the ionic conductivity might be tuned by oxidation of the iron centers. These materials may also prove useful as exploratory redox-controlled drug delivery agents as various water-soluble ferrocenium salts have been shown to display anticancer activity.

Another interesting application of these materials is as electrostatic superlattices formed via layer-by-layer (LbL) self-assembly. The technique involves the sequential adsorption of polyion monolayers from aqueous solution to form nanostructured multilayer polymer films of controlled thickness. Such film architectures can be manipulated to achieve unique and tunable physical properties, and can be used for the construction of a range of devices. In collaboration with Ozin, we have studied well-characterized organic–organometallic[31] and also all-organometallic[32] polymer electrostatic superlattices formed from PFS derivatives.[33] Alternate adsorption of the anionic polystyrenesulfonate (PSS) and the cationic water-soluble $[fcSiMe(C_6H_5NMe_3^+)]_n$ (**11**) were deposited on Si and Au substrates chemically modified with (3-aminopropyl)trimethoxysilane (AMPS) and 2-aminoethanethiol (AET), respectively (Fig. 4a). The wettability of the surface of the film was shown to be dependent on the outermost layer of the multilayer assembly as shown by the advancing contact angle measurements (Fig. 4b).[31] These LbL self-assembled PFS multilayers may be directly visualized via TEM techniques, allowing a useful way to monitor the growth of the superlattices (Fig. 5a).[32] Self-assembly of the multilayers can also be performed on curved surfaces. For example, LbL of PFS polyelectrolytes of opposite charge on silica nanospheres followed by etching of the inorganic core with HF yields hollow PFS spheres (Fig. 5b).

Future work on these composite superlattices will focus on patterning applications (e.g., using microcontact printing) and the generation of magnetic and redox-tunable multilayers that take advantage of the unique features of polyferrocenylsilanes.

IV. METAL-CONTAINING BLOCK COPOLYMERS: FORMATION OF SELF-ASSEMBLED, SUPRAMOLECULAR MATERIALS AND NANOSCOPIC CERAMIC PATTERNS

Thermal ROP of metallocenophanes leads to virtually no control over molecular weight and the molecular weight distribution is broad (PDI = ~1.5–2.5). Subsequently, living anionic and transition metal catalyzed ROP routes to polymetallocenes have been developed.[10,34–36] These have permitted unprecedented control of mainchain metal-containing polymer architectures. In particular, the access provided to the first block copolymers with metals in the mainchain has created unique opportunities for the generation of self-assembled, supramolecular materials.

Living anionic ROP of silicon-bridged [1]ferrocenophanes was reported by our group in 1994 and occurs at ambient or subambient temperatures using initiators such as *n*-BuLi or PhLi.[35] This has permitted the synthesis of PFSs with controlled molecular

weights and narrow molecular weight distributions, and has also allowed the preparation of end-functionalized polymers and block copolymers.[36] The prototypical PFS block copolymers contained inorganic [polydimethylsiloxane (PDMS)] and organic [polystyrene (PS)] coblocks, respectively.[36] The living anionic ROP of phosphorus-bridged [1]ferrocenophanes is also possible.[37] A range of diblock, triblock, and even pentablock materials with crystalline or amorphous polyferrocene blocks and a variety of different inorganic and organic coblocks are now available (Scheme 4).[36]

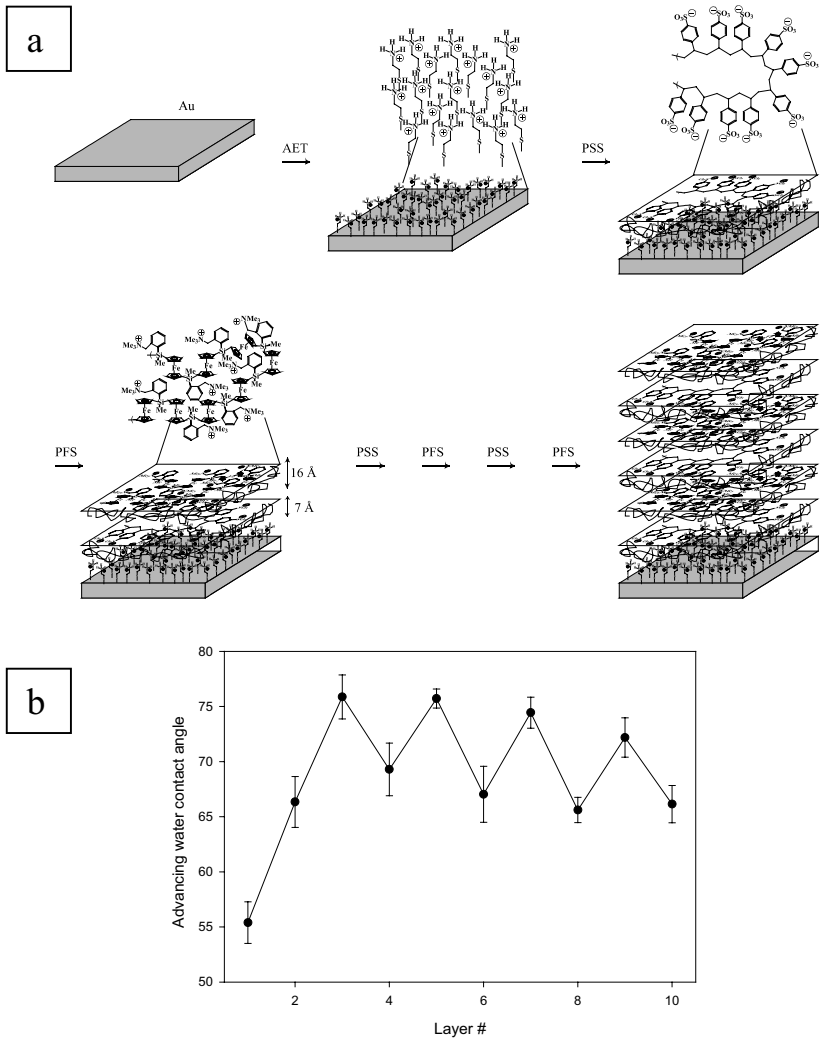

Figure 4 (a) Schematic representation of sequential polymer electrolyte adsorption for growing anionic polystyrenesulfonate–cationic water-soluble polyferrocenylsilane organic–organometallic multilayer thin films. (b) Advancing water contact angle on PSS (odd-numbered layers) and PFS **11** (even-numbered layers)-terminated multilayer films grown on Au substrates. (Adapted from Ref. 31.)

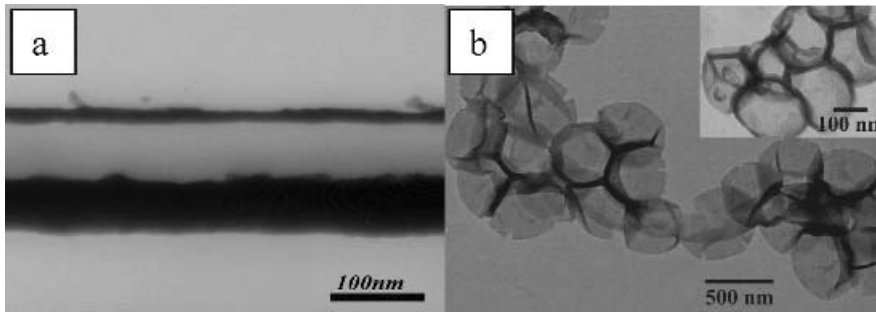

Figure 5 (a) TEM image of a cross section of 30 bilayers of positively charged PFS/negatively charged PSS deposited on a gold surface chemically modified with AET (adapted from Ref. 32). (b) SEM image of hollow spheres of 5 bilayers of positively charged PFS/negatively charged PSS obtained from templating on ~500-nm silica spheres followed by etching with HF.

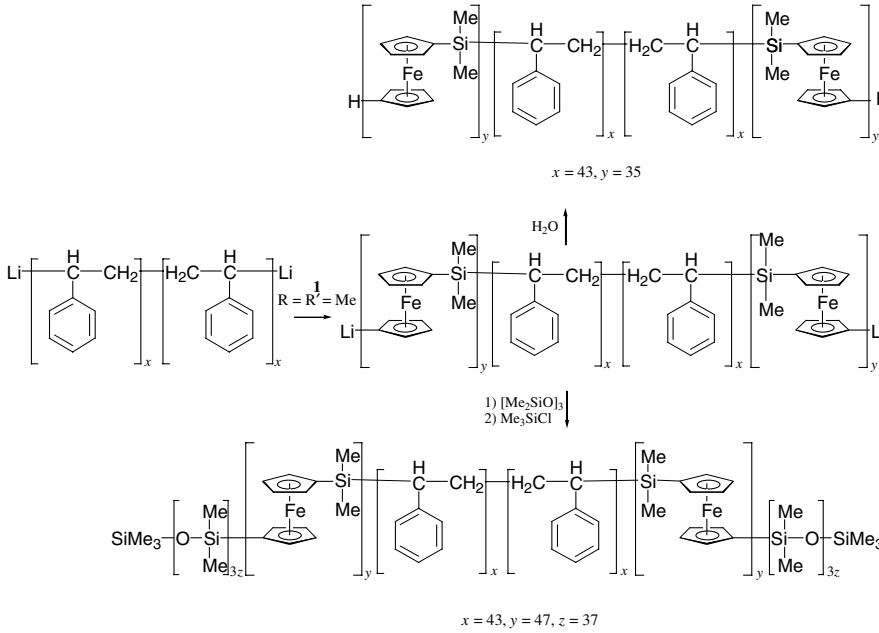

Scheme 4 Synthesis of PFS block copolymers via anionic polymerization.

Transition-metal-catalyzed ROP of silicon-bridged [1]ferrocenophanes was reported in 1995 and occurs in solution at room temperature in the presence of Pt^{II}, Pt^{0}, Rh^{I}, and Pd^{II} precatalysts. Transition-metal-catalyzed ROP is a mild method that does not require monomer with an exceptional degree of purity and has now been developed to the stage where considerable control over polymetallocene architectures is possible.[34]

On the basis of the behavior of all-organic analogs, polyferrocene block copolymers would be expected to self-assemble to form supramolecular

organometallic micellar aggregates in solvents selective for one of the blocks. In collaboration with the group of M. A. Winnik at Toronto we have shown that many polyferrocene block copolymers form spherical micelles with a polyferrocene core in nonsolvents for the organometallic block. In these cases, the PFS or PFP block present was amorphous. However, using crystallizable PFS blocks we found that well-defined cylindrical micellar structures can be generated. For example, the solution aggregation of PFS-*b*-PDMS block copolymers with a polyferrocenyldimethylsilane block in *n*-hexane as a PDMS-selective solvent yielded novel wormlike micelles (PFS–PDMS ratio 1–6).[38,39]

These structures maintain their integrity in the solid state and the structures are unchanged in size after heating in aliphatic hydrocarbon solvents to 80°C. In contrast, when micelles are formed above the T_m (melting point) of the polyferrocenyldimethylsilane block (~120–145°C), spherical aggregates are formed, suggesting that the crystallization of the core polymer is the key driving force for the formation of cylindrical structures below T_m.[40] The preference for the polyferrocenyldimethylsilane blocks to pack parallel to one another in the core, as appears to be the case in samples of the homopolymer, presumably results in a strong preference for the formation of a lower curvature cylindrical structure.[40] Block copolymers with crystallizable polyferrocenyldimethylsilane segments and polyisoprene (PI) coblocks similarly form cylindrical micelles with a PFS core in *n*-hexane.[41] Water-soluble PFS diblock copolymers with polyaminomethacrylate coblocks behave similarly.[42]

The self-assembled cylinders formed in *n*-hexane consist of a wirelike core of PFS surrounded by an insulating sheath or corona of polydimethylsiloxane or polyisoprene and are candidates for the formation of semiconducting nanowires. Furthermore, these well-defined aggregates may be of use as etching resists for semiconducting substrates such as GaAs or Si, and offer potential access to magnetic or semiconducting nanoscopic patterns on various substrates. As the accessibility of smaller and smaller length scales by lithographic techniques becomes more difficult, the use of such methods clearly becomes of interest. In collaboration with J. Spatz and M. Möller of the University of Ulm, Germany, the cylindrical block copolymer structures have been positioned on the surface of a GaAs resist by capillary forces along grooves that were previously formed from electron-beam etching of the surface.[43] Connected ceramic lines of reduced size were generated by subsequent reactive ion etching with hydrogen plasma (see Fig. 6). Such an approach allows the formation of nanolines that have widths as low as ~8–10 nm if easily etched organic coronas are present (e.g., PI) and lengths can reach >500 nm through a combined "top–down/bottom–up" approach. Current work focuses on detailed characterization of the nanoscopic lines and compositional tuning of their conductive and magnetic properties.

Self-assembling polyferrocene triblock copolymers are also accessible via living anionic or transition metal-catalyzed ROP.[34,44] We have reported studies of the self-assembly of PFS-*b*-PDMS-*b*-PFS triblock copolymers. If crystallizable PFS blocks are present, remarkable flowerlike architectures form on self-assembly in *n*-hexane as the PDMS-selective solvent with cylindrical micelles as a major component.[44] In contrast, analogs with amorphous PFS blocks form spherical micelles. In the former case it also appears that crystallization directs the self-assembly process and the ability of the

triblock copolymer to function as a tie molecule between individual micelles is critical to the hierarchical assembly to yield the flowerlike superstructures.[44]

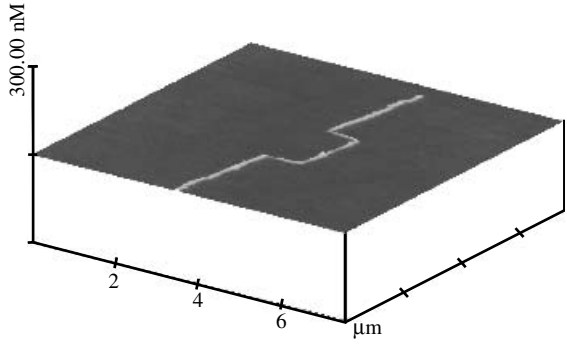

Figure 6 Scanning Force Microscopic (SFM) image of PFS-*b*-PDMS diblock copolymer cylinders deposited along a prepatterned groove on a resist film, followed by liftoff with acetone followed by hydrogen plasma treatment; the aligned nanoscopic line, height 4 nm, is composed of clusters of Fe, Si, O, and C (adapted from Ref. 43).

Polyferrocene block copolymers also phase separate in the solid state to generate periodic, nanoscopic metal-rich domains that can be observed by TEM without resorting to staining techniques (see Fig. 7a).[36,38] Pyrolysis methods can also be used to surface pattern substrates with magnetic nanostructures (see Fig. 7b),[45] and others[17] have shown that selective etching with plasmas yields ceramic patterns.

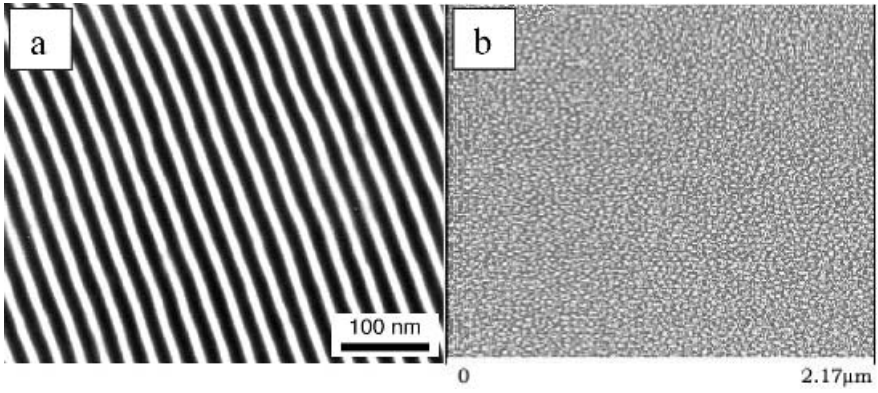

Figure 7 (a) TEM of films of PS-*b*-PFS (block ratio ~1–1) after annealing at 180°C showing lamellar ordering (interdomain spacing 310 Å). The white regions are PS domains while the darker regions are PFS domains. (Adapted from Ref. 38.) (b) AFM image of pyrolyzed sample at 600°C for 2 h under N_2, of a PS_{374}-*b*-PFS_{45} thin film (25 nm) in which the PS matrix had been crosslinked by UV radiation. The dot size is ~20–25 nm (Adapted from Ref. 45).

V. SUMMARY

ROP of silicon-bridged [1]ferrocenophanes has permitted access to polyferrocenylsilane homopolymers, a readily available class of processable metal-containing polymers with a range of interesting physical properties. Living anionic and transition-metal-catalyzed ROP have allowed the preparation of materials with controlled molecular weights and architectures, such as block copolymers. In this chapter examples of work by ourselves and our collaborators illustrate the interesting potential of these polymers in materials science, self-assembly, and nanoscience. With the immense structural diversity and range of properties made possible by the presence of transition elements, these results strongly suggest that supramolecular chemistry of metal-containing polymers is likely to be a broad and expanding area of future research.[3]

VI. ACKNOWLEDGMENTS

We would like to thank the remarkably motivated and talented students who have performed most of the research described in this chapter and whose names are cited in the references. We also acknowledge the scientists with whom we have collaborated with respect to the work described, particularly Profs. Geoffrey A. Ozin and Mitchell A. Winnik of our department and Profs. Joachim P. Spatz (now at the University of Heidelburg), Thomas P. Russell (University Massachusetts) and Martin Möller at Ulm Germany. Finally, I. M. acknowledges the University of Toronto for a McLean Fellowship (1997–2003), the Ontario Government for a Premier's Research Excellence Award (PREA) (1999–2004), the Alfred P. Sloan Foundation for a Fellowship (1994–98), and the Canadian Government for a Canada Research Chair for the duration of the work described.

VII. REFERENCES

1. R. D. Archer, *Inorganic and Organometallic Polymers,* Wiley-VCH, Weinheim, 2001.
2. R. P. Kingsborough, T. M. Swager, *Prog. Inorg. Chem*. **48,** 123 (1999).
3. I. Manners, *Science* **294,** 1664 (2001); P. Nguyen, P. Gómez-Elipe, I. Manners, *Chem. Rev.* **99,** 1515 (1999).
4. H. Nishihara, *Adv. Inorg. Chem.* **53,** 41 (2002).
5. C. U. Pittmann Jr., C. E. Carraher Jr., J. R. Reynolds, in *Encyclopedia of Polymer Science and Engineering,* J. Kroschwitz, ed., Wiley, 1987, Vol. 10, p. 541.
6. R. D. A. Hudson, *J. Organomet. Chem.* **637,** 47 (2001).
7. D. A. Foucher, B. Z. Tang, I. Manners, *J. Am. Chem. Soc.* **114,** 6246 (1992).
8. I. Manners, *Can. J. Chem.* **76,** 371 (1998).
9. R. Resendes, J. M. Nelson, A. Fischer, F. Jäkle, A. J. Lough, I. Manners, *J. Am. Chem. Soc.* **123,** 2116 (2001).

10. K. Kulbaba, I. Manners, *Macromol. Rapid Commun.* **22,** 711 (2001) (review on PFSs).
11. M. J. MacLachlan, M. Ginzburg, N. Coombs, T. W. Coyle, N. P. Raju, J. E. Greedan, G. A. Ozin, I. Manners, *Science* **287,** 1460 (2000).
12. K. Kulbaba, R. Resendes, A. Cheng, A. Bartole, A. Safa-Sefat, N. Coombs, H. D. H. Stöver, J. E. Greedan, G. A. Ozin, I. Manners, *Adv. Mater.* **13,** 732 (2001).
13. N. P. Reddy, H. Yamashita, M. Tanaka, *J. Chem. Soc. Chem. Commun.* 2263 (1995).
14. S. Barlow, A. L. Rohl, S. Shi, C. M. Freeman, D. O'Hare, *J. Am. Chem. Soc.* **118,** 7578 (1996).
15. L. I. Espada, M. Shadaram, J. Robillard, K. H. Pannell, *J. Inorg. Organomet. Polym.* **10,** 169 (2000).
16. Q. Sun, J. W. Y. Lam, K. Xu, H. Xu, J. A. K. Cha, P. C. L. Wong, G. Wen, X. Zhang, X. Jing, F. Wang, B.-Z. Tang, *Chem. Mater.* **12,** 2617 (2000).
17. J. Y. Cheng, C. A. Ross, V. Z.-H. Chan, E. L. Thomas, R. G. H. Lammertink, G. J. Vancso, *Adv. Mater.* **13,** 1174 (2001).
18. M. Hmyene, A. Yasser, M. Escorne, A. Percheron-Guegan, F. Garnier, *Adv. Mater.* **6,** 564 (1994).
19. X.-H. Liu, D. W. Bruce, I. Manners, *Chem. Commun.* 289 (1997).
20. V. S. Papkov, M. V. Gerasimov, I. I. Dubovik, S. Sharma, V. V. Dementiev, K. H. Pannell, *Macromolecules* **33,** 7107 (2000).
21. R. Rulkens, R. Resendes, A. Verma, I. Manners, K. Murti, E. Fossum, P. Miller, K. Matyjaszewski, *Macromolecules* **30,** 8165 (1997).
22. L. Bakueva, E. H. Sargent, R. Resendes, A. Bartole, I. Manners, *J. Mater. Sci, Mater. Electron.* **12,** 21 (2001).
23. L. Espada, K. H. Pannell, V. Papkov, L. Leites, S. Bukalov, I. Suzdalev, M. Tanaka, T. Hayashi, *Organometallics* **21,** 3758 (2002).
24. K. Kulbaba, M. J. MacLachlan, C. E. B. Evans, I. Manners, *Macromol. Chem. Phys.* **202,** 1768 (2001).
25. M. Ginzburg, M. J. MacLachlan, S. M. Yang, N. Coombs, T. W. Coyle, N. P. Raju, J. E. Greedan, R. H. Herber, G. A. Ozin, I. Manners, *J. Am. Chem. Soc.* **124,** 2625 (2002).
26. K. Kulbaba, A. Cheng, A. Bartole, S. Greenberg, R. Resendes, N. Coombs, A. Safa-Sefat, J. E. Greedan, H. D. H. Stöver, G. A. Ozin, I. Manners, *J. Am. Chem. Soc.* **124,** 12522 (2002).
27. J. Galloro, M. Ginzburg, H. Míguez, S. M. Yang, N. Coombs, A. Safa-Sefat, J. E. Greedan, I. Manners, G. A. Ozin, *Adv. Funct. Mater.* **12,** 382 (2002).
28. K. N. Power-Billard, I. Manners, *Macromolecules* **33,** 26 (2000).
29. F. Jäkle, Z. Wang, I. Manners, *Macromol. Rapid Commun.* **21,** 1291 (2000).
30. Z. Wang, A. Lough, I. Manners, *Macromolecules* **35,** 7669 (2002).
31. M. Ginzburg, J. Galloro, F. Jäkle, K. N. Power-Billard, S. M. Yang, I. Sokolov, C. N. C. Lam, A. W. Neumann, I. Manners, G. A. Ozin, *Langmuir* **16,** 9609 (2000).
32. J. Halfyard, J. Galloro, M. Ginzburg, Z. Wang, N. Coombs, I. Manners, G. A. Ozin, *Chem. Commun.* 1746 (2002); J. Galloro, M. Ginzburg, N. Coombs, V. Kitaev, S. M. Yang, I. Manners, G. A. Ozin, unpublished results.
33. For independent work by others, see M. A. Hempenius, N. S. Robins, R. G. H. Lammertink, G. J. Vancso, *Macromol. Rapid Commun.* **22,** 30 (2001).
34. P. Gómez-Elipe, R. Resendes, P. M. Macdonald, I. Manners, *J. Am.Chem. Soc.* **120,** 8348 (1998).
35. R. Rulkens, Y. Ni, I. Manners, *J. Am. Chem. Soc.* **116,** 12121 (1994).
36. Y. Ni, R. Rulkens, I. Manners, *J. Am. Chem. Soc.* **118,** 4102 (1996).
37. T. J. Peckham, J. A. Massey, C. H. Honeyman, I. Manners, *Macromolecules* **32,** 2830 (1999).
38. J. Massey, K. N. Power, M. A. Winnik, I. Manners, *Adv. Mater.* **10,** 1559 (1998).
39. J. Massey, K. N. Power, I. Manners, M. A. Winnik, *J. Am. Chem. Soc*. **120,** 9533 (1998).
40. J. A. Massey, K. Temple, L. Cao, Y. Rharbi, J. Raez, M. A. Winnik, I. Manners, *J. Am. Chem. Soc.* **122,** 11577 (2000).

41. L. Cao, I. Manners, M. A. Winnik, *Macromolecules* **35,** 8258 (2002).

42. X. -S. Wang, M. A. Winnik, I. Manners, *Macromol. Rapid Commun*. **23,** 210 (2002).

43. J. Massey, M. A. Winnik, I. Manners, V. Z.-H. Chan, J. M. Ostermann, R. Enchelmaier, J. P. Spatz, M. Möller, *J. Am. Chem. Soc.* **123,** 3147 (2001); L. Cao, J. A. Massey, M. A. Winnik, I. Manners, S. Riethmüller, F. Banhart, J. P. Spatz, M. Möller, *Adv. Func. Mater.* **13,** 271 (2003).

44. R. Resendes, J. A. Massey, K. Temple, L. Cao, K. N. Power-Billard, M. A. Winnik, I. Manners, *Chem. Eur. J*. **7,** 2414 (2001).

45. K. Temple, K. Kulbaba, K. N. Power-Billard, I. Manners, A. Leach, T. Xu, T. P. Russell, C. J. Hawker, *Adv. Mater.* **15,** 297 (2003).

CHAPTER 4

Synthesis and Solution Self-Assembly of Polyferrocene-Based AB Diblock and ABC Triblock Copolymers

Xiao-Song Wang, Mitchell A. Winnik, and Ian Manners

Department of Chemistry, University of Toronto, Toronto, Ontario, Canada

CONTENTS

Macromolecules Containing Metal and Metal-like Elements, Volume 2: Organoiron Polymers, Edited By Alaa S. Abd-El-Aziz, Charles E. Carraher, Jr., Charles U. Pittman, Jr., John E. Sheats, and Martel Zeldin
ISBN 0-471-45078-2

I. INTRODUCTION

Self-assembly of block copolymers provides a powerful route to nanostructured materials both in solution and the solid state.[1,2] For example, the micellization of organic diblock copolymers in a selective solvent for one of the blocks is currently attracting intense attention as a route to supramolecular nanostructures.[2] The incorporation of metallic elements into block copolymers offers potential new functions as ceramic precursors and redox-active materials which should complement those available from well-studied all-organic analogs.[3]

Well-defined polyferrocene block copolymers are accessible via the living anionic ring-opening polymerization (ROP) of [1]ferrocenophanes[4] [e.g., (**1**)] and self-assembly of these materials offers potential access to supramolecular structures with redox-active, high-refractive-index contrast, and preceramic properties.[5] We previously showed that crystalline-coil poly(ferrocenyldimethylsilane-*b*-dimethylsiloxane) (PFS-*b*-PDMS) (**2**), diblock copolymers (block ratio 1–6) form cylindrical micelles with an organometallic core and a polysiloxane corona in selective solvents such as hexane for the PDMS block.[6] As PFS homopolymers become semiconducting on oxidative doping[7] and also function as high-yield precursors to ceramics,[8] these cylinders are of interest as semiconducting nanowires and as nanoscopic etching resists.[9] We previously proposed that the formation of cylindrical structures rather than the spherical micelles expected on the basis of the block asymmetry is a result of the tendency of the PFS block to crystallize which favors the formation of low-curvature structures.[10] This assertion is further supported by the self-assembly of a polyferrocenyl phenylphosphine-*b*-polyisoprene (PFP-PI) block copolymer in hexane where spheres were formed as a result of the amorphous nature of the PFP block.[11] The extension of this concept to AB amphiphilic diblock or ABC triblock copolymer systems offers further opportunities for fabrication of water-soluble supramolecular organometallic assemblies and crystallization-directed micellar morphology control.

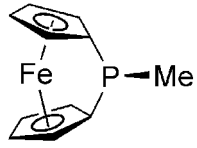

a

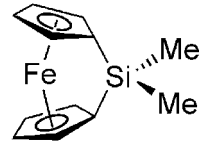

b

1

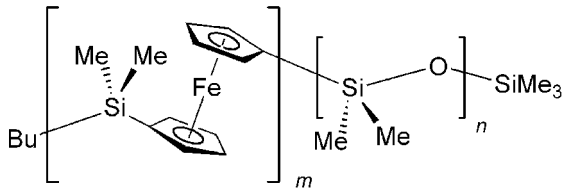

2

Herein, we discuss the synthesis of the first PFS block copolymers with a water-soluble polyacrylate coblock (**3**) by using an anionic ROP followed by anionic polymerization of dimethylethyl methacrylate,[12,13] as well as well-defined ABC triblock copolymers (**4**) conceptually derived from the PFS-*b*-PDMS system where a short, amorphous atactic polyferrocenylphenylphosphine (PFP) block is also attached to the PFS segment. The self-assembly behavior of these two types of novel block copolymers were investigated either in water or in hexane.

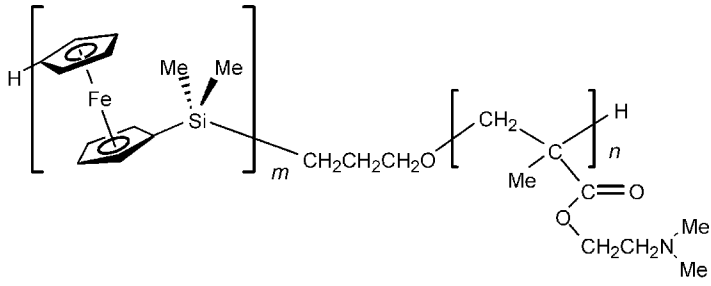

3

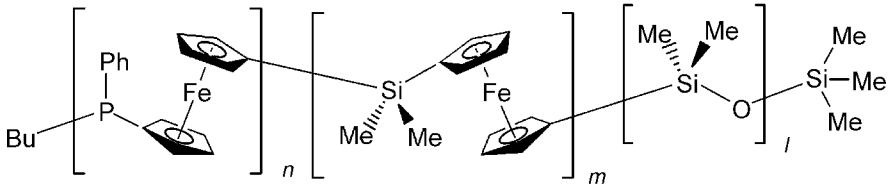

4

II. RESULTS AND DISCUSSION

A. Synthesis and Aqueous Micellization of PFS-PDMAEMA

The block copolymer polyferrocenyldimethylsilane-*b*-polydimethylaminoethyl methacrylate (PFS-*b*-PDMAEMA) was prepared by a two-step synthesis as illustrated in Scheme 1. The steps consisted of the synthesis of hydroxy terminated ferrocenyldimethylsilane (PFS-$CH_2CH_2CH_2OH$) (**5**) followed by the polymerization of DMAEMA initiated by PFS-$CH_2CH_2CH_2O^-K^+$, generated from the reaction of **5** with KH. Telechelic **5** was prepared by the (*tert*-butyldimethylsilyloxy)-1-propyl-lithium (*t*-BDMSPrLi)-initiated anionic ROP of **1** at room temperature. *t*-BDMSPrLi is well documented as a hydroxy group protected initiator for anionic polymerization[14,15] where the *t*-BDMS protecting group on the initiator is subsequently hydrolyzed to generate an −OH functionality in the presence of $[Bu_4N]F$ at room temperature over a time

period of 24 h. The molecular weight of **5** was M_n=2800 (PDI=1.1) measured by GPC with a light-scattering detector, corresponding to a degree of the polymerization (DP) of 11. The narrow polydispersity index of 1.1 is consistent with the living nature of the polymerization.

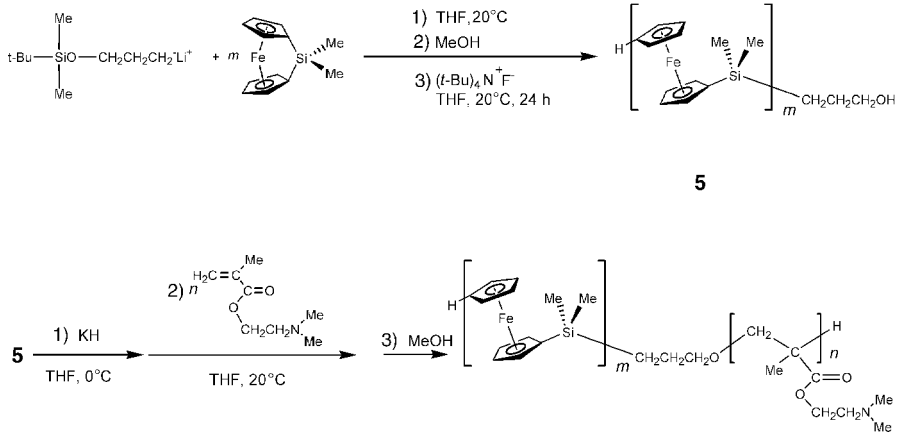

Scheme 1

Living anionic polymerization of tertiary amine methacrylates, such as 2-(diethylamino)ethyl methacrylate (DEAEMA) using potassium ethoxide as initiator in THF was first developed by Nagasaki in 1997.[12] Complexation of the potassium counterion with the nitrogen heteroatom of DEAEMA was attributed to this unexpected success. Armes and coworkers have successfully extended this polymerization technique to other tertiary amine methacrylates, such as 2-(dimethylamino) ethyl methacrylate (DMAEMA), 2-(*N*-morpholino)ethyl methacrylate (MEMA) to access a range of water-soluble block copolymers and macromonomers.[13] Reagents such as potassium naphthalide, potassium hydride (KH), or potassium methylsulfinyl carbanion ($DMSO^-K^+$) were used to convert a hydroxy end group into a potassium alkoxide to accomplish the initiation of DMAEMA polymerization. We used a slight excess of KH relative to **5** to ensure full conversion to PFS-$CH_2CH_2CH_2O^-K^+$ at 0°C. As soon as PFS-$CH_2CH_2CH_2O^-K^+$ was generated, the DMAEMA monomer was introduced to commence the 2-h room-temperature polymerization, which was finally quenched with methanol. The reaction mixture was precipitated in hexane at room temperature to isolate the amber block copolymers.

GPC characterization gave rise to a monomodal trace and a detected increase in M_n from 2800 to 11,000, suggesting a high efficiency for the crossover initiation and no contamination by either PFS or PDMAEMA. As excess KH was used, the possibility existed that PDMAEMA homopolymer might have been present in the

crude reaction mixture. No evidence of this homopolymer contamination was observed in the GPC trace, which suggests that either the contamination is minimal and can be neglected, or that the homopolymer was removed during the precipitation, since PDMAEMA homopolymer is slightly soluble in hexane at room temperature.[13] The polydispersity index of 1.3 is a reasonable value when using the oxyanionic initiation technique.[12,13]

From an integration of the ^{1}H NMR signals a block ratio (PFS–PDMAEMA) of 1–5 was deduced for this sample. The absolute degree of polymerization of PFS-$CH_2CH_2CH_2OH$ measured by GPC using a light-scattering detector indicates that the block copolymer has segment lengths of 11 and 55 repeat units for PFS and PDMAMA, respectively.

We have performed preliminary studies of the aqueous self-assembly of the PFS-*b*-PDMAEMA block copolymer. Stirring PFS_{11}-*b*-$PDMAEMA_{55}$ with water gradually gave a yellow colloidal dispersion, and a minimum of 20 days was required to achieve a well-dispersed solution free from any suspended material. The resulting solution was first aerosol sprayed onto a carbon film supported by mica. The carbon film was then floated off in water and deposited on a copper grid to facilitate the transmission electron microscopy (TEM) measurements. Although the block length of PFS is only 11 repeat units, cylindrical micelles were observed with a hydrophobic PFS core and a PDMAEMA corona (Fig. 1). TEM allows selective visualization of the electron-rich PFS core[9,10] which has an apparently uniform width of 16 nm, but a variation in length in the 50–500 nm range. Compared with the cylinders formed by PFS-*b*-PDMS in hexane,[5,6] the water-soluble cylinders have a similar width, but are shorter in length.

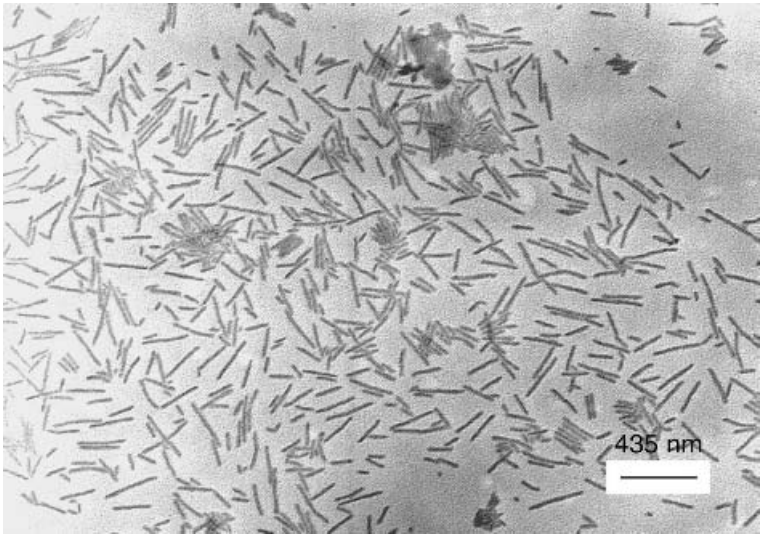

Figure 1 TEM of micelles associated in water from PFS_{11}-$PDMAEMA_{55}$.

B. Synthesis and Micellization of PFP-PFS-PDMS

The ABC triblock copolymers were synthesized by living anionic ROP initiated by *n*-BuLi with sequential monomer addition (see Scheme 2). The strategy for this synthesis is based on our previous experience with the individual [1]ferrocenophane monomers **1a** and **1b**, which we have shown undergo living ROP when treated with butyl lithium.[4] Thus the polymerization of **1a** and **1b** to form the PFP and PFS blocks were carried out at 23°C for (5 min for **1a**, 30 min for **1b**). Then the polymerization of the PDMS block was carried out at 0°C for 20 h. According to the changes in color of the solution, from the initial deep red color characteristic of the strained monomers to orange-yellow typical for ring-opened polyferrocenes, we inferred that there was quantitative conversion of **1a** and **1b** during the polymerization reaction. The well-defined nature of the PFP-*b*-PFS-*b*-PDMS triblock copolymers was demonstrated by the low polydispersities measured by GPC and also by ^{1}H NMR and ^{31}P NMR analysis. These results are listed in Table 1. In the text, the different block copolymers are denoted by PFP_n-*b*-PFS_m-*b*-$PDMS_l$, where *n, m*, and *l* represent the repeat units for the PFP, PFS, and PDMS blocks, respectively.

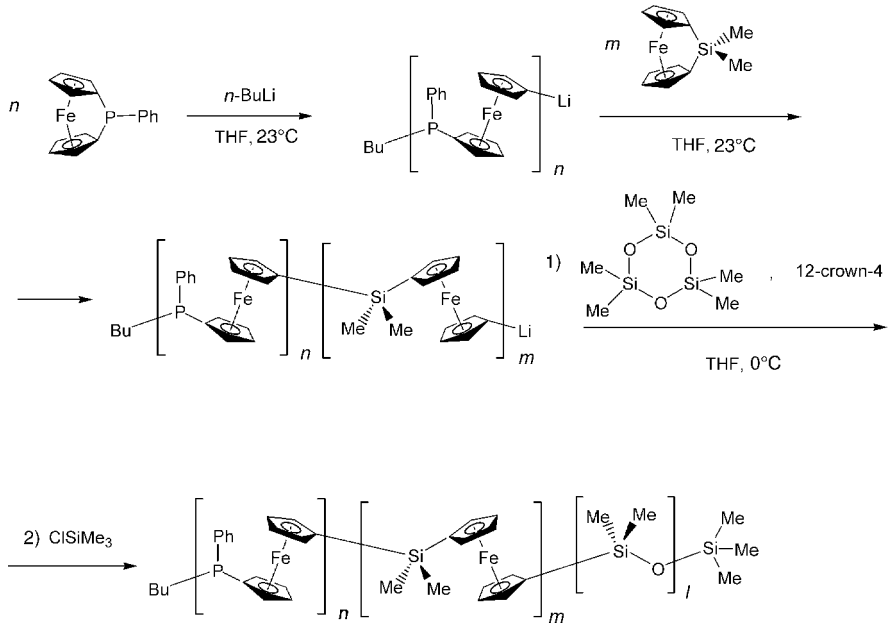

Scheme 2

The GPC data in Table 1 show that both the PFP-PFS diblock and PFP-*b*-PFS-*b*-PDMS triblock copolymers have narrow molecular weight distributions ($M_w/M_n < 1.10$) characteristic of living anionic polymerization. Because M_n values

measured by GPC are based on polystyrene standards, they do not reflect the true M_n values of the block copolymers. To overcome this problem, we characterized the absolute block lengths and block ratios of PFP-*b*-PFS-*b*-PDMS by ^{31}P and ^{1}H NMR, treating the PFP segment as the block copolymer end group. We took advantage of the fact that two resonances can be detected in the ^{31}P NMR spectrum of the PFP block. According to our previous study,[4d] a peak at −27 ppm was assigned to a single phosphorus in the ring-opened monomer unit next to the initiator moiety (*n*-BuP(Ph)Cp). A second signal at around −31 ppm was attributed to the phosphorus atoms in the mainchain ferrocenylphosphine units. By end-group analysis, the number of PFP repeat units *n* in the polymer can be deduced from the integration of these two peaks. The results obtained are in good agreement with the fcPPh/BuLi reactant ratio in each case. When one equivalent of **1a** was added to the BuLi initiator, *n*-BuP(Ph)fcLi was formed exclusively and quantitatively as inferred by the appearance of a single peak at −27 ppm. This result indicates that the reaction of BuLi with **1a** is much faster than the reaction of the *n*-BuP(Ph)fcLi anion with **1a**. This experiment provides evidence for very fast initiation in the ROP of ferrocenophane monomers with butyl lithium, and helps us to understand why we obtain polymers characteristic of good living character.

Table 1 M_n, PDI, Block Ratio, and Micellar Morphology for PFP-*b*-PFS-*b*-PDMS Triblock Copolymers in Hexane Characterized by GPC, ^{1}H, ^{31}P NMR, and TEM

No.	Block Copolymers	PFP_n-PFS_m Block M_n/PDI[a]	PFP_n-PFS_m-$PDMS_l$ M_n/PDI[a]	$n/m/l$[b]	Morphology[c]
1	1/40/304	10,400/1.10	40,500/1.04	1/40/304	Cylinders
2	2/45/300	13,400/1.01	38,300/1.05	2/45/300	Cylinders
3	6/45/220	13,000/1.06	31,200/1.06	6/45/220	Cylinders
4	11/50/600	15,000/1.06	74,300/1.04	11/50/600	Spheres

[a] GPC results with polystyrene standards.
[b] Evaluated from ^{1}H and ^{31}P NMR integration.
[c] Self-assembly in hexane as observed by TEM.

In the ^{1}H NMR spectrum of PFP-*b*-PFS-*b*-PDMS, signals due to the phenyl group attached to phosphorus are clearly visible at δ7.3 and δ7.5. On the basis of the absolute number of repeats unit of PFP deduced from the ^{31}P NMR spectrum, the overall composition of the polymer was calculated from the integrals of peaks representative of the PFS and PDMS blocks. For this purpose we chose as the reference the peak integrals of phenyl protons of the PFP block. We compared them with the $SiMe_2$ protons associated with the PFS block (δ=∼0.50 ppm) and those associated with PDMS (e.g., δ=∼0.15 ppm). For the results of these calculations, see Table 1.

Self-assembly of the ABC triblock copolymers was studied in hexane. Hexane is a nonsolvent for both PFP and for PFS, but a good solvent for PDMS. All micelle samples were prepared by slow addition of hexane to solutions of the polymer (0.1 wt/vol%)

in THF, a good solvent for all three blocks. THF was removed by slow dialysis against hexane. The micellar morphology was visualized by using TEM to analyze aerosol sprayed samples after solvent evaporation; the results are summarized in Table 1.

The length of the PFP end block influences the type of structures formed by the PFP-*b*-PFS-*b*-PDMS block copolymers in hexane. In Figure 2 we compared the morphologies for the micelles formed by three block copolymers with 1, 6, and 11 repeat units for the PFP block. Both PFP_1-*b*-PFS_{40}-*b*-$PDMS_{304}$ or PFP_6-*b*-PFS_{45}-*b*-$PDMS_{220}$ form cylinders, as shown in Figure 2a,b. The widths and lengths of these cylinders are similar to those obtained with PFS_{50}-$PDMS_{300}$ diblock copolymer in hexane,[6] suggesting that short PFP ($DP \leq 6$) end blocks have little effect on the overall micelle structure. Micelle solutions of PFP_{11}-*b*-PFS_{50}-*b*-$PDMS_{600}$ with 11 PFP repeat units do not contain cylindrical structures. Only spheres are seen in the TEM images (see Fig. 2c). This observation suggests that the presence of the longer PFP chains disrupted the crystallization of the PFS blocks in the micelle core. By comparison, crystalline–coil PFS-PDMS diblock copolymers of similar block ratio (1–12) form cylindrical structures that appear to be hollow.[6]

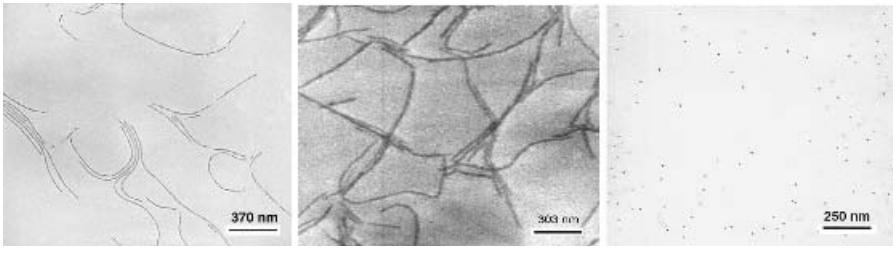

Figure 2 TEMs of micelles associated in hexane from PFP_1-*b*-PFS_{40}-*b*-$PDMS_{304}$ (a), PFP_6-*b*-PFS_{45}-*b*-$PDMS_{220}$ (b), and PFP_{11}-*b*-PFS_{50}-*b*-$PDMS_{600}$ (c), respectively.

In this context, it is also noteworthy that the effect of PFP units on the micelle structure was also detected in the sample of the cylinder-forming triblock PFP_6-*b*-PFS_{45}-*b*-$PDMS_{220}$ at elevated temperatures. On heating the cylindrical micelles to 70°C for 30 min., the formation of irregularly shaped aggregates was observed (see Fig. 3). This again can be explained by the disruptive influence of PFP on the crystallization of PFS, as cylindrical micelles of the diblock copolymer PFS-PDMS (PFS–PDMS = 1–6) without a PFP end block remain intact on heating at 80°C.[6]

To test the idea that the presence of the PFP block in the self-assembled structure could affect the crystallinity of the micelle core, we carried out wide-angle X-ray scattering (WAXS) measurements on films prepared from the micelles in hexane. The samples were prepared by casting a solution of the micelles in hexane onto an aluminum substrate and allowing the solvent to evaporate at ambient temperature. The WAXS pattern obtained from the wormlike micelles PFP_6-*b*-PFS_{45}-*b*-$PDMS_{220}$ has a peak at 6.4 Å. This peak appears at the same *d* spacing as that found in PFS homopolymer, confirming the crystalline nature of the PFS in this sample.[16]

The absence of higher-order peaks may indicate less well-defined crystals than in the homopolymer. In contrast, only an amorphous halo was observed in the WAXS spectrum of the film prepared from the solution of spherical micelles of PFP_{11}-*b*-PFS_{50}-*b*-$PDMS_{600}$. These results support the concept that crystallization plays a key role in the formation of cylindrical micelles in PFS block copolymers.

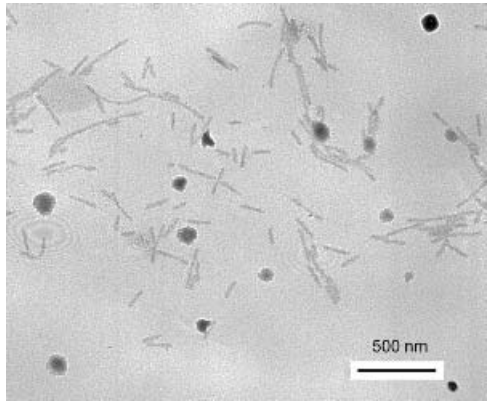

Figure 3 TEM illustrating the effect of heating on cylindrical micelles of PFP_6-*b*-PFS_{45}-*b*-$PDMS_{220}$ in hexane at 70°C for 30 min.

III. SUMMARY AND OUTLOOK

In conclusion, the well-defined organometallic amphiphilic AB block copolymer of PFS-PDMAEMA and ABC block polymers of PFP-*b*-PFS-*b*-PDMS were synthesized via anionic ROP approach.[17]

The crystallization of PFS chain and the amphiphilic nature of PFS-PDMAEMA drive the block copolymer forming cylindrical micelles on stirring with water. We expect the properties of PDMAEMA in water to vary with pH, temperature, and the degree of quaternization. Thus self-assembly studies of PFS-PDMAEMA may provide an opportunity to examine the interplay between the crystallization of PFS and corona chain stretching. Moreover, a wide range of redox-active, water-soluble micelle morphologies might be obtained simply by varying micelle preparation parameters. The water-soluble cylindrical micelles may also prove advantageous for lithographic applications.[9]

As for ABC triblock copolymers of PFP-PFS-PDMS, the PFP block is amorphous because of its atacticity, whereas the PFS block is crystalline at room temperature. These triblock copolymers form micelles in hexane, a solvent selective for the PDMS block. When the PFP block is very short (DP = 1 or 6) the polymer forms flexible wormlike micelles. A triblock copolymer with a longer PFP block (DP = 11) forms starlike spherical micelles. Films show a peak in the WAXS spectrum characteristic of a crystalline PFS block for the wormlike structures. There is no evidence

of crystallinity in the spherical micelles. We infer that the longer PFP block interferes with crystallization of the PFS block.

An interesting and as yet unanswered question for the self-assembly of PFP-PFS-PDMS ABC triblock copolymer is the location of the PFP component in these self-assembled micellar structures. The question is particularly important because the PFP segments present in these materials can coordinate to transition metals.[4] Studies of metal coordination to PFP-*b*-PFS-*b*-PDMS, and the types of nanostructures they form, are currently in progress.

IV. REFERENCES

1. I. W. Hamley, *The Physics of Block Copolymers,* Oxford Univ. Press, New York, 1998.
2. S. Forster, M. Antonietti, *Adv. Mater.* **10,** 195 (1998); P. F. W. Simon, R. Ulrich, H. W. Spiess, U. Wiesner, *Chem. Mater.* **13,** 3464 (2001); L. F. Zhang, A. Eisenberg, *Science* **268,** 1728 (1995); L. F. Zhang, A. Eisenberg, *J. Am. Chem. Soc.* **118,** 3168 (1996); G. J. Liu, *Curr. Opin. Interface Sci.* **3,** 200 (1998); M. Wilhelm, C. L. Zhao, Y. C. Wang, R. L. Xu, M. A. Winnik, J. L. Mura, G. Riess, M. D. Croucher, *Macromolecules* **24,** 1033 (1991).
3. I. Manners, *Science* **294,** 1664 (2001); S. Hou, W. K. Chan, *Macromol. Rapid Commun.* **20,** 440 (1999); C. L. Fraser, A. P. Smith, X. F. Wu, *J. Am. Chem. Soc.* **122,** 9026 (2000); J. F. Gohy, B. G. G. Lohmeijer, S. K. Varshney, U. S. Schubert, *Macromolecules* **35,** 7427 (2002).
4. R. Rulkens, Y. Ni, I. Manners, *J. Am. Chem. Soc.* **116,** 12121 (1994); Y. Ni, R. Rulkens, I. Manners, *J. Am. Chem. Soc.* **118,** 4102 (1996); C. H. Honeyman, T. J. Peckham, J. A. Massey, I. Manners, *Chem. Commun.* 2589 (1996); T. J. Peckham, J. A. Massey, C. H. Honeyman, I. Manners, *Macromolecules* **32,** 2830 (1999).
5. J. A. Massey, K. N. Power, M. A. Winnik, I. Manners, *Adv. Mater.* **10,** 1559 (1998).
6. J. A. Massey, K. N. Power, I. Manners, M. A. Winnik, *J. Am. Chem. Soc.* **120,** 9533 (1998); J. Raez, I. Manners, M. A. Winnik, *J. Am. Chem. Soc.* **124,** 10381 (2002).
7. K. Kulbaba, I. Manners, *Macromol. Rapid Commun.* **22,** 711 (2001).
8. M. J. MacLachlan, M. Ginzburg, N. Coombs, T. W. Coyle, N. P. Raju, J. E. Greedan, G. A. Ozin, I. Manners, *Science* **287,** 1460 (2000).
9. J. A. Massey, M. A. Winnik, I. Manners, V. Z-H. Chan, J. M. Ostermann, R. Enchelmaier, J. P. Spatz, M. Möller, *J. Am. Chem. Soc.* **123,** 3147 (2001).
10. J. A. Massey, K. Temple, L. Cao, Y. Rharbi, J. Raez, M. A. Winnik, I. Manners, *J. Am. Chem. Soc.* **122,** 11577 (2000).
11. L. Cao, I. Manners, M. A. Winnik, *Macromolecules* **34,** 3353 (2001).
12. Y. Nagasaki, Y. Sato, M. Kato, *Macromol. Rapid Commun.* **18,** 827 (1997).
13. S. F. Lascelles, F. Malet, R. Mayada, N. C. Billingham, S. P. Armes, *Macromolecules* **32,** 2462 (1999); M. Vamvakaki, N. C. Billingham, S. P. Armes, *Macromolecules* **32,** 2088 (1999); M. V. de Paz Báñez, K. L. Robinson, S. P. Armes, *Macromolecules* **33,** 451 (2000).
14. R. P. Quirk, S. H. Jang, H. M. Yang, Y. Lee, *Macromol. Symp.* **132,** 281 (1998); R. P. Quirk, S. H. Jang, J. Kim, *Rubber Rev., Rubber Chem. Technol.* **69,** 444 (1996).
15. P. Zhang, J. S. Moore, *J. Polym. Sci., Part A* **38,** 207 (2000).
16. J. Rasburn, R. Petersen, T. Jahr, R. Rulkens, I. Manners, G. J. Vancso, *Chem. Mater.* **7,** 871 (1995); R. Rulkens, A. J. Lough, I. Manners, S. R. Lovelace, C. Grant, W. E. Geiger, *J. Am. Chem. Soc.* **118,** 12683 (1996); V. S. Papkov, M. V. Gerasimov, I. I. Dubovik, S. Sharma, V. V. Dementiev, K. H. Pannell, *Macromolecules* **33,** 7107 (2000); Z. Chen, M. D. Foster, W. Zhou, H. Fong, D. H. Reneker, R. Resendes, I. Manners, *Macromolecules* **34,** 6156 (2001).
17. X. S. Wang, M. A. Winnik, I. Manners, *Macromol. Rapid Commun.* **23,** 210 (2002); X. S. Wang, M. A. Winnik, I. Manners, *Macromolecules* **35,** 9146 (2002).

CHAPTER 5

Synthesis and Self-Assembly of Polyisoprene-*block*-Polyferrocenyldimethylsilane Diblock Copolymers: Fabrication of Ceramic Nanolines on Semiconducting Substrates

Lan Cao, Mitchell A. Winnik, and Ian Manners

Department of Chemistry, University of Toronto, Toronto, Onatrio, Canada

CONTENTS

Macromolecules Containing Metal and Metal-like Elements, Volume 2: Organoiron Polymers, Edited By Alaa S. Abd-El-Aziz, Charles E. Carraher, Jr., Charles U. Pittman, Jr., John E. Sheats, and Martel Zeldin
ISBN 0-471-45078-2

I. INTRODUCTION

The self-assembly of amphiphilic block copolymers in block-selective solvents is of considerable interest as the resulting supramolecular micellar aggregates have a variety of potential applications.[1] As the chemical composition of the insoluble block and the lengths of the individual blocks can be varied, one can investigate systematically how these changes affect the size and structure of the micelles that are formed.[2–8] Most diblock copolymers form spherical micelles in a selective solvent. For this case, there is a rich body of theory to help us understand how the dominant interactions, the interplay of interfacial energy with the stretching entropies of the core and corona blocks, determine micelle size. We have a poorer understanding of the formation of other structures, such as cylinders and vesicles.[9–12]

When the insoluble block is crystalline, one would imagine that the energy of crystallization is so large that this block must pack in a folded structure. As a result, these diblock copolymers should form platelet structures consisting of a thin crystalline lamellar domain sandwiching a solvent-swollen corona of the soluble block protruding from both faces.[13] Experimental studies of micellar aggregates formed by semicrystalline diblock copolymers in dilute solution are rare. The first experiments, by Lotz et al.,[14–15] examined polystyrene-*block*-poly(ethylene oxide) (PS-*b*-PEO) diblock copolymers (with a crystalline PEO block) in ethylbenzene. They observed platelet micellar structures by transmission electron microscopy (TEM). Gast et al.[16] subsequently reported the coexistence of spherical and large lamellar aggregates from a PS-*b*-PEO diblock copolymer sample in cyclopentane. They also found some cylindrical aggregates protruding from the edge of the platelets. The authors attributed the multiple morphologies to different water content in the aggregates. More recently, Lin and Gast[17] used small-angle X-ray scattering and small-angle neutron scattering to study the platelet structures formed by PS-*b*-PEO in cyclopentane and by polyethylene-*block*-polyethylpropylene (PE-*b*-PEP, crystalline PE block) in decane. The latter system was also examined independently by Richter et al.[18]

The fabrication of numerous micrometer- and submicrometer-scale devices relies on the generation of periodic and aperiodic microstructures by the lithographic techniques. To create features smaller than 100 nm for further miniaturization, the use of conventional lithography becomes increasingly difficult and time-consuming. The ordered nanostructures arising from the self-assembly of diblock copolymers (size 10–100 nm) offer an alternative approach for lithographic purposes.[19–25] For example, spherical micellar aggregates from the self-assembly of diblock copolymers in block-selective solvents have been shown to function as etch resists to fabricate periodic features with dimensions smaller than 100 nm on substrates using selective etching processes.[26–28] To create connected structures such as lines, micellar aggregates with cylindrical morphology are more desirable.

Polyferrocenylsilanes are an interesting class of metal-containing polymers with a mainchain consisting of alternating ferrocene and organosilane units.[29–31] Well-defined diblock copolymers containing polyferrocenylsilane segments are readily

accessible via living anionic ring-opening polymerization (ROP) of silicon-bridged [1]ferrocenophane **1**.[32–34] The self-assembly of polyferrocenylsilane block copolymers in solid state and block-selective solvents results in the formation of nanosized materials possessing interesting electrical, magnetic, redox-active, and preceramic properties.[35–36] We have previously shown that the asymmetric block copolymers, polyferrocenyldimethylsilane-*block*-polydimethylsiloxane (PFDMS-*b*-PDMS) (block ratio 1–6) self-assemble in hexane solvent to form cylindrical micelles with an organometallic PFDMS core.[37] The formation of cylindrical supramolecular structures rather than the expected spherical micelles for these materials has been attributed to the crystalline nature of the core-forming PFDMS block.[38]

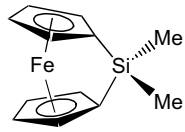

1

In this chapter, we describe the synthesis and solution self-assembly of organic–organometallic polyisoprene-*block*-polyferrocenyldimethylsilane (PI-*b*-PFDMS) diblock copolymers. We are interested in how the crystallization of core-forming PFDMS block and chain stretching of the corona-forming PI will affect the micelle morphology. In addition, we report our work on the fabrication and characterization of ceramic nanolines from plasma etching of cylindrical PI-*b*-PFDMS diblock copolymer micelles.

II. EXPERIMENTAL

The silicon-bridged [1]ferrocenophane **1** was synthesized as described before,[34] using a method modified from the original synthesis.[39] Isoprene was purified by distillation from CaH_2 and a second distillation over *n*-butyllithium immediately before the polymerization. Tetrahydrofuran was distilled over Na/benzophenone prior to use. All the other chemicals were used as received.

All reactions were carried out under an inert atmosphere using either a standard Schlenk line or a Mbraun glovebox. The block copolymers, PI-*b*-PFDMS, were synthesized by living anionic polymerization through sequential monomer addition. The polymerization was carried out in a flamed and vacuum-dried glass reactor equipped with a three-way stopcock and a rubber septum. Monomer, initiator, and solvent were transferred into the polymerization reactor via a stainless-steel canula or a glass syringe. Isoprene was polymerized first in THF at 0°C using *sec*-butyllithium as the initiator. On the completion of the synthesis of polyisoprene block, an aliquot

of the polymerization solution was drawn from the reaction flask for the analysis of that block. Then silicon-bridged [1]ferrocenophane **1** was added as a solution in THF. The reaction mixture was warmed to room temperature, and the polymerization was allowed to continue for another 30 min before it was quenched by adding a few drops of degassed methanol. The crude product was obtained by precipitation into methanol, filtered, and dried under vacuum.

Molecular weights of the polymer were estimated by size-exclusion chromatography (SEC) using Waters Associates 2690 Separations Module equipped with a column heater, ultrastyragel columns with pore sizes of 10^3–10^5 Å, inline degasser, and a differential refractometer. A flow rate of 1.0 mL/min was used, and the eluent was THF. Polystyrene standards purchased from American Polymer Standards were used for calibration purposes. The 200-MHz ^{1}H NMR spectra were recorded on a Varian Gemini 200 spectrometer with deuterated chloroform as the solvent.

The micelle solution was prepared by slow addition of hexane into the THF solution of the polymer. The concentration of the final micelle solution was around 1 mg/mL. Transmission electron microscopy (TEM) measurements were carried out on a Hitachi model 600 electron microscope. The specimen was prepared as follows. Thin carbon films were grown on mica as a support. Then 25 μL of a block copolymer micelle solution was sprayed onto the carbon film. Each carbon film was floated off the mica support in water and deposited onto a 300-mesh Gilder copper grid. The sample was air-dried before introduction into the electron microscope. Wide angle X-ray scattering (WAXS) analysis was performed using a Siemens D5000 diffractometer with a Cu Kα source operating at 50 kV and 35 mA in step scan mode. Scanning force microscopy (SFM) measurements were performed on a Nanoscope III instrument (Digital Instruments, Santa Barbara) operating in tapping mode. The oscillation frequency of the Si cantilever was set to 320–360 kHz. All images were recorded at a scan rate of 1 Hz.

Reactive ion etching experiments were carried out in a plasma etcher P300 (Plasma Electronics). The power was set at 100 W. The pressure inside the etching chamber and the etching time were varied. The samples for plasma etching were prepared by spin coating of the micelle solution onto cleaned Si substrates.

III. RESULTS AND DISCUSSION

A. Block Copolymer Synthesis

Polyisoprene-*block*-polyferrocenyldimethylsilane (PI-*b*-PFDMS) was synthesized by the anionic ring-opening polymerization of **1** initiated by living polyisoprene prepared in THF (Scheme 1). The products were recovered as amber gumlike materials.

Four block copolymers were synthesized in the current study and they were characterized by size-exclusion chromatography and ^{1}H NMR measurements. Their characteristics are summarized in Table 1. All polymers are narrow polydispersed from the SEC measurements and they have a PI–PFDMS block ratio ranging from 1–2 to 11.5–1.

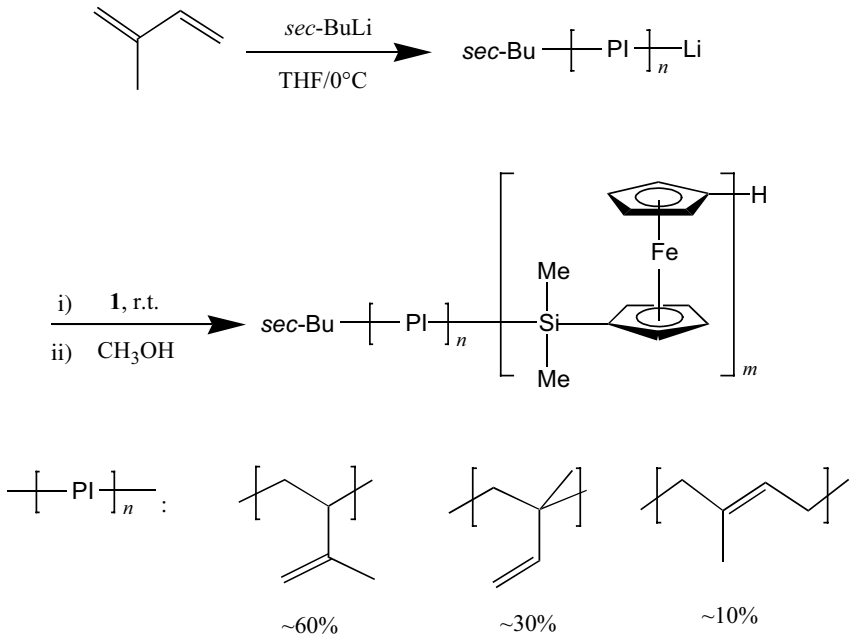

Scheme 1 Synthesis of polyisoprene-*block*-poly(ferrocenyldimethyl silane) (PI-*b*-PFDMS).

Table 1 Characteristics of PI_n-*b*-$PFDMS_m$

Samples	PI Block[a] M_n (g/mol)	PI_n-*b*-$PFDMS_m$[a] M_n (g/mol)	PDI	*n*–*m*[b]
PI_{30}-*b*-$PFDMS_{60}$	2000	17,400	1.03	1–2
PI_{70}-*b*-$PFDMS_{70}$	4800	23,600	1.03	1–1
PI_{320}-*b*-$PFDMS_{53}$	22,000	30,700	1.05	6–1
PI_{340}-*b*-$PFDMS_{30}$	23,000	29,300	1.05	11.5–1

[a] Apparent values based on SEC measurements.
[b] Calculated from ^{1}H NMR integration.

B. PI-*b*-PFDMS Micelles

To prepare micelle solutions, diblock copolymers were first dissolved in a small amount of THF, a common solvent for both blocks. Hexane, a precipitant for PFDMS, was added dropwise afterward with gentle stirring, and the solutions were monitored in a light-scattering apparatus. When a strong increase in light-scattering intensity indicated the onset of the aggregate formation, the addition of hexane was stopped. The solution was left to stir for 3 days at 23°C to equilibrate the micellar structures. All micelle solutions have a final polymer concentration of 1 mg/mL.

We employed TEM measurements to investigate the morphology of the aggregates. Figure 1 shows representative TEM micrographs of the micellar structures derived from these diblock copolymers in the THF/hexane mixture. No staining is necessary to visualize the Fe-rich PFDMS core.[34,37] Because of the low contrast between PI and the supporting carbon film, the objects on the TEM micrograph represent only the PFDMS domains. From Figure 1a,b, we see that PI_{320}-*b*-$PFDMS_{53}$ and PI_{340}-*b*-$PFDMS_{30}$ form cylindrical micellar aggregates consisting of a PFDMS core surrounded by a corona of PI chains. The cylinders seem stiff, with persistence lengths on the order of at least several hundred nanometers. The aggregates formed by PI_{30}-*b*-$PFDMS_{60}$ are very different. They appear as long strips of various sizes (Fig. 1c). The uniform electron density seen in the TEM image, even when the aggregate is folded or when two structures overlap, is indicative of thin tapelike structures. They have a high aspect ratio with straight edges and right-angle corners. These structures are expected to consist of a chain-folded PFDMS lamellar domain between solvated PI chains. For PI_{70}-*b*-$PFDMS_{70}$, we observed the coexistence of cylindrical and lamellar aggregates, as shown in Fig. 1d.

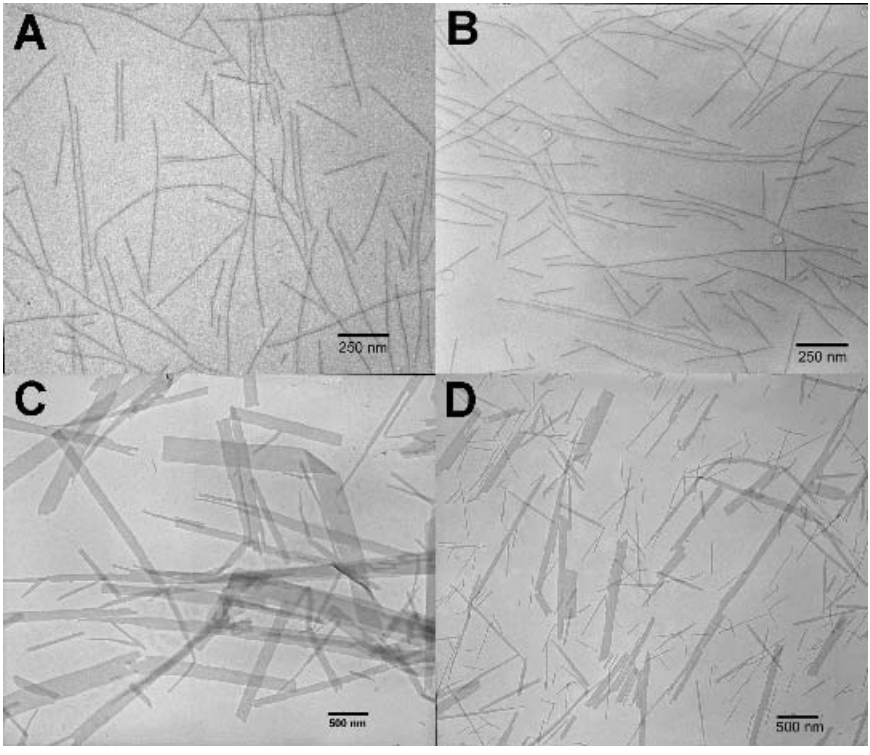

Figure 1 Representative TEM micrographs of the aggregates formed by (a) PI_{320}-*b*-$PFDMS_{53}$ in THF/hexane (2/8, v/v), (b) PI_{340}-*b*-$PFDMS_{30}$ in THF/hexane (1/9, v/v), (c) PI_{30}-*b*-$PFDMS_{60}$ in THF/hexane (3/7, v/v), (d) PI_{70}-*b*-$PFDMS_{70}$ in THF/hexane (3/7, v/v).

Bragg peaks are seen in the wide-angle X-ray scattering (WAXS) spectra of films formed from both the cylindrical and tapelike structures (Fig. 2). Both show a strong reflection at 6.4 Å similar to that seen in PFDMS homopolymer.[32]

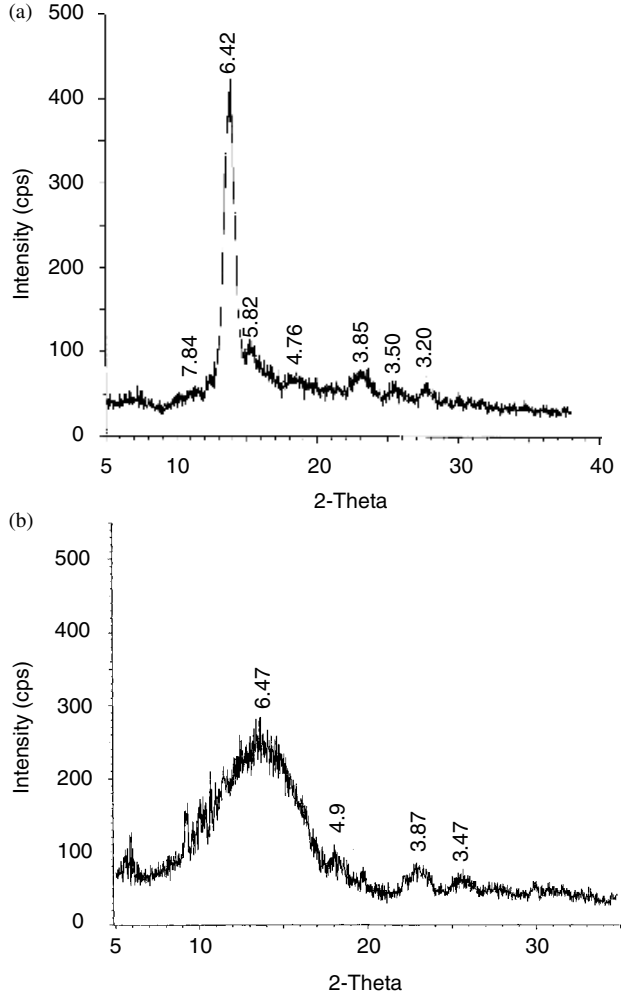

Figure 2 WAXS spectra of films formed from (a) cylindrical PI_{320}-*b*-$PFDMS_{53}$ and (b) tapelike PI_{30}-*b*-$PFDMS_{60}$ aggregates.

The scaling model of Vilgis and Halperin (VH) provides a theoretical framework to help us understand aspects of our observations.[40] VH consider a chain-folded crystalline core in which each chain experiences an integral number of chain

folds. Thicker cores have fewer folds, and this brings the junctions closer together. Overlap of the solvent-swollen coils of the soluble block leads to stretching of these chains. The equilibrium structure represents a balance between thick cores, which minimize the interfacial energy, and thin cores, which minimize the entropy penalty of stretching the corona chains. The formation of lamellar aggregates for PI_{30}-*b*-$PFDMS_{60}$ agrees very well with this theoretical prediction. For semicrystalline diblock copolymers with long coil blocks, VH predicted that cylindrical aggregates of finite length would be possible by the adjustment of the crystalline block in the micellar core. The core dimensions are truncated to accommodate the space-filling requirements of the soluble block.

PI_{30}-*b*-$PFDMS_{60}$ and PI_{320}-*b*-$PFDMS_{53}$ have similar PFDMS block lengths, but differ significantly in the PI block length. The formation of cylindrical aggregates for PI_{320}-*b*-$PFDMS_{53}$ is consistent with a strong competition between chain stretching of the PI corona and the energy of the crystalline PFDMS core. While crystallization of the PFDMS block would favor a lamellar morphology, the free-energy cost for stretching of the long corona chains will be substantial. Although the system could minimize the energy penalty from the stretching of PI chains by making more folds in the lamellar domain (i.e., a thinner lamellar region), every chain fold is energetically costly. A cylindrical structure provides the best balance between these effects. We also observe cylindrical aggregates for PI_{340}-*b*-$PFDMS_{30}$. This type of highly asymmetric diblock copolymer would form starlike spherical micelles if the PFDMS block were not crystalline.[38] The soluble block is stretched to a greater degree in a cylindrical structure than in a sphere. We see that the energy of crystallization is sufficient to overcome entropy of stretching associated with this shape transition.

C. Fabrication of Ceramic Nanolines

The cylindrical PI-*b*-PFDMS micelles consist of an Fe-rich core surrounded by an organic PI corona. In collaboration with Möller and coworkers we have explored the opportunity to fabricate ceramic nanolines on semiconducting substrates using reactive ion etching (RIE) process.

Before RIE, the PI_{320}-*b*-$PFDMS_{53}$ micellar aggregates were first deposited onto Si substrates by spin coating. Representative scanning force micrographs of the micelles before RIE on Si are shown in Figure 3. Cylindrical objects with uniform width are observed. The average height of the cylinders from the section analysis of the micrograph (shown below the micrograph) is around 9 nm.

The cylindrical PI_{320}-*b*-$PFDMS_{53}$ micelles on Si substrate were subject to oxygen or hydrogen plasma etching. Figure 4 shows the scanning force micrographs of the cylindrical micelles after the plasma treatment. It can be seen that the continuous lineshape was preserved during the etching process. Table 2 summarizes the dimensions of the cylinders before and after plasma etching. The average height of the cylinders decreases from 9 to 4 nm on oxygen plasma treatment and to only 2 nm when hydrogen plasma was used. No further decrease of the cylinder height was observed from SFM measurements with even longer etching time and varying pressure of the plasma, suggesting that most of the volatile component of the micelles

was removed under such etching conditions. It can also be noted that the cylinder height after treatment with hydrogen plasma was half of that when oxygen plasma was used. It was shown previously that a nonvolatile oxide layer at the surface of the polymer was formed on oxygen plasma etching of polyferrocenylsilane, which results in relatively low etching rate.[41] Because of the reductive nature of the hydrogen plasma, such protective oxide layer is less likely to be formed. This results in a larger extent of etching of the block copolymer micelles when hydrogen plasma was employed.

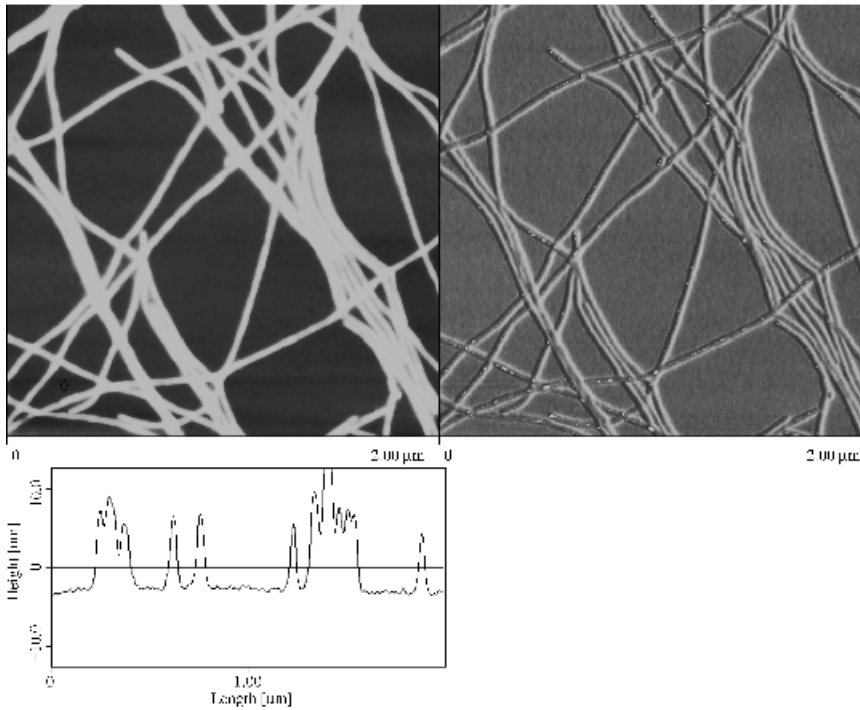

Figure 3 Representative SFM height (left) and phase (right) images of the cylindrical PI_{320}-*b*-$PFDMS_{53}$ micelles on Si substrate before reactive ion etching. The section analysis of the micrograph is shown underneath.

To quantify the widths of the nanolines from the SFM measurements, the SFM probe shape was calibrated using a procedure reported previously.[42] From the estimated probe dimensions, the width of the nanolines can be calculated from the section analysis of the SFM micrograph. These results are included in Table 2. It was demonstrated previously that reactive ion etching of polyferrocenyldimethylsilane predominantly removes organic components present in the polymer.[43,44] From Table 2, it is clear that the plasma treatment results in significant shrinkage of the original micellar aggregates and the nanolines after the plasma treatment should be ceramic materials containing Fe, Si, O, and C elements.

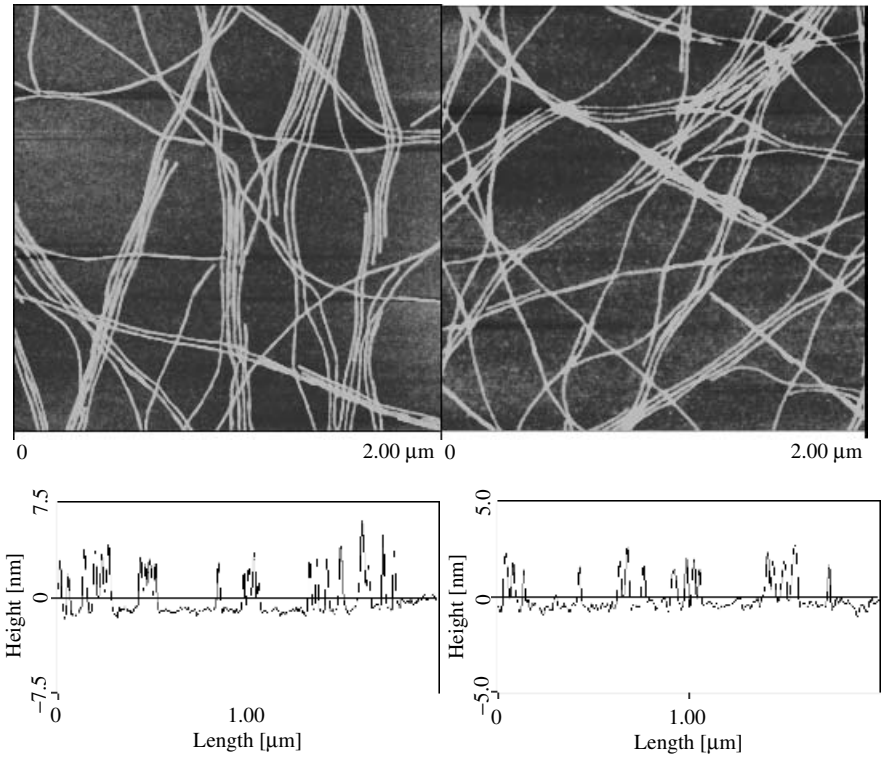

Figure 4 SFM height images of PI_{320}-*b*-$PFDMS_{53}$ micelles on Si substrate after O_2 (10 min, 1 mbar) (left) and H_2 (10 min, 1 mbar) (right) plasma etching. The section analysis of the micrograph is shown underneath.

Table 2 Dimensions of Ceramic Nanolines from Plasma Etching of Cylindrical PI_{320}-*b*-$PFDMS_{53}$ Micelles as Determined by SFM with Calibration of the Probe Shape

Etching Conditions	Height (nm)	Width (nm)
Before plasma	9	60
O_2, 10 min, 1 mbar	4	10
H_2, 10 min, 1 mbar	2	10

To characterize the nanolines after plasma treatment by TEM, the micelles were deposited onto a carbon-coated copper grid. The carbon film was thick enough that under the etching condition used (H_2 plasma, 10 min, 1 mbar), the carbon layer was not destroyed by the plasma. A representative transmission electron micrograph of the cylinders after the plasma treatment is shown in Figure 5. The nanolines were found to be continuous with a width of roughly 8 nm, which agrees well with the SFM measurements.

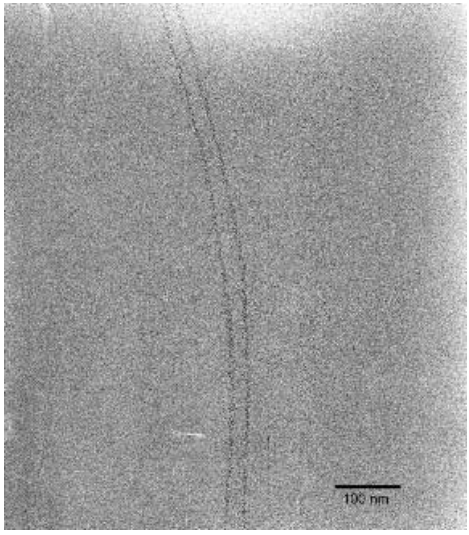

Figure 5 Transmission electron micrograph of two parallel cylindrical PI_{320}-*b*-$PFDMS_{53}$ micelles after H_2 plasma etching (10 min, 1 mbar).

IV. CONCLUSIONS

We have shown that a change in block length for coil–crystalline PI-*b*-PFDMS leads to a change in micelle structure. While the VH model provides separate scaling relationships for lamellar and cylindrical coil–crystalline aggregates in selective solvents, it cannot describe the requirements for a crossover between the two types of structures. The coexistence of both cylindrical and lamellar aggregates for PI_{70}-*b*-$PFDMS_{70}$ identifies a crossover composition. Our observations suggest that the use of crystalline blocks represent a potentially powerful approach to systematically control micellar morphology.

In addition, we have demonstrated that ceramic nanolines can be fabricated from the reactive ion etching of the cylindrical polyferrocenylsilane diblock copolymer micelles. The presence of inorganic elements in these micellar structures provides sufficient etching contrast. These continuous lines have length of micrometers and width as small as 8 nm. This represents a relatively simple method to prepare nanolines with large aspect ratio. These ceramic nanolines are potential candidates as etching resists to produce 2D quantum wires in semiconducting substrates.

V. ACKNOWLEDGMENTS

The authors thank NSERC Canada for the financial support of this project. The work on plasma etching was performed in collaboration with the group of Prof. Martin Möller at University of Ulm, Germany. In addition, L. C. is grateful to the

Ontario Government for an Ontario Graduate Scholarship (1999–2002). I. M. is grateful to the University of Toronto for a McLean Fellowship (1997–2003), to the Ontario Government for a PREA award (1999–2003), and to the Canadian Government for a Canada Research Chair (2001).

VI. REFERENCES

1. I. W. Hamley, *The Physics of Block Copolymers,* Oxford, New York (1999).
2. A. Halperin, M. Tirrell, T. P. Lodge, *Adv. Polym. Sci*. **100,** 31 (1992).
3. A. Halperin, *Macromolecules* **20,** 2943 (1987).
4. S. Förster, M. Antonietti, *Adv. Mater.* **10,** 195 (1998).
5. G. J. Liu, *Curr. Op. Coll. Interfac. Sci.* **3,** 200 (1998).
6. K. L. Wooley, *J. Polym. Sci. Polym. Chem.* **38,** 1397 (2000).
7. S. Liu, S. P. Armes, *J. Am. Chem. Soc.* **123,** 9910 (2001).
8. J. -F. Gohy, B. G. G. Lohmeijer, U. S. Schubert, *Macromolecules* **35,** 4560 (2002).
9. L. Luo, A. Eisenberg, *J. Am. Chem. Soc.* **123,** 1012 (2001).
10. L. Luo, A. Eisenberg, *Angew. Chem. Int. Ed.* **41,** 1001 (2002).
11. N. S. Cameron, M. K. Corbierre, A. Eisenberg, *Can. J. Chem.* **77,** 1311 (1999).
12. Y. Won, H. T. Davis, F. S. Bates, *Science* **283,** 960 (1999).
13. I. W. Hamley, *Adv. Polym. Sci.* **148,** 113 (1999).
14. B. Lotz, A. J. Kovacs, *Kolloid-Z. Z. Polym.* **209,** 97 (1966).
15. B. Lotz, A. J. Kovacs, G. A. Bassett, A. Keller, *Kolloid-Z. Z. Polym.* **209,** 115 (1966).
16. A. P. Gast, P. K. Vinson, K. A. Cogan-Farinas, *Macromolecules* **26,** 1774 (1993).
17. E. K. Lin, A. P. Gast, *Macromolecules* **29,** 4432 (1996).
18. D. Richter, D. Schneiders, M. Monkenbusch, L. Willner, L. J. Fetters, J. S. Huang, M. Lin, K. Mortenson, B. Farago, *Macromolecules* **30,** 1053 (1997).
19. H. -A. Klok, S. Lecommandoux, *Adv. Mater*. **13,** 1217 (2001).
20. K. E. Gonsalves, L. Merhari, H. Wu, Y. Hu, *Adv. Mater*. **13,** 703 (2001).
21. M. Park, C. Harrison, P. M. Chaikin, R. A. Register, D. H. Adamson, *Science* **276,** 1401 (1997).
22. M. Park, P. M. Chaikin, R. A. Register, D. H. Adamson, *Appl. Phys. Lett.* **79,** 257 (2001).
23. V. Z. -H. Chan, J. Hoffman, V. Y. Lee, H. Iatrou, A. Avgeropoulos, N. Hadjichristidis, R. D. Miller, E. L. Thomas, *Science* **286,** 1716 (1999).
24. M. -V. Meli, A. Badia, P. Grütter, R. B. Lennox, *Nano Lett.* **2,** 131 (2002).
25. T. Thurn-Albrecht, R. Steiner, J. DeRouchey, C. M. Stafford, E. Huang, M. Bal, M. Tuominen, C. J. Hawker, T. P. Russell, *Adv. Mater.* **12,** 787 (2000).
26. J. P. Spatz, P. Eibeck, S. Mössmer, M. Möller, T. Herzog, P. Ziemann, *Adv. Mater.* **10,** 849 (1998).
27. J. P. Spatz, T. Herzog, S. Mössmer, P. Ziemann, M. Möller, *Adv. Mater.* **11,** 149 (1999).
28. J. P. Spatz, S. Mössmer, C. Hartmann, M. Möller, T. Herzog, M. Krieger, H.-G. Boyen, P. Ziemann, B. Kabius, *Langmuir* **16,** 407 (2000).
29. D. A. Foucher, B. Z. Tang, I. Manners, *J. Am. Chem. Soc.* **114,** 6246 (1992).
30. I. Manners, *Science* **294,** 1664 (2001).
31. I. Manners, *J. Polym. Sci. Polym. Chem.* **40,** 179 (2002).
32. K. Kulbaba, I. Manners, *Macromol. Rapid. Commun.* **22,** 711 (2001).
33. R. Rulkens, Y. Ni, I. Manners, *J. Am. Chem. Soc.* **116,** 12121 (1994).

34. Y. Ni, R. Rulkens, I. Manners, *J. Am. Chem. Soc.* **118,** 4102 (1996).
35. J. Massey, K. N. Power, M. A. Winnik, I. Manners, *Adv. Mater.* **10,** 1559 (1998).
36. I. Manners, *Chem. Commun.* 857 (1999).
37. J. Massey, K. N. Power, I. Manners, M. A. Winnik, *J. Am. Chem. Soc.* **120,** 9533 (1998).
38. J. A. Massey, K. Temple, L. Cao, Y. Rharbi, J. Raez, M. A. Winnik, I. Manners, *J. Am. Chem. Soc.* **122,** 11577 (2000).
39. A. B. Fischer, J. B. Kinney, R. H. Staley, M. S. Wrighton, *J. Am. Chem. Soc*. **101,** 6501 (1979).
40. T. Vilgis, A. Halperin, *Macromolecules* **24,** 2090 (1991).
41. R. H. Lammertink, M. A. Hempenius, V. Z.-H. Chan, E. L. Thomas, G. J. Vancso, *Chem. Mater.* **13,** 429 (2001).
42. S. S. Sheiko, M. Möller, E. M. C. M. Reuvekamp, H. W. Zandbergen, *Phys. Rev. B* **48,** 5675 (1993).
43. J. Y. Cheng, C. A. Ross, V. Z.-H. Chan, E. L. Thomas, R. G. H. Lammertink, G. J. Vancso, *Adv. Mater.* **13,** 1174 (2001).
44. J. A. Massey, M. A. Winnik, I. Manners, V. Z.-H. Chan, J. M. Ostermann, R. Enchelmaier, J. P. Spatz, M. Möller, *J. Am. Chem. Soc*. **123,** 3147 **(**2001).
45. L. Cao, J. A. Massey, M. A. Winnik, I. Manners, S. Riethmuller, F. Banhart, J. P. Spatz, M. Moller, *Adv. Funct. Mater*. **13,** 271 (2003).

CHAPTER 6

Water-Soluble Polyferrocenylsilanes for Supramolecular Assemblies by Layer-by-Layer Deposition

Mark A. Hempenius, Mária Péter, Neil S. Robins, E. Stefan Kooij, Rob G. H. Lammertink, and G. Julius Vancso

Department of Chemical Technology, University of Twente, and MESA$^+$ Research Institute, Enschede, The Netherlands

CONTENTS

Macromolecules Containing Metal and Metal-like Elements, Volume 2: Organoiron Polymers, Edited By Alaa S. Abd-El-Aziz, Charles E. Carraher, Jr., Charles U. Pittman, Jr., John E. Sheats, and Martel Zeldin
ISBN 0-471-45078-2

I. INTRODUCTION

Macromolecules containing inorganic elements or organometallic units in the main chain are of considerable interest as they may combine potentially useful chemical, electrochemical, optical, and other interesting characteristics with the processability of polymers.[1]

Polyferrocenylsilanes, consisting of alternating ferrocenyl and alkylsilyl units in the mainchain, are among this class of materials. With the discovery of the anionic ring-opening polymerization (ROP) of silicon bridged ferrocenophanes,[1] well-defined polyferrocenylsilanes, block copolymers featuring corresponding organometallic blocks,[2] and end-functionalized polyferrocenylsilanes forming electroactive monolayers on gold,[3] have become accessible.

As polyferrocenyldimethylsilane was found to be an effective resist in reactive ion etching processes,[4] it became of interest to employ this polymer in surface patterning of silicon or other substrates, which has relevance in the fabrication of electrical, electrooptical, and magnetic storage devices; sensors; and other components. As a proof of principle, a line pattern of this polymer, deposited on silicon substrates using a MIMIC (micromolding in capillaries) microcontact printing technique, was transferred into the substrate by removing uncovered silicon areas in an O_2/CF_4 plasma.[4]

Block copolymers featuring polyferrocenylsilane blocks form nanoperiodic microdomain structures on phase separation.[5] In thin films of such block copolymers, such as poly(ferrocenyldimethylsilane-*block*-isoprene), the high resistance of the organometallic phase to reactive ion etching compared to the organic phase was used to form nanopatterned surfaces in a one-step etching process to transfer these patterns into silicon substrates.[6] The utility of ferrocenylsilane block copolymers in surface patterning was further demonstrated by the use of ferrocenylsilane-styrene block copolymers as templates in the fabrication of arrays of nanometer-sized cobalt magnetic dots.[7]

Water-soluble polyferrocenylsilane polycations, belonging to the rare class of main chain organometallic polyelectrolytes, have been reported by us and others.[8–11] These compounds are of interest because they combine the unusual properties of polyferrocenylsilanes with the processability of polyelectrolyte solutions, for example, enabling one to make use of ionic interactions to deposit these polymers onto substrates. Polyelectrolytes can be employed in layer-by-layer (LbL) self-assembly processes to form ultrathin multilayer films with controlled thickness and composition.[12,13]

The incorporation of metals in multilayer thin films significantly extends the scope of useful characteristics associated with these films. By employing for instance, polymeric Ru(II) complexes as polycationic species and poly(sodium acrylate) as polyanion in the LbL deposition process, efficient light-emitting solid-state devices could be fabricated.[14] In another example, a ferrocene-containing redox active polycation was combined with an enzyme to produce electrocatalytically active enzyme/mediator multilayer structures.[15] Multilayers composed of poly(4-vinylpyridine) complexed with $[Os(bpy)2Cl]^{+/2+}$ and, for example, poly(sodium 4-styrenesulfonate) were used to accomplish the electrocatalytic reduction of nitrite.[16]

Here we report on the use of a water-soluble polyferrocenylsilane polyanion and a corresponding polycation to form fully organometallic multilayer thin films.[17] Although cationic polyferrocenylsilanes have been used in combination with commercially available organic polyanions to manufacture heterostructured multilayer films,[11,18] because of the lack of availability of anionic organometallic polyions, no fully organometallic multilayers have been reported prior to our first communication.[19] In 2002 we succeeded in preparing the first polyferrocenylsilane polyanion.[20] This development broadens the range of accessible heterostructured organometallic multilayer films and enables the fabrication of all-organometallic multilayer thin films. Multilayer structures composed of polyferrocenylsilane polyanions and polycations are of interest as redox-active thin films, and are potentially useful as interlayers at the electrode/polymer interface in polymer light-emitting diodes.[21]

In addition to forming continuous organometallic multilayer thin films, we explored the LbL deposition of polyferrocenylsilane polyions onto, for instance, hydrophilically/hydrophobically modified substrates with the aim of building two-dimensionally patterned organometallic multilayers. In general, surfaces modified with microscopically patterned conducting,[22] luminescent,[23] or redox-active polymer[24] films have potential use in microelectronic and optoelectronic devices and microsensor arrays. Area-selective deposition of polyferrocenylsilane polyions can be an attractive method to obtain two-dimensionally patterned redox active films, which may be used as electrochemically modulated diffraction gratings.[24]

Patterned organometallic multilayers may be of interest also as etch barriers in RIE processes.[4] For this purpose it is essential that these films can be fabricated from etch resistant organometallic polyferrocenylsilane chains only, as organic polymers offer no resistance to reactive ion etching. This chapter deals with the formation of continuous organometallic multilayer thin films, and with the fabrication of patterned organometallic thin films, formed by area-selective deposition of organometallic polyions on prepatterned substrates.

II. SYNTHESIS OF POLYFERROCENYLSILANE POLYIONS

Any route to high-molar-mass polyferrocenylsilanes incorporates a ring-opening polymerization step of a strained silicon-bridged ferrocenophane.[1] Such ferrocenophanes are obtained by treating 1,1′-dilithioferrocene with a dichlorosilane of choice. Many functionalities, however, do not tolerate the highly basic dilithioferrocene or the reactive chlorosilane moieties, are incompatible with the reactive strained monomer itself, or hinder monomer purification. In principle, although two approaches to functional polyferrocenylsilanes can be envisaged—(1) functional group incorporation in the ferrocenophane monomer, usually as a substituent on silicon, or (2) functionalization after polymerization by side-group modification reactions—the latter will be used if polar or even ionic moieties are to be introduced.

We introduced and employed a polyferrocenylsilane, featuring chloropropylmethylsilane repeat units, as an organometallic main chain that already has reactive pendent groups in place for further functionalization by nucleophilic substitution (see Scheme 1).[11,25]

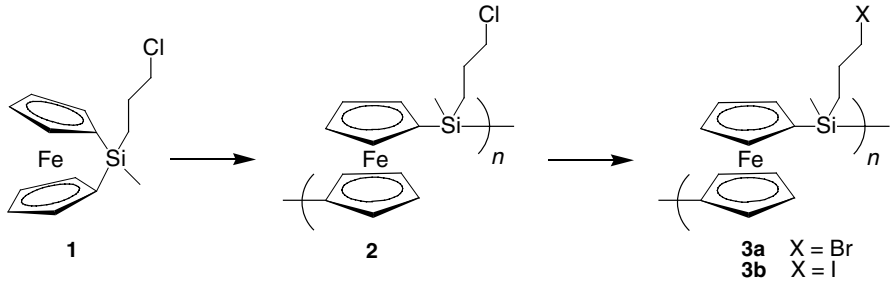

Scheme 1 Polyferrocenylsilanes featuring haloalkyl side groups.

Poly(ferrocenyl(3-chloropropyl)methylsilane) **2** was readily accessible by transition-metal-catalyzed ring-opening polymerization[1] of the corresponding (3-chloropropyl)methylsilyl[1]ferrocenophane **1**.[11] The chloropropyl groups are linked to silicon by Si–C bonds, which are stable to hydrolytic cleavage, as opposed to groups linked by Si–O bonds, for example. By means of halogen exchange,[26] **2** can be converted quantitatively into its bromopropyl (**3a**) or iodopropyl analogs (**3b**),[20] which are particularly suitable for functionalization by nucleophilic substitution. Thus, a wider range of nucleophiles can be employed to prepare functional polyferrocenylsilanes.

As an example, reaction of **2** with potassium 1,1,3,3-tetramethyldisilazide[27] and dicyclohexano-18-crown-6 in THF afforded a *N*,*N*-*bis*(dimethylsilyl)-protected poly(ferrocenyl(3-aminopropyl)methylsilane) **4**, which was hydrolyzed to the desired polycation **5** in aqueous acid[11] (see Scheme 2).

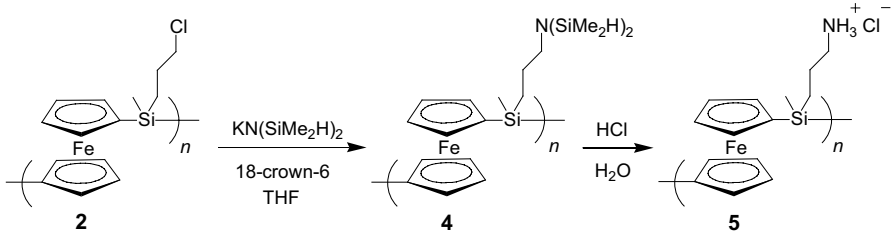

Scheme 2 Synthesis of a polyferrocenylsilane polycation.

The disilazide reagent has been reported[27] to convert reactive alkyl halides such as benzyl and allyl chlorides, alkyl bromides, and iodides into primary amines. We were able to expand its utility to the amination of the alkyl chloride moieties employed

here, by performing the amination in the presence of a crown ether. The more reactive poly(ferrocenyl(3-bromopropyl)methylsilane) **3a** can be converted into polycation **5** using lithium 1,1,3,3-tetramethyldisilazide, in the presence of dimethyl sulfoxide.

In case of functionalization by soft nucleophiles, poly(ferrocenyl(3-iodopropyl)methylsilane) **3b** is a suitable starting material. Malonic ester enolates such as dimethyl methylmalonate anion or dibenzyl methylmalonate anion smoothly react to produce the corresponding polyesters with quantitative conversions. By using hydrolytically labile ester enolates, such as methyl trimethylsilyl methylmalonate anion,[28] one can easily convert the corresponding pendent ester groups into carboxylate salts, thus forming an organometallic polyanion[20] (see Scheme 3).

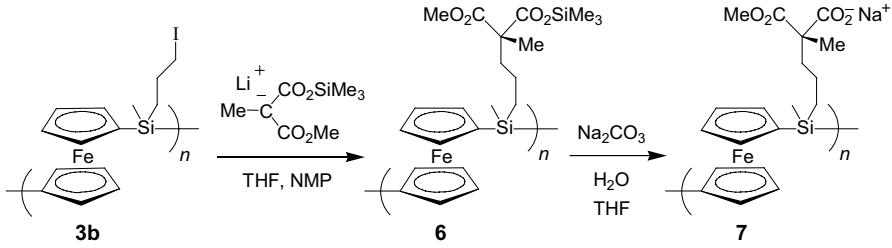

Scheme 3 Synthesis of a polyferrocenylsilane polyanion.[20]

Polyanion **7** is, to our knowledge, the first reported organometallic polyanion. The material is highly water soluble: it could be dissolved to concentrations exceeding 100 mg/mL. It must be noted that the solubility of the polyanion, which is a weak polyelectrolyte, decreases below pH 6.[29] In conclusion, a universal route to functionalized polyferrocenylsilanes, using nucleophilic substitution reactions, enabled us to produce water-soluble polyferrocenylsilane polycations and polyanions.

III. POLYMER CHARACTERIZATION

^{1}H and ^{13}C NMR spectroscopy support the high efficiency of the side-group modifications. As an example, the ^{13}C NMR spectrum of **7** is shown in Figure 1. No signals associated with residual iodopropyl moieties could be identified in the spectrum. In addition, elemental analysis of all polymers had excellent agreement between the expected and measured compositions. Polymers **2**, **3a**, and **3b** were characterized using gel permeation chromatography (GPC) in THF, using polystyrene standards, to ensure that no molar mass decline had occurred during the halogen exchange reaction. On the basis of GPC, polyferrocenylsilanes **2** and **3a**,**b** have a degree of polymerization $DP_n = 80$ and a polydispersity of $M_w/M_n = 1.8–1.9$. GPC measurements on polycation **5** and polyanion **7** had to be carried out in water, precluding a direct comparison with their precursors, but the corresponding GPC traces showed a single maximum, indicating that the organometallic mainchain had remained intact.

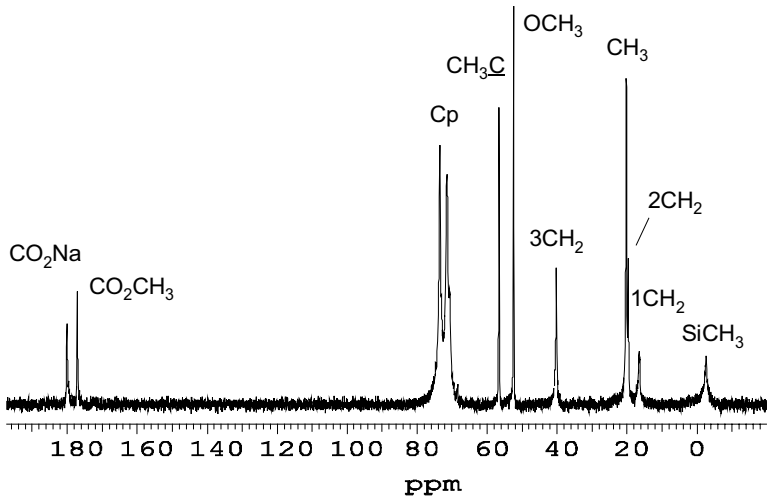

Figure 1 ^{13}C NMR spectrum of the polyferrocenylsilane polyanion **7** in D_2O. [Reproduced with permission from Ref. 20, © 2002 American Chemical Society (ACS).]

Polymers **5** and **7** were furthermore studied by viscometry in ultrapure water, in the absence of salt. As an example, values of the reduced viscosity, η_{sp}/C of **7** are plotted against polymer concentration C. For both polymers, the reduced viscosity increased strongly with decreasing polymer concentrations, exhibiting a pronounced concave-upward relationship (η_{sp} is the specific viscosity) (see Fig. 2). This behavior is typical of polyelectrolytes.[30]

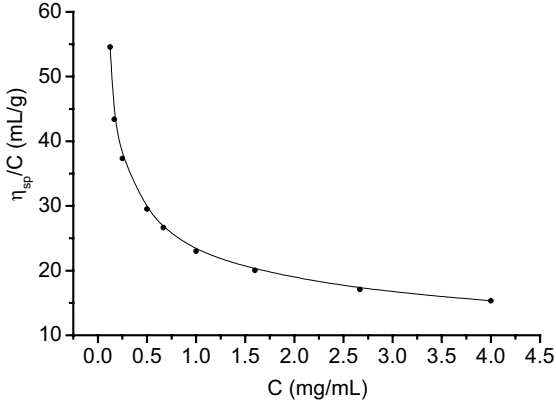

Figure 2 Reduced viscosity η_{sp}/C as a function of the concentration of polyanion **7** in salt-free water. (Reproduced with permission from Ref. 20, © 2002 ACS.)

IV. MULTILAYER CHARACTERIZATION

UV/Vis absorption spectroscopy was used to monitor the electrostatic self-assembly of the organometallic polyions. The increase in absorption at $\lambda_{max}=216$ nm as a function of the number of bilayers deposited on quartz slides is shown in Figure 3. An essentially linear dependence was found, with possibly a slight decrease in the amount of polyelectrolyte depositing per cycle as the number of bilayers approaches 20, but overall giving evidence for a well-defined deposition process.[31]

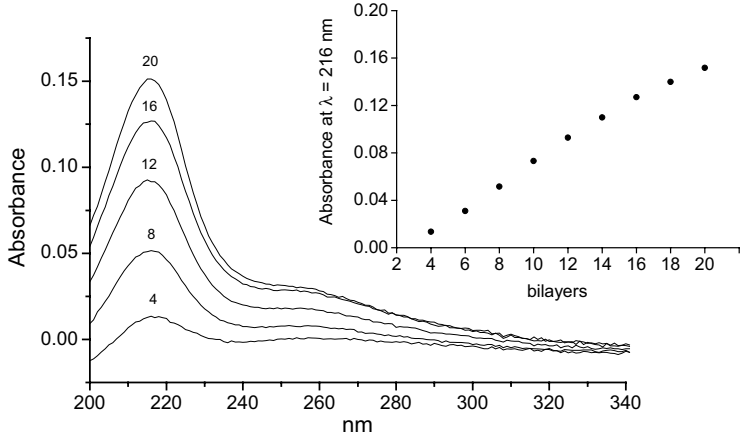

Figure 3 UV/Vis absorption spectra of sequentially adsorbed layers of polyferrocenylsilane polycation **5** and polyanion **7** on quartz.

Information on the increase of film thickness with the number of bilayers was obtained also from ellipsometry. Thickness measurements on the films, built up on silicon wafers, were carried out after each bilayer deposited. In Figure 4, ellipsometric spectra are shown for a bare substrate (solid lines) and after deposition of 3, 6, and 9 bilayers (dashed, dotted, and dashed–dotted lines, respectively). The ellipsometric angles Ψ and Δ are related to amplitude and phase changes, respectively, on reflection of elliptically polarized light on a planar surface.

With an increasing number of bilayers there is only a very small change in $\tan(\Psi)$, while the change in $\cos(\Delta)$ is much more substantial. This is in agreement with the fact that the phase contribution to the ellipsometric parameter $\rho=r_p/r_s=\tan(\Psi)\exp(i\Delta)$, is much more sensitive than the intensity contribution, in the case of very thin films.[32] The variation in $\tan(\Psi)$ and $\cos(\Delta)$ is approximately uniform over the measurement range, indicating that the multilayer film has a wavelength-independent refractive index for the investigated spectral domain.

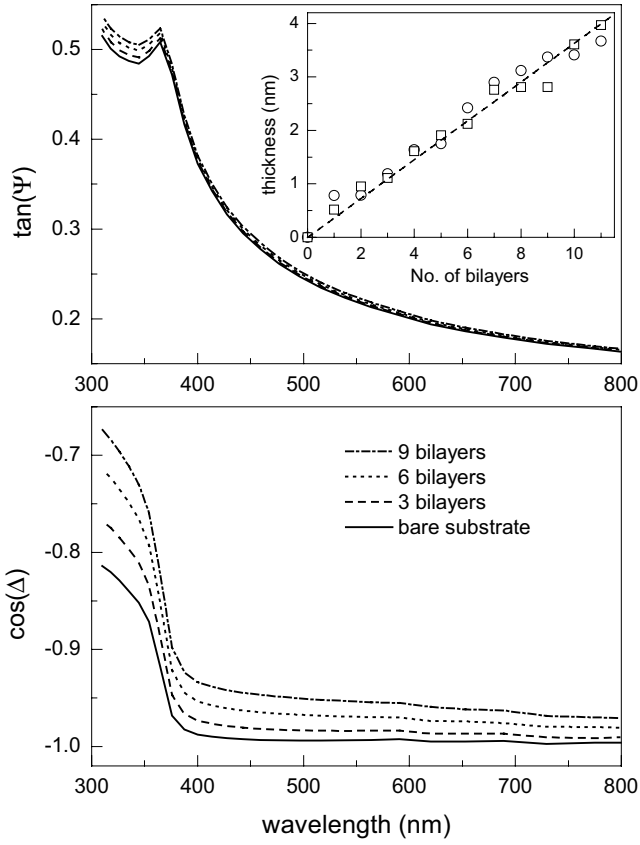

Figure 4 Ellipsometric spectra of 3, 6, and 9 polyferrocenylsilane bilayers (**5**/**7**) on silicon. The symbols ○ and □ represent two parallel deposition experiments.

The fitted multilayer thickness as a function of the number of deposited bilayers is shown in Figure 4, demonstrating that the thickness of the film is linearly related to the number of deposited bilayers, in accordance with the UV–Vis absorption spectroscopy results. The dashed line is a fit through the origin and indicates a thickness contribution of about 0.4 nm per bilayer. This result is influenced by the refractive index. Previously, combined ellipsometry and profilometry measurements led to a refractive index value of $n=1.687$ for spin-coated polyferrocenyldimethylsilane films on silicon wafers, and this value was also used for the polyferrocenylsilane multilayer thin films. However, the refractive index might be somewhat lower in this case, implying that the thickness contribution of 0.4 nm per bilayer we found could be a slight underestimate.

The elemental composition of the organometallic multilayer thin film (20 bilayers of **5** and **7** on quartz) was determined using X-ray photoelectron spectroscopy (XPS). The survey scan, shown in Figure 5, indicates the presence of all expected elements in the thin film. Atomic concentrations of the polyferrocenylsilane multilayer thin film are given in Table 1.

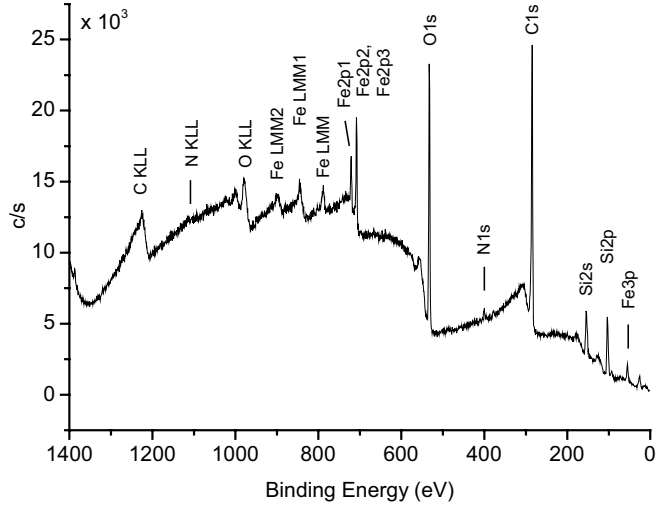

Figure 5 XPS survey spectrum of a multilayer thin film (20 bilayers) composed of polyferrocenylsilane polyions **5** and **7**.

Table 1 XPS Atomic Percentages of the Elements of a Polyferrocenylsilane Multilayer Thin Film $(\mathbf{5}/\mathbf{7})_{20}$ on Quartz

Element	Atom % (Found)	Binding Energy (eV)
C 1*s*	64.58	284.8[a]
N 1*s*	1.38	400.3
O 1*s*	19.66	532.5
Fe 2*p*	3.30	708.0
Si 2*p*	3.35	101.0[b]

[a]C 1*s* CO_2R 289.5 eV.
[b]Si 2*p* quartz 103.6 eV.

An experimental composition of a bilayer repeat unit $C_{39}N_{0.84}Fe_2Si_2$ was found, which agrees to within experimental error with the expected composition $C_{33}H_{43}NO_4Fe_2Si_2$. The oxygen signal in XPS spectra of these ultrathin films is dominated by contributions from the underlying quartz substrate.

Polyferrocenylsilanes are redox-active materials, showing fully reversible electrochemical oxidation and reduction.[1] A typical voltammogram shows two oxidation waves, indicating intermetallic coupling between neighboring iron centers in the polymer chain. The first oxidation wave was attributed to oxidation of ferrocene centers having neutral neighboring units. In the second wave, at higher potentials, oxidation of the remaining ferrocene centers, predominantly in positions next to oxidized units, is completed.[33–35] Thus, the charge ratio between the two oxidation peaks is approximately 1:1.

Multilayer films composed of polyferrocenylsilane polyions obtained by electrostatic self-assembly are of potential interest as ultrathin electroactive coatings, as one has accurate control over film thickness and redox surface concentration. In order to study the redox behavior of these thin films, multilayers were fabricated on gold electrodes. Stable multilayers were obtained by first adsorbing a sodium 3-mercapto-1-propanesulfonate monolayer on Au, producing a negatively charged surface that is ideally suited for polyion adsorption.[15] Cyclic voltammograms of the organometallic multilayer thin films were recorded for samples having an increasing number of bilayers (1–7), to monitor the electrochemical response as the surface concentration of redox sites increased. The CVs of thin films composed of 1, 3, and 6 bilayers (Fig. 6) show the two oxidation and reduction waves typical of polyferrocenylsilanes. Integration of the voltammetric peaks allows one to calculate the charge involved in the redox processes. From this the surface coverage Γ of ferrocene units can be obtained, using the relation $\Gamma = Q/nFA$, where Q is charge, n is the number of exchanged electrons ($n = 1$ in this case), F is Faraday's constant (96485 C/mol), and A is the electrode surface area employed in the measurements (0.44 cm^2).[36] Using this relation, one organometallic bilayer was found to correspond to a ferrocene surface coverage of 0.45 ferrocene units/nm^2. The surface coverage Γ (ferrocene units/nm^2) increased linearly with the number of bilayers.

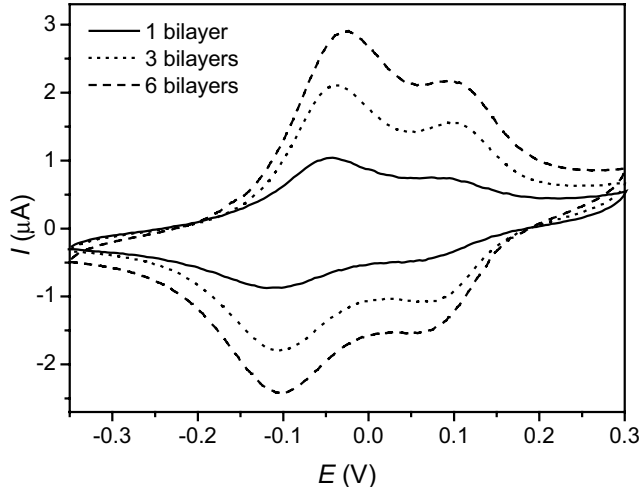

Figure 6 Cyclic voltammogram of 1, 3, and 6 organometallic bilayers (**5**/**7**), deposited on a gold electrode featuring a monolayer of sodium 3-mercapto-1-propanesulfonate. Scan rate $v = 30$ mV/s. (Reproduced with permission from Ref. 17, © 2002 ACS.)

V. PATTERNED POLYFERROCENYLSILANE MULTILAYER THIN FILMS

In addition to producing continuous fully organometallic multilayer thin films, we were interested in forming patterned organometallic multilayer

structures, specifically, to confine the deposition of the polyferrocenylsilane polyelectrolytes to selected areas on substrates, as this would broaden the applicability of such multilayers.[37] The selective deposition of polyelectrolytes on hydrophilically/hydrophobically patterned gold substrates has been described.[38,39] In this case, patterned self-assembled monolayers consisting of, for instance, methyl-terminated and oligo(ethyleneglycol)-terminated alkanethiols were introduced on gold substrates, using microcontact printing.[40] Areas covered with oligo(ethyleneglycol)-terminated alkanethiols were found to prevent adsorption of polyelectrolytes. Here, as a demonstration, a gold substrate was patterned with 5 μm wide methyl-terminated alkanethiol lines, separated by 3 μm, by microcontact printing of 1-octadecanethiol. The uncovered areas were subsequently filled in with 11-mercapto-1-undecanol, resulting in a hydrophilically/hydrophobically patterned substrate. AFM height and friction force images of these patterned self-assembled monolayers (Fig. 7a,b) show minimal height contrast but a large contrast in friction force, with the hydroxyl-terminated lines corresponding to the high friction areas.

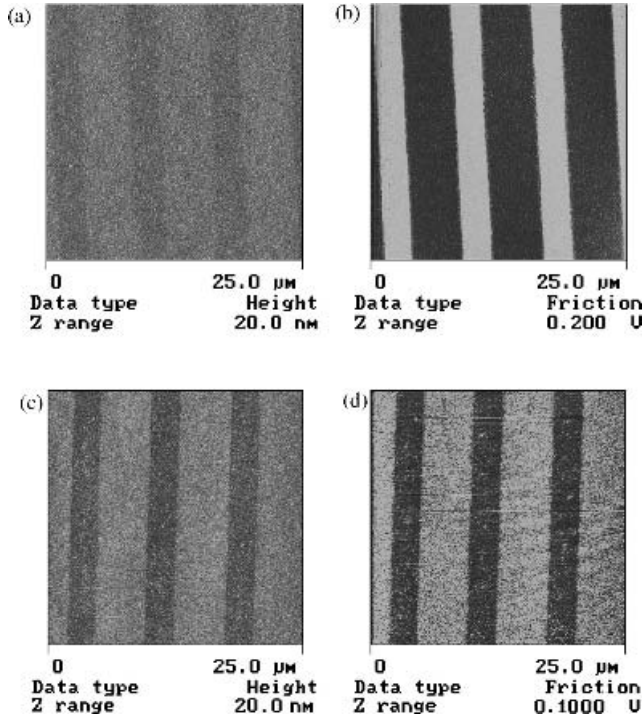

Figure 7 Multilayer deposition on a hydrophilically/hydrophobically patterned gold substrate. Upper AFM images: height (a) and friction force (b) images of patterned methyl- and hydroxyl- alkanethiol self-assembled monolayers. Adsorption of polyferrocenylsilane polyions (**5**/**7**, 12 bilayers) occurs selectively on the broad methyl-terminated stripes (c,d). (Reproduced with permission from Ref. 17, © 2002 ACS.)

The patterned substrate was then coated with 12 bilayers of organometallic polyions (**5**/**7**) and again examined by contact-mode AFM. Clearly, after deposition, the height contrast increased and the contrast in friction force was reversed, which shows that the multilayers grow selectively on the broad, methyl-terminated stripes (Fig. 7c,d).[17,41]

Resistivity of the hydroxyl-terminated areas to polyion deposition was demonstrated by forming a monolayer of 11-mercapto-1-undecanol on a gold substrate, which was then processed similarly as the patterned substrates, and subsequently analyzed by XPS. Fe 2*p* signals, indicating adsorbed polyions, were absent in the survey scan. The selective adsorption of the polyions on the methyl-terminated regions of the surface is most likely driven by favorable hydrophobic interactions between these areas and the hydrophobic polyferrocenylsilane backbone. Such favorable secondary interactions[42] with the hydrophilic regions are excluded. Furthermore, the charged segments of the polyions cannot compete with water in forming hydrogen bonds with the hydroxyl-terminated regions, which are hydrated under the processing conditions.[43] Thus, deposition occurs selectively on the methyl-terminated domains.

Further support for the role of hydrophobic interactions in the area-selective adsorption was obtained by reversing the dipping sequence. A single bilayer was adsorbed on a methyl- and hydroxyl-terminated stripe pattern (10 and 5 μm, respectively), in one case starting with the polycation, in the other case with first adsorbing the polyanion. Both substrates were subsequently analyzed by AFM in contact mode. The friction force images (Fig. 8) clearly show a reversal in contrast for both experiments, compared with the template without the polymers, indicating that in both cases one bilayer had been deposited selectively on the methyl-terminated areas.

VI. SUMMARY

A universal synthetic route to functional polyferrocenylsilanes, enabling us to produce water-soluble polyferrocenylsilane polycations/anions, is described. The polyferrocenylsilane polyions were successfully processed to novel, fully organometallic multilayer thin films. Furthermore, these organometallic polyions, featuring a hydrophobic backbone, enable one to make use of both electrostatic and hydrophobic interactions for manufacturing self-organized patterns on templated substrates. We demonstrated that adsorption of the polyions on hydrophilically/hydrophobically patterned substrates led to the formation of laterally structured polyferrocenylsilane multilayers. The hydroxyl-terminated monolayer regions used in this study prevent deposition of the polyions as a result of hydrogen bonding interactions with the solvent. We showed, using AFM friction force imaging of single bilayers, that the dipping sequence plays no role in the selectivity of the adsorption process.

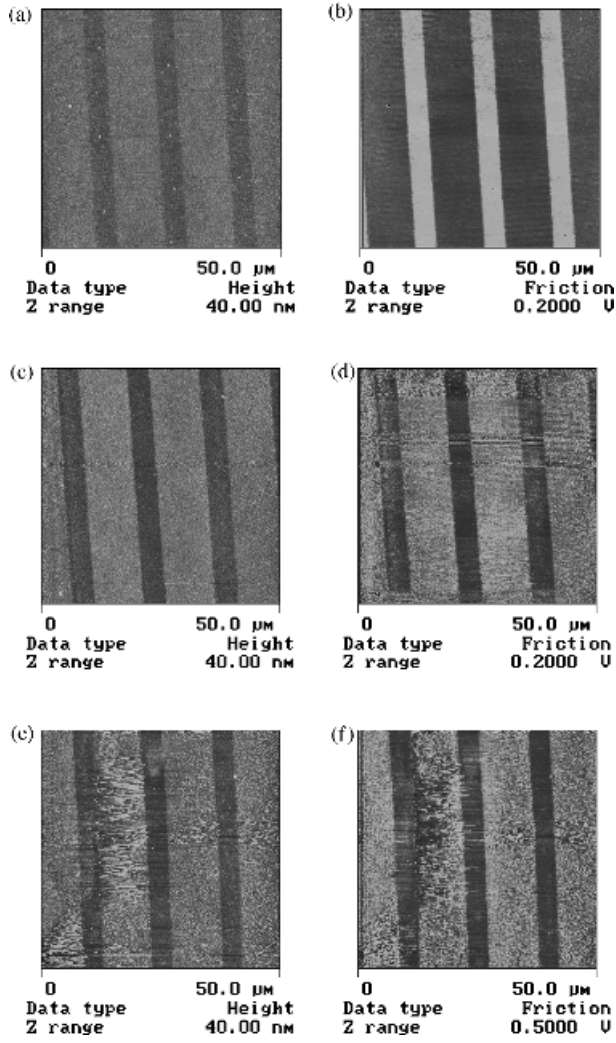

Figure 8 AFM height (a) and friction force (b) images of the hydrophilically (5 µm)/ hydrophobically (10 µm) patterned substrate and of single organometallic bilayers adsorbed on this prepatterned substrate. Adsorption sequence: cation–anion (c,d), anion–cation (e,f). In both cases the bilayer is selectively adsorbed on the hydrophobic areas. (Reproduced with permission from Ref. 17, © 2002 ACS.)

VII. EXPERIMENTATION

Multilayers (up to 20 bilayers) of polyions **5** and **7** were deposited on quartz, enabling the monitoring of film growth by UV/Vis absorption spectroscopy. UV/Vis spectra were recorded on a Varian Cary 300 Bio instrument in double-beam mode,

using an uncovered quartz slide as reference. XPS spectra were obtained on a Quantum 2000 Scanning ESCA Microprobe (Physical Electronics, Inc.), using monochromatic Al K_α (1486.6 eV) X-rays. The X-ray power was set at 25 W, the angle of detection was 45° with respect to the sample surface. Spectroscopic ellipsometry[32,44] was used to measure the thickness of the organometallic multilayers as a function of the number of bilayers. Multilayer films were deposited in parallel on two silicon substrates containing a thin oxide layer, and analyzed using a home-built spectroscopic ellipsometer (rotating polarizer–analyzer configuration) equipped with a xenon lamp and a scanning monochromator. Spectra were obtained in the visible region of the spectrum at wavelengths between 300 and 800 nm at a fixed incident angle of 70°. Optical measurements were performed after deposition of every bilayer on the same substrate, without changing the alignment and calibration of the ellipsometer. The spectra of the bare substrate were analysed in terms of a three-layer model,[44] consisting of a silicon substrate (with complex refractive index $\tilde{n}_{Si}(\lambda)=n_{Si} + ik_{Si}$),[45] and a silicon oxide layer with unknown thickness d_{ox} (with refractive index $n_{SiO_2}(\lambda)$),[46] in contact with air ($n=1$). By fitting to this model we obtained an oxide thickness $d_{ox}=1.4$ nm. The thickness of the bilayer assemblies was obtained by fitting the spectra to a four-layer model consisting of a silicon substrate [with $\tilde{n}_{Si}(\lambda)=n_{Si} + ik_{Si}$],[45] a silicon oxide layer with thickness $d_{ox}=1.4$ nm [refractive index $n_{SiO_2}(\lambda)$],[46] a PFS layer with thickness d_{PFS} and refractive index $n=1.687$ (determined previously by profilometry and ellipsometry), again in contact with air ($n=1$). Scanning force microscopy (SFM) measurements were performed with a NanoScope III AFM [Digital Instruments (DI), Santa Barbara, CA, USA] in contact mode. Images were obtained in air, using triangular Si_3N_4 cantilevers with a spring constant of 0.32 N/m.

VIII. ACKNOWLEDGMENT

The University of Twente, the MESA$^+$ Research Institute and IAESTE (N. R.) are gratefully acknowledged for financial support.

IX. REFERENCES

1. For a review on polyferrocenylsilanes, see K. Kulbaba, I. Manners, *Macromol. Rapid Commun.* **22,** 711 (2001).
2. Y. Ni, R. Rulkens, I. Manners, *J. Am. Chem. Soc.* **118,** 4102 (1996).
3. M. Péter, R. G. H. Lammertink, M. A. Hempenius, M. van Os, M. W. J. Beulen, D. N. Reinhoudt, W. Knoll, G. J. Vancso, *Chem. Commun.* 359 (1999).
4. R. G. H. Lammertink, M. A. Hempenius, V. Z. -H. Chan, E. L. Thomas, G. J. Vancso, *Chem. Mater.* **13,** 429 (2001).
5. R. G. H. Lammertink, M. A. Hempenius, E. L. Thomas, G. J. Vancso, *J. Pol. Sci. Part B, Pol. Phys.* **37,** 1009 (1999).

6. R. G. H. Lammertink, M. A. Hempenius, J. E. Van den Enk, V. Z. -H. Chan, E. L. Thomas, G. J. Vancso, *Adv. Mater.* **12,** 98 (2000).
7. J. Y. Cheng, C. A. Ross, V. Z. -H. Chan, E. L. Thomas, R. G. H. Lammertink, G. J. Vancso, *Adv. Mater.* **13,** 1174 (2001).
8. E. W. Neuse, F. B. D. Khan, *Macromolecules* **19,** 269 (1986).
9. S. Kelch, M. Rehahn, *Macromolecules* **32,** 5818 (1999).
10. K. N. Power-Billard, I. Manners, *Macromolecules* **33,** 26 (2000).
11. M. A. Hempenius, N. S. Robins, R. G. H. Lammertink, G. J. Vancso, *Macromol. Rapid Commun.* **22,** 30, (2001).
12. G. Decher, *Science* **277,** 1232 (1997).
13. P. Bertrand, A. Jonas, A. Laschewsky, R. Legras, *Macromol. Rapid Commun.* **21,** 319 (2000).
14. A. Wu, D. Yoo, J. -K. Lee, M. F. Rubner, *J. Am. Chem. Soc.* **121,** 4883 (1999).
15. J. Hodak, R. Etchenique, E. J. Calvo, K. Singhal, P. N. Bartlett, *Langmuir* **13,** 2708 (1997).
16. J. Sun, Y. Sun, S. Zou, X. Zhang, C. Sun, Y. Wang, J. Shen, *Macromol. Chem. Phys.* **200,** 840 (1999).
17. M. A. Hempenius, M. Péter, N. S. Robins, E. S. Kooij, G. J. Vancso, *Langmuir* **18,** 7629 (2002).
18. M. Ginzburg, J. Galloro, F. Jäkle, K. N. Power-Billard, S. Yang, I. Sokolov, C. N. C. Lam, A. W. Neumann, I. Manners, G. A. Ozin, *Langmuir* **16,** 9609 (2000).
19. M. A. Hempenius, M. Péter, E. S. Kooij, R. G. H. Lammertink, G. J. Vancso, Abstract ACS, *PMSE Preprint* **223,** 252, PMSE Part 2, April 7, 2002.
20. M. A. Hempenius, G. J. Vancso, *Macromolecules* **35,** 2445 (2002).
21. (a) A. Wu, J. Lee, M. F. Rubner, *Thin Solid Films* **327–329,** 663 (1998). (b) P. K. H. Ho, M. Granström, R. H. Friend, N. C. Greenham, *Adv. Mater.* **10,** 769 (1998).
22. W. S. Beh, I. T. Kim, D. Qin, Y. Xia, G. M. Whitesides, *Adv. Mater.* **11,** 1038 (1999).
23. S. L. Clark, E. S. Handy, M. F. Rubner, P. T. Hammond, *Adv. Mater.* **11,** 1031 (1999).
24. K. S. Schanze, T. S. Bergstedt, B. T. Hauser, C. S. P. Cavalaheiro, *Langmuir* **16,** 795 (2000).
25. M. A. Hempenius, N. S. Robins, R. G. H. Lammertink, G. J. Vancso, *IUPAC MACRO 2000 Proc.*, Vol. 2, Warsaw, July 2000, p. 900.
26. W. E. Willy, D. R. McKean, B. A. Garcia, *Bull. Chem. Soc. Japan* **49,** 1989 (1976).
27. S. Itsuno, T. Koizumi, S. Okumura, K. Ito, *Synthesis* 150 (1995).
28. J. W. F. K. Barnick, J. L. van der Baan, F. Bickelhaupt, *Synthesis* 787 (1979).
29. D. Yoo, S. S. Shiratori, M. F. Rubner, *Macromolecules* **31,** 4309 (1998).
30. R. M. Fuoss, *J. Polym. Sci.* **3,** 603 (1948).
31. M. Ferreira, J. H. Cheung, M. F. Rubner, *Thin Solid Films* **244,** 806 (1994).
32. R. M. A. Azzam, N. M. Bashara, *Ellipsometry and Polarized Light*, North-Holland, Amsterdam, 1987.
33. R. Rulkens, A. J. Lough, I. Manners, *J. Am. Chem. Soc.* **116,** 797 (1994).
34. D. A. Foucher, C. H. Honeyman, J. M. Nelson, B. Z. Tang, I. Manners, *Angew. Chem. Int. Ed. Engl.* **32,** 1709 (1993).
35. D. Foucher, R. Ziembinski, R. Petersen, J. Pudelski, M. Edwards, Y. Ni, J. Massey, C. R. Jaeger, G. J. Vancso, I. Manners, *Macromolecules* **27,** 3992 (1994).
36. (a) R. W. Murray, in *Electroanalytical Chemistry*, A. J. Bard, ed., Marcel Dekker, New York, Vol. 13, 1984, pp. 191–368; (b) H. O. Finklea, in *Electroanalytical Chemistry*, A. J. Bard, I. Rubinstein, eds., Marcel Dekker, New York, Vol. 19, 1996, pp. 109–335.
37. G. Decher, B. Lehr, K. Lowack, Y. Lvov, J. Schmitt, *Biosens. Bioelectron.* **9,** 677 (1994).
38. P. T. Hammond, G. M. Whitesides, *Macromolecules* **28,** 7569 (1995).
39. S. L. Clark, P. T. Hammond, *Adv. Mater.* **10,** 1515 (1998).

40. Y. Xia, G. M. Whitesides, *Angew. Chem. Int. Ed.* **37,** 550 (1998).
41. The first example of a patterned heterostructured organometallic multilayer film, fabricated from **5** and poly(sodium vinylsulfonate) on a substrate featuring CH3- and OH-terminated alkanethiol monolayer areas, appeared on the cover of *Macromol. Rapid Commun.* **22**(1)**,** 2001.
42. S. L. Clark, P. T. Hammond, *Langmuir* **16,** 10206 (2000).
43. M. Sprik, E. Delamarche, U. Rothlisberger, M. L. Klein, H. Wolf, H. Ringsdorf, *Langmuir* **10,** 4116 (1994).
44. H. G. Tompkins, W. A. McGahan, *Spectroscopic Ellipsometry and Reflectometry: A User's Guide*, J. Wiley, New York, 1999.
45. D. F. Edwards, in *Handbook of Optical Constants of Solids*, E. D. Palik, ed., Academic Press, Orlando, FL, 1985, pp. 563–565.
46. H. R. Philipp, in *Handbook of Optical Constants of Solids*, E. D. Palik, ed., Academic Press, Orlando, FL, 1985, pp. 728–729.

CHAPTER 7

Metal-Containing Polymers for High-Performance Resist Applications

Rob G. H. Lammertink, Igor Korczagin, Mark A. Hempenius, and G. Julius Vancso

University of Twente, MESA$^+$ Research Institute, Enschede, The Netherlands

CONTENTS

Macromolecules Containing Metal and Metal-like Elements, Volume 2: Organoiron Polymers, Edited By Alaa S. Abd-El-Aziz, Charles E. Carraher, Jr., Charles U. Pittman, Jr., John E. Sheats, and Martel Zeldin
ISBN 0-471-45078-2

I. INTRODUCTION

Optical lithography remains the predominant technology for device manufacturing in the semiconductor industry. As feature dimensions continue to decrease, more and more performance is required from the resist formulations used. Here, special attention is directed to resists that are used for mask fabrication. For such applications, contamination by metallic impurities is not an issue. Two main types of polymeric resists have been widely applied: (1) especially for e-beam (electron-beam) lithography, the resist functions by a chain scission process; and (2) for both e-beam and UV lithography, the resist functions by a deprotection reaction. The development of e-beam resist systems used for photomask fabrication has been directed to improve the sensitivity, resolution, and etch resistance of the material.[1] Driven by strong demand, there has been major interest in materials and composites beyond organic species. Current progress in metal containing macromolecule synthesis may in principle result in advancement of high-performance resist materials.

Within microfabrication technology, materials science and particularly polymer chemistry has been of utmost importance. The demand is driven by a single reason: scale. Electronic systems are rapidly moving toward small, fast, and high-density information storage devices. As early as 1959, Richard Feynman addressed the possibility of manipulating matter on small scales.[2]

The lithographic process (Fig. 1) fabricates patterns in two steps.[3] First the pattern is delineated into a radiation sensitive thin film called a *resist*. This step is followed by pattern transfer into the underlying substrate by an appropriate etching technique, such as reactive ion etching.

In the following sections, we briefly review the resist technologies that are available, with a particular focus on e-beam resists. The reason for this is that complications may arise from the use of metal containing resists for microelectronic fabrication. E-beam lithography is typically used for fabrication of photomasks, in which metallic impurities are not relevant.

II. ORGANIC RESISTS

A classical example of a chain scission resist is poly(methyl methacrylate) (PMMA) (see Scheme 1).[1] The high molecular weight PMMA resist undergoes chain scission induced by e-beam radiation. The low molecular weight fractions in the exposed areas are soluble in the developer, resulting in positive-tone features.

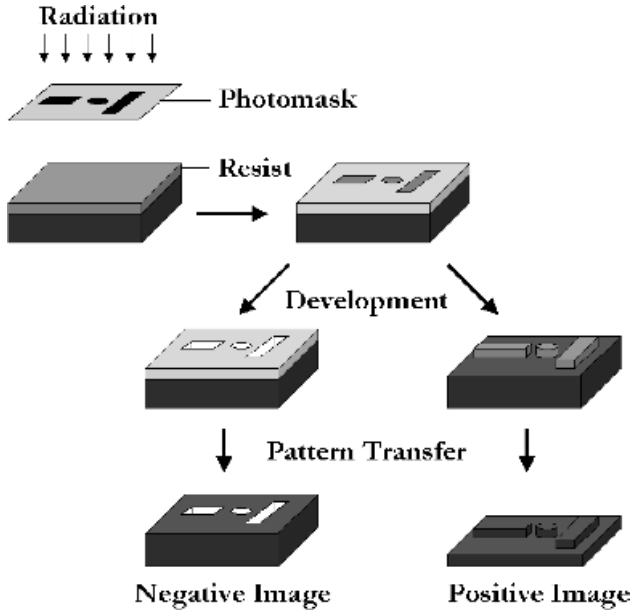

Figure 1 Illustration of the lithographic process.

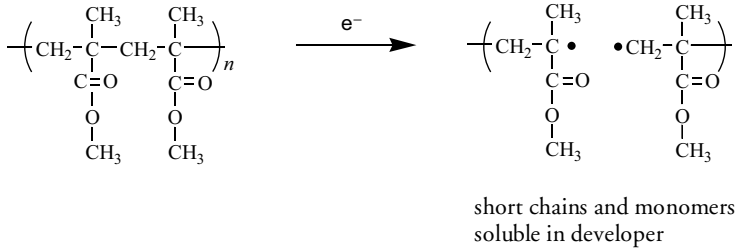

Scheme 1 Chain scission mechanism for PMMA e-beam resists.

The majority of semiconductor fabrication processes exploits diazonaphthoquinone (DNQ)-based photoresists for light-exposure-based lithography.[4] The photoactive DNQ is dispersed in a phenolic matrix resin, also known as *Novolac*, and acts as a dissolution inhibitor for the matrix. Irradiation of the hydrophobic DNQ results in its transformation into hydrophilic indenecarboxylic acid. A tremendous amount of research has been directed toward designing organic materials for high-resolution imaging, using light sources with decreasing wavelengths.[5–8] These purely organic materials are being used for pattern transfer to fabricate microelectronic devices. Such applications are sensitive to contamination by metallic impurities. Although this area receives considerable attention both from academia as well as

industry, it is not the scope of this chapter. Instead the reader is referred to excellent general reviews in the literature.[9,10]

For e-beam resists, there have been several reports of new materials. For example, in order to circumvent the disadvantages of polydisperse polymer systems, calixarenes have been employed as negative resists.[11] E-beam resists consisting of liquid crystals have also been reported, based on polysubstituted derivatives of triphenylene.[12] Patterns of approximately 14 nm were defined using these materials.

A. Chemical Amplification

In contrast to chain scission, chemical amplification (CA) employs an acid catalyzed deprotection or crosslinking reaction, which changes the solubility of the resist in the exposed areas. Therefore, a typical CA resist consists of a matrix polymer and a photoacid generator (PAG).[13] The PAG is converted into a strong acid on absorption of a photon. The acid catalyzes the deprotection or crosslinking reaction and is regenerated (Scheme 2), which explains the amplification effect in the system. A variety of acid generator chemistries are available, both ionic and nonionic, but are not considered here.

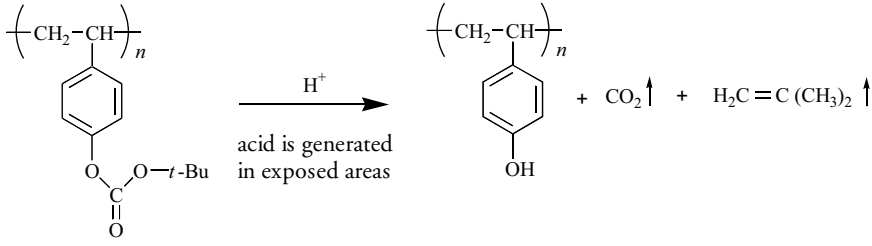

Scheme 2 Example of a chemically amplified resist scheme.

The chemically amplified resist mechanism was the breakthrough that ultimately led to the next generation of 248-nm lithography. The initial work by Ito and Willson[14] employed the acid labile *tert*-butyloxycarbonyl (*t*-BOC) group. The acid catalyzes the decomposition of the *t*-BOC groups, and thereby modifies the chemical composition. Several different trajectories can be followed from here, leading to both positive and negative tone resists.

The CA resists are suitable candidates for introducing inorganic constituents into resist systems. Functional groups, generated in exposed areas, react in a subsequent step with, for instance, a silylating agent.[15] A silicon-containing material exhibits a high-oxygen-plasma etch resistance. Such photoresists can therefore be developed by a plasma. Besides silicon, a variety of other inorganic elements, such as tin,[16] germanium,[17] or titanium,[18] can be employed to selectively alter the etch resistance.

Contrary to organic polymers, inorganic materials form products with very reduced, or no volatility when treated with an oxygen plasma. Therefore, their removal takes place via sputtering processes only.

III. INORGANIC RESISTS

Although PMMA is the most commonly used e-beam resist,[19] it suffers from poor resistance to most etching processes.[1] Inorganic resists seem to be promising materials for $<$10-nm pattern fabrication.[20] When films of metal halides are exposed to high-energy electron-beam irradiation, these resists undergo radiolysis.[21] As this dissociation takes place in a high vacuum, the resist becomes volatile in the exposed regions, resulting in a positive-tone resist. Alternatively, if the exposure is done at lower doses and/or at lower vacuum, the metal halide films may act as negative resists. In this case, the irradiation causes a difference in dissolution rates between exposed and unexposed areas in an appropriate developer. A series of metal halides provided better resolution than did PMMA.[22] Furthermore, high etch resistance was observed in fluorine-containing plasmas.[23] The stress in the deposited films was an important parameter for these metal fluoride resists.

Another approach reported the use of fullerene C_{60} films as e-beam resist.[24] The irradiation of a C_{60} film was found to reduce the dissolution rate in organic solvents. Furthermore, the inorganic films have higher dry etch resistance compared to conventional Novolac resists.

IV. ORGANIC–INORGANIC COMPOSITE RESISTS

Employing composites of organic and inorganic components represents a novel trend in the design of resists.[25] In order to accommodate the fabrication of small features, at least one of the components needs to be structured on a nanoscale level. The bottleneck for preparing such nanocomposites lies in the tailoring of the surface and interfaces of the components, such that a homogeneous dispersion is obtained.

Approaches involving nanocomposite resists benefit from higher softening temperatures and increased rigidity, thereby reducing the probability of pattern collapse. Furthermore, increased etch resistance is also warranted.

The plasma etch rates of nanocomposites, consisting of PMMA resists, impregnated with C_{60} fullerenes, were compared with those of commercially available resists.[26] Fullerenes were found to be successful at improving the etch resistance under CF_4 and Cl_2 reactive ion etch conditions. The basic idea of this concept is the reduction of free volume in the polymer resist film. This then results in improved mechanical and etch resistance.

The addition of silica particles to the polymer resist resulted in a higher etch resistance to plasma etching with O_2 gas.[25,27] Furthermore, when using electron-beam

lithography, the nanocomposite was shown to drastically reduce the electron proximity effect, which fundamentally results from the interactions of electrons with polymers.[28]

Molecular silica cages, such as polyhedral oligomeric silsesquioxanes (POSSs), were incorporated into organic polymer backbones.[29] By optimizing the polymer composition the contrast could be maximized, while a sensitivity comparable to that of standard PMMA was maintained.

The same molecular silica cage was incorporated into chemically amplified resists, using TBMA as the deblocking component, in order to improve resist performance.[30] Methacrylate resists for 193-nm lithography have been successful in terms of sensitivity and resolution, but generally lack the reactive ion etching resistance required for the subsequent pattern transfer. Again, the incorporation of inorganic moieties, namely, oligosilsesquioxane, proved to be effective in improving the RIE resistance when using an oxygen plasma source.[30]

A bilayer resist consisting of hydrogen silsesquioxane and Novolac was investigated for fabricating high-aspect-ratio structures.[31] In the bilayer combination, the silicon-containing top layer allowed nanoscale structures with aspect ratios exceeding 15 to be etched into the hard-baked Novolac bottom layer.

Recently, a true nanocomposite was reported,[32] incorporating 1–2-nm silica particles into a commercial e-beam resist, namely, ZEP520 [poly(α-chloro acrylate-co-α-methyl styrene]. The surface of the silica particles was chemically pretreated to promote their compatibility with the resist. In another study, in which the concept of encapsulated inorganic resist technology (EIRT) was proposed,[33] 8–10-nm colloidal silica particles were dispersed in another commercial resist. It was shown that high degrees of loading could be obtained and that 150-nm imaging was still feasible.[34]

In an almost purely inorganic approach, surfactant stabilized metal or bimetal clusters were irradiated with electron beams directly, leading to a partial destruction of the organic stabilizer.[35] The unexposed colloids and the destroyed organic stabilizers were then removed under ultrasonic rinsing.

V. ORGANOMETALLIC POLYMERS

Organometallic species seem attractive candidates to enhance the etch resistance of a resist. Particularly, such materials can be used for maskmaking applications, where contamination by metallic impurities is not a problem.

Previously, incorporation of organometallic functionalities into resist materials showed a great enhancement of the etch resistance of the resist.[1] The incorporation can be accomplished either by direct covalent attachment or by blending the organometallic additives into the resist matrix. Blending may be limited by miscibility problems or inadequate solubility.

A series of organometal-containing polysulfones were studied to improve the poor stability of poly(olefin sulfone) resists that have been used for e-beam lithography (Scheme 3).[36] It was found that the germanium containing poly(*p*-(trimethylgermyl)styrene sulfone) possessed a higher etch resistance compared to the silane containing poly(*p*-(trimethylsilyl)styrene sulfone).

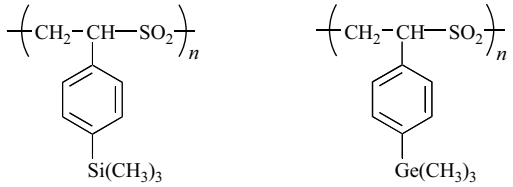

Scheme 3 Organometal-containing polysulfones for e-beam resists.

To manufacture deep structures in a device, plasma etching requires the presence of a thick perpendicularly structured resist layer, unless the etch resistance of the resist is far greater then that of the substrate. Thick resist layers suffer from a variety of problems, especially when they are employed for high-resolution lithography.[37] More specifically, high-aspect-ratio structures, specifically, tall and narrow features, suffer from collapse during the development steps due to capillary forces.

To circumvent some of these problems, bilayer resist schemes have proved to be useful.[38] In such resist schemes, an etch resistant layer is combined with an imageable layer, thus obtaining the best of both worlds. Such bilayer resists are developed by a plasma. Therefore, the top layer of these resists requires a high resistance against removal by the developing plasma. It is for such applications that organometallic polymers may prove to be of interest.

Novel organometallic polymers became available via ring-opening polymerization.[39,40] A variety of strained metallocenophanes were used as monomeric precursors to obtain high molecular weight organometallic polymers. The ring-opening polymerization can proceed thermally, by heating the monomer above a certain polymerization onset temperature. Furthermore, some metallocenophanes were found to be polymerizable in solution as well, by using anionic initiators[41] or transition metal catalysts, or in the solid state.[42,43]

Since the discovery of the ring-opening polymerization of strained metallocenophanes, a diverse series of metal-containing macromolecules have been synthesized and characterized (see Scheme 4). These include the following variations: substituents on silicon,[44] number and type of bridging atoms,[45] and substituents on the cyclopentadienyl rings.[46]

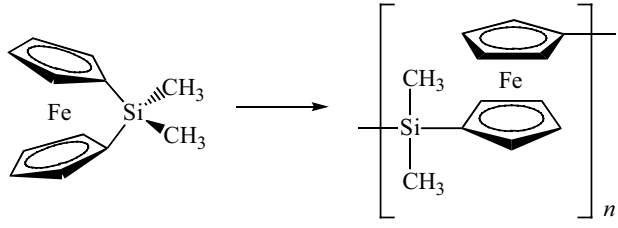

Scheme 4 Ring-opening polymerization of strained dimethylsilyl[1]ferrocenophane.

A. Polyferrocenyldimethylsilane as Reactive Ion Etch Barrier

Oxygen and oxygen-containing plasmas are frequently used to modify polymer surfaces.[47] When an organometallic polymer is exposed to an oxygen plasma, two etching processes—namely, chemical and physical etching—take place. *Chemical etching* refers to the chemical reactions that occur between the plasma and the surface of interest. Contrary to organic polymers, some products of chemical etching with oxygen plasmas are nonvolatile and therefore do not desorb from the surface. This is the fundamental reason for the low etch rates found for inorganic species when using oxygen plasmas. *Physical etching*, on the other hand, is caused by the bombardment of positive ions that break bonds on impact. Therefore, physical etching is less specific for chemical composition of the polymer film. The balance between the two etching mechanisms depends on many variables, such as gas pressure and composition, reactor design, and temperature.

From the Auger electron spectroscopy (AES) depth profile (Fig. 2), it can be seen that relatively less carbon and a significant amount of oxygen is present at the surface. Furthermore, a higher intensity of iron and an equal amount of silicon compared to the bulk of the film were measured. Compared with XPS observations, it was clear that an Fe–Si–oxide layer was formed at the exposed surface.[48] The thickness of this oxide layer is approximately 10 nm.

Radiofrequency discharges in low-pressure fluorocarbon gases are often used for etching silicon, silicon oxide, and silicon nitride.[49,50] The gas mixtures are

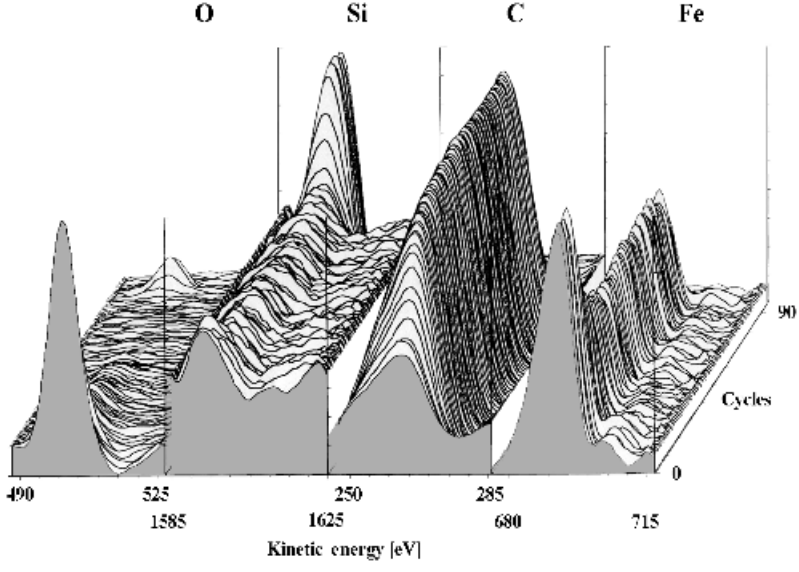

Figure 2 Auger electron spectroscopy depth profile of an oxygen plasma-treated film of polyferrocenyldimethylsilane. The front of the image corresponds to the exposed free surface. (Reproduced with permission from Ref. 48, © 2001 ACS.)

composed of compounds such as CF_4, CHF_3, and C_2F_6. By adjustment of the composition of the gas, the nature of the plasma can be dramatically changed.[51]

Tetrafluorocarbon (CF_4) shows the highest relative etching characteristics towards materials reactive with fluorine atoms. Its decomposition in the plasma is characterized by the highest concentration of fluorine atoms (F) and the lowest concentration of CF and CF_2 radicals. If the F/C atomic ratio of the feed-in gas decreases, the concentration of CF and CF_2 radicals will be higher at the expense of F, and the plasma becomes "polymerizing," due to the deposition of polymer film, rather than "etching." Frequently, O_2 is added to the feed-in gas in order to reduce the "polymerizing" effect, thereby significantly increasing the etch rate of silicon.

The pattern in Figure 3 demonstrates the potential of organometallic polymers as etch resists. The top half of the AFM image corresponds to the untreated pattern of polyferrocenyldimethylsilane (PFS). The bottom half displays the same pattern after it has been exposed to a CF_4/O_2 plasma treatment.

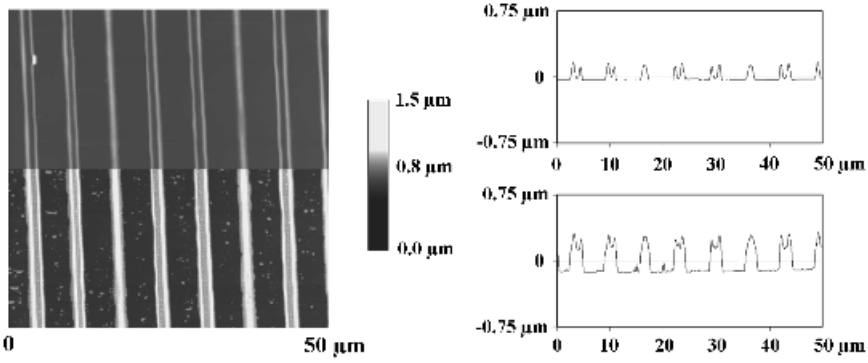

Figure 3 AFM images (left) and single-line scans (right) of a ferrocenyldimethylsilane homopolymer pattern, before and after CF_4/O_2 plasma treatment. The top half of the AFM image corresponds to an unetched film, and the bottom half displays the etched area. The sample was etched for 10 min, which led to the removal of approximately 200 nm of unprotected substrate. (Reproduced with permission from Ref. 48, © 2001 ACS.)

Since the potential of polyferrocenyldimethylsilane as an etch barrier has been demonstrated above, we now want to focus on pathways to generate patterns of these polymers. Masking layers with such high etching resistance are potentially useful for very thin resist layer applications: thin layers that prevent pattern collapse when fabricating high-aspect-ratio structures.

B. Printing of Organometallic Polymers by Soft Lithography

Printing of high-etch-resistance polymers is an attractive economic alternative for the fabrication of lithographic masks. Microcontact printing is a frequently used

technique to generate chemically distinct patterns on solid substrates. Mostly small molecules are employed as inks that upon contact will react with the substrate. Approaches in which the ink consists of a macromolecule are now more commonly employed.

The limited use of macromolecular inks can be attributed to poor wetting characteristics of PDMS surfaces by many polymers. A variety of approaches exist for patterning macromolecules on substrates using microcontact printing methods.

PDMS stamps can be treated briefly by an oxygen plasma to generate an oxide surface that can be wetted by the organometallic polymer. However, during the plasma treatment, the surface of the PDMS thermally expands. On cooling this thermally expanded oxide layer buckles the surface in order to relieve the stress caused by the expansion.[52] When a stamp was prepatterned, as demonstrated in Figure 4, the corrugated structure is formed with an orientation perpendicular to the original pattern.[53]

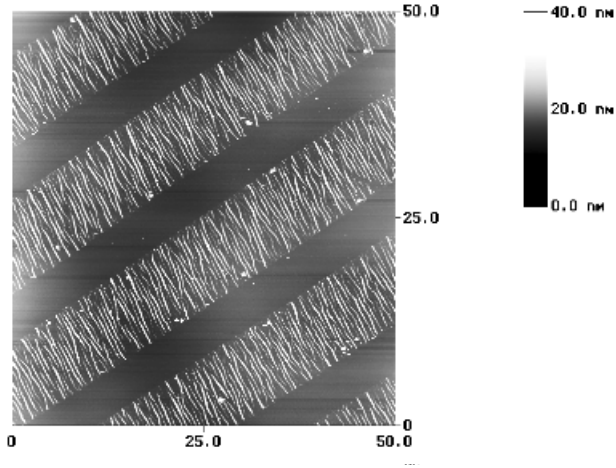

Figure 4 AFM image of a PFS pattern printed with an oxygen plasma-treated PDMS stamp. The corrugated structure is a result of the stress generated by the difference in thermal expansion between the PDMS matrix and the oxidized surface.

When using less aggressive cleaning and oxidation techniques, it is also possible to eliminate the corrugation formation. Cleaning the PDMS stamp in a mild ozone/UV environment will still render the PDMS surface hydrophilic, but will not result in extensive surface heating and therefore thermal expansion related stress. This is demonstrated in Figure 5.

The lines shown in Figure 5 demonstrate the very high etch resistance of these organometallic polymers. The initial PFS film thickness was approximately 30 nm. After the plasma etching treatment (10 min in CF_4/O_2 plasma) the features exhibited a height of approximately 250 nm.

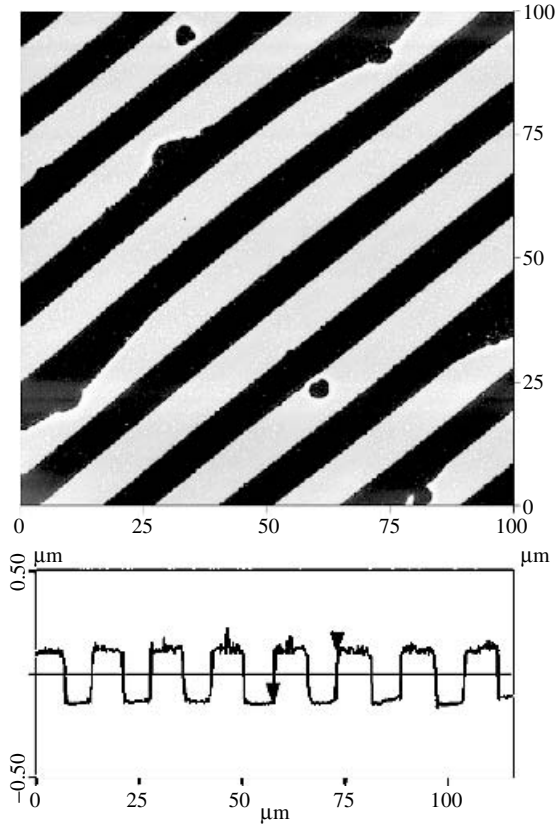

Figure 5 Pattern of PFS on silicon fabricated by direct stamping using a ozone/UV-cleaned PDMS stamp. Subsequently, the pattern was etched into the substrate by a CF_4/O_2 plasma. The features of the resulting pattern consisted primarily of lines narrowed by dewetting. Full lines, however, were observed at the borders of the patterned area.

1. Directed Dewetting

In some cases a microcontact printed substrate is used as a template that directs the subsequent adsorption of macromolecules. This is demonstrated in Figure 6. A substrate was printed with a self-assembling monolayer, generating hydrophobic and hydrophilic areas. The PFS is then spincoated onto this patterned substrate, which directs the dewetting of the polymer film.

Microcontact printing-based approaches are cost-effective methods to generate patterns on the micrometer lengthscale. Such lengthscales are still large compared to the high-resolution lithography processes that are being developed continuously. In order to bridge the lengthscale gap, research can be directed toward generating novel resists that combine a radiation-sensitive material with the etch barrier properties of organometallic materials. So-called bilevel resists have been considered for high-resolution resist materials.[38] Very thin layers are needed in such resists, reducing the probability of pattern collapse when fabricating high-aspect-ratio structures.

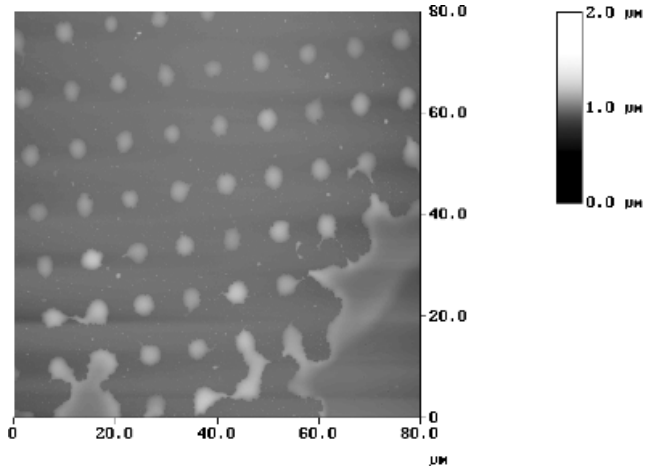

Figure 6 AFM image of a printed substrate, partially dewetted by an organometallic polymer film.

VI. ORGANIC–ORGANOMETALLIC BLOCK COPOLYMERS

A. Structure Formation via Block Copolymer Self-Assembly

All resists and technologies described so far originate from pursuing a top–down approach. Smaller features can be obtained by using lower wavelength irradiation, more sensitive resists for smaller wavelengths, and better optics. In a bottom–up approach structures can be fabricated by self-assembly processes as well.

Well-controlled architectures can be obtained in block copolymers (see examples in Fig. 7), and the equilibrium structures can be controlled by macromolecule design. The morphology of microdomains formed by pure diblock copolymers has been intensively researched and is by now a relatively well-understood area.[54]

In neat diblocks three "classical" ordered microphases are usually distinguished. These include alternating lamellae, hexagonally packed cylinders, and body-centered-cubic packed spheres. In addition, some other, more complex microstructures may appear, especially near the order–disorder transition.

Figure 7 The classical morphologies in block copolymer systems.

1. Synthesis of Organometallic–Organic Block Copolymers

Well-defined block copolymers can be synthesized by sequential anionic polymerizations.[55] The living end of the first polymeric block must be reactive enough to initiate the polymerization of the second block.

A variety of block copolymers containing a ferrocenylsilane block (see Scheme 5) have been synthesized by anionic polymerization. These include dimethylsiloxane,[56] styrene,[57] isoprene,[58] aminoalkylmethacryate,[59] and ethylene oxide.[60]

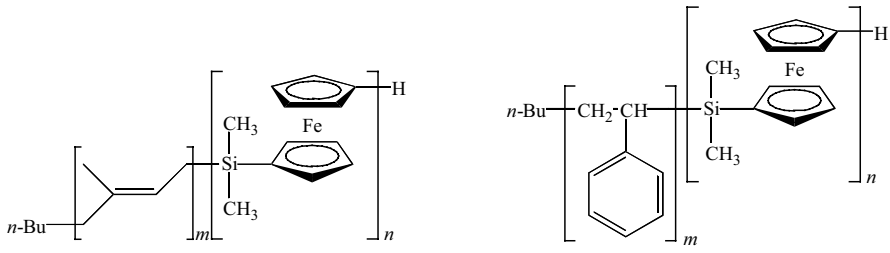

PI-*b*-PFS : *IF* **PS-*b*-PFS : *SF***

Scheme 5 Examples of two organic-ferrocenylsilane block copolymers.

2. Periodic Nanodomain Structures

A series of styrene-ferrocenyl dimethylsilane block copolymers form periodic structures on a lengthscale comparable to the size of the polymers.[61]

Pure diblock copolymers (e.g., see Fig. 8) phase-separate into an equilibrium structure that depends on the corresponding χ parameter,[62] the length of the block copolymer, and the volume fraction of the two phases. Knowledge of the χ parameter will allow one to target a specific morphology by adjusting the molar mass and composition of the diblock copolymer accordingly.

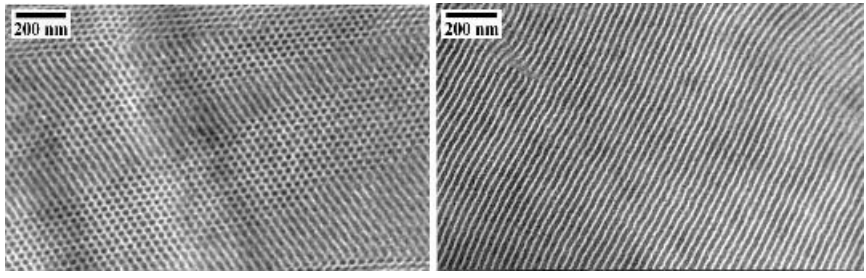

Figure 8 Bright-field TEM micrograph of a cylinder-forming and a lamella-forming PS-*b*-PFS diblock copolymer. (Reproduced with permission from Ref. 61, © 1999 Wiley & Sons.)

Another approach involves the blending of diblock copolymers with the corresponding homopolymer (Fig. 9). Thus, instead of synthesizing a specific block copolymer in order to obtain a certain morphology, it is possible to mix in a corresponding homopolymer to alter the overall composition.[61]

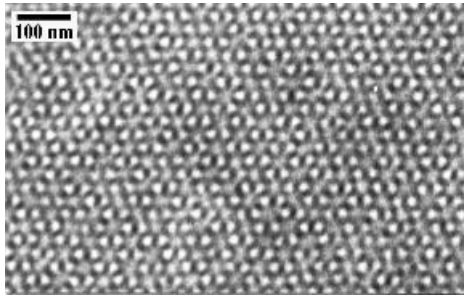

Figure 9 Bright-field TEM micrograph of a (PS-*b*-PFS) diblock/PS homopolymer blend displaying the double-gyroid morphology. The pure diblock displayed a lamellar morphology. (Reproduced with permission from Ref. 61, © 1999 Wiley & Sons.)

3. Thin Films of Block Copolymers

Constraining block copolymers onto substrates induces an orientation of the microdomains with respect to the substrate. One block will preferentially wet the substrate, and similarly, one block will be present at the free surface. This preferential wetting results in a parallel orientation of the microdomains to the substrate.[63]

In relatively thick block copolymer films, a mismatch between the film thickness and the bulk lattice spacing can be distributed over many layers. As the film thickness is decreased to a value equal to a few domain periods, the frustration due to the mismatch becomes more significant and can be released by the formation of islands or holes (see Fig. 10).[64]

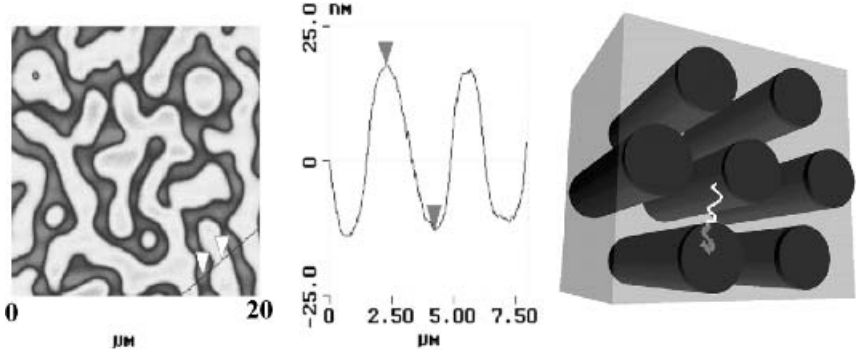

Figure 10 Representation of a cylinder-forming (PS-*b*-PFS) block copolymer (right). When confined in a thin film with a thickness 2 times the lattice spacing, islands and holes are formed (left) as the result of an incommensurate film thickness.

Film thickness constraints can also be exploited to control the orientation of the nanodomains. More specifically, when the thickness of the film approaches the lattice constant of the block copolymer, the orientation of the nanodomains is sometimes altered with respect to the substrate. Simply stated, the stress generated by the incommensurate film thickness can be relieved by a change in domain orientation. This is further illustrated by an example in Figure 11. A styrene-ferrocenyl dimethylsilane block copolymer (PS-*b*-PFS) consisting of a styrene fraction of 0.73 forms a cylindrical structure in the bulk.[61] Within a thin film, the pattern that is formed by the block copolymer also depends on the film thickness.[65]

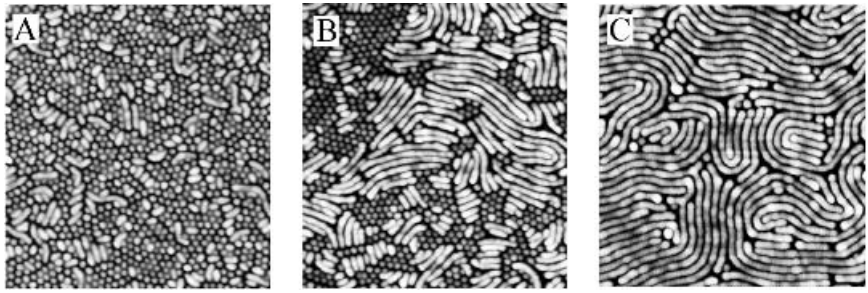

Figure 11 AFM images of PS-*b*-PFS block copolymer films of different initial thicknesses: (a) 30 nm; (b) 35 nm; (c) 40 nm—each scan size is 1 μm^2 (reproduced with permission from Ref. 65, © 2001 ACS).

Alternatively, the morphology of a thin diblock film can be altered by a subtle change in composition. It was demonstrated for a series of isoprene-ferrocenyl dimethylsilane block copolymers (PI-*b*-PFS) that the structure within a 30-nm-thin film could be significantly changed by a slight compositional difference, although the bulk structures all had the same morphology.[58] This is demonstrated in Figure 12.

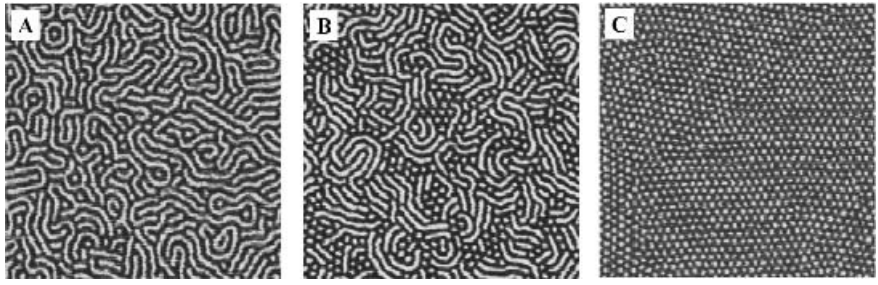

Figure 12 Tapping-mode AFM images of 30-nm thin PI-*b*-PFS copolymer films of different compositions: (a) PI volume fraction of 0.72; (b) PI fraction of 0.76; (c) PI fraction of 0.80 (reproduced with permission from Ref. 58, © 2000 ACS).

4. Self-Assembling Resists

Block copolymers can be employed as templates to direct the deposition of inorganic nanostructures. Park et al.[66] used an OsO_4-stained microphase separated thin film of poly(styrene-*block*-butadiene) that produced holes on RIE in silicon nitride substrates. The etch ratio between the two phases, stained butadiene and styrene, was only about 1–2. Möller et al. discussed the use of poly(styrene-*block*-2-vinylpyridine), to prepare masks for nanolithography by loading the PVP domains with gold particles[67] or by selective growth of Ti on top of the PS domains.[68]

The thin films of organic–organometallic block copolymers self-assemble to form lateral regions that have a significantly different etching behavior. Furthermore, the two phases already contain all the elements necessary to generate large etching contrast, without the need for staining or loading. The organometallic areas enclose a high resistance against removal by oxygen and fluorocarbon plasmas, whereas the organic phase is quickly removed. This opens up the possibility to transfer the pattern, generated by block copolymer self-assembly, in a one-step etching process into the underlying substrate.[69]

A nanostructured silicon surface, obtained after etching, is visualized in Figure 13. The organic constituents of the block copolymer have been selectively removed by the action of the oxygen plasma, leaving the oxidized metal-containing phase behind. Such self-assembling nanolithographic templates have been employed to obtain high-density magnetic arrays in cobalt substrates.[70]

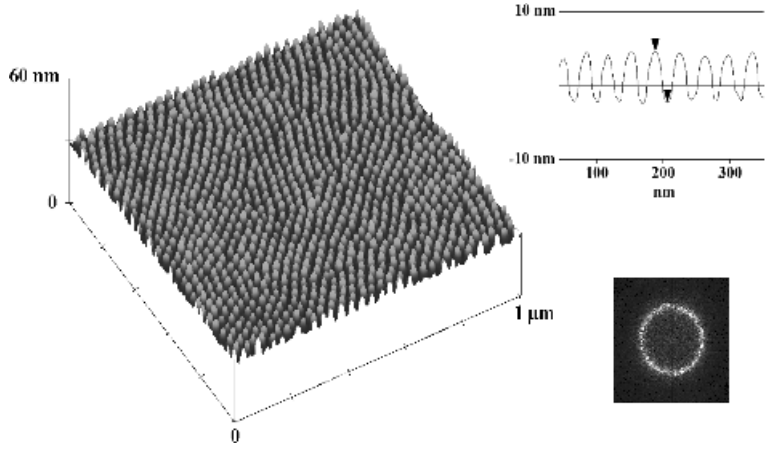

Figure 13 Tapping-mode AFM height image of an etched PI-*b*-PFS organic–organometallic diblock copolymer film. The dots result from block copolymer phase separation. (Reproduced with permission from Ref. 69, © 2000 ACS.)

VII. CONCLUSIONS AND OUTLOOK

Metal-containing polymers appear to be valuable candidates for developing highly etch-resistant resists. The increasing understanding and possibilities of e.g. the

ring-opening polymerization of metallocenophanes might lead to the development of novel high-performance resists. They may, for example serve as the etch-resistant top layer within bilayer system resists.

Advances in printing techniques of polymers may also contribute to the progress in cost-effective pattern replication procedures. The ability to replicate and print polymer patterns on micrometer and submicrometer lengthscales opens up a route to economically fabricate etch resistant patterns for applications, where metallic contaminations are not relevant. Examples of such applications can be the fabrication of photomasks, microfluidic devices, optical components, and data storage arrays.

It is now up to the imagination of the chemist, materials scientist, and physicist to design and develop novel organometallic-based materials and methods for creating and/or replicating patterns that can then be easily transferred into substrates.

VIII. ACKNOWLEDGMENT

The University of Twente and the MESA$^+$ Research Institute are gratefully acknowledged for financial support.

IX. REFERENCES

1. D. R. Medeiros, A. Aviram, C. R. Guarnieri, W. S. Huang, R. Kwong, C. K. Magg, A. P. Mahorowala, W. M. Moreau, K. E. Petrillo, M. Angelopoulos, *IBM J. Res. Dev.* **45,** 639 (2001).
2. Annual meeting of the American Physical Society at the California Institute of Technology on December 29, 1959. A transcript of the talk is located in the Caltech library in the February issue of *Engineering & Science* 1960.
3. C. G. Willson, M. D. Stewart, in *Encyclopedia of Materials: Science and Technology*, Elsevier Science, Kidlington, UK, 2001, p. 6973.
4. R. A. Dammel, *Diazonaphthoquinone-Based Resists*, SPIE Optical Engineering Press, Bellingham, WA 1993.
5. M. Rothschild, T. M. Bloomstein, J. E. Curtin, D. K. Downs, T. H. Fedynyshyn, D. E. Hardy, R. R. Kunz, V. Liberman, J. H. C. Sedlacek, R. S. Uttaro, A. K. Bates, C. Van Peski, *J. Vac. Sci. Technol*. *B* **17,** 3262 (1999).
6. C. Brodsky, J. Byers, W. Conly, R. Hung, S. Yamada, K. Patterson, M. Somervell, B. Trinque, H. V. Tran, S. Cho, T. Chiba, S.-H. Lin, A. Jamieson, H. Johnson, T. Vander Heyden, C. G. Willson, *J. Vac. Sci. Technol*. *B* **18,** 3396 (2000).
7. A. K. Bates, M. Rothschild, T. M. Bloomstein, T. H. Fedynyshyn, R. R. Kunz, V. Liberman, M. Switkes, *IBM J. Res. Dev.* **45,** 605 (2001).
8. J. M. Klopp, D. Pasini, J. D. Byers, C. G. Willson, J. M. J. Fréchet, *Chem. Mater.* **13,** 4147 (2001).
9. E. Reichmanis, O. Nalamasu, F. M. Houlihan, *Acc. Chem. Res*. **32,** 659 (1999).
10. G. M. Wallraff, W. D. Hinsberg, *Chem. Rev*. **99,** 1801 (1999).
11. Y. Ohnishi, J. Fujita, Y. Ochiai, S. Matsui, *Microelectron. Eng*. **35,** 117 (1997).
12. N. Boden, R. C. Borner, R. J. Bushby, A. N. Cammidge, M. V. Jesudason, *Liq. Cryst.* **15,** 851 (1993).

13. E. Reichmanis, F. M. Houlihan, O. Nalamasu, T. X. Neenan, *Chem. Mater*. **3,** 394 (1991).
14. H. Ito, C. G. Willson, *Polym. Sci. Eng*. **23,** 1012 (1983).
15. S. A. MacDonald, H. Schlosser, H. Ito, N. J. Clecak, C. G. Willson, *Chem. Mater*. **3,** 435 (1991).
16. T. M. Wolf, G. N. Taylor, *J. Electrochem. Soc*. **131,** 1664 (1984).
17. H. Fujioka, H. Nakajima, S. Kishimura, H. Nagata, *Proc. SPIE* **1262,** 554 (1990).
18. O. Nalamasu, F. A. Baiocchi, G. N. Taylor, *ACS Symp. Ser*. **412,** 189 (1989).
19. W. Chen, H. Ahmed, *Appl. Phys. Lett.* **62,** 1499 (1993).
20. J. Fujita, H. Watanabe, Y. Ochiai, J. S. Tsai, S. Matsui, *Appl. Phys. Lett*. **66,** 3064 (1995).
21. W. Langheinrich, H. Beneking, *Microelectron. Eng*. **23,** 287 (1994).
22. E. Kratschmer, M. Isaacson, *J. Vac. Sci. Technol*. *B* **5,** 369 (1987).
23. W. Langheinrich, B. Spangenberg, H. Beneking, *J. Vac. Sci. Technol*. *B* **10,** 2868 (1992).
24. T. Tada, T. Kanayama, *Jpn. J. Appl. Phys. Part 2, Lett*. **35,** L63 (1996).
25. K. E. Gonsalves, L. Merhari, H. Wu, Y. Hu, *Adv. Mater*. **13,** 703 (2001).
26. P. M. Dentinger, J. W. Taylor, *J. Vac. Sci. Technol. B* **15,** 2575 (1997).
27. L. Merhari, K. E. Gonsalves, Y. Hu, W. He, W.-S. Huang, M. Angelopoulos, W. H. Bruenger, C. Dzionk, M. Torkler, *Microelectron. Eng*. **63,** 391 (2002).
28. Y. Hu, H. Wu, K. Gonsalves, L. Merhari, *Microelectron. Eng*. **56,** 289 (2001).
29. K. E. Gonsalves, J. Wang, H. Wu, *J. Vac. Sci. Technol. B* **18,** 325 (2000).
30. H. Wu, Y. Hu, K. E. Gonsalves, M. J. Yacaman, *J. Vac. Sci. Technol. B* **19,** 851 (2001).
31. F. C. M. J. M. van Delft, J. P. Weterings, A. K. Van Langen-Suurling, H. Romijn, *J. Vac. Sci. Tech. B* **18,** 3419 (2000).
32. K. E. Gonsalves, Y. Hu, H. Wu, L. Mehari, in *Collected Abstracts 12th Int. Conf. Photopolymers, Society of Plastics Engineers*, McAfee, NJ, Oct. 16–18, 2000.
33. T. H. Fedynyshyn, S. P. Doran, I. Sondi, M. L. Lind, E. Matijevic, *Proc. SPIE-Int. Soc. Opt. Eng.* (*Adv. Resist Technol. Proc.*) **3999,** 627 (2000).
34. I. Sondi, T. H. Fedynyshyn, R. Sinta, E. Matijevic, *Langmuir* **16,** 9031 (2000).
35. M. T. Reetz, M. Winter, G. Dumpich, J. Lohau, S. Friedrichowski, *J. Am. Chem. Soc*. **119,** 4539 (1997).
36. S.-J. Kim, J.-H. Kim, D.-Y. Lee, Y.-H. Ko, B.-S. Park, C.-G. Park, *Mol. Cryst. Liq. Cryst*. **227,** 317 (1993).
37. K. Wiesauer, G. Springholz, *J. Appl. Phys.* **88,** 7289 (2000).
38. I. Zharov, J. Michl, M. H. Sherwood, R. Sooriyakamaran, C. E. Larson, R. A. DiPietro, G. Breyta, G. M. Walraff, *Chem. Mater.* **14,** 656 (2002).
39. D. A. Foucher, B. Z. Tang, I. Manners, *J. Am. Chem. Soc*. **114,** 6246 (1992).
40. For a review, see K. Kulbaba, I. Manners, *Macromol. Rapid Commun*. **22,** 711 (2001).
41. R. Rulkens, A. J. Lough, I. Manners, *J. Am. Chem. Soc*. **116,** 797 (1994).
42. Y. Ni, R. Rulkens, J. K. Pudelski, I. Manners, *Macromol. Rapid Commun*. **16,** 637 (1995).
43. J. Rasburn, R. Petersen, T. Jahr, R. Rulkens, I. Manners, G. J. Vancso, *Chem. Mater*. **7,** 871 (1995).
44. D. A. Foucher, R. Ziembinski, B. Z. Tang, P. M. Macdonald, J. Massey, C. R. Jaeger, G. J. Vancso, I. Manners, *Macromolecules* **26,** 2878 (1993).
45. J. M. Nelson, H. Rengel, I. Manners, *J. Am. Chem. Soc*. **115,** 7035 (1993).
46. J. M. Nelson, A. J. Lough, I. Manners, *Angew. Chem. Int. Ed. Engl*. **33,** 989 (1994).
47. R. d'Agostino, *Plasma Deposition, Treatment, and Etching of Polymers,* Academic Press, New York, 1990; J. W. Coburn, in *Encyclopedia of Materials: Science and Technology,* Elsevier Science, Kidlington, UK, 2001, p. 7015.

48. R. G. H. Lammertink, M. A. Hempenius, V. Z.-H. Chan, E. L. Thomas, G. J. Vancso, *Chem. Mater*. **13,** 429 (2001).
49. R. Knizikevicius, A. Galdikas, A. Grigonis, *Vacuum* **66,** 39 (2002).
50. G. Kokkoris, E. Gogolides, A. G. Boudouvis, *J. Appl. Phys*. **91,** 2697 (2002).
51. M. Strobel, S. Corn, C. S. Lyons, G. A. Korba, *J. Polym. Sci. A* **25,** 1295 (1987).
52. N. Bowden, W. T. S. Huck, K. E. Paul, G. M. Whitesides, *Appl. Phys. Lett*. **75,** 2557 (1999).
53. D. B. H. Chua, H. T. Ng, S. F. Y. Li, *Appl. Phys. Lett*. **76,** 721 (2000).
54. F. S. Bates, J. H. Rosedale, G. H. Fredrickson, *J. Chem. Phys*. **92,** 6255 (1990).
55. H. L. Hsieh, R. P. Quirk, *Anionic Polymerization: Principles and Practical Applications*, Marcel Dekker, New York, 1996.
56. R. Rulkens, Y. Z. Ni, I. Manners, *J. Am. Chem. Soc*. **116,** 12121 (1994).
57. Y. Z. Ni, R. Rulkens, I. Manners, *J. Am. Chem. Soc*. **118,** 4102 (1996).
58. R. G. H. Lammertink, M. A. Hempenius, G. J. Vancso, *Langmuir* **16,** 6245 (2000).
59. X. S. Wang, M. A. Winnik, I. Manners, *Macromol. Rapid Commun*. **23,** 210 (2002).
60. R. Resendes, J. Massey, H. Dorn, M. A. Winnik, I. Manners, *Macromolecules* **33,** 8 (2000).
61. R. G. H. Lammertink, M. A. Hempenius, E. L. Thomas, G. J. Vancso, *J. Polym. Sci., Polym. Phys*. **37,** 1009 (1999).
62. H. B. Eitouni, N. P. Balsara, H. Hahn, J. A. Pople, M. A. Hempenius, *Macromolecules* **35,** 7765 (2002).
63. G. Coulon, T. P. Russell, V. R. Deline, P. F. Green, *Macromolecules* **22,** 2581 (1989).
64. G. Coulon, D. Auserre, T. P. Russell, *J. Phys.* (*France*) **51,** 777 (1990).
65. R. G. H. Lammertink, M. A. Hempenius, G. J. Vancso, K. Shin, M. H. Rafailovich, J. Sokolov, *Macromolecules* **34,** 942 (2001).
66. M. Park, C. Harrison, P. M. Chaikin, R. A. Register, D. H. Adamson, *Science* **276,** 1401 (1997).
67. J. P. Spatz, T. Herzog, S. Mössmer, P. Ziemann, M. Möller, *Adv. Mater*. **11,** 149 (1999).
68. J. P. Spatz, P. Eibeck, S. Mössmer, M. Möller, T. Herzog, P. Ziemann, *Adv. Mater*. **10,** 849 (1998).
69. R. G. H. Lammertink, M. A. Hempenius, J. E. van den Enk, V. Z.-H. Chan, E. L. Thomas, G. J. Vancso, *Adv. Mater*. **12,** 98 (2000).
70. J. Y. Cheng, C. A. Ross, V. Z.-H. Chan, E. L. Thomas, R. G. H. Lammertink, G. J. Vancso, *Adv. Mater*. **13,** 1174 (2001).

CHAPTER 8

Proton-Coupled Intramolecular Electron Transfer in Ferrocene–Quinone Conjugated Oligomers and Polymers

Masaki Murata and Hiroshi Nishihara

Department of Chemistry, School of Science, The University of Tokyo, Tokyo, Japan

CONTENTS

Macromolecules Containing Metal and Metal-like Elements, Volume 2: Organoiron Polymers, Edited By Alaa S. Abd-El-Aziz, Charles E. Carraher, Jr., Charles U. Pittman, Jr., John E. Sheats, and Martel Zeldin
ISBN 0-471-45078-2

I. INTRODUCTION

Proton-coupled electron transfer (PCET) between donor and acceptor molecules is a fundamentally important chemical reaction closely related to various energy conversion events in biological systems including photosynthesis and respiration.[1–8] In the photosynthetic process, especially the rapid electron transfer reaction occurring within protein-bound pigment complexes,[9,10] the main function of the reaction center complexes of the photosynthesis is to create an energy gradient, using successive multistep intermolecular electron transfer processes through a group of donor and acceptor moieties around the cytoplasmic membrane.[11] During photosynthesis, because the redox sites are widely spaced ($\sim$70 Å) and extremely long-lived, charge-separated states ($\tau_{1/2} > 1$ s) are formed; unitary quantum efficiency for charge separation is achieved by virtue of a large expenditure of photon energy. It has been recognized that hydrogen bonds must play an important role in mediating such electron transfer processes, and that their function most likely extends beyond simply providing the structural scaffolding for the donors and the acceptors that participate in the redox process.[4–8] The relationship between electron transfer and proton motion has been elucidated in photoinduced electron transfer within an electron donor–acceptor pair juxtaposed by a proton transfer interface.[7,8] The theoretical studies are based on experiments that directly compare the rate of electron transfer through a donor (amidinium-carboxylate)–acceptor salt bridge and corresponding switched interface donor (carboxylate-amidinium)–acceptor complex, which are related to the aspartate-arginine salt bridges found in a range of biological systems, including RNA and DNA complexes and enzymes.

For the attainment of marvelous electron transfer processes in the natural sequential potential fields, many noncovalentaly-bound donor–acceptor (DA) systems[12] and covalently-bound DA systems[13–24] have been previously reported. Most of them are artificial models of the photosynthesis comprising simple assemblies of the dyad (DA) or triad [donor–spacer–acceptor (DSA)] functional molecules with a chromophore such as a porphyrin. The quantum efficiency of such systems is lower ($<$25%) compared with the biological systems ($\cong$100%), and thus more efforts for constructing more efficient systems are necessary. Some of the covalentaly-bound DA systems have been designed for the fabrication of molecule-scale devices based on a molecular electron-transport wire and/or highly ordered molecular arrays on the surface.[20–29] Most of such studies employed the DA nonconjugated molecules.

Relative to the development of new molecule-scale devices, intelligent molecules, the structures and properties of which are facilely and reversibly changeable by application of external physical and chemical stimuli, have attracted much attention.[30] One category of such molecules consists of transition metal complexes with π-conjugated spacers; the combination of flexibility of *d* and π-orbitals can yield unique optical, magnetic, and electronic properties. Because the ferrocenyl moiety works as a good donor, conjugated ferrocene systems constructed by combining ferrocene with electron-accepting molecular units have attracted attention for their fluctuating electronic structures,[31–34] which are sensitive to outer fields, and exhibit

novel behavior resulting from their second-order nonlinear optical (NLO) properties[35–38] and facile intramolecular electron transfer, which causes drastic changes in their structure and physical properties.

The electronic structure of metallocenes has been well and systematically investigated by Hendrickson and Gray et al.,[39,40] and a molecular orbital diagram of ferrocene is shown in Figure 1 [where the subscripts *g* and *u* denote *gerade* (symmetric) and *ungerade* (unsymmetric), respectively]. The electronic structure of ferrocene includes the three metal-based highest filled levels derived from the d_{z2} orbital (a_{1g}), and the d_{xy}, $d_{x^2-y^2}$ orbitals, which are degenerated to give e_{2g} in staggered D_{5d} geometry. The $1e^-$-oxidized form, the ferrocenium ion, has a similar electronic structure except that the energy levels of e_{2g} and a_{1g} are reversed, which leads to a singly occupied molecular orbital (SOMO) of the ferrocenium ion of e_{2g}. The e_{2g} orbitals have some character of *d* backbonding through interaction with a combination of the cyclopentadienyl (Cp) anion LUMOs, and the a_{1g} orbital involves some interaction of d_{z2} with the metal *s* orbital and with the Cp rings. The next-highest orbitals, e_{1u}, of ferrocene are primarily ligand-based, with some contribution from the metal p_x and p_y orbitals. In contrast, the LUMO of ferrocene is derived from an out-of-phase π interaction between the d_{xz}/d_{yz} and Cp orbitals and has e_{1g} symmetry. Bonding of the electron-donating moieties to the Cp rings raises the energies of both the filled *d* orbitals and the highest ligand-based orbitals, and the electron-withdrawing group does the opposite. However, because of the presence of the Cp rings, when a conjugated system is attached to ferrocene, the most significant perturbation is not of the metal-based HOMOs but of the orbitals just below them. Actually, in a ferrocene derivative with a moderate electron-withdrawing conjugated substituent, the first ionization potential and electrochemical oxidation potential are similar to those of ferrocene.[41–43] It should be emphasized that the ferrocene derivatives do not undertake protonation and its redox potential is almost independent of the solvent because of their electronic structures.

One of the most versatile electron-accepting molecules is the quinonoid compound, and the redox reaction of the quinone–hydroquinone couple is one of the most thoroughly studied proton-coupled electron transfer systems of organic molecules.[44] Quinones show the reversible two-step $1e^-$ reduction in aprotic organic solvents (Fig. 2).[45] One-electron addition to quinone forms the semiquinone radical with five π electrons. The stability of the semiquinone form is affected by the existence of a minute amount of proton, which appears as the large shift of the reduction potentials in the positive direction.[46] This implies that quinonoid compounds are representative acceptor molecules of which redox properties are influenced by external perturbation, such as protonation and solvation (Fig. 2).[47,48] They are employed in covalently and noncovalently linked donor–acceptor systems of particular interest in the study of proton-coupled electron transfer[49–51] and photoinduced electron transfer.[1–3,52]

From the observations noted above, the quinonoid compound linked to ferrocene by a π-conjugated spacer model provides insight into proton-coupled intramolecular electron transfer, because the redox potential of the quinonoid molecule can be readily controlled by external perturbation such as protonation and

solvation,[4,5] and thus the redox potentials of the two molecules can become similar to each other (Fig. 3). This chapter presents an overview of the more recent studies concerning ferrocene-quinone π-conjugated donor–acceptor system in the following two categories: (1) the ferrocene-anthraquinone (FcAq) system and (2) the ferrocene-benzoquinone (FcBq) system. The protonation-induced studies of oligomers and polymers of the FcAq system are also included in the former. The complexes exhibit novel structural changes into fulvene-cumulene complexes induced by proton-coupled intramolecular reactions. Previous studies on the transition metal complexes containing allenylidene and cumulenylidene are surveyed before the description of the FcAq system in the following section.

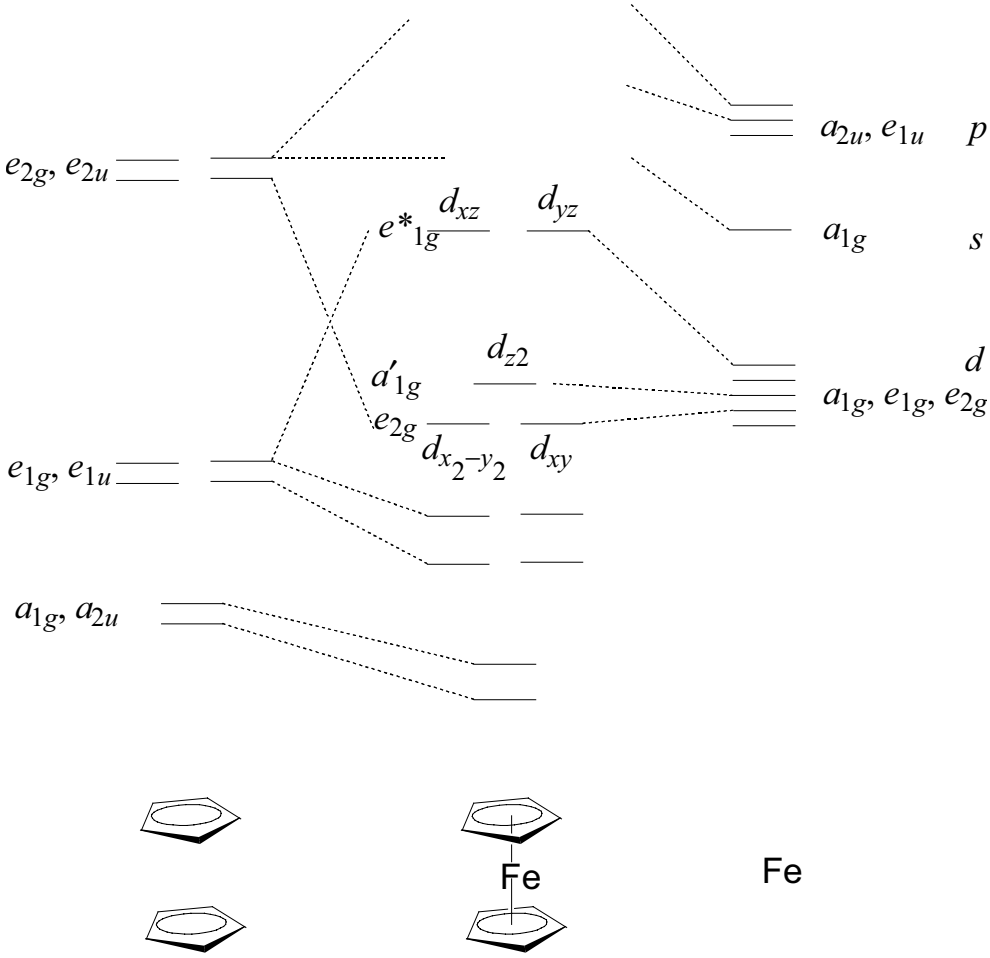

Figure 1 Electronic structure of ferrocene.

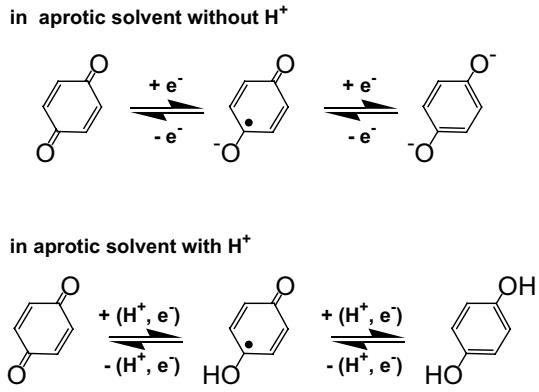

Figure 2 The stabilized structure of the redox isomers of quinonoid compounds without or with the proton source in aprotic solvent.

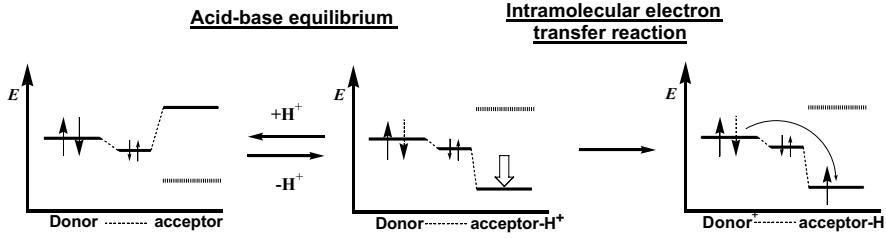

Figure 3 Concepts of protonation-induced intramolecular electron transfer.

II. ETHYNYLENE-BRIDGED FERROCENE-ANTHRAQUINONE (FcAq) COMPLEXES

A. Transition Metal Complexes Containing Allenylidene and Cumulenylidene

Current interest in the chemistry of π-conjugated diyne and polyyne metal complexes linked with ferrocenyl groups have resulted in further discoveries of novel unsaturated carbene ($M{=}CR^1R^2$; R^1 = ferrocene, R^2 = ferrocene, Ph, H, etc.) complexes derived from the resonance effects of the electron fluctuated spacers. This term of the metal complexes containing allenylidene and cumulenylidene derivatives has been considered and systematically investigated by Bruce in 1998.[37]

Vinylidenes ($M{=}C{=}CR^1R^2$) are tautomers of 1-alkynes and reformed by a formal 1,2-shift of the alkyne hydrogen from C1 to C2 ($H{-}C{\equiv}C{-}H \rightarrow :C{=}CH_2$). The lifetime of the vinylidene in the free state, $H_2C{=}C{=}CH_2$ is extremely short ($>10^{-10}$ s); therefore, unsaturated cumulenylidenes are extremely reactive and are considered to be important intermediates. The presence of a lone-pair (or two unpaired electrons) on the terminal carbon atom enables vinylidenes to be stabilized by coordination to a transition metal center. This is because some degree of backbonding from the metal to the carbon ligand may further strengthen the

carbon-to-metal donation bond. Stabilization of allenylidenes ($M{=}C{=}C{=}CR^1R^2$) by two heteroatom substituents is indicated by the resonance structures ($[M]{=}C{=}C{=}C(R^1R^2) \leftrightarrow [M]^+{-}C{\equiv}C{-}C^-(R^1R^2) \leftrightarrow [M]^+{-}C{\equiv}C{-}(C{=}R^1)^-R^2$), and thus strongly dipolar characteristics are expected, particularly when heteroatoms are present.

Several studies of electronic interactions between metal centers in ferrocenyl-alkynyl and -diynyl derivatives, metal-*bis*-acetylide complex–bridged ferrocenyl-alkynyl monomer ($MCl(-C{\equiv}C-Fc)(dppm)_2$: M = Ru, Os; Fc = ferrocenyl, dppm = diphenylphosphinomethane) and dimer ($M(-C{\equiv}C-Fc)_2(dppm)_2$), have been reported.[53–56]

The cyclic voltammogram of ferrocenyl-alkynyl monomer shows two quasi-reversible processes, and the redox potentials for the metal centers are considerably less anodic than those for $MCl_2(dppm)_2$. This is interpreted as electron donation to the metal center from the ferrocenyl group occurs through the $-C{\equiv}C-$ linker. In contrast, the redox potentials of the ferrocenyl moieties are more positive. These data are consistent with contributions of the resonance effect from the fulvene-carbene (cyclopentadienylidene) form ($[M]{-}C{\equiv}C{-}Fc \leftrightarrow [M]^+{=}C{=}C{=}Fv$, Fv; ($\eta^5$-cyclopentadienyl-$\eta^4$-2,4-cyclopentadiene)iron(I)) (Fig. 4).

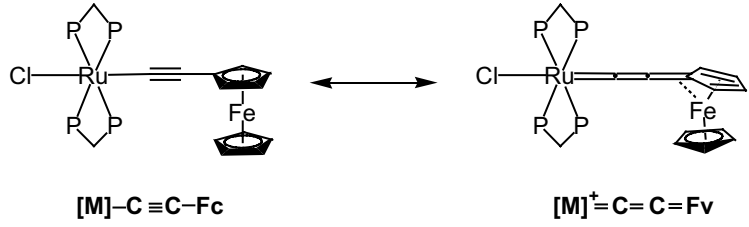

Figure 4 Contributions of the resonance effect from the fulvene-carbene (cyclopentadienylidene) form in the metal-acetylide-ferrocenyl complex.

On the other hand, the ruthenium complex of ferrocenyl-alkynyl dimer shows a separation of redox potentials of two ferrocene units through the alkyne-Ru-alkyne ligand at 0.22 V.[57,58] This result indicates that the mixed-valence state of ferrocenyl groups in $Ru(-C{\equiv}C-Fc)_2(dppm)_2$ complex are much more stable because of the strong donor–acceptor interaction through the ruthenium core metal with two σ-bonding alkynyl chains. The four oxidation states could be experimentally found for $Ru(-C{\equiv}C-Fc)_2(dppm)_2$ complex ($Fe(II){-}Ru(II){-}Fe(II) \leftrightarrow Fe(III){-}Ru(II){-}Fe(II) \leftrightarrow Fe(III){-}Ru(II){-}Fe(III) \leftrightarrow Fe(III){-}Ru(III){-}Fe(III)$), where the redox potential of the ruthenium center is positively shifted as noted above.

B. 1–1-FcAq Complexes

The expected protonation-induced phenomena of the ferrocene-quinone (FcQ) π-conjugated system are shown in Figure 3, which includes two basic and important processes of "acid–base equilibrium" and "intramolecular PCET." The former process is the interaction of the quinonoid moieties with protic solvent or acid. The latter process can appear when the donor and acceptor levels are close and the

donor–acceptor interaction is conducted by the π-conjugated linker. When the protonation occurs to the quinone moiety in the acid–base equilibrium, the acceptor level of the quinone moiety is lowered, so that the electron transfer from the ferrocene moiety to the quinone moiety through the π-conjugated chain can be expected (Fig. 3). In this condition, two spins would be generated separately at D and A sites, and because of this uneasy electronic configuration not a single structure derived from the resonance effect of these π-conjugated structure with the valence exchange of the iron center in the ferrocenyl moiety and the redox reaction of the quinone moiety, namely, "valence tautomers," may exist. Thus, unique structures and physical (magnetic and optical) properties may be exhibited.

We here start to describe the protonation behavior of ferrocenyethynylanthraquinones from the simplest D/A 1–1 complexes, 1-ferrocenylethynylanthraquinone (1-FcAq)[59] and 2-ferrocenylethynylanthraquinone (2-FcAq).[60] There are two carbonyl groups in each compound, and only one of them is conjugated to the ferrocenyl group as shown in Scheme 1. This conjugation affords a specific absorption band at 510 nm attributable to the metal-to-ligand charge transfer (MLCT) transition from the Fe(II) to the π* orbital of ethynylanthraquinone moiety, of which molar extinction coefficient ε, is larger for 2-FcAq (2.5×10^3 mol^{-1} dm^3 cm^{-1}) than 1-FcAq (1.7×10^3 mol^{-1} dm^3 cm^{-1}). The difference between the two isomers also appear in their X-ray crystallographic structures (Fig. 5), showing that the cyclopentadienyl (Cp) rings of the ferrocenyl moiety are perpendicular and parallel to the plane of the anthraquinone moiety for 1-FcAq and 2-FcAq, respectively.

The protonation behavior of 1-FcAq and 2-FcAq in a benzonitrile solution supplemented with CF_3SO_3H is also entirely different. The color of the 1-FcAq solution changed immediately from red to deep-reddish-pink after the addition of the stoichiometric amount of CF_3SO_3H. This corresponds to the spectral change in which the *n*-π* band decreased and the band at 510 nm increased in intensity, and in which a new broad band with the half-width, $\Delta\nu_{1/2} = 5.2 \times 10^3\,cm^{-1}$ appears visible in the near-IR regions ($\lambda_{max} = 939$ nm) (Fig. 6). Judging from the NMR spectra as described below, the protonated complex of 1-FcAq is a diamagnetic complex in benzonitrile with a unique structure involving a fulvene complex (Fv) moiety, $[1\text{-FvAqH}]^+CF_3SO_3^-$. The band at $\lambda_{max} = 939$ nm can be ascribed to the valence tautomerization of $[1\text{-FvAqH}]^+$ into a spin-separated form containing a ferrocenium (Fc^+) moiety, $[1\text{-Fc}^{\bullet}\text{AqH}^{\bullet}]^+$ (see Scheme 1), given that such a broad low-energy band has been recognized in other valence tautomerization complexes.[61,62] This consideration is supported by the fact that the solvent effect on λ_{max} is large; $\lambda_{max} =$ 1051 nm in dichloromethane, which is less polar than benzonitrile.

Notable features in the ^1H NMR spectrum of $[1\text{-FvAqH}]^+CF_3SO_3^-$ in CD_3CN include a new singlet due to the hydroxyl group appearing at δ 8.23 ppm, and two double doublets, one at 4.67 and one at 4.33 ppm, due to the Cp ring connecting to the ethynyl group of 1-FcAq, shift to the lower field by 1 ppm in comparison with 1-FcAq. This shift of the signals for the Cp ring is in accordance with the conversion into the fulvene structure. Instead of the two signals of the ethynyl carbons at 96.2 and 86.1 ppm, two signals ascribable to cumulene carbons appear in significantly lower field positions (171.1 and 167.8 ppm). These chemical shift values of $[1\text{-FvAqH}]^+$ are quite similar to those of $[Fe(C_5H_5)(fulvene)]^+$,[63–66] the molecular

structure of which, with a marked bent of exocyclic C=C bond, indicates that the fulvene unit of $[Fe(C_5H_5)(fulvene)]^+$ is characterized by both η^4 and η^6 coordination.[67] This implies a significant contribution of the $18e^-$ form rather than the $16e^-$ form. The IR spectrum of $[1\text{-FvAqH}]^+$ shows the disappearance of the $\nu(C{\equiv}C)$ band of 1-FcAq, and the molecular ion peak of $[1\text{-FvAqH}]^+$ (*m/z* 417) detected in the electrospray ionization (ESI) mass spectrum indicates the addition of one hydrogen atom to the composition of 1-FcAq (*m/z* 416).

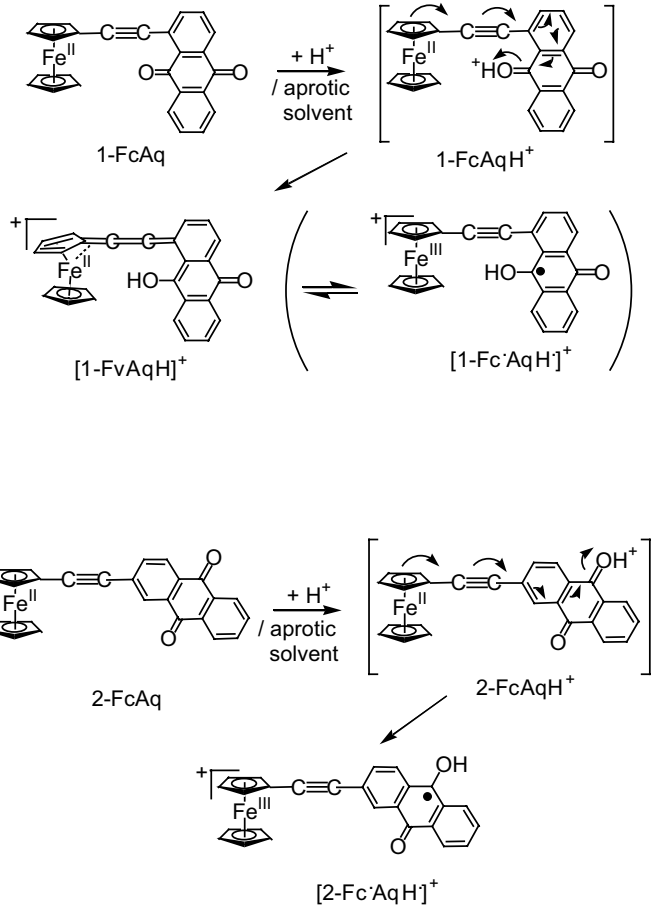

Scheme 1 Protonation reaction pathway of 1-FcAq and 2-FcAq.

The deprotonated form, 1-FcAq, shows reversible two-step $1e^-$ reduction at $E^{\circ\prime} = -1.26$ and -1.71 V versus ferrocenium/ferrocene (Fc^+/Fc) derived from the anthraquinone moiety, and reversible $1e^-$ oxidation at $E^{\circ\prime} = 0.22$ V due to the ferrocenyl moiety in *n*-Bu_4NClO_4-CH_2Cl_2 (Table 1). The first reduction potential shifts

dramatically in the positive direction to $E^{\circ\prime} = -0.06$ V, and the oxidation potential shifts moderately in the positive direction to $E^{\circ\prime} = 0.33$ V in the protonation product, $[1\text{-FvAqH}]^+$, whereas the second reduction potential is little changed. These results correspond to the structural changes in both ferrocenyl and anthraquinone moieties by protonation.

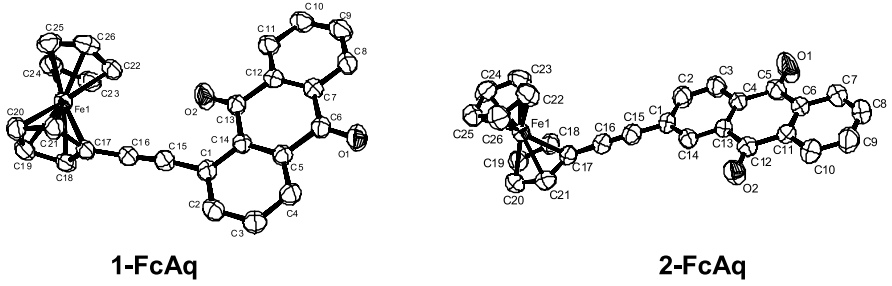

Figure 5 ORTEP (Oak Ridge thermal ellipsoid plot) diagrams of 1-FcAq and 2-FcAq with probability levels of 50% (reprinted with permission from Ref. 59).

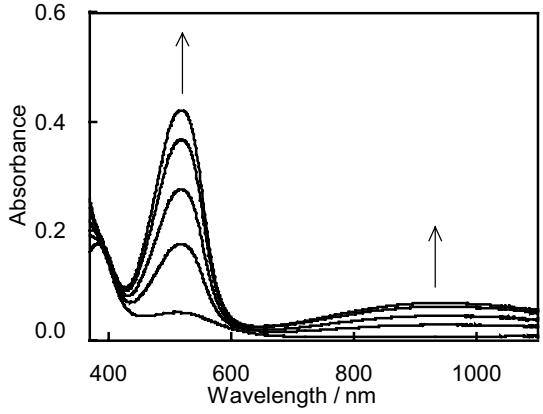

Figure 6 UV–vis–near-IR absorption spectral change of 1-FcAq (3.0×10^{-4} mol dm^{-3}) in benzonitrile on stepwise addition of 0–2 eq of CF_3SO_3H (reprinted with permission from Ref. 59).

Contrary to the facile change of 1-FcAq, the deep red solution of 2-FcAq did not change significantly after the addition of the stoichiometric amount of CF_3SO_3H. The color of the solution changed gradually to deep green by addition of an excess amount (50 eq) of CF_3SO_3H. The n-π^* and the MLCT bands decreased in intensity, and two new bands appeared at 414 and 615 nm. The intense band at 414 nm is appreciably consistent with that of the semiquinone form of anthraquinone derivatives.[68] The ^{1}H NMR spectrum of a CD_2Cl_2 solution of 2-FcAq indicated that the

Table 1 Redox Potentials of Ferrocene-Anthraquinone Complexes and Their Protonated Species in 0.1 mol dm^{-3} Bu_4NClO_4– CH_2Cl_2[a]

	$E^{\circ\prime}_{red}$ (V) versus Fc^+/Fc					$E^{\circ\prime}_{ox}$ (V) versus Fc^+/Fc			
1-FcAq	−1.83 (Aq)	−1.39 (Aq)	—	—	—	0.11 (Fc)	—	—	—
$[1\text{-FvAqH}]^+$	—	−1.05 (AqH)	−0.31 (AqH)	—		—	—	0.30 (Fv)	
$1,8\text{-Fc}_2\text{Aq}$	−1.75 (Aq)	−1.33 (Aq)	—	—	0.07 (Fc)	—	0.14 (Fc)	—	—
$[1,8\text{-FcFvAqH}]^+$	—	−1.01 (AqH)	−0.31 (AqH)	—	—	—	0.19 (Fc)	0.30 (Fv)	—
$1,5\text{-Fc}_2\text{Aq}$	−1.78 (Aq)	−1.39 (Aq)	—	—	—	0.11 ($2e^-$, Fc)	—	—	—
$[1,5\text{-FcFvAqH}]^+$	—	−1.07 (AqH)	−0.32 (AqH)	—	—	—	0.11 (Fc)	0.27 (Fv)	—
$[1,5\text{-Fc}^{\cdot}\text{FvAqH}_2^{\cdot}]^{2+}$	—	—	−0.16 (AqH_2)	0.11 (Fc^+)	—	—	—	0.27 (Fv)	0.42 (AqH_2)
1,1′-$FcAq_2$	−1.85 ($2e^-$, Aq)	−1.39 ($2e^-$, Aq)	—	—	—	0.21 (Fc)	—	—	—
$[1,1'\text{-FvAq}_2\text{H}]^+$	−1.85 (Aq)	−1.39 ($2e^-$, Aq&AqH)	−0.32 (AqH)	—	—	—	—	0.43 (Fv)	—
$[1,1'\text{-FvAq}_2\text{H}_2]^{2+}$	—	−1.39 ($2e^-$, AqH × 2)	−0.14 (AqH)	−0.06 (AqH)	—	—	—	0.43 (Fv)	—

[a] The number of electrons for the reaction is one except otherwise stated in parentheses.

complex lost the diamagnetic nature by the protonation. The EPR spectrum of 2-FcAq in benzonitrile on addition of 6 eq of CF_3SO_3H at 6.5 K showed well-resolved signals interpreted as superposition of a ferrocenium cation including paramagnetic low-spin Fe(III) nuclei ($g_{\|} = 4.26$, $g_{\perp} = 1.49$) and a semiquinone radical of the anthraquinone moiety ($g = 2.00$). The latter signal did not exhibit a hyperfine structure due to the coupling between the electron spin and the protons of the anthrasemiquinone moiety, indicating slight fluctuation of the electron spin state. From the results of the UV–vis absorption and the EPR spectra, it is postulated that 2-FcAq is changed into a "spin-separated" ferrocenium–semiquinone combination linked by an ethynyl group $[2\text{-Fc}^{\bullet}\text{AqH}^{\bullet}]^{+}$ through protonation (Scheme 1).

In conclusion, the electron transfer to the protonated anthraquinone moiety occurs from the cyclopentadienyl ring (e_{1u} orbital) of the ferrocene moiety when 1-FcAq is protonated in benzonitrile and from the iron center (a_{1g} or e_{2g} orbital) when 2-FcAq is protonated.

C. 2–1-FcAq Complexes

The next simplest complexes are 2–1-D/A compounds, 1,8-*bis*(ferrocenylethynyl)anthraquinone, 1,8-Fc_2Aq, and 1,5-*bis*(ferrocenylethynyl)anthraquinone, 1,5-Fc_2Aq.[69] Comparison of protonation behavior between them is intriguing because the quinone moiety can undergo double protonation, drastically changing the acceptor level and because there is a significant difference in conjugation of the ferrocenyl groups with the carbonyl groups of the anthraquinone moieties between the isomers. Two ferrocenyl groups in 1,5-Fc_2Aq conjugate with different carbonyl moieties, whereas those in 1,8-Fc_2Aq conjugate with the same carbonyl moiety (see Scheme 2). This actually influences the protonation behavior of the isomers; namely only 1,5-Fc_2Aq undergoes a facile two-step proton response, leading to a doubly protonated species with unique physical properties due to the existence of three possible valence tautomers, whereas 1,8-Fc_2Aq does only single protonation as described below.

The X-ray crystallographic analysis of both 1,8-Fc_2Aq and 1,5-Fc_2Aq indicates that the Cp rings and the anthraquinone plane are nearly perpendicular to each other as displayed in Figure 7. The spectroscopic responses of 1,8-Fc_2Aq and 1,5-Fc_2Aq to CF_3SO_3H in benzonitrile are significantly different. The solution of 1,8-Fc_2Aq changed immediately from deep red to deep reddish-purple after the addition of the acid, corresponding to the UV–Vis–near-IR absorption spectral change. The n-π^* band of the anthraquinone moiety decreased, two visible bands increased in intensity at 491 and 546 nm, and a new broad band with the half-width $\Delta\nu_{1/2} = 5.4 \times 10^3\ \text{cm}^{-1}$ appeared over the visible and near-IR regions ($\lambda_{max} = 934$ nm). This spectral change is quite similar to that of 1-FcAq.[59] The protonated species of 1,8-Fc_2Aq was isolated from the acidic solution, and its ESI-mass, ^{1}H NMR, ^{13}C NMR, and IR spectra revealed that 1,8-Fc_2Aq undergoes a single protonation of the carbonyl oxygen adjacent to the ethynylene bond, causing a structural change to create a compound involving both ferrocenyl-ethynyl and η^6-fulvene-cumulene moieties, $[1,8\text{-FcFvAqH}]^{+}$ (Scheme 2).

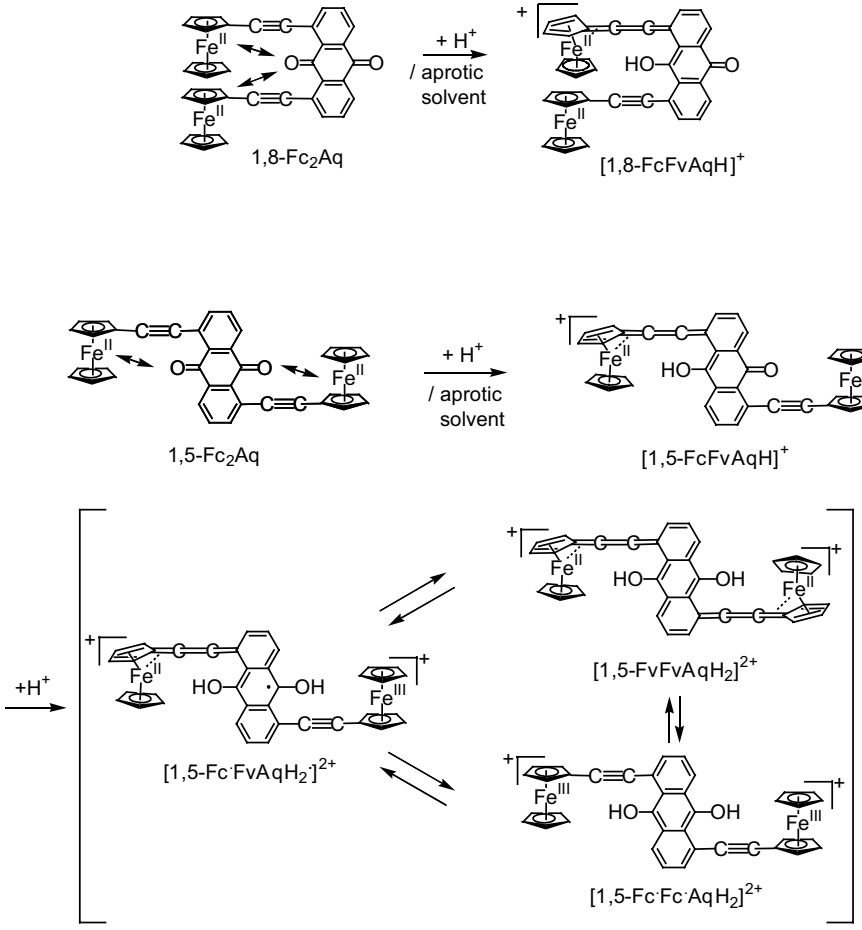

Scheme 2 Protonation reaction pathway of 1,8-Fc_2Aq and 1,5-Fc_2Aq. The arrow ↔ indicates conjugation between Fe and Carbonyl groups.

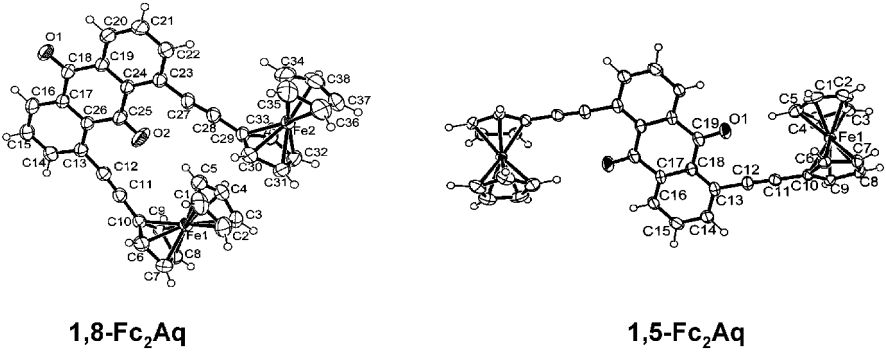

Figure 7 ORTEP diagrams of 1,8-Fc_2Aq and 1,5-Fc_2Aq with probability levels of 50% (reprinted with permission from Ref. 69).

In contrast, the addition of several equivalents of CF_3SO_3H into a benzonitrile solution of 1,5-Fc_2Aq resulted in two-step color changes, initially to deep reddish-purple, and then to deep green. ESI-mass spectra indicated that deep reddish-purple and deep green solutions were derived from singly and doubly protonated species, respectively. The first spectral change in the UV–Vis–near-IR absorption spectra, as depicted by the dotted lines in Figure 8, is quite similar to those of 1-FcAq and 1,8-Fc_2Aq, suggesting a conversion to a similar fulvene-Fe(II) complex–cumulene structure, $[1,5\text{-FcFvAqH}]^+$. In the second step, the MLCT band at $\lambda_{max} = 522$ nm decreased in intensity, two intense bands appeared at 748 and 850 nm, and the broad band with the half-width ($\Delta\nu_{1/2} = 7.2 \times 10^3\ cm^{-1}$, $\lambda_{max} = 909$ nm) was shifted to longer wavelength ($\Delta\nu_{1/2} = 5.2 \times 10^3\ cm^{-1}$, $\lambda_{max} = 1309$ nm) (Fig. 8, solid line). The two bands in the visible region are quite similar to those of the semiquinone form of anthraquinone derivatives.[68] The EPR spectrum of the frozen acidic acetonitrile solution of 1,5-Fc_2Aq at 5.0 K showed a strong, sharp signal at $g = 2.02$ assignable to a semiquinone radical of the anthraquinone moiety as well as weak broad signals at $g_{\|} = 4.12$ and $g_{\perp} = 1.5$ originating from a ferrocenium cation including a Fe(III) nucleus.[70,71] These spectroscopic results suggest the generation of a spin-separated form, $[1,5\text{-Fc}^{\bullet}\text{FvAqH}_2{}^{\bullet}]^{2+}$ (Scheme 2).

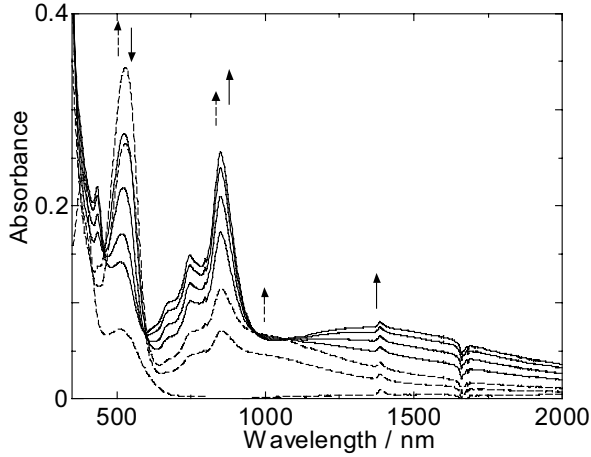

Figure 8 UV–Vis–near-IR absorption spectral change of 1,5-Fc_2Aq in (3.0×10^{-4} mol dm^{-3}) in benzonitrile on stepwise addition of 0–2 eq (dotted lines and arrows) and 2–4 eq (solid lines and arrows) of CF_3SO_3H.

Electrochemistry of the protonated compounds supported the reactions given in Scheme 2. The series of monoprotonated complexes exhibits a reversible two-step one-electron reduction of the protonated anthraquinone moiety (AqH) in the cyclic voltammograms, whose potentials are largely shifted in the more positive direction than those of nonprotonated forms (Table 1). The reversible oxidation waves of non- and monoprotonated complexes are derived from the metal-centered oxidation of the ferrocenyl and fulvene complex moieties. In $[1,5\text{-Fc}^{\bullet}\text{FvAqH}_2{}^{\bullet}]^{2+}$, the redox reaction

occurs in a pattern different from that of non- and monoprotonated complexes, with the rest potential positioned between the reduction wave of the ferrocenium moiety and the oxidation waves of Fv. Therefore, according to these results, the spin-separated form, $[1,5\text{-Fc}^{\bullet}\text{FvAqH}_2^{\bullet}]^{2+}$, among the three possible canonical structures, $[1,5\text{-Fc}^{\bullet}\text{FvAqH}_2^{\bullet}]^{2+}$, $[1,5\text{-FvFvAqH}_2]^{2+}$, and $[1,5\text{-Fc}^{\bullet}\text{Fc}^{\bullet}\text{AqH}_2]^{2+}$, is considered to be the most thermodynamically favorable in solution as the doubly protonated species of 1,5-Fc_2Aq.

Protonation of 1,5-Fc_2Aq with CF_3SO_3H in dichloromethane afforded a deep green precipitate, of which the ESI-mass spectrum indicated the formation of doubly protonated structure. Its UV–Vis–near-IR absorption spectrum in Nujol mull, showing the $^2E_{2g} \rightarrow {}^2E_{1u}$ transition characteristic of a ferrocenium ion (λ_{max} = 766 nm)[30] and significantly broad absorption (1456 nm), is different from that of $[1,5\text{-Fc}^{\bullet}\text{FvAqH}_2^{\bullet}]^{2+}$ (Fig. 9). The spectrum was gradually changed into that of $[1,5\text{-Fc}^{\bullet}\text{FvAqH}_2^{\bullet}]^{2+}$, with isosbestic points appearing after dissolution in acetonitrile. These results suggest that the green precipitate is a valence tautomer of $[1,5\text{-Fc}^{\bullet}\text{FvAqH}_2^{\bullet}]^{2+}$.

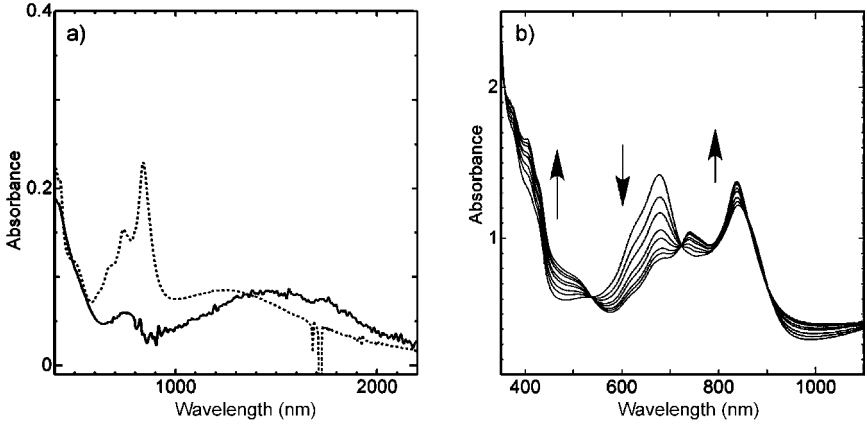

Figure 9 UV–Vis–near-IR absorption spectral change of doubly protonated 1,5-Fc_2Aq with CF_3SO_3H suspended in Nujol mull.

The ^{57}Fe Mössbauer spectra of the green precipitate designate strong temperature dependence, as shown in Figure 10. The spectrum at 10 K shows the superposition of two components of Fe(II) (QS = 2.10 mm/s, IS = 0.40 mm/s) and Fe(III) nuclei (QS = 0.30 mm/s, IS = 0.40 mm/s), for which the areal intensity ratio (ϕ = Fe(III)/ Fe(II) + Fe(III)) is 0.44 ($\pm$0.01). The QS value of the Fe(II) component is smaller than the value of the Fe(II) nucleus of the nonprotonated 1,5-Fc_2Aq (QS = 2.39 mm/s, IS = 0.55 mm/s, at 9.2 K), and this smaller QS value indicates a conversion to the fulvene-Fe(II) complex structure through protonation.[72,73] The absorption of the ferrocenium-Fe(III) nucleus increased compared to that of Fe(II), when the temperature was raised, as shown in the spectrum at 293 K (Fig. 9). The ϕ values at 50, 150, 220, and 293 K were estimated to be 0.51 ($\pm$0.04), 0.70 ($\pm$0.08), 0.70 ($\pm$0.08), and 1.00 ($\pm$0.09), respectively.

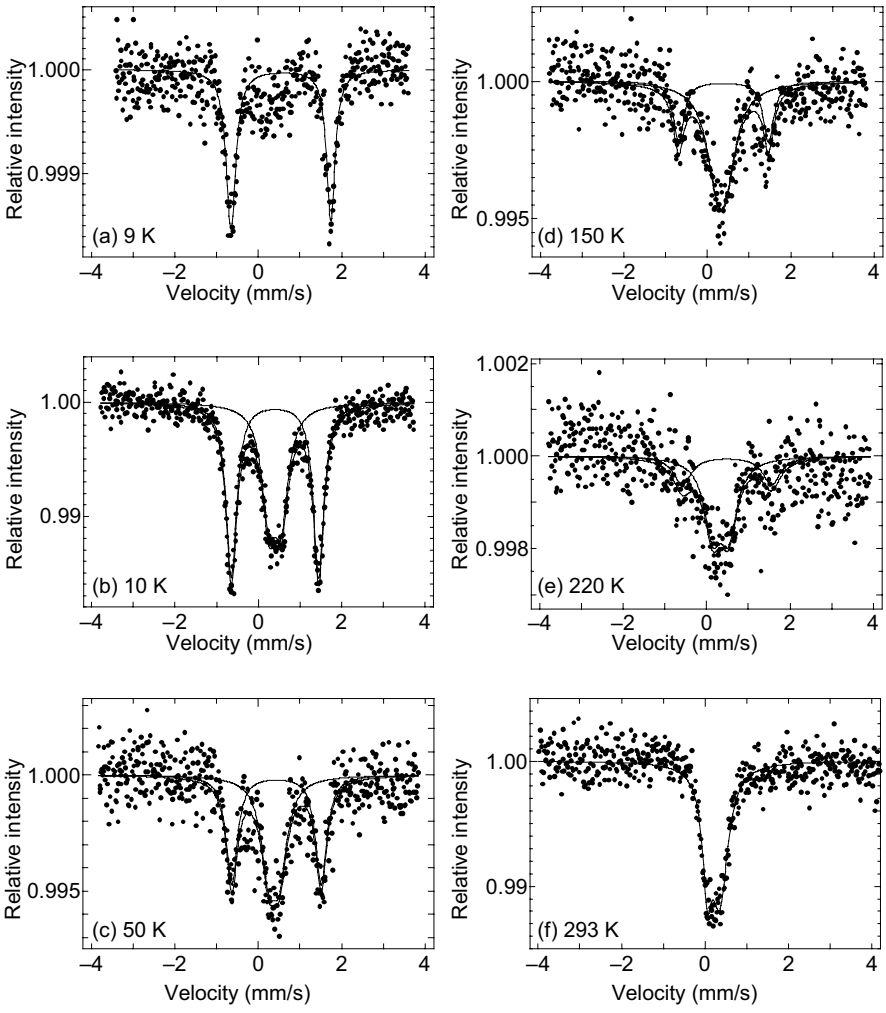

Figure 10 ^{57}Fe Mössbauer spectra of 1,5-Fc_2Aq at 9 K (a), and doubly protonated 1,5-Fc_2Aq at 10 K (b), 50 K (c), 150 K (d), 220 K (e), and 293 K (f) (reprinted with permission from Ref. 69).

The EPR spectrum of the solid state of the doubly protonated 1,5-Fc_2Aq at 6.6 K showed a superposition of two components of Fe(III) nuclei from a ferrocenium cation ($g_{\|} = 3.93$, $g_{\perp} = 1.59$) and a semiquinone radical of the anthraquinone moiety ($g = 2.00$). The ratio in signal intensity of the semiquinone radical to the ferrocenium cation was considerably smaller in the solid state than in the frozen solution state. The $\chi_M T$–T plot of this doubly protonated 1,5-Fc_2Aq is shown in Figure 11. The $\chi_M T$ value decreased with decreasing temperature.

The temperature-dependent change of the ^{57}Fe Mössbauer spectra can be ascribed to the thermal equilibrium between the three valence tautomers,

$[1,5\text{-FvFvAqH}_2]^{2+}$, $[1,5\text{-Fc}^{\bullet}\text{FvAqH}_2^{\bullet}]^{2+}$, and $[1,5\text{-Fc}^{\bullet}\text{Fc}^{\bullet}\text{AqH}_2]^{2+}$ in the solid state (Scheme 2). At higher temperatures, the paramagnetic $[1,5\text{-Fc}^{\bullet}\text{Fc}^{\bullet}\text{AqH}_2]^{2+}$, with its two ferrocenium Fe(III) nuclei, is dominantly formed. The $\chi_M T$ value at 348 K is 0.95 $cm^3\ mol^{-1}$ K, which is close to the calculated $\chi_M T$ value of 1.05 for $[1,5\text{-Fc}^{\bullet}\text{Fc}^{\bullet}\text{AqH}_2]^{2+}$, as estimated from the EPR *g* values. With decreases in temperature, $[1,5\text{-Fc}^{\bullet}\text{Fc}^{\bullet}\text{AqH}_2]^{2+}$ might primarily be transformed into the diamagnetic $[1,5\text{-FvFvAqH}_2]^{2+}$, which has two fulvene-Fe(II) and doubly protonated anthrahydroquinone moieties, as the calculated $\chi_M T$ values in typical temperatures estimated from the EPR *g* values and ^{57}Fe Mössbauer ϕ values correspond well with the experimental $\chi_M T$ values (Fig. 11). A small distribution of $[1,5\text{-Fc}^{\bullet}\text{FvAqH}_2^{\bullet}]^{2+}$, which is dominant in the solution, cannot be ruled out at low temperature in the solid state because of the existence of a weak EPR signal for the radical.

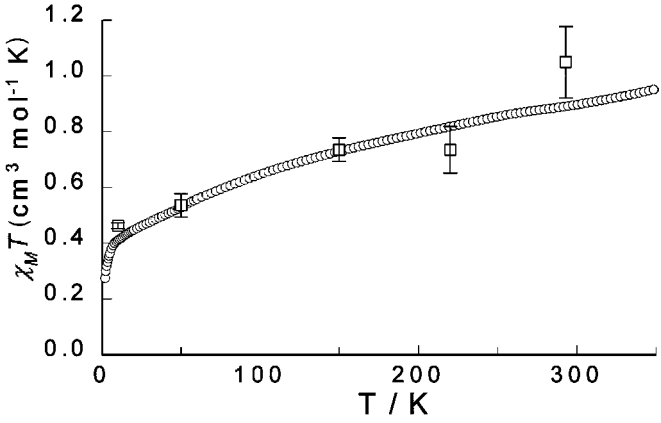

Figure 11 The $\chi_M T$–*T* plot of doubly protonated 1,5-Fc_2Aq (○) and $\chi_M T$ values estimated from the EPR *g* values and ^{57}Fe Mössbauer ϕ values (□) (b) (reprinted with permission from Ref. 69).

D. A 1–2-FcAq Complex

The other simplest combination of the nonequivalent donor–acceptor members is a 1–2-D/A compound, 1,1′-*bis*(1-(anthraquinonyl)ethynyl)ferrocene (1,1′-$FcAq_2$). To this complex, two-step protonation occurs, while only the first protonation causes the intramolecular electron transfer reaction.[31]

When 8 eq of CF_3SO_3H were added to a benzonitrile solution of 1,1′-$FcAq_2$, the color of the solution changed immediately from red to deep reddish-pink. This color change corresponds to the spectral change in which the band at $\lambda_{max} = 510$ nm with $\varepsilon = 2.8 \times 10^3$ mol^{-1} dm^3 cm^{-1} increases 4 times in intensity with a slight blueshift to $\lambda_{max} = 504$ nm, together with an appearance of a new broad band with the half-width over visible and near-IR regions ($\lambda_{max} = 936$ nm, $\varepsilon = 1.3 \times 10^3$ mol^{-1} dm^3 cm^{-1}). These spectral changes are similar to those of other FcAq complexes,[59,69] indicating that the ferrocenyl moiety is converted into butatriene-fulvene-Fe(II)-Cp.

The spectroscopic change due to the proton-coupled phenomenon of 1,1′-$FcAq_2$ in benzonitrile continued even after the addition of 8 eq of CF_3SO_3H. This spectroscopic behavior with the acid was also observed in dichloromethane and chloroform, and in these cases, there was saturation of the spectral change, which is indicative of complete protonation. The degree of spectral change was not proportional to the amount of added CF_3SO_3H in any solvent, suggesting that this spectral change is not due to a single-step reaction. Possible rationales for this result are the existence of double protonation to both anthraquinone moieties and/or the acid–base equilibrium of the anthraquinone moiety.

The addition of 1 eq of CF_3SO_3H to the concentrated 1,1′-$FcAq_2$ solution in chloroform produced reddish-brown precipitate that could be separated by filtration. The mass spectrum of the product shows a molecular ion peak at $m/z = 647\,MH+$, indicating the addition of one hydrogen atoms to 1,1′-$FcAq_2$ [FAB-mass (m/z): 646 M+]. When 6 eq of CF_3SO_3H were added to the concentrated 1,1′-$FcAq_2$ solution in chloroform, a precipitate with the molecular ion peak at $m/z = 648\,MH_2+$ was detected, indicating a formation of doubly protonated species. These results suggest that 1,1′-$FcAq_2$ undergoes a two-step protonation; the first step occurs with the addition of 1 eq of CF_3SO_3H involves the monoprotonation of 1,1′-$FcAq_2$ causing a structure conversion identical to that of 1-FcAq, producing a unique structure involving an AqH–butatriene–fulvene–Fe(II)–Cp–ethynylene–Aq moiety, $[1,1'\text{-}FvAq_2H]^+$ (Scheme 3), while the second step achieved by the addition of 6 eq of CF_3SO_3H involves the double protonation of 1,1′-$FcAq_2$ to give $[1,1'\text{-}FvAq_2H_2]^{2+}$, with the UV–Vis–near-IR absorption not changing significantly. This process results in no additional intramolecular electron transfer, which is reasonable since the butatriene-fulvene-Fe(II)-fulvene-butatriene structure should be unstable.

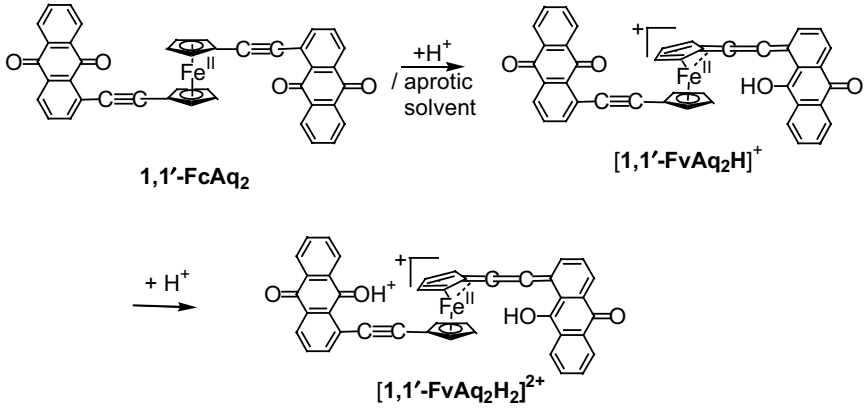

Scheme 3 Protonation reaction pathway of 1,1′-$FcAq_2$.

The results of cyclic voltammetry of 1,1′-$FcAq_2$ with the stepwise addition of CF_3SO_3H in Bu_4NClO_4-CH_2Cl_2 are shown in Table 1. The nonprotonated complex, 1,1′-$FcAq_2$ shows reversible two-step $2e^-$ reductions derived from the two

anthraquinone moieties (−1.85 and −1.39 V vs. Fc^+/Fc), with reversible $1e^-$ oxidation originating from the ferrocene moiety (0.21 V), respectively. The reduction of two neutral anthraquinone units occurs simultaneously, due to the relatively small interaction between the two units through the linked ethynylene and ferrocene units. The addition of 1 eq of CF_3SO_3H for 1,1′-$FcAq_2$ shows the redox behavior of $[1,1'\text{-}FvAq_2H]^+$. This monoprotonated complex exhibits three reversible reduction waves at −1.85 ($1e^-$), −1.39 ($2e^-$), and −0.32 V ($1e^-$) and an oxidation wave at 0.43 V ($1e^-$), which can be interpreted as the overlapping of redox waves of anthraquinone (Aq; −1.85 and −1.39 V), protonated anthraquinone (AqH; −1.39 and −0.32 V), and fulvene–Fe(II) (Fv; 0.43 V). Further addition of the acid to cause one more protonation to $[1,1'\text{-}FvAq_2H]^+$ produces a serious change in the redox wave of the anthraquinone moiety, and this behavior appears identical to that occurring with the formation of $[1,1'\text{-}FvAq_2H_2]^{2+}$. The reduction waves at −1.85 ($1e^-$), −1.39 ($2e^-$), and −0.32 V ($1e^-$) are changed to −1.39 ($2e^-$), −0.14 ($1e^-$) and −0.06 V ($1e^-$), whereas the oxidation wave derived from the fulvene–Fe(II) unit is not influenced by the further addition of CF_3SO_3H (0.43 V), indicating that the fulvene–Fe(II) structure is not changed. Disappearance of the most negative wave at −1.85 V ($1e^-$) derived from the nonprotonated anthraquinone unit of $[1,1'\text{-}FvAq_2H]^+$ indicates that the second protonation for $[1,1'\text{-}FvAq_2H]^+$ occurs at the nonprotonated anthraquinone moiety. Consequently, two monoprotonated anthraquinone moieties are formed in the double protonation of 1,1′-$FcAq_2$.

E. Polymeric 1–1-FcAq Complexes

The results noted above present peculiar structure conversion and spin separation behavior of a series of ferrocenylethynylanthraquinones caused by protonation, which depends on the substituent position, the number of donor and acceptor units. This predicts the intriguing properties of polymer complexes of this series. From this point of view, 1–1-D/A polymer, $(1,1'\text{-Fc-1,8-Aq})_n$, comprising ferrocenylethynyl–anthraquinone units in the mainchain, was synthesized and its PCET behavior investigated.[74]

The polymer $(1,1'\text{-Fc-1,8-Aq})_n$ was synthesized by the reaction of 1,1′-*bis*(trimethylstanylethynyl)ferrocene and 1,8-dibromoanthraquinone. The polymer was obtained as a deep brown powders, containing soluble and insoluble components in regular organic solvents. The soluble part gave a film when it was dried, and its average molecular weight determined by GPC based on the polystyrene standard was ∼2000. As for the insoluble component of the polymer, the addition of CF_3SO_3H changed the polymer soluble in common organic solvents such as acetonitrile or dichloromethane, and the color changes from deep red to deep purple-pink.

The UV–Vis–near-IR absorption spectrum of the solution of the protonated polymer exhibited the MLCT bands and valence tautomerization and similar to those of 1,8-Fc_2Aq as shown in Figure 12, indicating the formation of fulvene complexes in the mainchain in solution. The infrared spectrum of the protonated polymer also showed the similarity with that of 1,8-Fc_2Aq; specifically, half of the C–C triple bond remain. These results indicate a formation of $([1,1'\text{-Fv-1,8-AqH}]^+)_n$ as shown in Scheme 4.

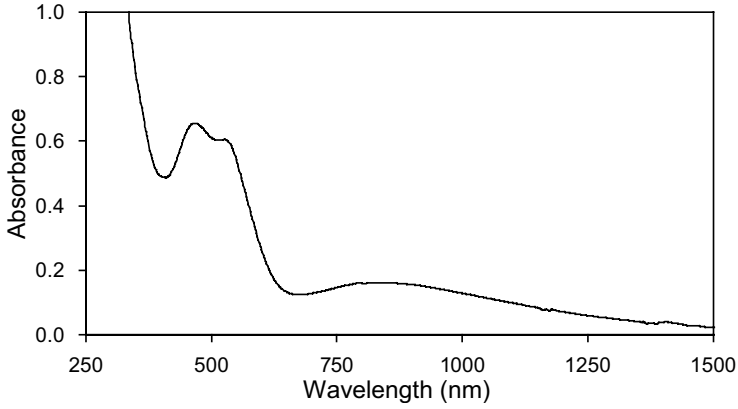

Figure 12 UV–vis–near-IR absorption spectrum of protonated $(1,1'\text{-Fc-1,8-Aq})_n$ (1.3×10^{-3} mol/dm^3 as FcAq monomer unit) in acetonitrile.

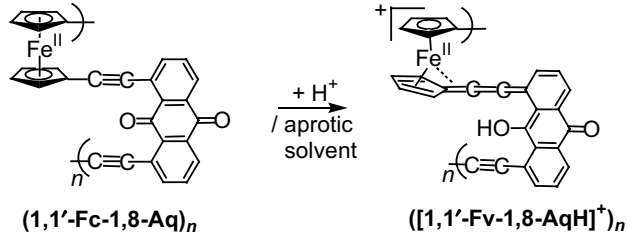

Scheme 4 Protonation reaction pathway of $(1,1'\text{-Fc-1,8-Aq})_n$.

III. VINYLENE-BRIDGED FERROCENE-BENZOQUINONE COMPLEX

Proton-coupled intramolecular electron transfer was investigated for another quinonoid compound, $FcCHCHBQH_2$, linked to the ferrocene moiety by a π-conjugated spacer.[75] The compound $FcCHCHBQH_2$ was synthesized by the Wittig coupling of ferrocenylmethyltriphenylphosphonium bromide with 2,5-ditosylbenzaldehyde,[76] followed by deprotection of the tosyl groups. Chemical oxidation of $FcCHCHBQH_2$ by $[Fe(\eta^5\text{-}C_5H_4Cl)_2]PF_6$ in methanol showed a drastic decrease of the UV–Vis absorption band at 342 nm, and an increase of the band at 312 nm, as shown in Figure 13a, affording the $2e^-$-oxidized form, FcCHCBQH, which consists of an unusual allene and a quinonoid structure, with the loss of two hydrogen atoms from $FcCHCHBQH_2$ (Scheme 5).

In the ^{1}H NMR spectrum of FcCHCBQH in acetone-d_6, two doublets at δ 6.88 and 7.02 ppm derived from the vinylene protons of $FcCHCHBQH_2$ disappeared and a new singlet appeared at 6.67 ppm. One of the two singlets at 7.60 and 7.81 ppm, due to nonequivalent hydroxyl protons of $FcCHCHBQH_2$, was not detected in

FcCHCBQH, and the remaining singlet at 8.00 ppm immediately disappeared by H/D exchange on addition of D_2O. As a result of one of the two vinylene carbons of $FcCHCHBQH_2$, a new ^{13}C NMR signal as a quaternary carbon appeared in a lower field position at 131.6 ppm with disappearance of the signal. The ^{13}C NMR spectrum of FcCHCBQH has also indicated that the ferrocenyl structure is maintained without the oxidation-induced significant change into a fulvene-like structure.[59,77] The IR spectrum of FcCHCBQH exhibited weak bands around 1900 cm^{-1} that are ascribable to C=C stretching of the allene structure. The compound FcCHCBQH is considered to be a structural isomer of both 2-(2-ferrocenylvinyl)-*p*-benzoquinone and 2-(ferrocenylethynyl)hydroquinone. It is of substantial interest that the oxidation of $FcCHCHBQH_2$ favors the release of two hydrogen atoms—one from the vinylene and one from the hydroxyl group—to disintegrate the ordinarily stable aromatic structure of $FcCHCHBQH_2$.

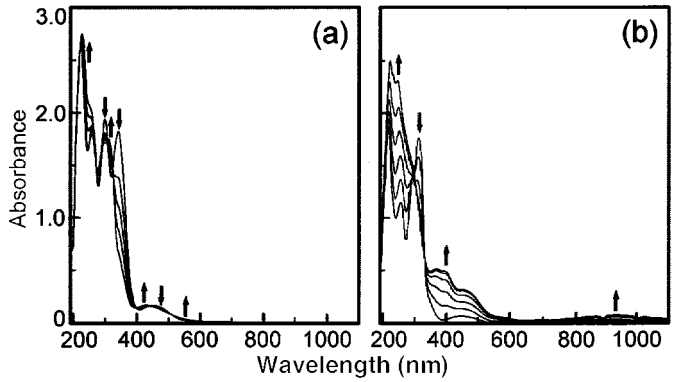

Figure 13 (a) UV–Vis–near-IR absorption spectral change of $FcCHCHBQH_2$ (1.2 mM) in methanol on stepwise addition of 0–2.0 eq of 1,1′-dichloroferrocenium *hexa*fluorophosphate under a nitrogen atmosphere. Light pathlength is 1 mm. (b) UV–Vis–near-IR absorption spectral change of FcCHCBQH (1.2 mM) in acetonitrile on stepwise addition of 0–100 eq of CF_3SO_3H under a nitrogen atmosphere. Light pathlength is 1 mm. (Reprinted with permission from Ref. 75.)

A proposed formation mechanism of FcCHCBQH is shown in Scheme 5. The oxidation of $FcCHCHBQH_2$ initially occurs at the ferrocenyl site to form a ferrocenium state of Fe(III), based on the fact that the reversible redox wave due to the ferrocenyl site is observed at the potential $E^{\circ\prime} = -0.11$ V versus Fc^+/Fc, more positive than the potentials of irreversible oxidation waves due to the hydroquinone site ($E_{p,a} = 0.39$ and 0.79 V) in acetonitrile, and the redox potential of the oxidizing agent $[Fe(C_5H_4Cl)_2]PF_6$ (0.23 V vs. Fc^+/Fc) is located between the potentials of the ferrocenyl and the hydroquinone sites.[78] The strong electron-withdrawing effect of the ferrocenium moiety causes the immediate elimination of a proton. The proton elimination from the hydroquinone moiety and the vinylene moiety followed by further $1e^-$ oxidation resulted in formation of the semiquinone radical intermediates

$[Fc^{\bullet}CHCHBQH^{\bullet}]^{+}$ and $[Fc^{\bullet}CHCBQH_2^{\bullet}]^{+}$, respectively. The structural change between $[Fc^{\bullet}CHCHBQH^{\bullet}]^{+}$ and $[Fc^{\bullet}CHCBQH_2^{\bullet}]^{+}$ likely occurs through the proton exchange between the carbonyl oxygen and the allene carbon, which are located nearby. A further proton-elimination reaction from the vinylene carbon of $[Fc^{\bullet}CHCHBQH^{\bullet}]^{+}$ or from the hydroxyl group of $[Fc^{\bullet}CHCBQH_2^{\bullet}]^{+}$ affords the stable compound FcCHCBQH, in which the iron center is reduced. It is considered that the deprotonation of $[Fc^{\bullet}CHCHBQH^{\bullet}]^{+}$is less likely than that of $[Fc^{\bullet}CHCBQH_2^{\bullet}]^{+}$, and that the structural change between $[Fc^{\bullet}CHCHBQH^{\bullet}]^{+}$ and $[Fc^{\bullet}CHCBQH_2^{\bullet}]^{+}$ plays an important role in the formation mechanism of FcCHCBQH including the allene and quinonoid structure.

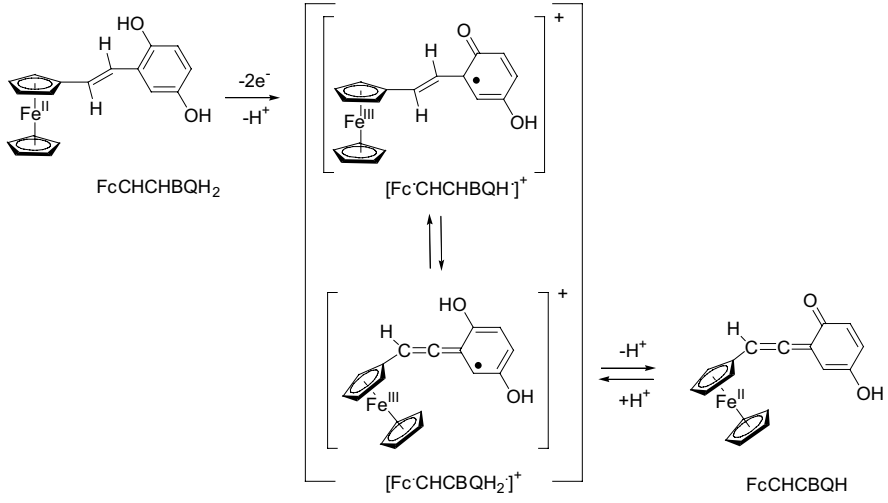

Scheme 5 Redox and proton-coupled reaction of $FcCHCHBQH_2$.

The UV–Vis–near-IR absorption spectral change of FcCHCBQH in acetonitrile, on stepwise addition of CF_3SO_3H (0–100 eq), indicated an interesting proton response, as shown in Figure 13b. The new intense bands appearing at 400 and 456 nm, the molar extinction coefficients, ε values, of which were estimated at 4.0×10^3 and $2.5 \times 10^3\,mol^{-1}dm^3cm^{-1}$, respectively, were appreciably similar to those of the free semiquinone radical,[44,79,80] and the weak shoulder band at 600 nm with $\varepsilon = 350\ mol^{-1}dm^3cm^{-1}$ can be attributed to the $^2E_{2g} \rightarrow {}^2E_{1u}$ transition of the ferrocenium ion.[81] The EPR spectrum of the frozen solution of the product at 6.4 K exhibited a well-resolved signal ($g_{\parallel} = 3.97$, $g_{\perp} = 1.64$) attributable to a ferrocenium cation, including paramagnetic Fe(III) nuclei.[70,82–84] The appearance of the ferrocenium state of Fe(III) from diamagnetic FcCHCBQH resulted in generation of an odd number of electrons, that is, in generation of a semiquinone radical through an intramolecular electron transfer. The semiquinone radical was not detected in the

EPR spectrum, probably due to fluctuation of the electron spin states, which is supported by the significant broadening of the axial signal of the ferrocenium moiety. These facts indicate that the diamagnetic FcCHCBQH can be converted to the paramagnetic semiquinone-ferrocenium compound $[Fc^{\bullet}CHCHBQH^{\bullet}]^{+}$ through the protonation of FcCHCBQH. A broad absorption band was observed at 1000 nm in the near-IR spectrum of $[Fc^{\bullet}CHCHBQH^{\bullet}]^{+}$. This band may be due to LMCT at the Fe(III) center—photoinduced valence tautomerization[61,62] between the Fe(III) center and the semiquinone—given that radical complexes exhibit long-wavelength bands due to low-lying transitions originating from the singly occupied molecular orbitals (SOMOs).[85]

Two protonation sites exist in FcCHCBQH to form $[Fc^{\bullet}CHCHBQH^{\bullet}]^{+}$. The protonation of the allene carbon leads to the direct formation of $[Fc^{\bullet}CHCHBQH^{\bullet}]^{+}$ via an intramolecular electron transfer from the ferrocenyl to the quinonoid site. The protonation of the carbonyl oxygen of the quinonoid site forms $[Fc^{\bullet}CHCBQH_2^{\bullet}]^{+}$, and requires the structural change into $[Fc^{\bullet}CHCHBQH^{\bullet}]^{+}$, that is, from the allene to the vinylene bonding. When 100 eq of CF_3SO_3H was added all at once, a transient UV–Vis absorption spectrum was observed, and this spectrum gradually changed to that of $[Fc^{\bullet}CHCHBQH^{\bullet}]^{+}$. This implies a two-step transformation, and supports the idea that the transient species is produced by the protonation of the carbonyl oxygen. Intriguingly, when $FcCHCHBQH_2$ was oxidized by 2 eq of $[Fe(C_5H_4Cl)_2]PF_6$ in acetonitrile, the observed UV–Vis–near-IR absorption spectrum at room temperature and the EPR spectrum at 6.9 K were quite similar to those of the protonated form of FcCHCBQH. The addition of methanol into the acetonitrile solution of $[Fc^{\bullet}CHCHBQH^{\bullet}]^{+}$ caused the UV–Vis– near-IR absorption spectrum to change into that of FcCHCBQH. This means that methanol assists in the proton elimination from $[Fc^{\bullet}CHCHBQH^{\bullet}]^{+}$, and supports the consideration that the intermediate $[Fc^{\bullet}CHCHBQH^{\bullet}]^{+}$ should be included in the formation process of FcCHCBQH from $FcCHCHBQH_2$ in methanol.

In summary, an unusual structural change of a vinylene-bridged ferrocene-hydroquinone compound, $FcCHCHBQH_2$, was observed to occur by two-electron oxidation and two-proton elimination in methanol. The oxidation product, FcCHCBQH, which includes an allene and a quinonoid structure, exhibited a unique proton response, leading to an exchange of the magnetic properties.

IV. CONCLUDING REMARKS

In this chapter, novel intramolecular PCET phenomena of ethynylene-bridged ferrocene-anthraquinone complexes, 1-FcAq, 2-FcAq, 1,8-Fc_2Aq, 1,5-Fc_2Aq, 1,1′-$FcAq_2$, and $(1,1'\text{-Fc-1,8-Aq})_n$ and a vinylene-bridged ferrocene-benzoquinone complex, $FcCHCHBQH_2$ have been described. In these donor–acceptor-conjugated compounds, drastic changes in structure and physical properties are observed. The singly and doubly protonated forms of the FcAq complexes reach an equilibrium involving two and three valence tautomers, depending on the matrix and temperature. The events in the FcBq complex are strongly dependent of the solvents. These findings should be useful in designing novel functional ferrocene-containing molecular

systems from mononuclear to polynuclear compounds based on strong intramolecular donor–acceptor interaction triggered by chemical perturbation.

V. REFERENCES

1. D. Gust, T. A. Moore, A. L. Moore, *Acc. Chem. Res.* **26,** 198 (1993).
2. A. Harriman, J. -P. Sauvage, *Chem. Soc. Rev.* **25,** 41 (1996).
3. D. Gust, T. A. Moore, A. L. Moore, S.-J. Lee, E. Bittersmann, D. K. Luttrull, A. A. Rehms, J. M. DeGraziano, X. C. Ma, F. Gao, R. E. Belford, T. T. Trier, *Science* **248,** 199 (1990).
4. D. A. Williamson, E. B. Bruce, *J. Am. Chem. Soc.* **120,** 10902 (1998).
5. A. Soudackov, S. H. Schiffer, *J. Am. Chem. Soc.* **121,** 10598 (1999).
6. T. Maki, Y. Araki, Y. Ishida, O. Onomura, Y. Matsumura, *J. Am. Chem. Soc.* **123,** 3371 (2001).
7. J. P. Kirby, J. A. Roberts, D. G. Nocera, *J. Am. Chem. Soc.* **119,** 9230 (1997), and references cited therein.
8. P. J. Piotrowiak, *Chem. Soc. Rev*. **28,** 143 (1999).
9. M. A. Smitha, E. Prasad, K. R. Gopidas, *J. Am. Chem. Soc.* **123,** 1159 (2001).
10. J. Deisenhofer, H. Michel, *Angew. Chem., Int. Ed. Engl.* **28,** 829 (1989).
11. R. Huber, *Angew. Chem., Int. Ed. Engl.* **28,** 848 (1989).
12. L. Ouahab, *Coor. Chem. Rev.* **178–180,** 1501 (1998).
13. D. M. Guldi, M. Maggini, G. Scorrano, M. Prato, *J. Am. Chem. Soc.* **119,** 974 (1997).
14. K. Ogawa, Y. Kobuke, *Angew. Chem., Int. Ed. Engl.* **39,** 4070 (2000).
15. M. Diekers, A. Hirsch, S. Pyo, J. Rivera, L. Echegoyen, *Eur. J. Org. Chem.* 1111 (1998).
16. P. D. Beer, S. S. Kurek, *J. Organomet. Chem.* **366,** C7 (1989).
17. J. Zhang, H.-R. Sun, G.-Y. Yang, K. Wen, L.-X. Yu, X.-Z. Cao, *Electrochim. Acta* **48,** 2693 (1998).
18. N. B. Thornton, H. Wojtowiez, T. Netzel, D. W. Dixon, *J. Phys. Chem. B* **102,** 2101).
19. H. Hokari, M. Fujihira, *Thin Solid Films* **273,** 185 (1996).
20. M. Fujihira, M. Sakomura, *Thin Solid Films* **179,** 471 (1989).
21. K. Uosaki, T. Kondo, X.-Q. Zhang, M. Yanagida, *J. Am. Chem. Soc.* **119,** 8367 (1997).
22. A. Ikeda, T. Hatano, S. Shinkai, T. Akiyama, S. Yamada, *J. Am. Chem. Soc.* **123,** 4855 (2001).
23. H. Imahori, M. Arimura, T. Hanada, Y. Nishimura, I. Yamazaki, Y. Sakata, S. Fukuzumi, *J. Am. Chem. Soc.* **123,** 335 (2001).
24. H. Imahori, H. Yamada, Y. Nishimura, I. Yamazaki, Y. Sakata, *J. Phys. Chem. B* **104,** 2099 (2000).
25. D. K. Smith, G. A. Lane, M. S. Wrighton, *J. Phys. Chem.* **92,** 2616 (1988) and references therein.
26. X.-U. Yi, L.-Z. Wu, C.-H. Tung, *J. Phys. Chem. B* **104,** 9468 (2000).
27. M. Skupin, G. Li, W. Fudickar, J. Zimmermann, B. Röder, J.-H. Fuhrhop, *J. Am. Chem. Soc.* **123,** 3454 (2001).
28. I. Willner, B. Willner, *J. Mater. Chem.* **8,** 2543 (1998) and references therein.
29. D. Mandler, I. Turyan, *Electroanalysis* **8,** 207 (1996).
30. C. Joachim, J. K. Gimzewski, A. Aviram, *Nature* **408,** 541 (2000).
31. H. Nishihara, "Organometallic Conductive Polymers", in *Handbook of Organic Conductive Molecules and Polymers*, H. S. Nalwa, ed., Wiley, 1997, Vol. 2, Chap. 19, pp. 799–832.
32. H. Nishihara, *Bull. Chem. Soc. Jpn.* **74,** 19 (2001).

33. M. Kurihara, H. Nishihara, *Coord. Chem. Rev.* **226,** 125 (2002).
34. H. Nishihara, *Adv. Inorg. Chem.* **53,** 41–86 (2002).
35. S. Barlow, H. E. Bunting, C. Ringham, J. C. Green, G. U. Bublitz, S. G. Boxer, J. W. Perry, S. R. Marder, *J. Am. Chem. Soc.* **121,** 3715 (1999).
36. S. Barlow, S. R. Marder, *Chem. Commun.* **2000,** 1555 (2000).
37. M. I. Bruce, *Chem. Rev.* **98,** 2797 (1998), and references cited therein.
38. K. N. Jayaprakash, P. C. Ray, I. Matsuoka, M. M. Bhadbhade, V. G. Puranik, P. K. Das, H. Nishihara, A. Sarkar, *Organometallics* **18**(19), 3851 (1999).
39. Y. S. Shon, D. N. Hendrickson, H. B. Gray, *J. Am. Chem. Soc.* **93,** 3603 (1971).
40. V. N. Sapunov, K. Kirchner, R. Schmid, *Coord. Chem. Rev.* **214,** 143 (2001).
41. S. Barlow, H. E. Bunting, C. Ringham, J. C. Green, G. U. Bublitz, S. G. Boxer, J. W. Perry, S. R. Marder, *J. Am. Chem. Soc.* **121,** 3715 (1999).
42. B. J. Coe, C. J. Jones, J. A. McCleverty, D. Bloor, G. H. Cross, *J. Organomet. Chem.* **464,** 225 (1994).
43. B. J. Coe, J.-D. Foulon, T. A. Hamor, C. J. Jones, J. A. McCleverty, D. Bloor, G. H. Cross, T. L. Axon, *J. Chem. Soc., Dalton Trans.* 3427 (1994).
44. S. Patai, ed., *The Chemistry of the Quinonoid Compounds*, Parts 1, 2, Wiley, Bristol, UK, 1974.
45. J. S. Jaworski, E. Lesniewska, M. K. Kalinowski, *J. Electroanal. Chem.* **105,** 329 (1979).
46. N. Gupta, H. Linschitz, *J. Am. Chem. Soc.* **119,** 6384 (1997).
47. P. Tissot, A. Huissoud, *Electrochim. Acta* **41,** 2451 (1996).
48. C. Degrand, *Annali di Chimica* **75,** 1 (1985).
49. S. Fukuzumi, K. Ishikawa, K. Hironaka, T. Tanaka, *J. Chem. Soc., Perkin Trans.* **2,** 751 (1987).
50. M. S. Graige, M. L. Paddock, J. M. Bruce, G. Feher, M. Y. Okamura, *J. Am. Chem. Soc.* **118,** 9005 (1996).
51. Y. -Z. Hu, S. Tsukiji, S. Shinkai, S. Oishi, I. Hamachi, *J. Am. Chem. Soc.* **122,** 241 (2000).
52. M. R. Wasielewski, *Chem. Rev.* **92,** 435 (1992).
53. M. Sato, E. Mogi, S. Kumakura, *Organometallics* **14,** 3157 (1995).
54. M. Sato, E. Mogi, M. Katada, *Organometallics* **14,** 4837 (1995).
55. J. A. Mata, E. Falomir, R. Llusar, E. Peris, *J. Organomet. Chem.* **616,** 80 (2000).
56. N. J. Long, A. J. Martin, R. Vilar, A. J. P. White, D. J. Williams, M. Younus, *Organometallics* **18,** 4261 (1999).
57. M. C. B. Colbert, J. Lewis, N. J. Long, P. R. Raithby, A. J. P. White, D. J. Williams, *J. Chem. Soc., Dalton Trans.* 99 (1997).
58. N. D. Jones, M. O. Wolf, *Organometallics* **16,** 1352 (1997).
59. M. Murata, T. Fujita, M. Yamada, M. Kurihara, H. Nishihara, *Chem. Lett.* **2000,** 1328 (2000).
60. M. Murata, Ph.D. thesis, Univ. Tokyo, 2002.
61. D. M. Adams, D. N. Hendrickson, *J. Am. Chem. Soc.* **118,** 11515 (1996), and references cited therein.
62. C. G. Pierpont, C. W. Lange, *Prog. Inorg. Chem.* **41,** 331 (1994).
63. T. D. Turbitt, W. E. Watts, *J. Chem. Soc., Perkin Trans.* **2,** 177 (1974).
64. G. A. Olah, G. Liang, *J. Org. Chem.* **40,** 1849 (1975).
65. N. Cully, W. E. Watts, *J. Organomet. Chem.* **182,** 99 (1979).
66. A. Ceccon, G. Giacometti, A. Venzo, D. Paolucci, D. Benozzi, *J. Organomet. Chem.* **185,** 231 (1980).
67. U. Behrens, *J. Organomet. Chem.* **182,** 89 (1979).
68. B. E. Hulme, E. J. Land, G. O. Phillips, *J. Chem. Soc., Faraday Trans. I* **68,** 1992 (1972).

69. M. Murata, M. Yamada, T. Fujita, K. Kojima, M. Kurihara, K. Kubo, Y. Kobayashi, H. Nishihara, *J. Am. Chem. Soc.* **123,** 12903 (2001).
70. W. H. Morrison, Jr., D. N. Hendrickson, *Inorg. Chem.* **14,** 2331 (1975).
71. Y. S. Shon, D. N. Hendrickson, B. Gray, *J. Am. Chem. Soc.* **93,** 3603 (1971).
72. U. Behrens, *J. Organomet. Chem.* **182,** 89 (1979).
73. Barlow, S. R. Marder, *Chem. Commun.* 1555 (2000).
74. H. Nishihara, M. Murata, K. Kojima, T. Fujita, K. Kubo, M. Kurihara, *Polym., Mater. Sci. Eng.* **86,** 87 (2002).
75. M. Kurihara, H. Sano, M. Murata, H. Nishihara, *Inorg. Chem.* **40,** 4 (2001).
76. K. R. Thomas, J. T. Lin, Y. S. Wen, *J. Organomet. Chem.* **575,** 301 (1999).
77. A. Masuda, Y. Masuda, Y. Fukuda, *J. Phys. Chem. A* **101,** 2245 (1997).
78. T. Hirao, K. Aramaki, H. Nishihara, *Bull. Chem. Soc. Jpn.* **71,** 1817 (1998).
79. X. Zhao, H. Imahori, C.-G. Zhan, Y. Sakata, S. Iwata, T. Kitagawa, *J. Phys. Chem. A* **101,** 622 (1997).
80. N. Okumura, B. Uno, *Bull. Chem. Soc. Jpn.* **72,** 1213 (1999).
81. Y. S. Sohn, D. N. Hendrickson, H. B. Gray, *J. Am. Chem. Soc.* **93,** 3603 (1971).
82. M. Kurihara, T. Matsuda, A. Hirooka, T. Yutaka, H. Nishihara, *J. Am. Chem. Soc.* **122,** 12373 (2000).
83. D. O. Cowan, G. A. Candela, F. Kauffman, *J. Am. Chem. Soc.* **93,** 3889 (1971).
84. T.-Y. Dong, D. N. Hendrickson, C. G. Pierpont, M. F. Moore, *J. Am. Chem. Soc.* **108,** 963 (1986).
85. V. Kasack, W. Kaim, H. Binder, J. Jordanov, E. Roth, *Inorg. Chem.* **34,** 1924 (1995).

CHAPTER 9

Organization of Ferrocenoyl Amino Acids

Heinz-Bernhard Kraatz

Department of Chemistry, University of Saskatchewan, Saskatoon, Saskatchewan, Canada

CONTENTS

Macromolecules Containing Metal and Metal-like Elements, Volume 2: Organoiron Polymers, Edited By Alaa S. Abd-El-Aziz, Charles E. Carraher, Jr., Charles U. Pittman, Jr., John E. Sheats, and Martel Zeldin
ISBN 0-471-45078-2

I. INTRODUCTION

Since the early 1990s there have been numerous accounts of novel functional biomaterials. Peptides in particular have received much attention. In solution and in the crystalline state, amino acids and peptides often assemble into extended supramolecular three-dimensional structures guided by hydrogen bonding between individual molecules.[1,2] The properties of such extended peptide networks are related to the molecular arragement of the individual molecules and offer a fascinating array of structures. Considerable effort has focused on the design of secondary structural elements,[3,4] and on the design of new peptidic materials, such as nanotubes[5–9] and hydrogels,[10–12] with potential applications in drug delivery and biomedical engineering. In many cases, scaffolds are used to assist the design and guide formation of a particular peptide structural mimic. More recently, significant efforts have been directed at equipping noncovalent supramolecular peptide assemblies with redox-active groups and give them specific electric properties that may be exploited.

This review focuses on ferrocene peptide systems, with particular attention to mono and 1,1′-disubstituted ferrocene derivatives. Both systems have been successfully explored as templates in an effort to create highly ordered electroactive supramolecular systems.

II. SYNTHESIS OF FERROCENOYL PEPTIDES

Fc-amino acids and Fc-peptides have been prepared by various different methods. Most of them use commercially available ferrocenecarboxylic acid (FcOH, **1**) or ferrocenecarboxylic acid chloride (FcCl, **2**). Historically, amide bond formation was achieved starting from **2** and a suitable amino component, such as an amino acid or peptide, having an available NH_2 group, to give the desired Fc-amino acid esters (**3**) or Fc-peptides (**4**)[13] (Scheme 1).

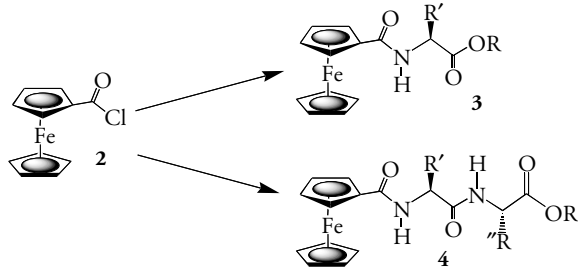

Scheme 1 Synthesis of ferrocenoyl amino acid esters (**3**) and peptides (**4**) via the acid chloride method.

The acid chloride method was successfully employed to produce a number of 1,1′-disubstituted ferrocenoyl peptide and amino acid systems, such as Herrick's 1,1′-ferrocenoyl-prolinylmethylester (**5**)[14] and Hirao's 1,1′-ferrocenoyl-*bis*-alanyl-prolinylesters (**6**).[15]

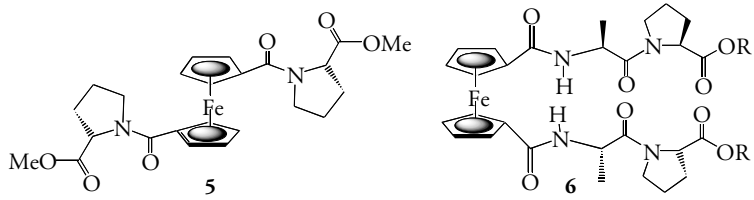

More recently, a convenient method for linking peptides or amino acids to the ferrocenoyl group was developed using FcOH as a starting material and carbodiimides such as dicyclohexylcarbodiimide (DCC) or 1-(3-dimethylaminopropyl)-3-ethyl-carbodiimide (EDC) in conjunction with hydroxybenzotriazole (HOBt)[16–18] or succinimide (HOSu) (Scheme 2). The intermediates HOBt- or HOSu-active esters (**7**) can be isolated as dark red crystalline materials. Both are stable toward hydrolysis, and readily react with the available amino groups of amino acid esters or peptide esters to give the corresponding Fc-amino acid ester (**3**) or peptide esters (**4**) in high yields. Similarly, Fc-amino acids and peptides can be directly obtained by employing amino acids or peptides instead of the C-protected esters.

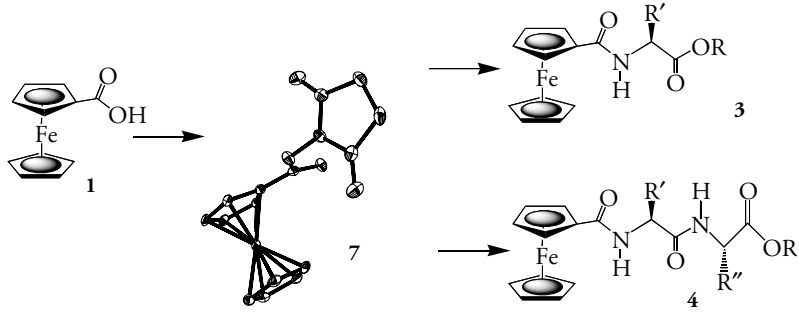

Scheme 2 Synthesis of ferrocenoyl amino amino acids (**3**) and peptides (**4**) via the FcOSu (**7**) active ester.

The synthetic procedures and workup are similar to those employed in standard solution peptide synthesis and hence are suitable for labelling larger biomolecules at the ε-amino group of lysines, as was shown by Degani and Heller.[19,20] The Fc-amino acid esters and peptides can be deprotected under basic conditions and can serve as useful building blocks for formation of more complex structures. This procedure was used successfully for the preparation of helical Fc oligoproline benzyl esters, in which the oligoproline exists exclusively in the all-*trans* conformation in solution and the solid state.[21]

Using this approach, symmetric Fc-peptide-cystamines were synthesized in high yields. For example, [Fc-Gly-CSA]$_2$ (**10**), an orange crystalline materials, was obtained by coupling of Fc-OBt or Fc-Osu with the symmetric tetrapeptide [Boc-Gly-CSA]$_2$ (**9**) (CSA = cysteamine), as summarized in Scheme 3.[22] Similarly, a wide range of symmetric Fc-peptide cystamines were synthesized and used for the electrochemical electron transfer studies of organized Fc-peptide monolayers on gold.

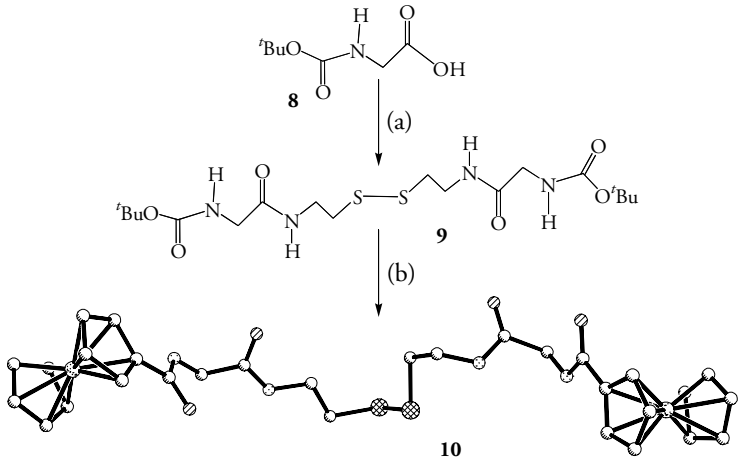

Scheme 3 Synthesis of ferrocenoyl glycyl cystamine (**10**): (a) DCC or EDC, HOBt, cystamine dihydrochloride, Et_3N; (b) Fc-OBt or Fc-OSu.

A series of 1,1′-oligoprolinoyl-ferrocenes (**5**, **15**–**17**) were obtained from 1,1′-ferrocenedicarboxylic acid (**11**), HOBt, EDC, and a series of oligoproline esters (Scheme 4).[23,24] The monoproline derivative **5** was first obtained by Herrick via the acid chloride route.[14]

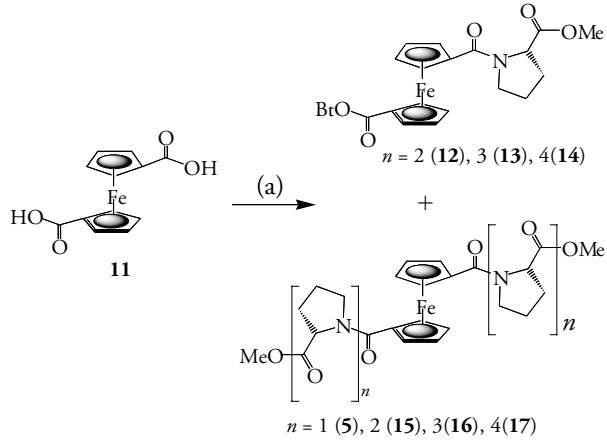

Scheme 4 Synthesis of 1,1′-*bis*-peptide ferrocene derivatives peptides (**4**) via the HOBt/EDC protocol: (a) HOBt, EDC, CH_2Cl_2, H-Pro$_n$-OMe (n = 1–4) (Sta = statine).

Interestingly, using the HOBt, 1-oligoprolinoyl-1′-OBt-ferrocene derivatives (**12**–**14**) were obtained as byproducts. This class of compounds is a convenient starting material en route to asymmetrically substituted ferrocenoyl derivatives, such as compound **18**.

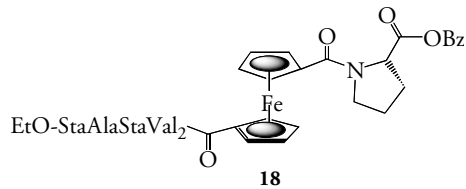

18

An alternative route to Fc-peptides, developed by Beck and coworkers, uses ferrocenyl oxazolones,[17] which can be obtained by the reaction of Fc-amino acids (**19**) with a carbodiimide (Scheme 5). The resulting oxazolone (**20**) undergoes a nucleophilic ring-opening reaction with the amino group of a C-protected amino acid to give the desired Fc-peptide (**4**).

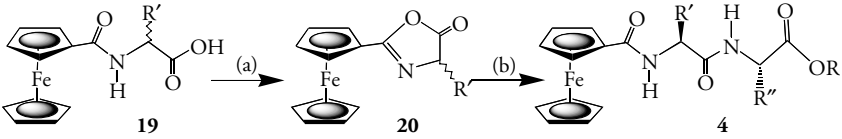

19 **20** **4**

Scheme 5 Synthesis of ferrocenoyl peptides (**4**) via the ferrocenyl oxazolone (**20**) starting from a ferrocenoyl amino acid (**19**); (a) DCC or EDC, (b) amino acid.

The crude Fc-amino acids and Fc-peptides are readily purified by chromatographic methods or by recrystallization. In many cases, this results in crystalline materials of sufficient quality for crystallographic investigations.

III. STRUCTURE OF FERROCENOYL PEPTIDES

A. General Parameters

Table 1 summarizes some pertinent structural features for some Fc-amino acids (**21**–**24**) and Fc-peptides (**5**, **25**–**31**). In general, the two cyclopentadienyl (Cp) rings of most structurally investigated Fc-amides are in a coplanar arrangement[25] with very small bent angles, which is the angle of the Cp rings away from coplanarity (**II**), and coplanarity between the amide and Cp planes (**I**) as defined in Scheme 6.

Steric pressures or interactions of the substituents with adjacent molecules may result in a loss of coplanarity of the Cp rings. The group attached to ferrocenoyl moiety has a significant influence on the coplanarity of the Cp and amide planes. Generally, with increasing size of the substituent, the twist angle between the Cp and amide planes will increase (Scheme 6), which will result in poor electronic coupling between Cp and amide for large twist angles. In general, for all ferrocenoyl amino acids and peptides, the Cp bent angle is relatively small ($<$1–4.5°), but as the peptide

becomes larger, the angle becomes greater because of the relief of steric pressures.[26] In the solid-state structure of Fc-Pro_4-OBz (**27**) the two Cp rings adopt a Cp-bent angle of 16.0°.[21]

Table 1 Common Structural Parameters for Ferrocenoyl Amino Acids and Peptides

				Angle	
Compound	*d*(C=O)	*d*(C=C)	<(O–C–N)	Bent	Twist
Fc-(Pro-OMe)$_2$ (**5**)	1.219(11)	1.515(14)	129.2(9)	<1	—
	1.227(11)	1.481(14)	120.1(9)	<1	—
Fc-(AlaPro-OMe)$_2$ (**6a**)	1.219(7)	1.506(9)	121.7(7)	0.53	3.77, 5.64
Fc-(AlaPro-OEt)$_2$ (**6b**)[a]	1.222(7)	1.478(8)	121.7(6)	2.45	5.27
Fc-(AlaPro-OPr)$_2$ (**6c**)	1.22(1)	1.47(1)	119(1)	1.75	1.70, 4.38
Fc-(AlaPro-OBzl)$_2$ (**6d**)	1.22(1)	1.51(1)	121(1)	2.60	2.64, 2.84
[Fc-Gly-CSA]$_2$ (**10**)[b]	1.252(2)	1.478(3)	122.08(18)	3.1	14.0
	1.232(3)	1.508(3)	122.4(2)	2.6	8.7
Fc-Asp(OH)-OH (**21**)	1.252(2)	1.472(2)	121.74(17)	<1	4.3
Fc-Glu(OBzl)$_2$ (**22**)	1.236(6)	1.499(7)	122.5(4)	1.8	14.1
Fc-Cys(SBzl)-OMe (**23**)	1.21(2)	1.43(2)	123.6(26)	1.8	5.4
Fc-Pro-OH (**24**)	1.257(14)	1.48(2)	116.6(11)	1.9	24.6
Fc-Pro_2-OBz (**25**)	1.23(3)	1.50(4)	120.6(30)	2.5	19.2
Fc-Pro_3-OBz (**26**)	1.222(12)	1.50(2)	118.1(11)	4.0	14.2
Fc-Pro_4-OBz (**27**)	1.223(5)	1.489(6)	120.8(4)	16.0	8.0
Fc-Gly_2-OEt (**28**)[c]	1.240(2)	1.477(2)	120.96(15)	2.1	<1
	1.233(2)	1.484(2)	122.32(16)	1.9	<1
Fc-AlaPro-OEt (**29**)[c]	1.234(7)	1.498(9)	122.8(7)	2.64	22.50, 24.30[b]
Fc-AlaPro-NHpy (**30**)	1.224(10)	1.490(8)	122.9(6)	—	—
Fc-LeuPhe-OMe (**31**)	1.215(8)	1.485(10)	121.2(7)	4.5	18.9
Fc-Pro_2Phe-OH (**32**)	1.244(9)	1.463(10)	119.7(7)	1.0	11.4

[a] The Fe atom is on a special position.
[b] Two parts of the molecule.
[c] Two independent molecules per asymmetric unit.

The Cp-amide twists for most Fc-peptides are generally small, allowing significant electronic interaction between the π systems of the Cp and the amide group. However, there are some exceptions in which larger twist angles are realized, most likely as the result of intramolecular strain and repulsion between the Cp ring and the peptide substituents or as a result of intermolecular interactions, discussed in the following section.

The distances of the carbonyl carbon to the Cp rings for all structurally characterized Fc-peptides are well within established bond distances for a normal C–C single bond in Fc-amides [range *d*(C–C) = 1.43–1.507 Å].[25] Furthermore, the amide C(O)–N group is planar in all Fc-amino acids and Fc-peptides, and the carbonyl C=O distances compare well with simple ferrocene amides. Similarly, the bond distances and angles of the Fc moiety itself are well within established parameters for ferrocene derivatives.[25]

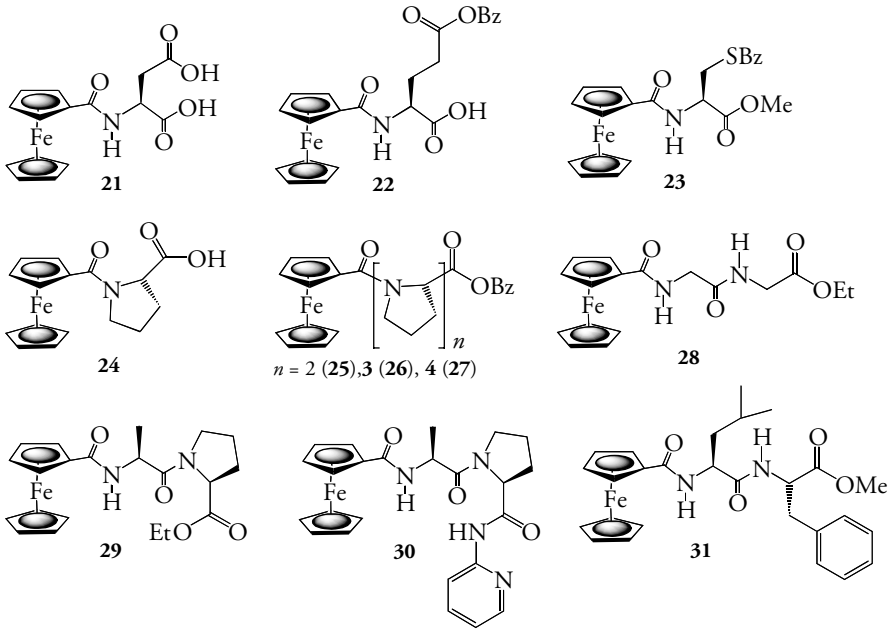

B. Hydrogen Bonding and Ordering in the Solid State

Even simple Fc-peptides exhibit a fascinating array of intermolecular hydrogen bonding interactions, which result in an ordered packing of the molecules in the solid state. In all structures investigated to date, the Fc group does not interfere with the peptides' instrinsic ability to assemble into larger aggregates via intermolecular hydrogen bonding.

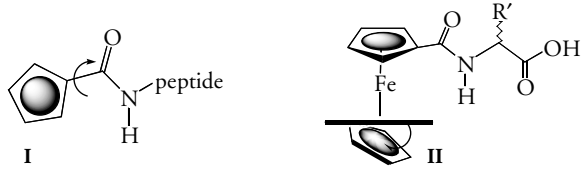

Scheme 6 Twist angle (**I**) and bent angle (**II**) in substituted ferrocenes.

The crystal structures of Fc-Gly$_2$-OEt (**28**),[27] Fc-AlaPro-OEt (**29**),[28] and Fc-LeuPhe-OMe (**31**)[27] provide examples. The structure of **28** is shown in Figure 1. The asymmetric unit contains two independent molecules. In addition, it contains a water molecule, disordered over two positions. The two independent molecules of **28** are held together by H bonding involving the Cp-amide carbonyl and NH groups [d(O1−N11) = 3.073 Å and d(N2−O12) = 2.992 Å] (Fig. 1a). Compound **28** forms a layered structure with H bonding between adjacent units forming a layered structure. The individual layers are connected through H bonding to a water molecule. The

arrangement between the Fc-diglycine molecules in the layers is best described as a parallel β sheet (Fig. 1b). In fact, the torsion angles, Φ and ψ, in **28** are −120° and +116° respectively, which is close to the literature values of Φ = −119° and ψ = +113° for a parallel β sheets.[29]

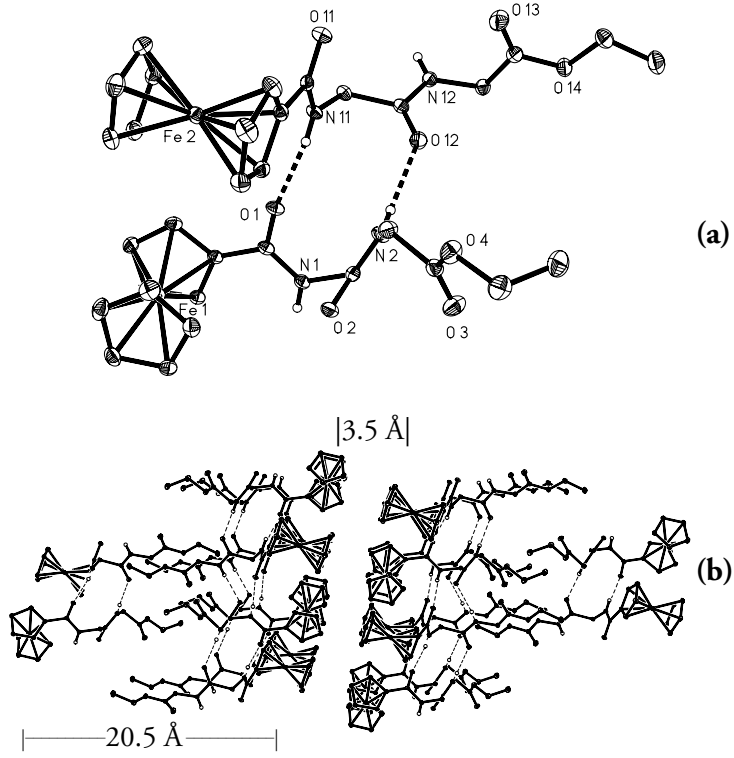

Figure 1 (a) Molecular structure of Fc-Gly_2-OEt (**28**). Two adjacent molecules interacting in a head-to-head fashion engaging in H bonding, resembling structures commonly found in parallel β sheets. (b) View of the β sheet. Two β sheets form tail-to-tail bilayers having the peptide substituents on the inside of the bilayer with a thickness of 20.5 Å and an interlayer distance of 3.5 Å. (Reprinted with permission from Ref. 27. Copyright 2001 American Chemical Society.)

The Fc-dipeptide β-sheet layers form a supramolecular bilayer structure with the peptide substituents pointing towards each other, as shown in Figure 1b. The bilayer thickness is 20.5 Å, and its separation from the adjacent bilayer is 3.5 Å. Studies of simple diglycine show that it crystallizes in a layered structure with strong N–H···O=C H bonds linking molecules, resulting in a parallel β-sheet-like structure.[30–33]

This demonstrates that in essence, the H-bonding ability of diglycine substituent is not significantly perturbed by the presence of the Fc group. In fact, the

Gly_2 substituent on Fc controls the arrangement of the molecules in the solid state, resulting in a strongly H-bonded structure similar to that found in diglycine. Strongly H-bonded networks leading to an antiparallel assembly of the Fc-dipeptide were reported by Hirao and coworkers for Fc-AlaPro-NHpy (**30**).[34]

Figure 2 shows an ORTEP of **30** together with the highly organized supramolecular assembly formed by H bonding involving the Fc-Ala CO and NH and the pyridine amide NH and ring N, thereby maximizing the H-bonding interactions. In contrast, Fc-AlaPro-OEt (**29**), having only the Fc-Ala amide linkage as a functional group able to interact with adjacent molecules, assembles into a simple linear chain, as shown in Figure 3.

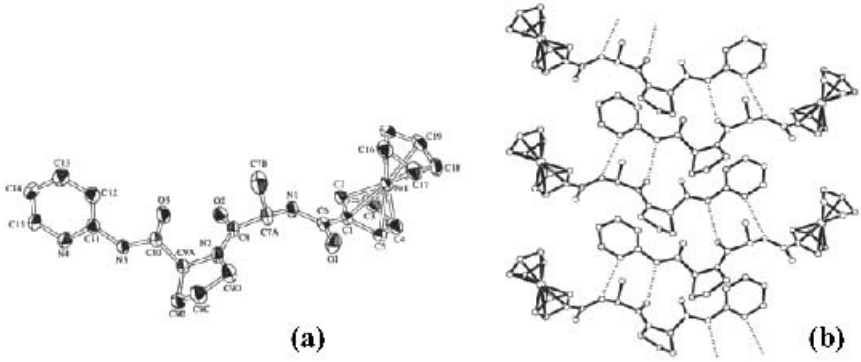

Figure 2 (a) Molecular structure of Fc-AlaPro-NHpy (**30**). (b) A view of the layered structure formed by association of the molecules in an antiparallel head-to-tail fashion.

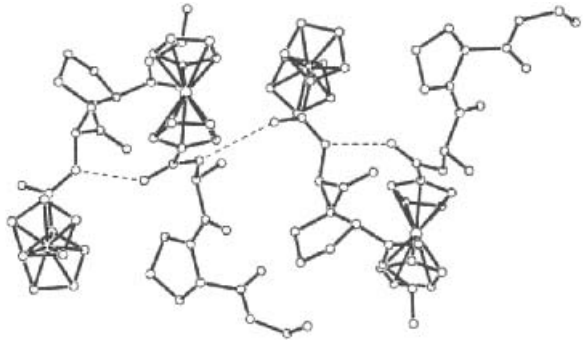

Figure 3 H-bonding involving the Fc-amide NH and CO groups in Fc-AlaPro-OEt (**29**) results in a linear chain.

It is noteworthy that the Cp/amide twist angle is large most likely due to the involvement of the carbonyl group in H bonding. The H bonding in **31** is similar to that of **28** in that it involves the interaction of two Fc-amides [Fc-C=O···H–N–C(O)-Fc; d(O1–N1B) = 2.977 Å] and two peptide amides [$C{=}O_{Phe}{\cdots}H{-}N_{Phe}$;

d(O2B–N2) = 2.983 Å] of two adjacent molecules (Fig. 4). Thereby a maximum of four interactions are established to adjacent molecules, which can be best described as a parallel sheetlike interaction.[27] However, the supramolecular arrangement is distinctly different from that of a β sheet. Instead, the intermolecular H-bonding interactions enable the formation of supramolecular helicates. Four molecules are required to complete one helical turn, giving a pitch of 14.6 Å and a width of approximate 12.7 Å (Fc to Fc). Interestingly, both aromatic residues, Fc and Ph groups are located on the outside of the helix (Fig. 4) and the isobutyl substituents are on the inside of the helix. Presumably, this supramolecular structure is adopted to satisfy the steric requirements of the Leu and Phe groups. The solvent molecules occupy positions in between individual helicate stacks. In a more detailed structural study by Hirao and coworkers, a series of disubstituted ferrocenoyldipeptides was studied.[35] It was shown that only intramolecular H bonding is present in the C_2 symmetric molecules of the Fc-(AlaPro-OR)$_2$ series, forcing the two Cp rings into a 1,2′ conformation, which has been observed frequently in other disubstituted ferrocenes. Two strong intramolecular H-bonding interactions are present between the C=O of Ala of the Cp ring and the amide NH of Ala of another strand on the Cp′ ring giving *d*(O···HN) distances of 1.88 and 2.15 Å (Fig. 5). One would expect that the size of the peptide would lead to a significant twist. However, the strong intramolecular H bonding is the dominant factor, forcing the two amide planes to be coplanar to their respective Cp ring.

Changing the ester substituent in this series of compounds has virtually no effect on their molecular conformation. Importantly, the intramolecular H bonding is preserved in solution, which contrasts the behaviour of the monosubstituted Fc-AlaPro-OEt (**29**), in which the intermolecular interactions break down in solution. Despite the lack of intermolecular H bonding, these molecules assemble in a chirality-directed selfassembly into helical structures. The helicity depends on the chirality of the podant peptide. The L-Ala-L-Pro podant peptide chain will result in a helical arrangement, with the podant D-Ala-D-Pro giving the exact mirror image (Fig. 5). Both have a pitch height of >14 Å and a Fc–Fc distance of approximately 4.5 Å. The related GlyPro and ProGly systems form related supramolecular arrangements in which intramolecular H bonding determines the structure of the assembly.[36]

A very recent (as of 2003) example from our laboratory shows chiral ordering in the achiral Fc-glycylcystamine (**10**).[22] The ORTEP of **10** was shown in Scheme 3. In the solid state, each molecule maximizes its H bonding interaction with adjacent molecules. Interestingly, for each Fc-Gly-CSA (CSA = cysteamine) half of the molecule engages in H bonding through the Fc-amide and cystamine functions with the identical portion of two neighboring molecules, one on each face, resulting in each molecule interacting with four adjacent molecules. However, the two portions establish different H-bonding patterns, as shown in Scheme 7.

The H bonding O1···N1* and N2···O2* is virtually symmetric and forms a 12-membered ring, as observed in other Fc-peptide structures (Scheme 7a) and

commonly found in parallel peptide β sheets. The pair of H bond acceptors O3 and O4 are *cis*-oriented on the same face of the molecule, whereas the H bond donors N3 and N4 are *cis* but located on the other face of the molecule. The result is a H-bonding pattern involving a 12-membered ring novel to Fc-peptides (Scheme 7b). The H-bonding is very asymmetric [O3···N3* = 2.976(12) Å and O4···N4* = 2.789(12) Å]. This complex intermolecular H-bonding interaction requires the molecules to turn with respect to each other, where each Fc-Gly fragment of **10** is involved in a different supramolecular helical arrangement. The result is a fascinating arrangement of the molecules giving two types of helices with H-bonded cores linked to each other through a disulfide bridge, as shown in Figure 6.

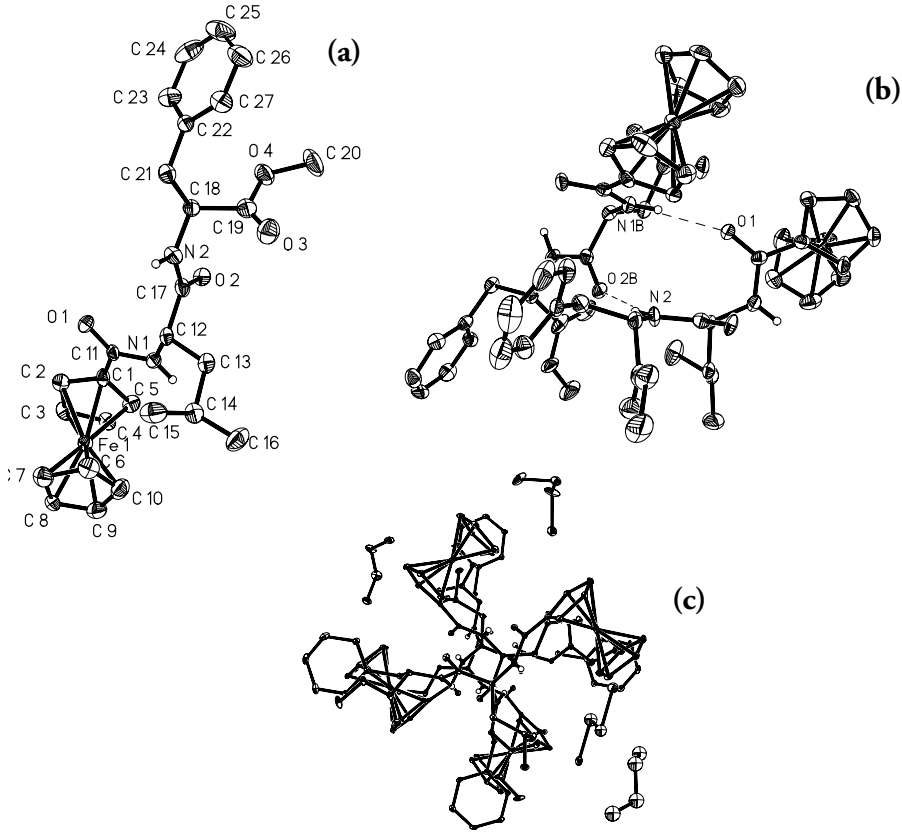

Figure 4 (a) Molecular structure of Fc-LeuPhe-OMe (**31**). (b) Two adjacent molecules engaging in H bonding in a head-to-head fashion. Please note that the steric pressure forces a rotation of the molecules of about 90° with respect to each other. (c) View down the supramolecular helical axis. The solvent of crystallization ($C_2H_4Cl_2$) is shown. (Reprinted with permission from Ref. 27. Copyright 2001 American Chemical Society.)

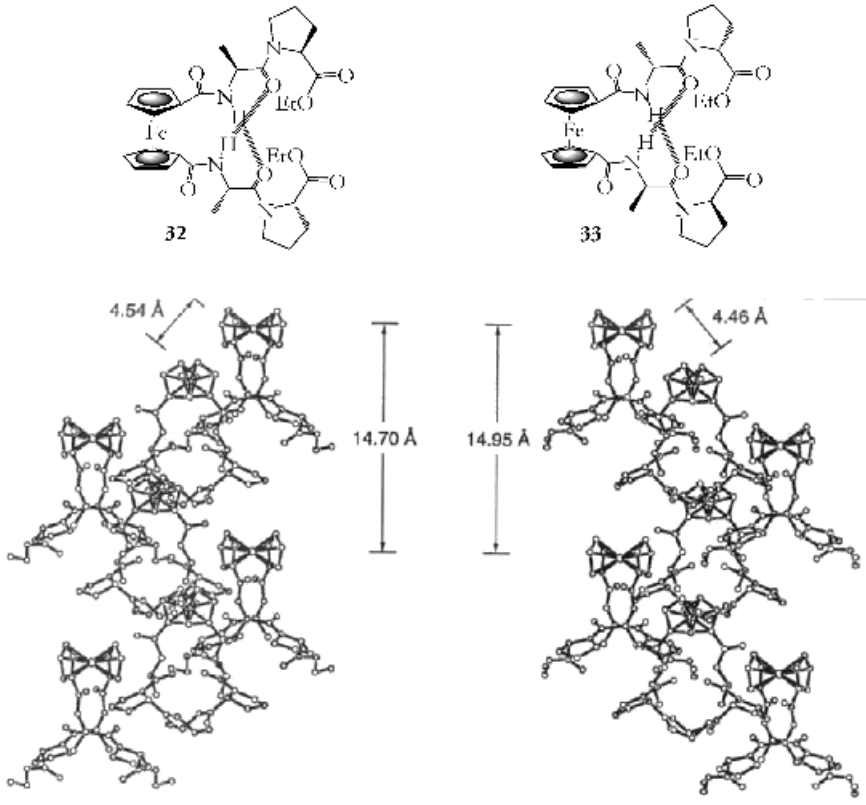

Figure 5 (a) Molecular structure of Fc-(L-Ala-L-Pro-OEt)$_2$ (**32**) and Fc-(D-Ala-D-Pro-OEt)$_2$ (**33**). (b) View at the supramolecular helical axis. (Reprinted with permission from Ref. 35. Copyright 2001 American Chemical Society.)

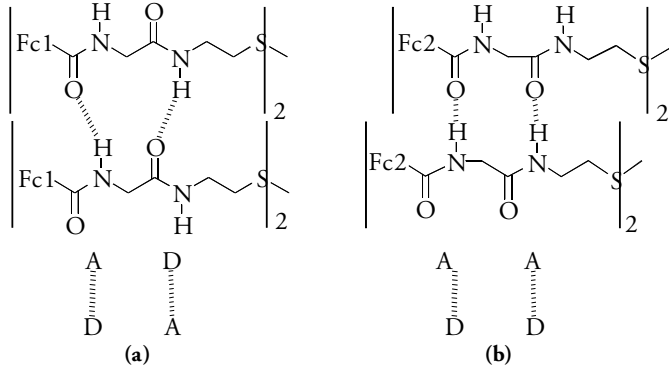

Scheme 7 Two types of hydrogen bonding interactions exhibited by the two different Gly-cystamine residues of compound 10: (a) D···A and A···D interactions and (b) D···A and D···A interactions.[22] (Reproduced by permission of The Royal Society of Chemistry.)

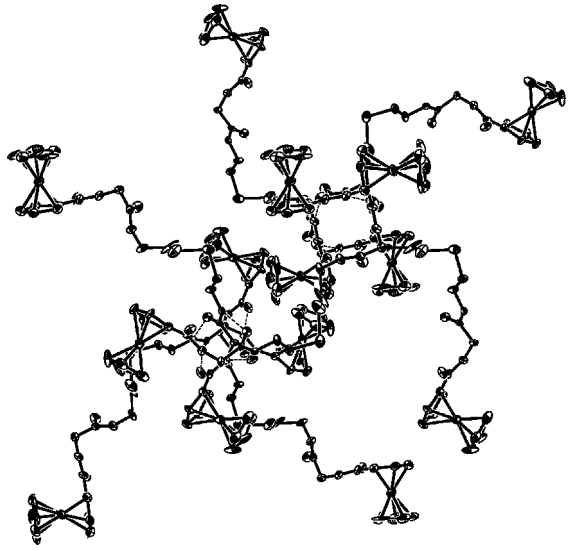

Figure 6 A view down the helical axes. Interaction between molecules resulting in the formation of a supramolecular helicate. The two parts of the molecule participate in two different types of interactions. Fc1 is involved in the right-handed "square helix" and Fc2 in the left-handed "twisted helix."[22] (Reproduced by permission of The Royal Society of Chemistry.)

The redox-active ferrocenoyl moieties are surrounding a central H-bonded peptide core. Fc1 is involved in the "square helix" having a right-handed twist, as observed in most β sheets, and Fc2 is involved in the "twisted helix." Both helices have a pitch height of ~14 Å. The "square helix" and "twisted helix" have an inner diameter of 3.8 Å and 4.1 Å, respectively. Although peptide-disulfides often exhibit unusual structural features,[37,38] a supramolecular assembly as exhibited by Fc-glycylcystamine was never before observed in peptide conjugates.

IV. MONOLAYERS OF FERROCENE PEPTIDE CONJUGATES

Electrochemical techniques have been used extensively to investigate the kinetics of electron transfer (ET) through self-assembled monolayers (SAMs) of molecules connected to a gold surface,[39–44] leading to information about the distance dependence and the influence of solvation.

For the purpose of studying the electron transfer kinetics through peptides and ordered peptide assemblies supported on a gold surface, we began to prepare a series of rigid helical ferrocenoyl-oligoprolinyl benzylesters [Fc-Pro$_n$-OR, $n = 1$ (R = H, **25**), 2 (R = Bz, **26**), 3 (R = Bz, **27**), 4 (R = Bz, **28**)[21]] and the related

ferrocenoyl-oligoprolinyl cystamines [[Fc-Pro$_n$-CSA]$_2$, n = 0 (**35**), 1 (**36**), 2 (**37**), 3 (**38**), 4 (**39**), 5 (**40**), 6 (**41**)].[45] Fc-peptide cystamines [Fc-Xxx$_n$-CSA]$_2$ are of particular interest since they allow bonding of the Fc-peptide to a gold surface through the disulfide linkage. Disulfides, such as cystamine, are well suited for the preparation of SAMs on gold.[46,47] Fc-oligoprolines are ideal candidates for ET studies since they possess a well-defined rigid polyproline II secondary structure with a translational distance of 3.1 Å per proline residue. As expected for polyproline II, the solution NOESY (nuclear overhauser enhancement spectroscopy) spectrum shows strong $\alpha(n) - \delta(n + 1)$ nOe crosspeaks. In addition, all compounds display a strong negative CD (circular dichroism) signal at λ = 210–215 nm, and a weak positive band at 230 nm (for the Pro$_5$-derivative **40** and the Pro$_6$-derivative **41**) characteristic for polyproline-II[48] (Fig. 7). Importantly, [Fc-Pro-CSA]$_2$ (**36**) and [Fc-Pro$_2$-CSA]$_2$ (**37**) exhibit a significant broadening of this CD signal, indicating a higher flexibility and potentially the ability to undergo *cis–trans* isomerism in solution. This was confirmed by nOe studies indicating that the proline residue adjacent to the CSA is indeed undergoing a facile *cis*-to-*trans* interconversion [crosspeak for $\alpha(n) - \alpha(n + 1)$ CH interaction]. Other proline residues in **36** and **37** are not affected by this process. Subsequently, Fc-amino acid cystamine conjugates were included in this study, which were not expected to adopt a stable secondary peptide structure on the surface, such as [Fc-Gly-CSA]$_2$ (**10**), [Fc-Ala$_n$-CSA]$_2$ [n = 1 (**42**), 2 (**43**)], and [Fc-PheAla-CSA]$_2$ (**44**).

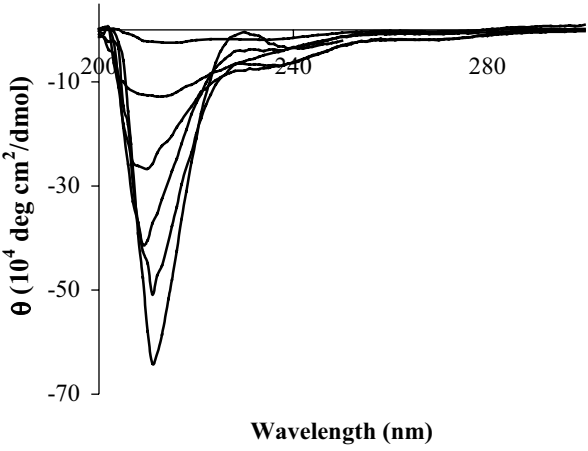

Figure 7 Circular dichroism spectra of compounds **36–41** in 0.1 mM ethanol. All compounds exhibit a negative CD signal at 210–215 nm typical for a polyproline II structure in solution.[21] The signal intensity increases with the number of proline residues (36 weakest–41 strongest). (Taken with permisson from Ref. 45.)

Compounds **35–41** exhibit a fully reversible one-electron oxidation wave, attributed to the oxidation of the Fc moiety. The oxidation potentials for **35–41** are influenced by the number of the attached proline residues, which is similar to the redox behavior of the related Fc-Pro$_n$-OBz (n = 1–4) (**24–27**). In both systems, the

Fc electrophore becomes easier to oxidize as the length of the podant oligoproline chain increases (Fig. 8). The redox potential of [Fc-CSA]$_2$ (**35**) is typical of that of simple ferrocene amides (635 mV vs. Ag/AgCl). However, the attachment of a proline residue to the Fc group causes a drop in the redox potential to 610 mV (vs. Ag/AgCl) for **36**. [Fc-Pro$_3$-CSA]$_2$ (**38**) having a single fully completed helical polyproline II turn exhibits a redox potential at 600 mV (vs. Ag/AgCl), which is in line with measurements in the Fc-Pro$_n$-OBz series. The exception is the Fc-diprolinyl-CSA complex **37**, containing the Pro$_2$-Xxx motif, which is often found in β turns.[21] However, this is not too surprising since the Pro$_2$-Xxx motif appears to cause shifts to higher potential, as was the case in the related Fc-Pro$_2$Phe-OH (**32**).

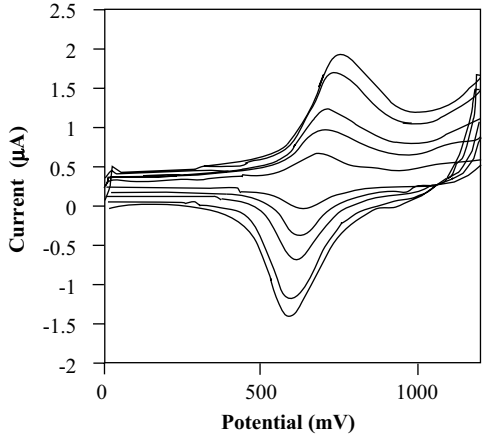

Figure 8 Cyclic voltammogram of a SAM of [Fc-Pro$_5$-CSA]$_2$ (**40**) on gold at various scan rates using a Pt counterelectrode and a Ag/AgCl reference electrode: 100–700 V/s, with 1 M *tetra*-butylammonium perchlorate (TBAP) in CH_3CN at 20 ± 1°C. (Taken with permisson from Ref. 45.)

In order to prepare Fc-peptide-modified gold surfaces suitable for electron transfer studies, cleaned gold microelectrodes (diameter 50 μm) were immersed in degassed ethanolic solutions of **36–41**, which should allow the Fc-oligoprolines to attach in the desired polyproline II conformation. Figure 8 shows a series of typical cyclic voltammograms taken at various sweep rates for [Fc-Pro$_5$-CSA]$_2$ (**40**) attached on the gold surface. The SAM of **40** and those of all other compounds studied exhibited a well-defined and fully reversible one-electron oxidation. The relationship between the peak currents and the sweep rates is linear, indicating that the electrochemical response arises from surface-bound Fc-peptides and thus show a successful immobilization of the Fc-peptides on the gold surface.[49,50]

Multiple scanning experiments on this and other Fc-peptide cystamine monolayers shows only small decreases in the signal intensity, indicating the stability of the monolayers to scanning. For a SAM of **40**, over a period of 60 s, the peak current decreased by ~10%, indicating that loss of the Fc label is minimal (Fig. 9). Some

loss is expected since Fc^+ readily reacts with nucleophiles resulting in decomposition of the ferrocenium cation.[51] CV experiments of Fc-Pro_n-CSA-modified gold electrodes in an aqueous solution of 0.1 M $K_3[Fe(CN)_6]$ showed that the SAMs of the longer proline systems **38–41**, were able to efficiently block the direct electron transfer between the electrode and $[Fe(CN)_6]^{3-}$ anion in solution and thus indicating the absence of defects, such as pinholes, that may otherwise contribute to the observed electrochemistry (Fig. 10).

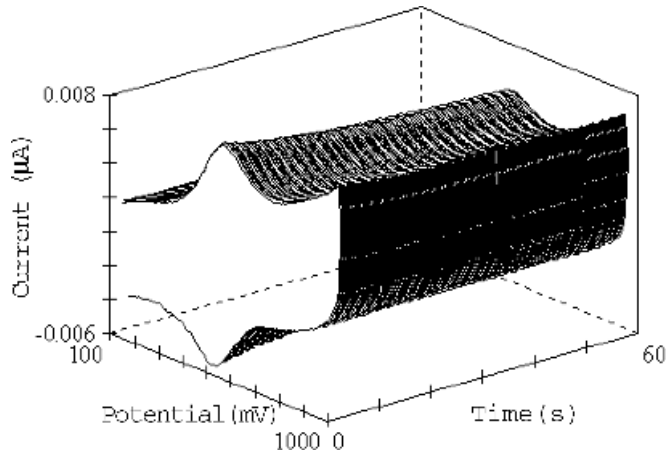

Figure 9 A typical multiple-scan cyclic voltammogram of a $[FcPro_5CSA]_2$ (**40**) SAM. Experiment time 60 s, scan rate 8 V/s; number of scans 254.

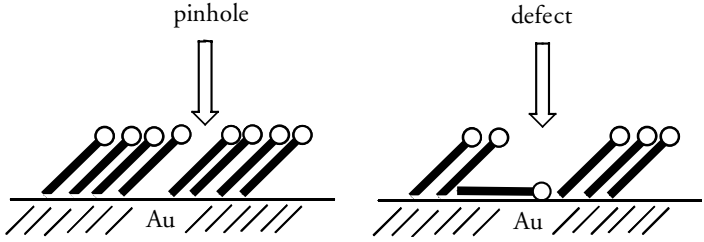

Figure 10 Diagram showing the difference between monolayer pinholes and defects.

The signal intensity was reduced by a factor of 139–220 compared to the signal for a bare electrode (Fig. 11). It can be assumed that ability of the CSA residue to engage in intermolecular H-bonding to adjacent CSAs is partly responsible for the tightly packed monolayers. A similar behavior was observed by Hutchinson for modified Fc-alkylthiols SAMs in which the alkylthiol was able to H-bond to adjacent molecules within the monolayer.[52–54] Exceptions are the shorter Fc-amino acid CSA

systems and $[Fc\text{-}CSA]_2$, which exhibited some residual signal, attesting to the poor packing of the molecules on the surface.

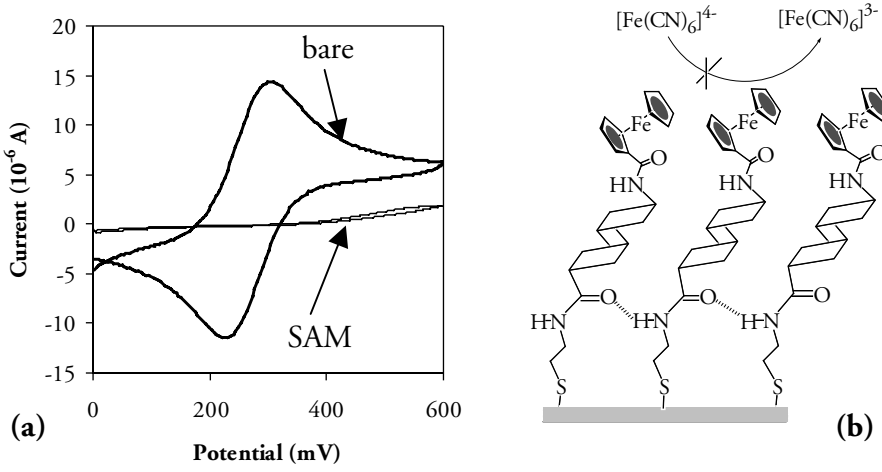

Figure 11 (a) Blocking studies comparing the cyclic voltammograms of $K_3[Fe(CN)_6]$ (0.1 M in 1 M KCl) on a bare gold electrode and a gold electrode modified by a SAM of $[Fc\text{-}Pro_5\text{-}CSA]_2$ (**40**). Scan rate 8 V/s, electrode diameter 50 μm; (b) monolayer model showing the inability of the $[Fe(CN)_6]^{3-}$ anions to penetrate the SAM.

The double-layer capacitance is a measure of monolayer permeability by the electrolyte. As expected, the presence of the Fc-oligoproline SAMs causes a drop in the capacitance compared to clean Au electrodes. Thus we were able to rule out the presence of significant surface defects, incomplete monolayer formation, and electrolyte permeation of the peptide monolayer, all of which may contribute to the electrochemical event. The integration of the oxidative peak currents was used to evaluate the spatial requirements for the Fc-oligopeptides and are summarized in Table 2. The space occupied by compounds **38–41** is in the range of 180–240 $Å^2$, which compares well with values obtained by Mihira and coworkers for helical fluoresence-labeled peptides.[50] Shorter Fc-peptide cystamines that are not able to adopt a helical conformation require less space. These include the mono- and diprolinyl systems $[Fc\text{-}Pro\text{-}CSA]_2$ (**36**) and $[Fc\text{-}Pro_2\text{-}CSA]_2$ (**37**), and $[Fc\text{-}Gly\text{-}CSA]_2$ (**10**), $[Fc\text{-}Ala\text{-}CSA]_2$ (**42**), $[Fc\text{-}Ala_2\text{-}CSA]_2$ (**43**), and $[Fc\text{-}PheAla\text{-}CSA]_2$ (**44**).

The orientations of the adsorbed Fc-oligoproline were investigated by reflectance–absorbance infrared spectroscopy (RAIRS). A typical spectrum of a SAM of **40** is shown in Figure 12. The amide I band for all compounds investigated is centered around 1650–1640 cm^{-1}, indicating a helical structure of the peptide for the longer proline systems.[55–57] Surface selection rules allow the determination of the angle θ of the peptide to the surface normal. Vibrations with components normal to the surface will experience an enhancement over vibrations in KBr. Thus, the ratio of amide I to amide II bands is a measure of the adsorbed peptide angle relative to

the gold surface. For compounds **38–41**, angles of 30–50° relative to the surface normal were observed (Table 2), which compare well with angles observed for other longer peptide SAMs.[58]

Table 2 Summary of Results of the Electrochemical and RAIRS Results Obtained for SAMs of Compounds **10** and **35–44** on Gold

Compound	E^0 (mV)	Specific Area (Å^2)	Ratio Amide I/II	θ (deg)
[Fc-Gly-CSA]$_2$ (**10**)	475	70(3)	<1	~90
[Fc-CSA]$_2$ (**35**)	630	80 (26)	<1	~90
[Fc-Pro-CSA]$_2$ (**36**)	600	123(38)	<1	~90
[Fc-Pro$_2$-CSA]$_2$ (**37**)	605	157(18)	<1	~90
[Fc-Pro$_3$-CSA]$_2$ (**38**)	590	180(21)	4.2	32
[Fc-Pro$_4$-CSA]$_2$ (**39**)	580	190(27)	2.2	47
[Fc-Pro$_5$-CSA]$_2$ (**40**)	610	220(40)	1.9	51
[Fc-Pro$_6$-CSA]$_2$ (**41**)	575	240(13)	5.3	28
[Fc-Ala-CSA]$_2$ (**42**)	480	81(9)	<1	~90
[Fc-Ala$_2$-CSA]$_2$ (**43**)	475	103(20)	<1	~90

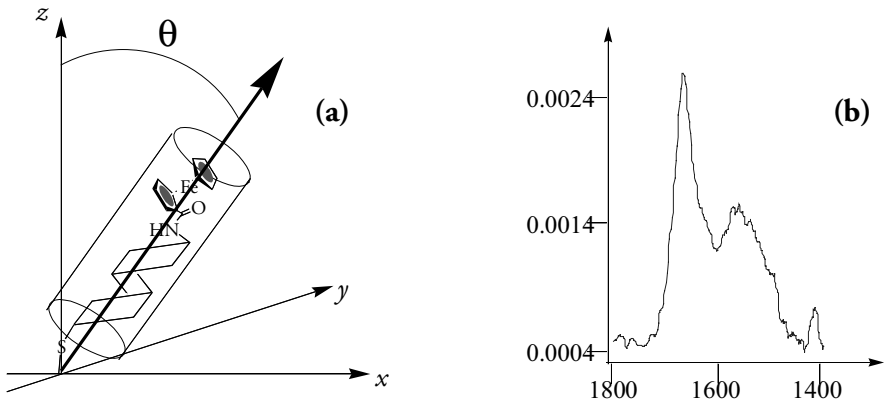

Figure 12 (a) Schematic representation of a Fc-peptide-CSA on a surface indicating the angle θ from the surface normal; (b) reflectance–absorbance IR spectrum (RAIRS) of the amide I and II regions of [Fc-Pro$_5$-CSA]$_2$ (40) on gold. (Taken with permisson from Ref. 45.)

On the other hand, shorter, more flexible Fc-peptides exhibit ratios for the amide I and II bands of <1, suggesting that the molecules are flat on the gold surface. In contrast, the longer proline systems having a rigid polyproline II conformation are able to pack on the surface in a vertical orientation. At present it appears that there is no correlation between the length of the peptide linker and the angle it adopts on the gold surface.

The theory enabling the determination of electron transfer rates from the dependence of the peak potential difference (ΔE_{peak}) in cyclic voltammetric experiments on the scan rates was first described by Laviron for diffusionless processes. Thus we were able to obtain the ET rates from the CVs at selected scan rates (Fig. 8) applying the Butler–Volmer formalism.[59] A typical experimental example is shown in Figure 13.

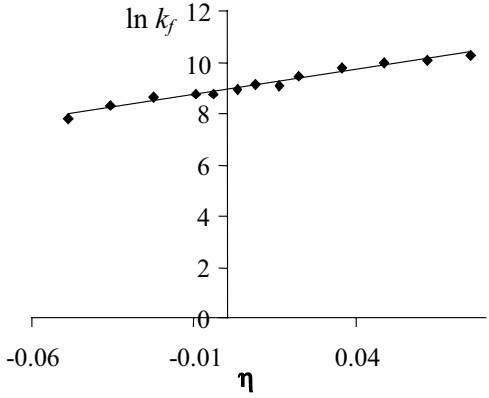

Figure 13 Relationship between the forward electron transfer rate and the overpotential η for [Fc-Pro-CSA]$_2$ (**36**) on gold.

Murray and Creager have extensively reported on the use of CV for the evaluation of electron transfer rate constants in ferrocenyl-labeled alkylthiol monolayers.[42,43] Table 3 summarizes the results of our electron transfer studies for **35–41**. For **36** an electron transfer rate of 11.2×10^3 s^{-1} was observed. For compounds having a longer oligoproline chain, the rate of electron transfer decreased. For three proline residues, the rate drops to 5.2×10^3 s^{-1} for **38** and to 3.6×10^3 s^{-1} for **39**. For **40** and **41** possessing Pro_5 and Pro_6 linkers, respectively, the ET rate is decreasing even further. An exponential relationship between k_{ET} and Fc−Au separation is predicted by Marcus theory. An increase in distance between the electrode surface and the Fc group by ~2 Å should result in a decrease in the k_{ET} by an order of magnitude. Although we observe an exponential decay with increasing number of proline residues and thus a distance dependence (maximum 3.1 Å per proline residue), the decrease is less than expected from a through-space ET (Fig. 14). Thus, the distance relationship deviates significantly from Marcus-type behavior, implicating a through-bond mechanism for the electron transfer process, as was suggested by others. A low electron transfer coefficient β value of 0.12 Å^{-1} was observed by us for ET in these Fc-peptide monolayers, which is significantly lower than was reported by Schanze and Sauer[60] and Isied and coworkers[61,62] for photoinduced ET studies of various labeled oligoprolines in solution.

Table 3 Summary of Results of Electron Transfer Studies of Compounds **35–41**

Compound	$E°$ (mV)	E_{FWHM} (mV)	k_{ET} (σ) ($s^{-1} \times 10^3$)	α
$[Fc\text{-}CSA]_2$ (**35**)	651	148	8.3(1.3)	0.50
$[Fc\text{-}Pro\text{-}CSA]_2$ (**36**)	639	133	11.2(2.8)	0.51
$[Fc\text{-}Pro_2\text{-}CSA]_2$ (**37**)	621	127	7.5(1.2)	0.52
$[Fc\text{-}Pro_3\text{-}CSA]_2$ (**38**)	620	124	5.2(1.1)	0.53
$[Fc\text{-}Pro_4\text{-}CSA]_2$ (**39**)	623	127	3.6(1.3)	0.55
$[Fc\text{-}Pro_5\text{-}CSA]_2$ (**40**)	627	140	2.5(0.3)	0.51
$[Fc\text{-}Pro_6\text{-}CSA]_2$ (**41**)	604	133	1.8(0.6)	0.51

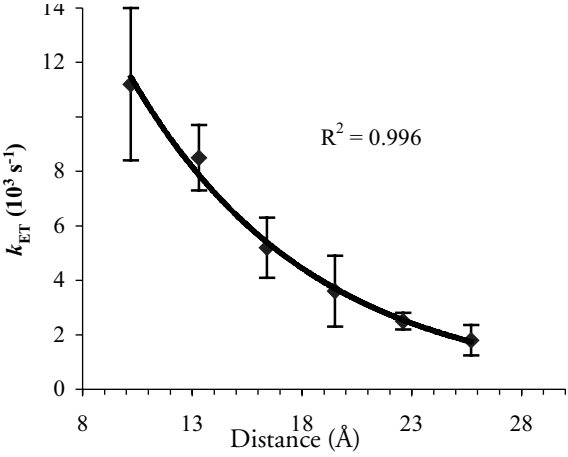

Figure 14 Relationship between the heterogeneous ET rates and donor–acceptor distance for SAMs of compounds **35–41**. (taken with permisson from Ref. 45).

In general, the β values for ET through polyproline II spacers are significantly lower than the average β values of proteins (0.9–1.2 $Å^{-1}$). In contrast, Faraggi and Klapper[63] proposed a through-bond mechanism to explain the low β value of 0.2–0.4 $Å^{-1}$ found in H-Tyr(Pro)$_n$-TrpOH and H-Trp(Pro)$_n$-TyrOH. It was suggested that ET could occur primarily through a strained conformation in which the electron donor–acceptor distances are shorter than estimated on the basis of the thermodynamically dominant structures. Thus the "true" value of β would be larger than the apparent value, especially if ET was through-space. Pulse radiolysis studies by Bobrowski and coworkers[64] on H-Trp-(Pro)$_n$–TyrOH gave low β values in the range between 0.2 and 0.28 $Å^{-1}$, suggesting a combined through-space/through-bond pathway, which is dependent on the peptide chain length. It appears that the low β and the fast ET rates fpr Fc-oligoproline SAMs are related to the rigidity of the two-dimensional Fc-peptide array on the Au surface. Hydrogen bonding between adjacent Fc-oligoproline cystamine molecules on the surface may significantly contribute to the monolayer packing and its rigidity. Moverover, the close proximity of the redox-active Fc head groups appears to allow for a lateral interaction of the redox centers.

V. SUMMARY

Ferrocenoyl peptides can be rationally designed are readily obtained by a variety of peptide coupling techniques from often commercially available synthons. The podant peptide chains are able to engage in inter- and intramolecular hydrogen bonding, giving rise to an array of helical and nonhelical supramolecular assemblies in solution and the solid state, having the redox-active ferrocenoyl group decorate the outside of the assemblies. In the long term, this may open up the fascinating possibility of generating tailor-made redox-active peptidic materials of fixed lengths and electronic makeup with potential application in nanoelectronics. It is clear from the data available that the interpeptide interactions largely govern the supramolecular assembly of the Fc-peptides and dipeptides. Unfortunately, details of the supramolecular assembly cannot be predicted from the amino acid sequence at the present time. Thus, most structural discoveries in this area are accidental.

With regard to its electronic properties, no studies are available that clearly demonstrate that electron transfer through such a supramolecular assembly is possible. Solid-state electrochemical studies on the crystalline material are not available at the present time. The closest to "supramolecular electrochemistry" are studies of ordered two-dimensional peptide arrays on gold. For some Fc-peptide cystamines, self-assembled monolayers of Fc-peptide cystamines were prepared that allow the quantification of the electron transfer kinetics by electrochemical techniques. Similar to the supramolecular assemblies, H-bonding plays an important role. At the present time (2003), only a few systems were studied and offer a rather complex picture of the ET properties. Additional experimental work is required to obtain definite results on the influence of the peptide primary and secondary structure on ET kinetics. In addition, the issue of lateral interactions needs to be addressed by detailed dilution studies with alkylthiols.

VI. ACKNOWLEDGMENTS

This work was supported by the National Science and Engineering Research Council. HBK is Canada Research Chair in Biomaterials. I wish to thank Dr. T. Sutherland for his useful comments while preparing this manuscript.

VI. REFERENCES

1. A. Aggeli, I. A. Nyrkova, M. Bell, R. Harding, L. Carrick, T. C. B. McLeish, A. N. Semenov, N. Boden, *Proc. Natl. Acad. Sci.* (*USA*) **98,** 11857 (2001).
2. W. A. Petka, J. L. Harden, K. P. McGrath, D. Wirtz, D. A. Tirrell, *Science* **281,** 389 (1998).
3. J. P. Schneider, J. W. Kelly, *Chem. Rev.* **95,** 2169 (1995).
4. J. S. Nowick, *Acc. Chem. Res.* **32,** 287 (1999).

5. M. R. Ghadiri, J. R. Granja, R. A. Milligan, D. E. McRee, Khazanovich, *Nature* **366,** 324 (1993).
6. J. D. Hartgerink, J. D., J. R. Granja, R. A. Milligan, M. R. Ghadiri, *J. Am. Chem. Soc.* **118,** 43 (1996).
7. T. D. Clark, J. M. Buriak, K. Kobayashi, M. P. Isler, D. E. McRee, M. R. Ghadiri, *J. Am. Chem. Soc.* **120,** 8949 (1998).
8. D. Ranganathan, V. Haridas, C. S. Sundari, D. Balasubramanian, K. P. Madhusudana, R. Roy, I. L. Karle, *J. Org. Chem.* **64,** 9230 (1999).
9. D. Ranganathan, M. P. Samant, I. L. Karle, *J. Am. Chem. Soc.* **123,** 5619 (2001).
10. R. P. Lyon, W. M. Atkins, *J. Am. Chem. Soc.* **123,** 4408 (2001).
11. J. H. Collier, B. -H. Hu, J. W. Ruberti, J. Zhang, P. Shum, D. H. Thompson, P. B. Messersmith, *J. Am. Chem. Soc.* **123,** 9463 (2001).
12. T. C. Holmes, S. deLasalle, X. Su, G. Liu, A. Rich, A. Zhang, *Proc. Natl. Acad. Sci.* (*USA*) **97,** 6728 (2000).
13. K. Severin, R. Bergs, W. Beck, *Angew. Chem. Int. Ed.* **37,** 1634 (1998).
14. R. S. Herrick, R. M. Jarret, T. P. Curran, D. R. Dragoli, M. B. Flaherty, S. E. Lindyberg, R. A. Slate, L. C. Thornton, *Tetrahedron Lett.* **37,** 5289 (1996).
15. A. Nomoto, T. Moriuchi, S. Yamazaki, A. Ogawa, T. Hirao, *Chem. Commun*. 1963 (1998).
16. H. B. Kraatz, J. Lusztyk, G. D. Enright, *Inorg. Chem.* **36,** 2400 (1997).
17. W. Bauer, K. Polborn, W. Beck, *J. Organomet. Chem.* **579,** 269 (1999).
18. P. Saweczko, H. B. Kraatz, *Coord. Chem. Rev.* **190–192,** 185 (1999).
19. Y. Degani, A. Heller, *J. Phys. Chem.* **91,** 1285 (1987).
20. Y. Degani, A. Heller, *J. Am. Chem. Soc.* **110,** 2615 (1988).
21. H. B. Kraatz, D. M. Leek, A. Houmam, G. D. Enright, J. Lusztyk, D. D. M. Wayner, *J. Organomet. Chem.* **589,** 38 (1999).
22. I. Bediako-Amoa, R. Silerova, H. B. Kraatz, *Chem. Commun.* (in press).
23. Y. Xu, P. Saweczko, H. B. Kraatz, *J. Organomet. Chem.* **637–639**, 355 (2001).
24. Y. Xu, H. B. Kraatz, *Tetrahedron Lett.* **42,** 2601 (2001).
25. L. Lin, A. Berces, H. B. Kraatz, *J. Organomet. Chem.* **556,** 11 (1998).
26. H. B. Kraatz, J. Lusztyk, G. D. Enright, *Inorg. Chem.* **36,** 2400 (1997).
27. P. Sawezcko, G. D. Enright, H. B. Kraatz, *Inorg. Chem.* **40,** 4409 (2001).
28. T. Moriuchi, A. Nomoto, K. Yoshida, T. Hirao, *J. Organomet. Chem.* **589,** 50 (1999).
29. T. E. Creighton, Proteins, 2nd ed., Freeman, New York, 1993.
30. A. B. Biswas, E. W. Hughes, B. D. Sharma, J. N. Wilson, *Acta Cryst.* **B24,** 40 (1968).
31. E. W. Hughes, *Acta Cryst.* **B24,** 1128 (1968).
32. H. C. Freeman, G. L. Paul, T. M. Sabine, *Acta Cryst.* **B26,** 925 (1970).
33. J. F. Griffin, P. Coppens, *J. Am. Chem. Soc.* **97,** 3496 (1975).
34. T. Moriuchi, K. Yoshida, T. Hirao, *J. Organomet. Chem.* **637–639,** 73 (2001).
35. T. Moriuchi, A. Nomoto, K. Yoshida, A. Ogawa, T. Hirao, *J. Am. Chem. Soc.* **123,** 68 (2001).
36. T. Moriuchi, A. Nomoto, K. Yoshida, T. Hirao, *Organometallics* **20,** 1008 (2001).
37. I. L. Karle, D. Ranganathan, V. Haridas, *J. Am. Chem. Soc.* **118,** 10916 (1996).
38. D. Ranganathan, V. Haridas, R. Hagaraj, I. L. Karle, *J. Org. Chem.* **65,** 4415 (2000).
39. C. D. E. Chidsey, *Science* **251,** 912 (1991).
40. C. D. E. Chidsey, C. R. Bertozzi, T. M. Putvinski, A. M. Mujsce, *J. Am. Chem. Soc.* **112,** 4301 (1990).
41. J. N. Richardson, S. P. Peck, L. S. Curtin, L. M. Tender, G. K. Rowe, S. E. Creager, *J. Chem. Phys.* **99,** 766 (1995).
42. S. E. Creager, G. K. Rowe, *J. Electroanal. Chem.* **370,** 203 (1994).

43. L. Tender, M. T. Carter, R. W. Murray, *Anal.Chem.* **66,** 3173 (1994).
44. M. S. Ravencroft, H. O. Finklea, *J. Am. Chem. Soc.* **98,** 3843 (1994).
45. M. M. Galka, H. B. Kraatz, *Chem. Phys. Chem.* **3,** 356 (2002).
46. A. Ulman, *Chem. Rev.* **96,** 1533 (1996).
47. M. Wirde, U. Gelius, L. Nyholm, *Langmuir* **15,** 6370 (1999).
48. R. W. Woody, *Peptides* **7,** 15 (1985).
49. H. O. Finklea, in *Electroanalytical Chemistry*, Vol. 19, A. J. Bard, I. Rubinstein, eds., Marcel Dekker, New York, 1993, Chap. 3, pp. 110–335.
50. S. Sakamoto, H. Aoyagi, N. Nakashima, H. Mihara, *J. Chem. Soc. Perkin Trans*. *2* 2319 (1996).
51. R. Prins, A. R. Kirswagen, A. G. T. G. Kortbeek, *J. Organomet. Chem.* **39,** 335 (1972).
52. R. S. Clegg, J. E. Hutchinson, *Langmuir* **12,** 5239 (1996).
53. R. S. Clegg, J. E. Hutchinson, *J. Am. Chem. Soc.* **121,** 5319 (1999).
54. R. S. Clegg, S. M. Reed, R. K. Smith, B. L. Barron, J. A. Rear, J. E. Hutchinson, *Langmuir* **15,** 8876 (1999).
55. P. I. Harris, D. Chapman, *Biopolymers* **37,** 251 (1995).
56. X. Cha, K. Ariga, T. Kunitake, *Bull. Chem. Soc. Jpn.* **69,** 163 (1996).
57. A. E. Strong, B. D. Moore, *J. Chem. Soc. Chem. Commun.* 473 (1998).
58. N. Higashi, T. Koga, M. Nina, *Langmuir* **16,** 3482 (2000).
59. A. J. Bard, L. R. Faulkner, *Electrochemical Methods*, 2nd ed., Wiley, New York, 2001.
60. K. S. Schanze, K. Sauer, *J. Am. Chem. Soc.* **110,** 1180 (1988).
61. S. S. Isied, M. Y. Ogawa, J. Wishart, *Chem. Rev.* **92,** 381 (1992).
62. S. S. Isied, I. Moereia, M. Y. Ogawa, A. A. Vassalian, B. Arbo, J. Sun, *J. Photochem. Photobiol. A* **82,** 203 (1994).
63. A. K. Mishra, R. Chandrasekar, M. Faraggi, M. H. Klapper, *J. Am. Chem. Soc.* **116,** 1414 (1994).
64. K. Bobrowski, J. Holcman, J. Poznanski, M. Ciurak, K. Wierzchowski, *J. Phys. Chem*. **96,** 10036 (1992).

CHAPTER 10

Polyaromatic Ethers and Thioethers Coordinated to Cyclopentadienyliron Cations

Alaa S. Abd-El-Aziz and Erin K. Todd

Department of Chemistry, The University of Winnipeg, Winnipeg, Manitoba, Canada

CONTENTS

Macromolecules Containing Metal and Metal-like Elements, Volume 2: Organoiron Polymers, Edited By Alaa S. Abd-El-Aziz, Charles E. Carraher, Jr., Charles U. Pittman, Jr., John E. Sheats, and Martel Zeldin
ISBN 0-471-45078-2

I. INTRODUCTION

The past few decades have seen increasing interest in the design of thermally stable polymers as replacements for metals and ceramics in the aerospace and automotive industries.[1–3] Polyaromatic ethers and thioethers are two classes of thermally stable polymers that have been examined for this purpose because of their ability to withstand temperatures in excess of 200°C and their stability toward acids, bases, and organic solvents. Rigid polymers such as polyaromatic ethers and thioethers often exhibit limited solubility in organic solvents at room temperature, and their high melting points can limit their processability.

There are a limited number of methodological approaches to the synthesis of polyaromatic ethers; however, the most successful method has been found to be nucleophilic aromatic substitution reactions. Electrophilic aromatic sulfonylation or acylation, metal-catalyzed coupling, oxidative coupling of disubstituted phenols, and ring-opening polymerization have also been utilized to prepare these classes of polymers.[1,2] Polyaromatic thioethers are commonly synthesized by reaction of 1,4-dichlorobenzene with sodium sulfide, via reaction of disulfide monomers or catalysts and by ring-opening polymerization.[3]

Nucleophilic aromatic substitution reactions of haloarenes complexed to transition metal moieties with oxygen-, sulfur-, and nitrogen-containing nucleophiles allows for the synthesis of a wide variety of aryl ethers, thioethers, and amines.[4–8] These metal-mediated reactions proceed under very mild conditions and allow for the incorporation of a number of different functional groups. Nucleophilic substitution reactions of chloroarenes complexed to the cyclopentadienyliron moiety have been the focus of many studies directed toward the design of functionalized organic monomers.[9–16]

Since the early 1980s, a number of research groups have investigated the incorporation of transition metal moieties π-coordinated to phenylene units in the polymer backbones. The metallic groups have included chromium tricarbonyl,[17–26] molybdenum tricarbonyl,[25–29] cyclopentadienyliron,[29–39] pentamethylcyclopentadienylruthenium,[38–41] and cyclopentadienylruthenium.[42] A number of studies have shown that the incorporation of metallic moieties pendent to polymeric materials resulted in enhanced solubilities of the organometallic polymers. While many of these polymers were synthesized using nucleophilic aromatic substitution reactions mediated by the electron-withdrawing ability of the metallic moieties, they have also been prepared via coordination of a metallic moiety to a preexisting organic polymer, polycondensation reactions and supramolecular assembly of arene complexes.

II. LINEAR POLYAROMATIC ETHERS, THIOETHERS, AND AMINES

A. Polyethers

The synthesis of polyaromatic ethers coordinated to cyclopentadienyliron moieties was achieved via nucleophilic displacement of the chloro groups from

complex **1** using the diphenolic nucleophiles **2a–h** as shown in Scheme 1.[31,32] It is well known that the type of aromatic linkage incorporated into polyaromatic ethers has a strong influence on their thermal and physical properties. Therefore, a wide range of aromatic spacers were incorporated into the polymers under investigation. The electron-withdrawing cyclopentadienyliron moiety pendent to the dichloroarene complex allowed these polymerization reactions to occur at 60°C over a period of 6–12 hs.

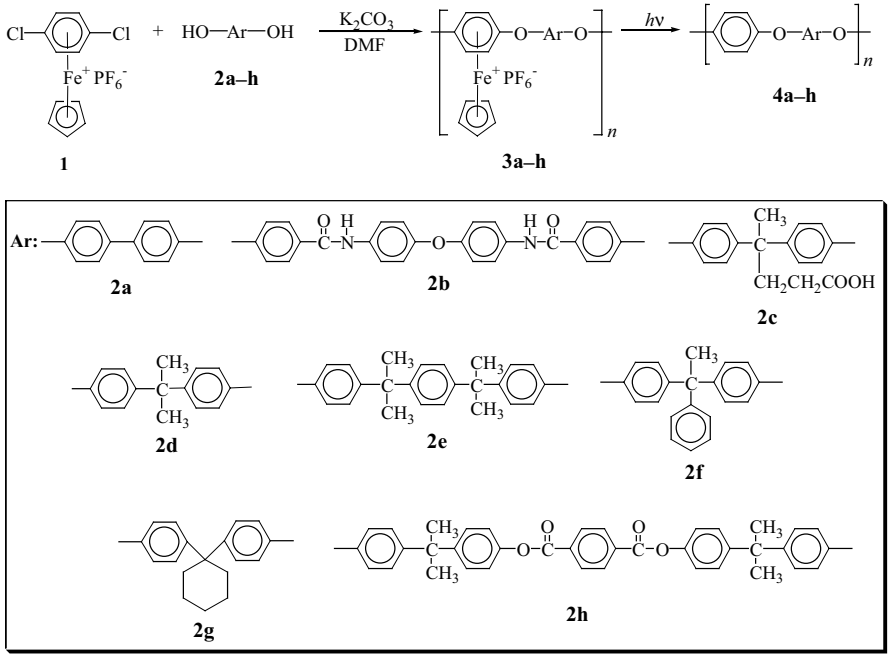

Scheme 1

The organoiron polyethers were isolated as beige powders in yields ranging from 89 to 99%. These polymeric materials were soluble in polar aprotic solvents such as DMAc, DMF, and DMSO and displayed varying degrees of solubility in solvents such as acetone, dichloromethane, and acetonitrile. The solubilities of all the organoiron-coordinated polyethers are listed in Table 1.[32] Polymer **3c**, with carboxylic acid groups pendent to its backbone, was also soluble in a water solution containing sodium hydroxide. Because of the flexibility imparted by alkyl groups, polymers **3d–h** displayed much higher solubilities than did polymers **3a,b**. The enhanced solubilities of the metallated polymers allowed for the solution characterization of polymers **3a–h**.

The photolytic demetallation of polymers **3a–h** was achieved in solutions of acetonitrile, or acetonitrile/DMF, resulting in the isolation of polymers **4a–h**. The photolytic reactions were conducted for 4 h, and after that time, there was no evidence of the cyclopentadienyliron moieties in the NMR spectra of the organic polymers

(**4a–h**). These polymers (**4a–h**) exhibited varying degrees of solubility in polar solvents such as chloroform and tetrahydrofuran; however, polymers **4a–c** were insoluble in all solvents tested. The molecular weights of the organic polymers (**4d–h**) were determined using gel permeation chromatography (GPC), with chloroform as the eluent (Table 2). Although the solubilities of the organic materials were often much lower than those of their organoiron analogs, the molecular weights of the metallated polymers could not be determined by GPC because of interactions of the cationic organometallic moieties with GPC columns. However, the molecular weights of the demetallated polymers allowed for the determination of the approximate molecular weights of the organoiron polymers. For example, polymer **4d** had a weight-average molecular weight (M_w) of 18,100, which corresponds to a degree of polymerization of about 60, and a M_w value of 34,000 for the corresponding organoiron polymer (**3d**).

Table 1 Solubility of Organoiron Polymers in Polar Organic Solvents[a]

Polymer	CH_2Cl_2	Acetone	CH_3CN	DMAc	DMF	DMSO
3a	I	I	PS	PS	PS	PS
3b	I	I	I	S	S	S
3c[b]	I	PS	PS	PS	S	S
3d	PS	S	S	S	S	S
3e	PS	S	S	S	S	S
3f	I	I	PS	S	S	S
3g	I	PS	PS	S	S	S
3h	I	I	PS	S	PS	S

[a] Solubility at room temperature: (S), soluble; (PS), partially soluble; (I), insoluble.
[b] Also soluble in a solution of dilute sodium hydroxide.

Table 2 Molecular Weight Analysis of Polyethers **4d–h**

Polymer	M_w	M_n	M_w/M_n
4d	18,100	8,800	2.1
4e	21,400	9,900	2.2
4f	7,300	3,500	2.1
4g	8,800	3,700	2.4
4h	16,100	7,400	2.2

^1H and ^{13}C NMR analysis of the cyclopentadienyliron-coordinated polyaromatic ethers was very useful in determining the success of the polymerization reactions. The ^1H NMR spectrum of the *p*-dichlorobenzene complex (**1**) is very simple, with the cyclopentadienyl resonance appearing as a singlet at 5.45 ppm, and the complexed aromatic protons resonating as a singlet at 6.99 ppm. After polymerization, the resonances corresponding to both of these peaks underwent quite noticeable upfield shifts to 5.0–5.3 ppm and 6.2–6.6 ppm, respectively. Figure 1 shows the ^1H NMR spectrum of polymer **3e**. The five cyclopentadienyl protons appear as a singlet at

5.20 ppm, and the singlet at 6.23 ppm is assigned to the four complexed aromatic protons. The protons of the isopropylidene groups resonate at 1.65 ppm, and the protons corresponding to the bridging aromatic rings appear as a multiplet integrating for eight protons at 7.18 ppm and a doublet integrating for four protons at 7.36 ppm.

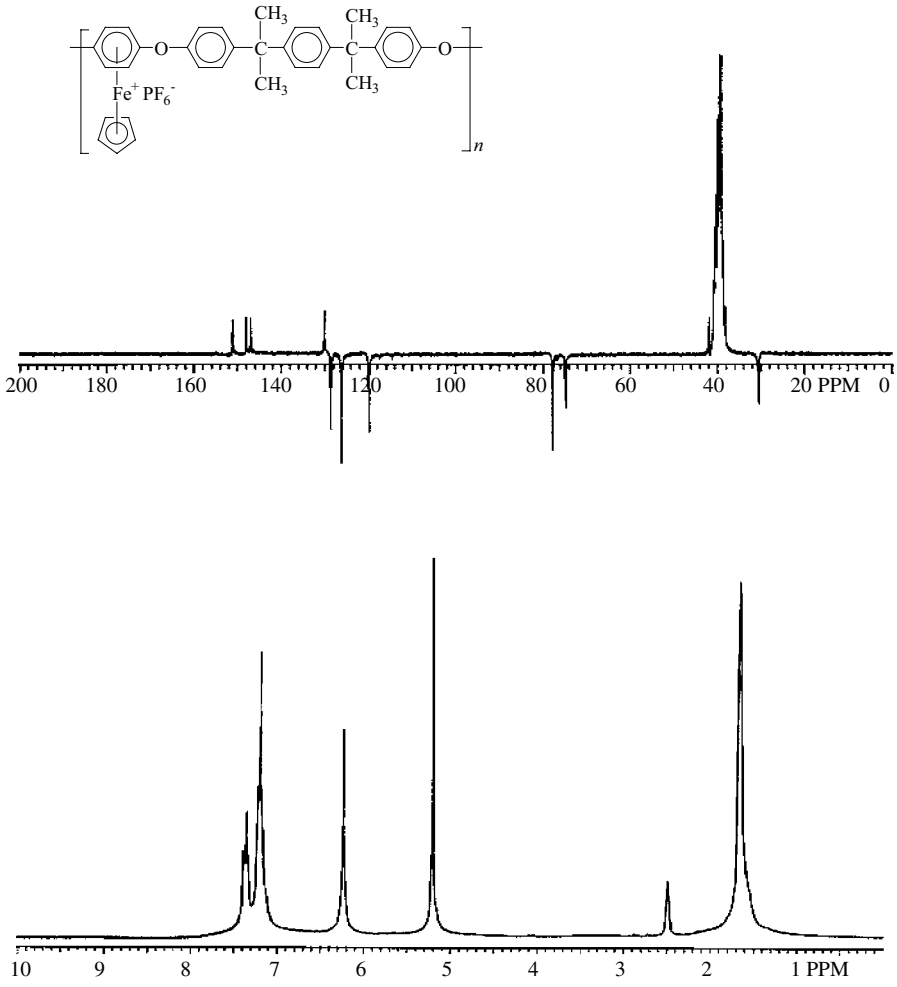

Figure 1 ^{1}H and ^{13}C NMR spectra of polymer **3e** in DMSO-d_6.

The ^{13}C NMR spectrum of polymer **3e** was run as an attached proton test (APT). This spectrum shows the methyl carbons appearing as a downward peak at 30.39 ppm and the quaternary carbon of the isopropylidene group as an upward peak at 41.83 ppm. The cyclopentadienyl resonance appears at 77.74 ppm as an intense peak pointing down. The complexed aromatic CH carbons appear at 74.76 ppm, while

the quaternary complexed aromatic carbons appear at 130.07 ppm. The uncomplexed aromatic carbon peaks appear further downfield at 119.77, 126.12, and 128.62 ppm, and the quaternary carbons resonate at 146.98, 147.99 and 151.09 ppm.

NMR analysis of polymers **4a–h** verified the success of the photolytic reactions. The most noticeable differences in the spectra were the absence of the cyclopentadienyl resonances and the downfield shift of the complexed aromatic resonances to ~7–7.5 ppm in the ^{1}H spectra and to ~120–130 ppm in the ^{13}C spectra of the organic polymers. Figure 2 shows the ^{1}H and ^{13}C NMR spectra of polymer **4e**. The ^{1}H NMR spectrum shows a singlet at 1.62 ppm, corresponding to the 12 methyl protons, two broad singlets at 6.87 and 6.95 ppm corresponding to 8 aromatic protons, and another broad singlet at 7.10 ppm, assigned to the remaining 8 aromatic protons. The ^{13}C NMR spectrum also indicates that the cyclopentadienyl rings were cleaved from the polymer backbone. The aromatic CH carbons appear at 117.53, 120.33, 126.25, and 128.03 ppm, and the quaternary carbons appear at 145.33, 147.67, 152.65, and 155.49 ppm. The methyl carbon appears at 30.88 and the quaternary isopropylidene carbon appears at 42.05 ppm.

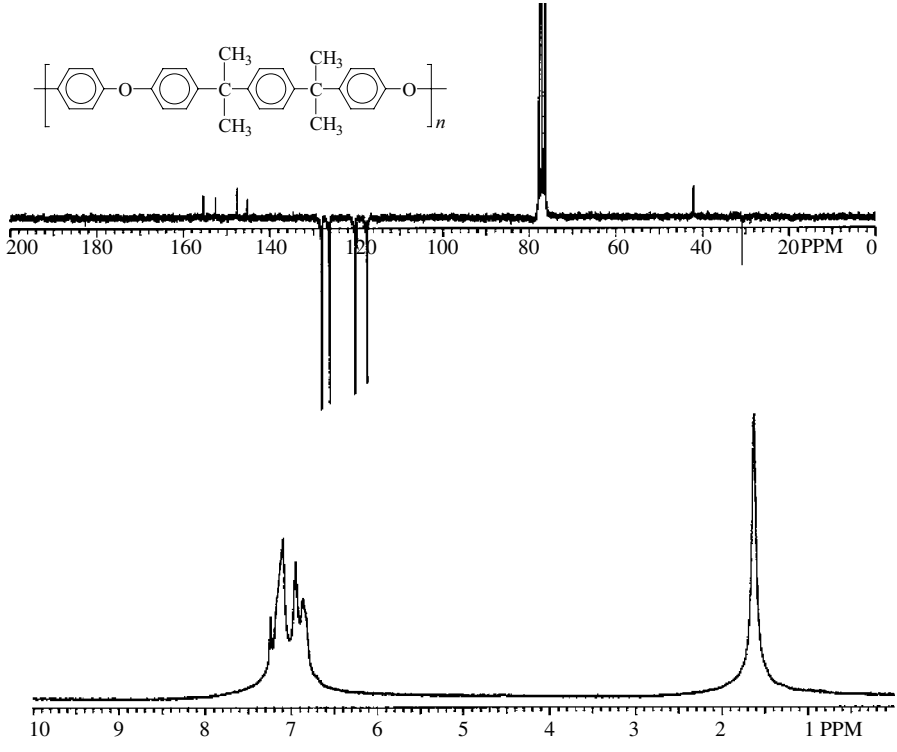

Figure 2 ^{1}H and ^{13}C NMR spectra of polymer **4e** in $CDCl_3$.

Electrochemical analysis of the cyclopentadienyliron-coordinated polyaromatic ethers was accomplished using cyclic voltammetry.[43] It has previously been established that cationic arene complexes of cyclopentadienyliron undergo monoelectronic reduction processes to produce neutral 19-electron species.[44–46] These radicals can undergo a second reduction to produce highly unstable anionic 20-electron complexes. The cyclic voltammograms of polymer **3e** and an oligomeric analog were compared. In general, the redox couples of the polymer were less reversible than the couples of the oligomer at low scan rates. The cyclic voltammogram of **3e** is shown in Figure 3, and the CV of its oligomeric analog is shown in Figure 4. The CV for the polymer is much broader and has an $E_{pc} = -1.61$ V, $E_{pa} = -1.18$ V, and $E_{1/2} = -1.40$ V.

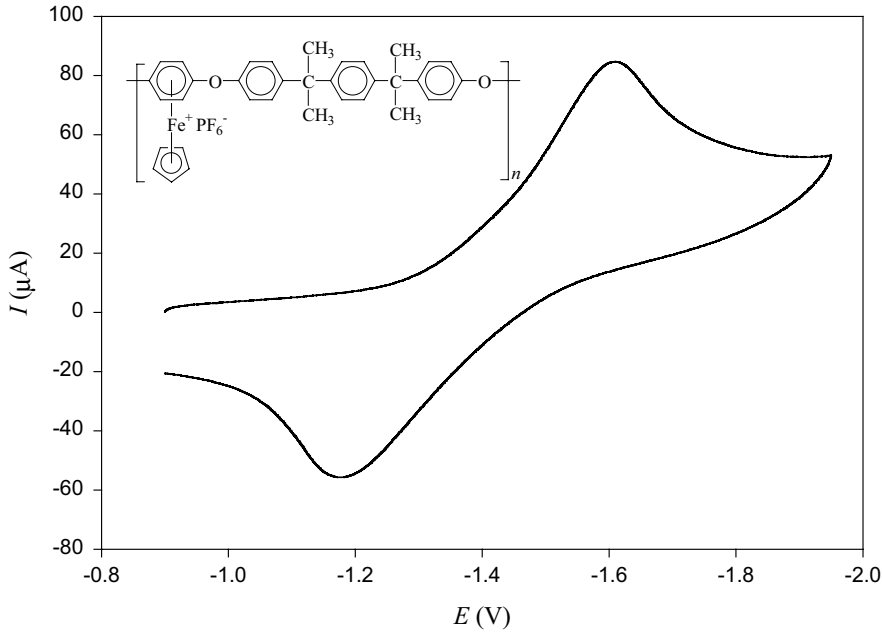

Figure 3 Cyclic voltammogram of **3e** obtained in a DMF solution containing TBAP as the supporting electrolyte at −20°C with a scan rate of 1 V/s.

The CV of the oligomeric complex in Figure 4 shows the reversible reduction of this diiron complex. The redox wave is much narrower and the E_{pc} was found at −1.28 V, the E_{pa} was at −1.08 V, and the $E_{1/2}$ for this complex occurred at −1.18 V.

Many of the cyclopentadienyliron-coordinated polymers also adsorbed onto the working electrode during the cyclic voltammetry experiments, and this phenomenon was most noticeable at low scan rates. The CVs of polymer **3f** obtained at −30°C in DMF are shown in Figure 5 at scan rates of 0.1, 0.2, 1, and 5 V/s. From these curves, it is quite obvious that the current increases significantly with increased scan rate, while the $E_{1/2}$ values obtained for these curves occurred at −1.03, −1.04, −1.04, and −1.06 V, respectively.

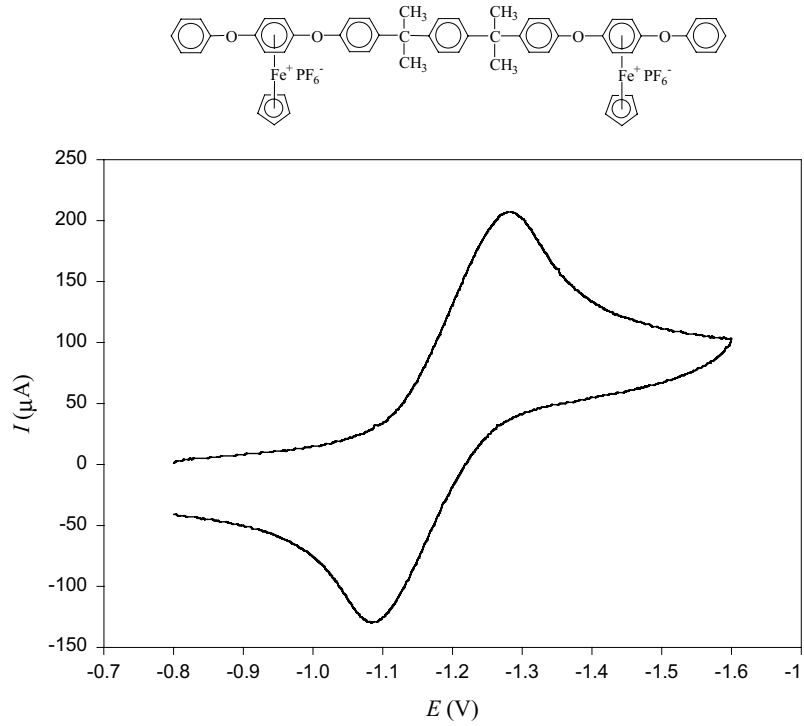

Figure 4 Cyclic voltammogram obtained in a DMF solution containing TBAP as the supporting electrolyte at −20°C with a scan rate of 1 V/s.

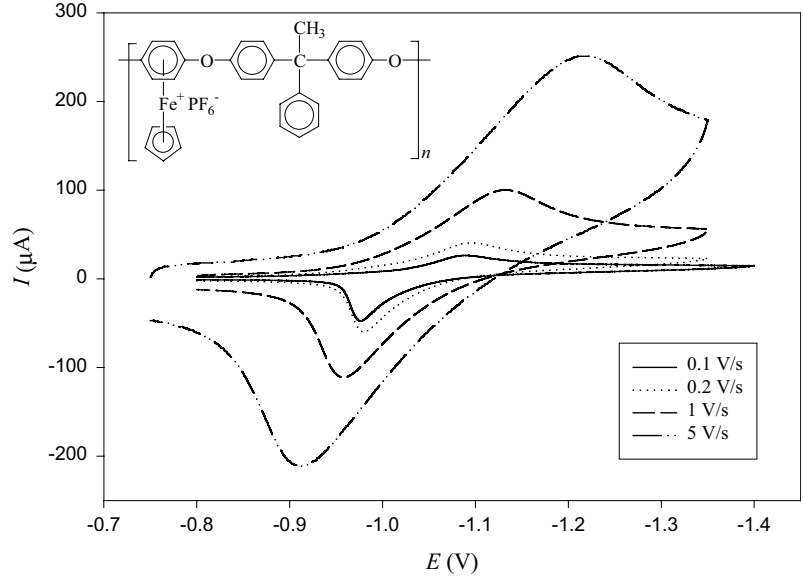

Figure 5 Cyclic voltammogram of **3f** obtained at scan rates of 0.1, 0.2, 1, and 5 V/s.

Polymer **3h** displayed interesting electrochemical properties. This polymer exhibited two redox waves corresponding to two distinct reduction processes. Figure 6 shows the CV of this polymer obtained at −40°C in a DMF solution. This CV was obtained at a scan rate of 0.2 V/s, and the $E_{1/2}$ values for the two redox processes occurred at −0.988 and −1.11 V. An oligomeric complex containing the same bridging aromatic spacer exhibited the same redox behavior.

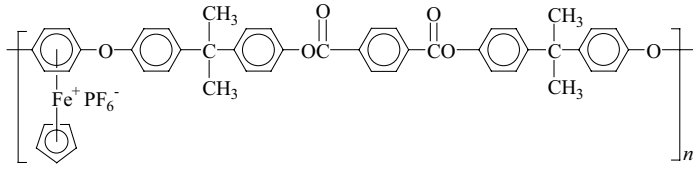

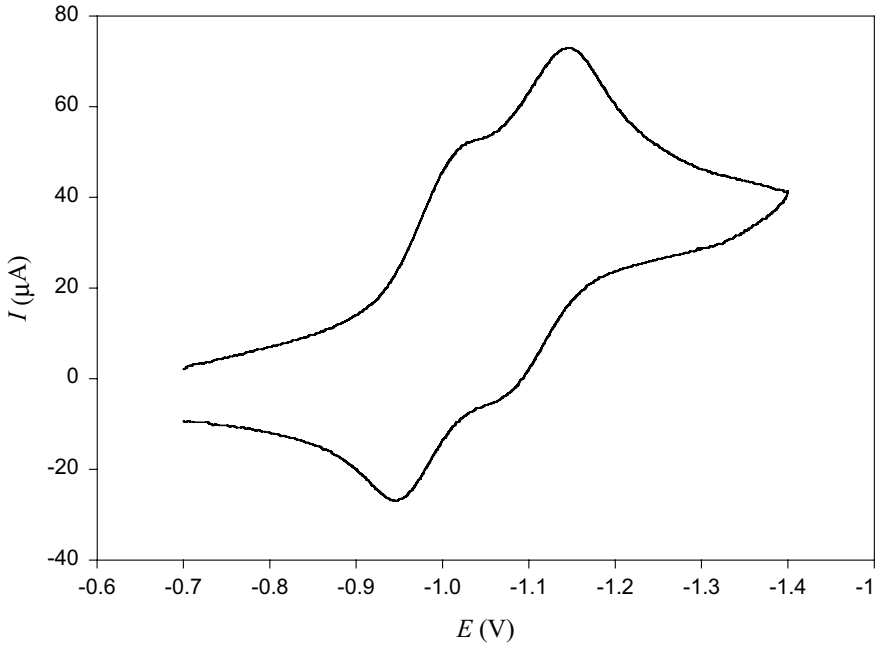

Figure 6 Cyclic voltammogram of **3h** obtained at a scan rate of 0.2 V/s.

The thermal properties of the metallated and demetallated polymers were investigated using thermogravimetric analysis (TGA).[32] All of the metallated polymers (**3a–h**) exhibited a 17–27% weight loss between 219 and 296°C, corresponding to cleavage of the cyclopentadienyliron moieties. Following this initial weight loss, the polymers experienced second weight losses that were dependent on the aromatic linkages in their backbones. For example, the polymers lost anywhere between 20 and 39% of their original weight starting from 417 to 521°C. Following photolytic demetallation, the thermal stability of polymers **4a–h** was examined. It was noted that there was only one weight loss present in the organic polymers' thermograms

corresponding to decomposition of the polymer backbones. These results indicated that the presence of organoiron moieties did not significantly influence the thermal stability of the polymer backbones. Figure 7 shows the TGA thermograms of polymers **3d** and **4d**. It can be seen that polymer **3d** displayed an initial 23% weight loss at 247°C and a second weight loss of 34% beginning at 517°C and ending at 554°C. Following demetallation, polymer **4d** had a 62% weight loss that began at 533°C and continued until 562°C.

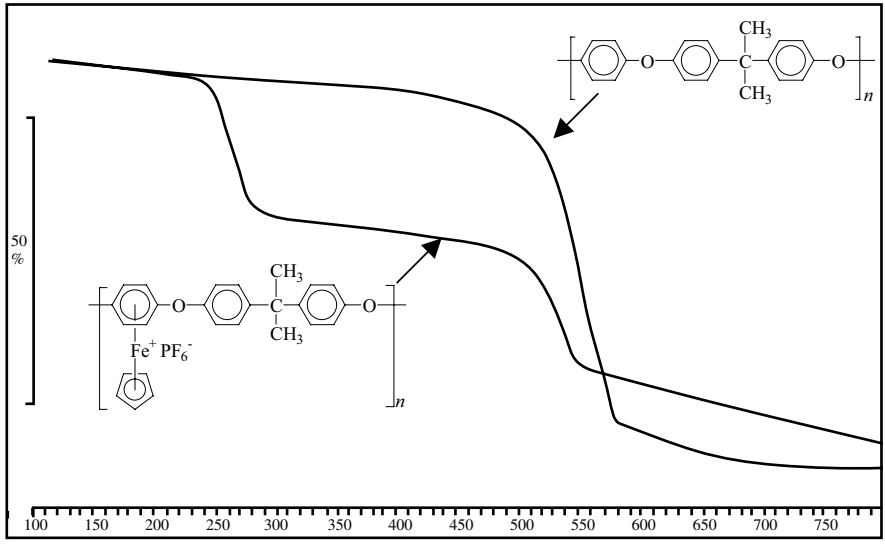

Figure 7 TGA thermograms of polymers **3d** and **4d**.

The thermal properties of the organic polyethers were also examined using differential scanning calorimetry (DSC).[32] DSC indicated that the glass transition temperatures (T_g) of the polyaromatic ethers ranged from 113 to 165°C (Table 3). The glass transition temperatures of the cyclopentadienyliron-coordinated polymers were investigated; however, they were determined to be above their decomposition temperatures. Figure 8 shows the DSC thermograms for polymers **4d–f**. It can be seen that polymer **4f**, with the aromatic groups pendent to the polymer backbone, has the highest glass transition temperature of this series, while polymer **4d** has the lowest T_g. As expected, polymers with polar groups in their structures possessed higher T_g values. For example, polymer **4c** had the highest T_g (165°C) because of the presence of carboxylic acid groups pendent to its backbone.

Table 3 DSC Results for Polyethers **4a–h**

Polymer	**4a**	**4b**	**4c**	**4d**	**4e**	**4f**	**4g**	**4h**
T_g (°C)	150	146	165	119	130	142	113	144

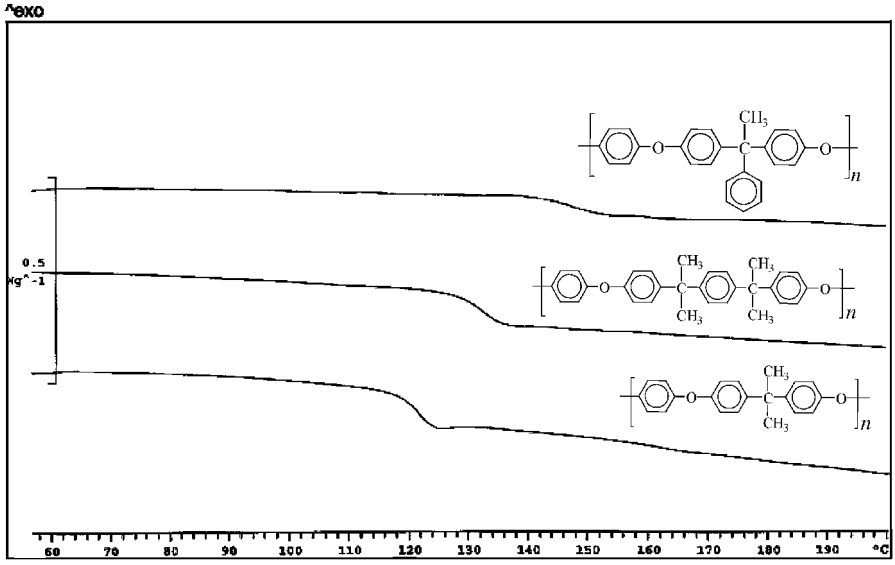

Figure 8 DSC curves of polymers **4d–f**.

B. Polythioethers

A number of polythioethers with aromatic and aliphatic spacers were also synthesized. The 1,2-, 1,3- and 1,4-dichlorobenzene complexes were reacted with 4,4′-thio-*bis*-benzenethiol in the presence of potassium carbonate to produce the corresponding polyaromatic thioethers shown in Scheme 2.[31,32] Poly(phenylene sulfide) (PPS) is a well-known engineering thermoplastic that has been the topic of many studies.[3] This polymer is usually prepared under very harsh conditions, and is insoluble below 200°C. Reaction of 1,2-, 1,3-, and 1,4-dichlorobenzene complexes (**1**, **5**, and **6**) with 4,4′-thio-*bis*-benzenethiol (**7**) gave the corresponding organoiron polyphenylene sulfides (**8a–c**) as yellow solids in very high yields (92–96%).[32] The synthesis of these cyclopentadienyliron-coordinated polymers occurred rapidly, which could be readily observed by the viscous nature of the reaction solutions within approximately 30 mins. These organometallic polymers were soluble in polar solvents such as DMAc, DMF, and DMSO but displayed very limited solubility in less polar solvents such as acetone, acetonitrile, and dichloromethane. On cleavage of the cyclopentadienyliron cations from the polymer backbones, polymers **9a** and **9b** were insoluble in all solvents tested, while polymer **9c** displayed fair solubility in polar solvents. The M_w of **9c** was found to be 16,200, with a polydispersity index of 3.0. This corresponds to a degree of polymerization of ~50 and a molecular weight for the metallated analog (**8c**) of 29,500.

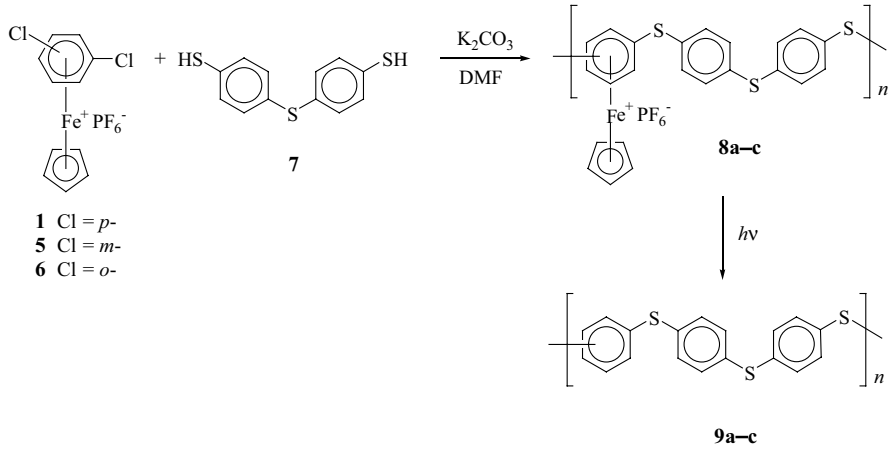

Scheme 2

Cyclic voltammetric studies of the organoiron polyphenylene sulfide (**8a**) were undertaken in DMF and propylene carbonate.[43] The influence of solvents on the reversibility of the redox waves of these complexes is related to their coordinating ability.[45,46] It was found that the polymer adsorbed to the working electrode in DMF but not in propylene carbonate.[43] The half-wave potential of **8a** in propylene carbonate at −30°C was −0.85 V using a scan rate of 2 V/s. This cyclic voltammogram is shown in Figure 9.

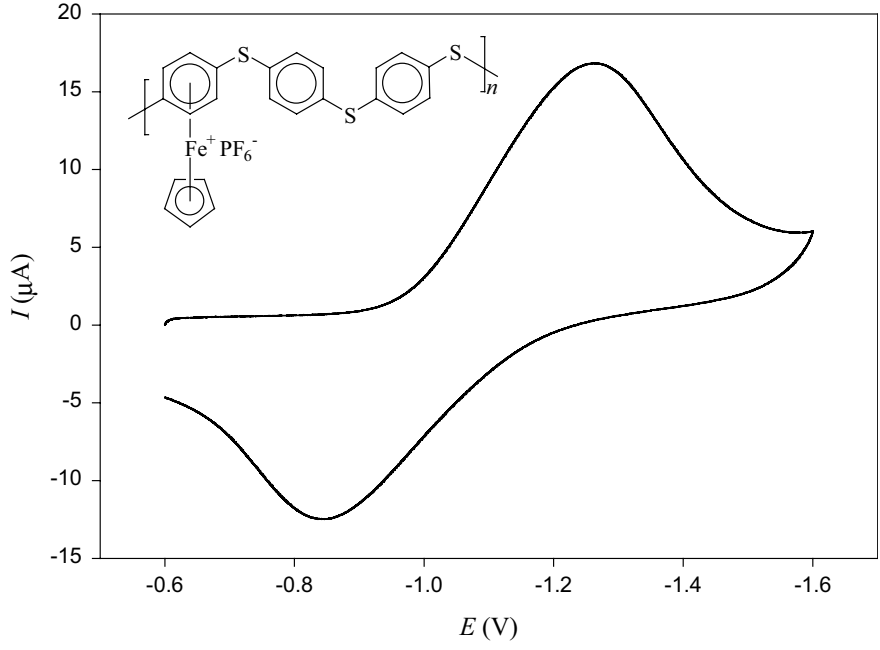

Figure 9 Cyclic voltammogram of **8a** obtained at −30°C in propylene carbonate with a scan rate of 2 V/s.

The thermal properties of the *para-, meta-*, and *ortho*-substituted polyphenylene sulfides (**8a–c, 9a–c**) were examined using thermogravimetric analysis.[32] Although all of these polymers exhibited good thermal stability, TGA results indicated that the thermal stability of these polymers decreased in the order *p-* > *m-* > *o-*. For example, the onsets for weight loss in polymers **9a–c** were 512, 491, and 448°C, respectively.

The DSC thermograms of polymers **9a–c** were also obtained. The T_g of the *o*-substituted polymer was 88°C, followed by the *p*-substituted polymer at 86°C, while the *m*-substituted polymer's T_g was 72°C. The DSC trace of the *p*-substituted polyphenylene sulfide is shown in Figure 10. This curve shows a glass transition at 86°C, a crystallization point at 140°C, and a melting point at 278°C.[32] These values are in agreement with literature T_g and T_m values for *p*-polyphenylene sulfide, which are 85 and 285°C, respectively.[3]

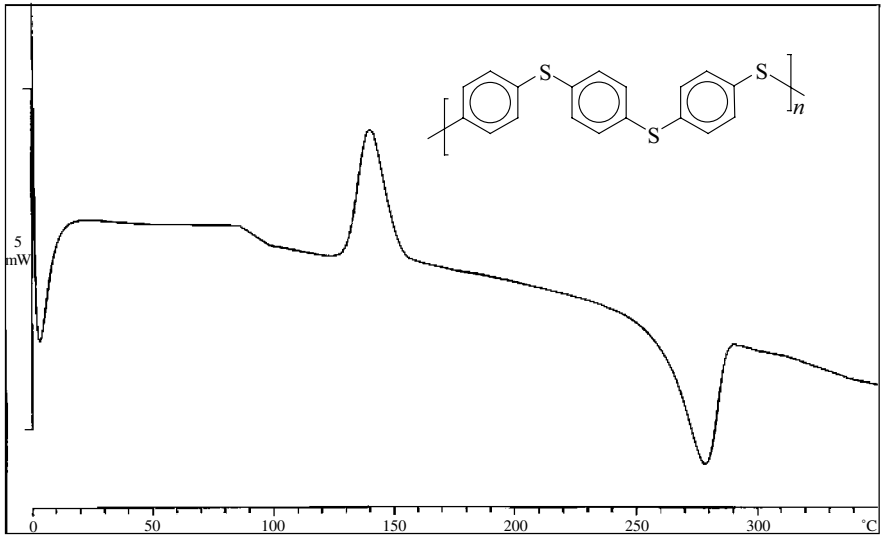

Figure 10 DSC trace of polymer **9a**.

The influence of aliphatic spacers in the backbones of polythioethers was examined by reacting complex **1** with **10a–d** as shown in Scheme 3.[32] Polymers **11a–d** were isolated in 88–91% yield as beige or brown materials. Polymers **11c** and **11d** were often elastomeric in nature and formed sticky solids, while polymers **11a** and **11b** were precipitates. Polymer **11a** displayed very low solubility in polar solvents and precipitated from DMF during the polymerization reactions. It was noted that with increases in the number of methylene units in the polymer backbones, there were corresponding increases in polymer solubility. For example, the polymer prepared using 1,8-octanedithiol was formed more rapidly, was more soluble, and had a higher molecular weight than polymers with shorter aliphatic spacers in their backbones. Moreover, the hexamethylene (**11c**) and octamethylene (**11d**) bridged polymers were much more stable at high temperatures during the polymerization reactions, which is likely related to their higher solubilities.

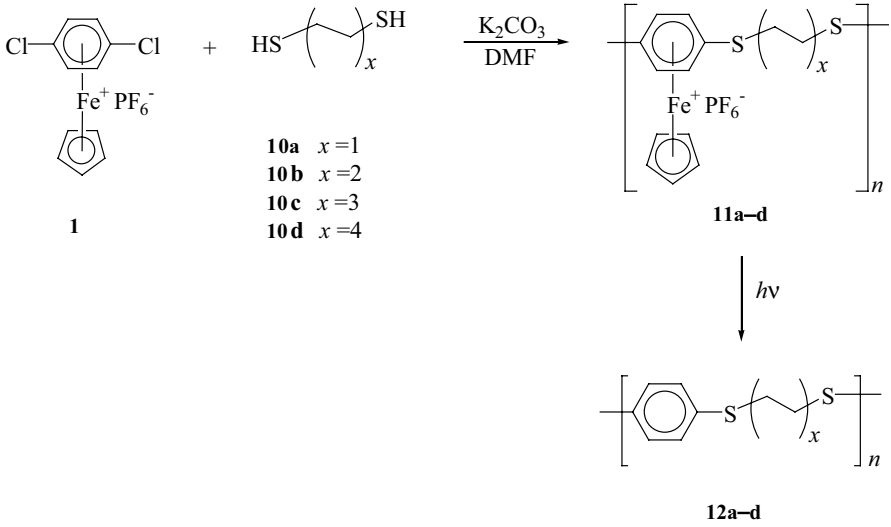

Scheme 3

Figure 11 shows the ^{1}H NMR spectrum of polymer **11c**. There are three resonances corresponding to the methylene peaks in the polymer backbone at 1.42, 1.71, and 3.26 ppm, and each of these peaks integrated for four protons, demonstrating the symmetry within the hexamethylene bridges. The cyclopentadienyl protons appear as a singlet integrating for five protons at 5.01 ppm, while the complexed aromatic protons appear as a singlet integrating for four protons at 6.41 ppm. Following demetallation, the aromatic resonance in the polymer backbone of **12c** shifted downfield and appeared as a singlet at 7.20 ppm.

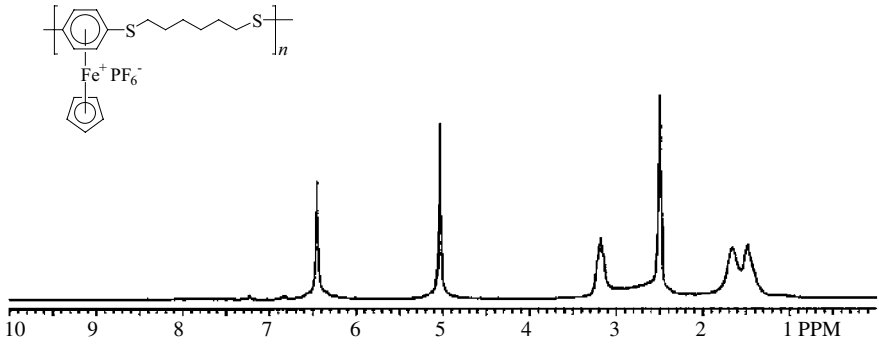

Figure 11 ^{1}H NMR spectrum of polymer **11c** in DMSO-d_6.

The solubilities of polymers **12a–d** were also highly dependent on the number of methylene units in their backbones. It was found that polymers **12c** and **12d** were soluble in organic solvents such as THF and chloroform in light of the 6- and 8-carbon aliphatic chains in their backbones. These polymers were determined to have weight average molecular weights of 13,500 and 21,400, respectively. Because of the short aliphatic spacers in polymers **12a** and **12b**, these polymers were found to be insoluble.

The cyclic voltammogram of polymer **11d** containing an octamethylene bridge is shown in Figure 12.[43] This CV shows the two sequential one-electron reduction steps that the iron centers pendent to the polymer backbone undergo at a scan rate of 5 V/s. It was found that at low scan rates, the second reduction step was irreversible; however, the reversibility increased with higher scan rates. The $E_{1/2}$ values corresponding to formation of the neutral 19-electron, and anionic 20-electron iron species occurred at −1.07 and −1.77 V, respectively.

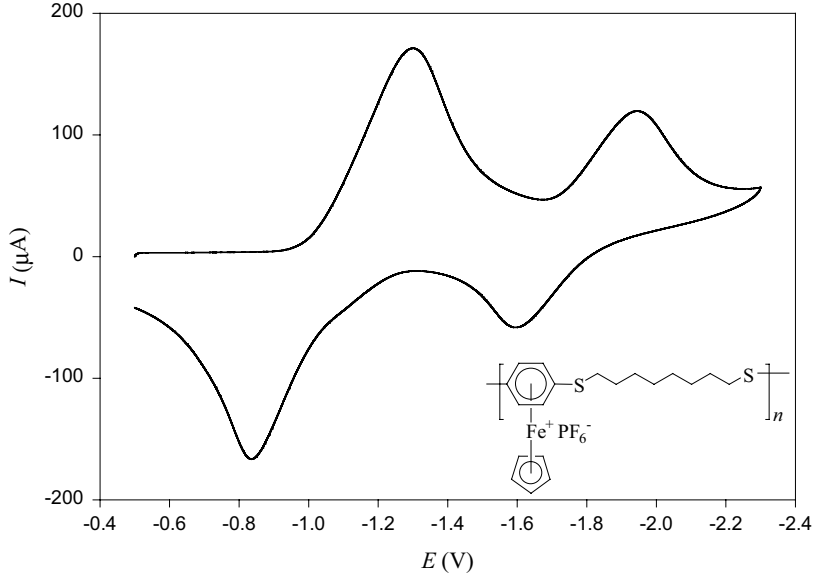

Figure 12 Cyclic voltammogram of **11d** obtained at a scan rate of 5 V/s.

TGA analysis indicated that the polythioethers with aliphatic spacers were less thermally stable than the aromatic polyethers and thioethers.[32] Following the initial weight losses due to the cleavage of the metallic moieties, secondary weight losses of 41–46% were observed starting from 347 to 402°C. In contrast, the lowest onset for weight loss recorded for polyethers **3a–h** occurred at 417°C, and the percent weight losses corresponding to degradation of the polymer backbones were all approximately 25%. For polymers **11a–d**, there was an initial weight loss of 17 to 25% between 200 and 250°C, due to loss of the cyclopentadienyliron moieties. Thereafter, the organic portions of these polymers began to decompose at around 350°C.

DSC of the organic polythioethers provided the glass transition temperatures of these polymers.[32] The T_g values of these polymers were approximately 100°C lower than those observed for the polyaromatic ethers and about 50°C lower than those of the polyaromatic thioethers. This is due to both the flexible aliphatic spacers in the polymer backbones and the presence of thioether rather than ether bridges. The T_g values of polymers **12b–d** were 33, 34, and 37°C, respectively. It can be concluded that increasing the length of the aliphatic spacers decreased the glass transition temperatures of these materials slightly.

C. Copolymers with Ether–Thioether and Amine–Thioether Spacers

It was also of interest to examine the properties of polymers with different types of spacers within their backbones.[32] Scheme 4 shows the synthesis of diiron complexes containing amine bridges (**14a, 14b**). These complexes were synthesized in 74 and 76% yields, respectively, by reaction of 2 equivalents of complex **1** with 1 equivalent of the diamine compounds (**13a**, **13b**).

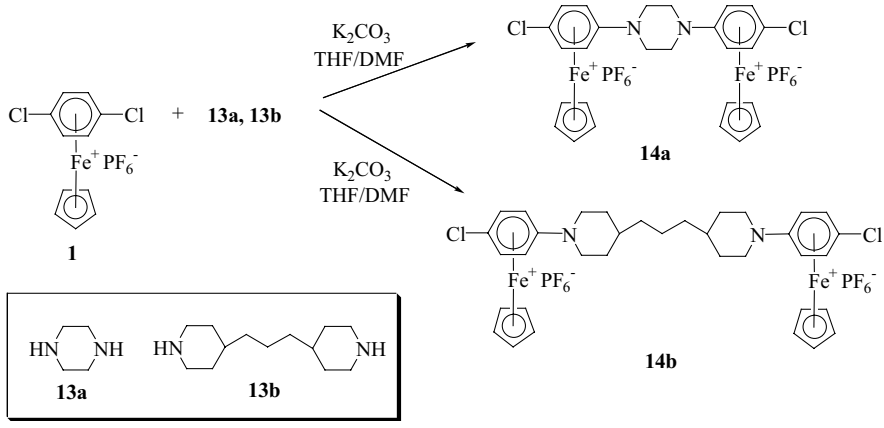

Scheme 4

Figure 13 shows the ^{1}H and ^{13}C NMR spectra of complex **14b**. The interesting feature of the ^{1}H NMR spectrum of complex **14b** is that the protons of the methylene groups on the cyclic units (H_a and H_b) appeared as four separate peaks rather than two. Assignment of these peaks was accomplished using HH and CH correlation spectroscopy (COSY) experiments. The multiplet at 1.35 ppm corresponds to H_d and H_b', while the broad peak at 1.47 was assigned to H_e. The singlet at 1.64 ppm corresponds to the two H_c protons while the doublet at 1.93 ppm corresponds to H_b''. The triplet at 3.05 ppm integrating for four protons is assigned to H_a', while the four protons at 4.01 ppm are assigned to H_a''. The singlet integrating for 10 protons at 5.14 ppm, was assigned to the cyclopentadienyl protons, and the two doublets at 6.05 and 6.51 ppm correspond to the complexed aromatic protons.

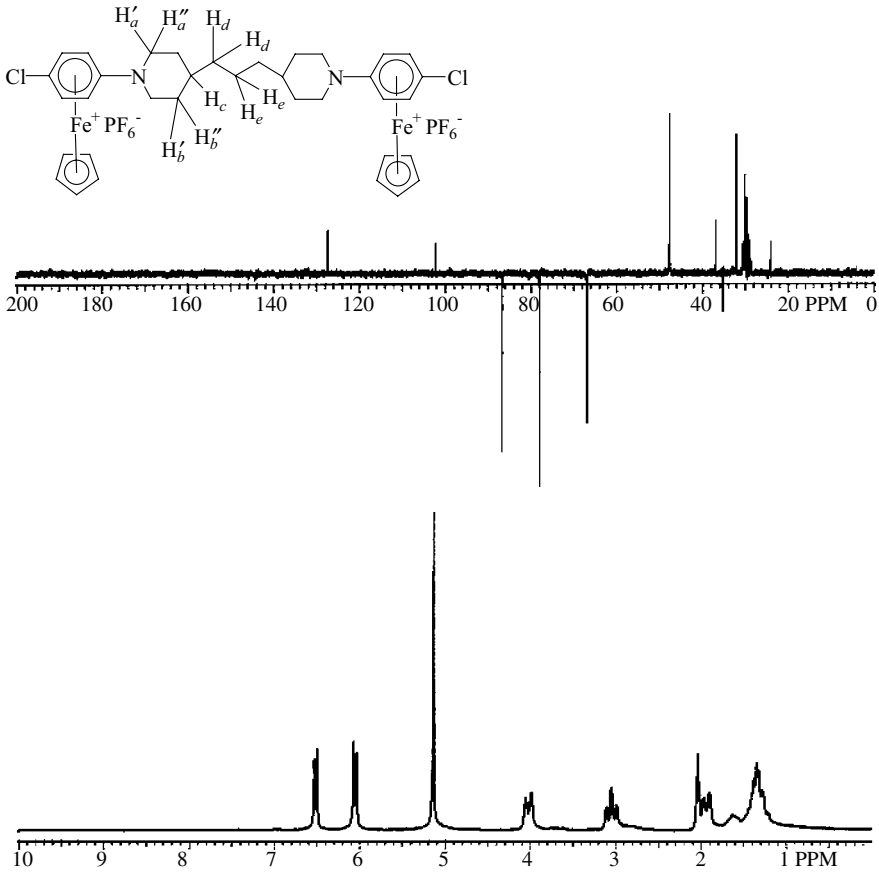

Figure 13 ^{1}H and ^{13}C NMR spectra of complex **14b** in acetone-d_6.

The ^{13}C NMR spectrum of complex **14b** is quite simple relative to the ^{1}H NMR spectrum. The methylene carbons can be seen at 24.24, 32.13, 36.92, and 47.66 ppm, while the methine carbons appear at 35.41 ppm. The cyclopentadienyl carbons are present at 78.00 ppm, while the complexed aromatic CH carbons appear at 66.79 and 86.65 ppm and the quaternary complexed aromatic carbons appear at 102.29 and 127.48 ppm.

The syntheses of polymers **15a** and **15b** are shown in Scheme 5.[32] These polymers, with alternating amine/thioether linkages, were prepared by reacting the diiron amine complexes **14a** and **14b** with 4,4′-thio-*bis*-benzenethiol (**7**). These polymers were isolated as orange precipitates in 93 and 98% yields, respectively. The resulting polymers (**15a**, **15b**) exhibited relatively good solubility in polar organic solvents. On demetallation, polymer **16a** was insoluble while polymer **16b** had a weight-average molecular weight of 9100 with a polydispersity of 1.5.

Figure 14 shows the ^{1}H NMR spectra of polymers **15b** and **16b**. The aliphatic protons in **15b** are seen between 1.21 and 3.84 ppm, and the cyclopentadienyl resonance appears at 5.00 ppm as a broad singlet. The complexed and uncomplexed

aromatic protons each appear as two broad peaks. The signals corresponding to the complexed and uncomplexed aromatic protons each integrated for four hydrogens. The ^{1}H NMR spectrum of **16b** shows the same pattern observed in the alkyl resonances as **15b**. In this polymer, the complexed aromatic protons shifted downfield and all of the aromatic protons appear as four sets of doublets between 6.88 and 7.32 ppm.

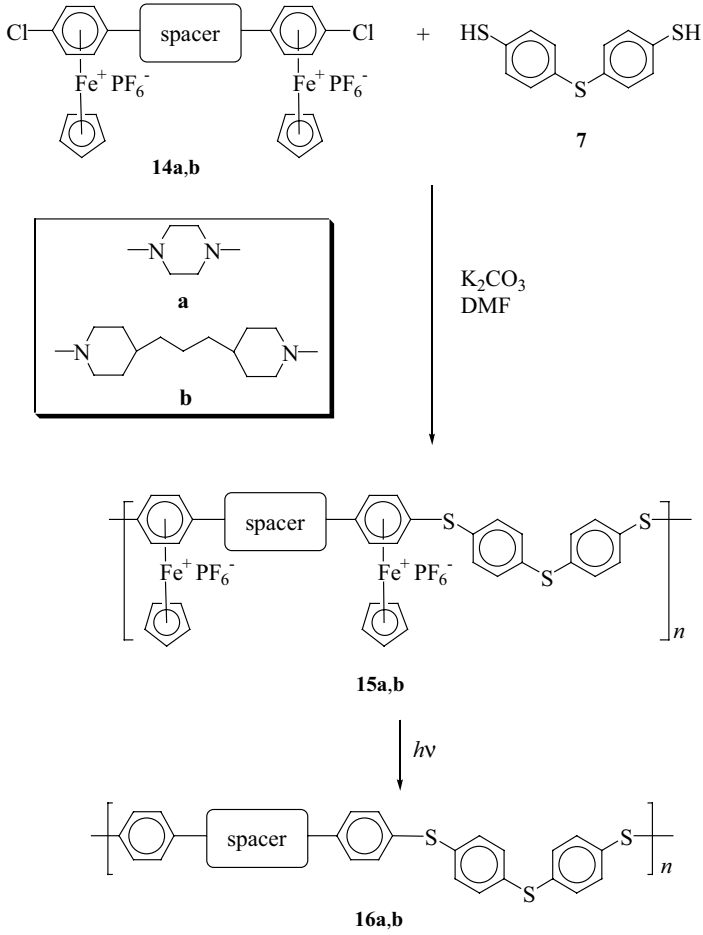

Scheme 5

Using a similar strategy, polymers with alternating ether and thioether bridges in their backbones were synthesized as shown in Scheme 6. Two different dithiols were explored in the polymerization reaction with complex **18**,[6] 4,4′-thio-*bis*-benzenethiol (**7**) and 1,8-octanedithiol (**10d**).[32] The two resulting polymers (**19a** and **19b**) had very different solubilities due to their respective aromatic and aliphatic thioether bridges. Although both of these polymers were soluble in polar

organic solvents while coordinated to the cyclopentadienyliron moieties, polymer **19b**, with the aliphatic spacers was much more soluble in organic solvents such as acetone, acetonitrile and dichloromethane than **19a**. The fully aromatic polymer **19a** could only be solubilized in very polar solvents such as DMSO and DMF, and often formed a gel. Polymer **20a** was insoluble in all common organic solvents at room temperature because of the rigid nature of its backbone, while polymer **20b** could be solubilized and its M_w was determined to be 21,700 with a PDI of 2.4.

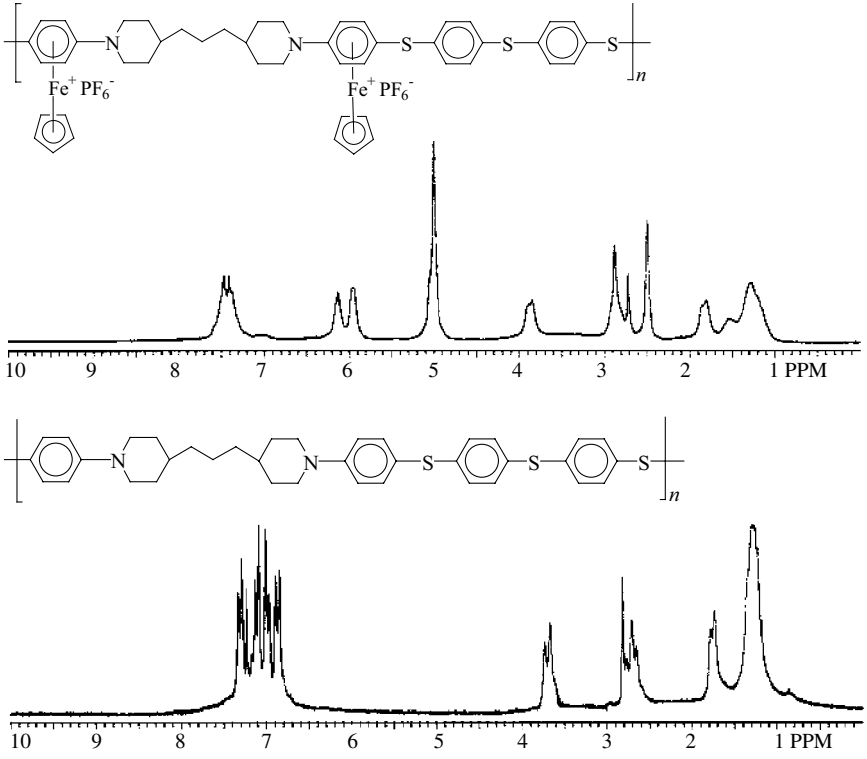

Figure 14 ^{1}H NMR spectra of polymer **15b** in DMSO-d_6 and polymer **16b** in $CDCl_3$.

In order to complete the electrochemical investigations, the redox properties of the copolymers were also studied.[43] The cyclic voltammogram of polymer **19a**, containing aromatic ether and thioether bridges was examined. Figure 15 shows the CV obtained at −30°C using a scan rate of 1 V/s. The E_{pc}, E_{pa}, and $E_{1/2}$ for this polymer were calculated to be −1.23, −0.955, and −1.09 V, respectively.

The thermal stabilities of the polyether/thioethers were examined using thermogravimetric analysis, and it was determined that the incorporation of aliphatic bridges into the backbones of **19b** and **20b** decreased their thermal stabilities. The completely aromatic-bridged **20a** had a 38% weight loss at an onset temperature of 523°C, whereas **20b** with aliphatic spacers between the aromatic ether bridges displayed a 72% weight loss commencing at 380°C.[32] These thermograms are shown in Figure 16.

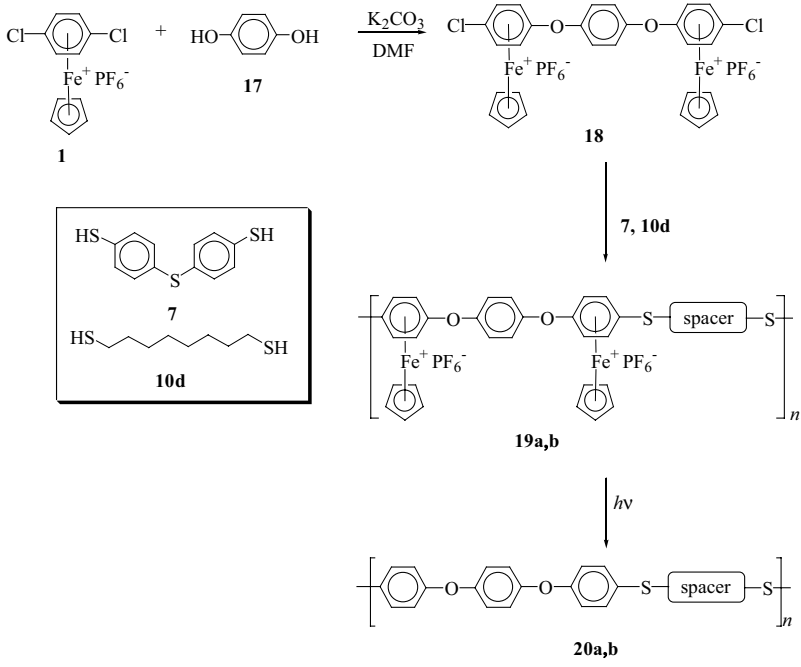

Scheme 6

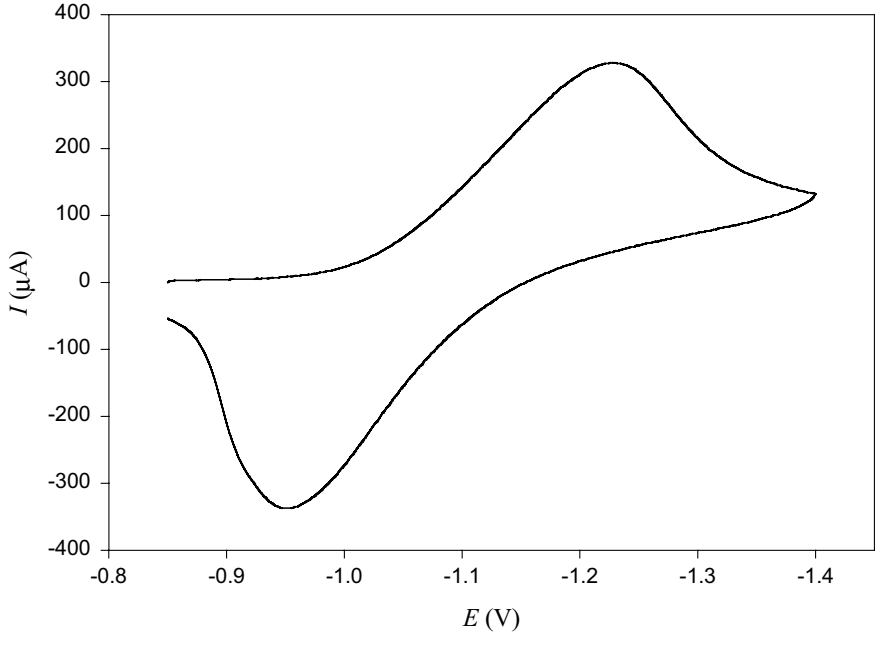

Figure 15 Cyclic voltammogram of **19a** obtained at a scan rate of 1 V/s in DMF.

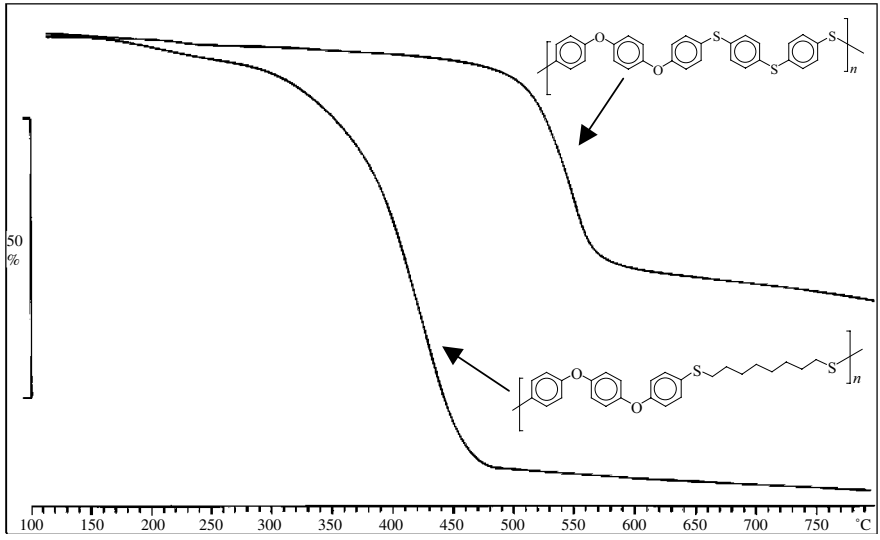

Figure 16 TGA thermograms of polymers **20a** and **20b**.

Differential scanning calorimetry of the organic polymers demonstrated that their glass transition temperatures were strongly influenced by the nature of the spacers in their backbones.[32] For example, polymers **20a** and **20b** both had aromatic ether spacers in their backbones, but while **20a** also had an aromatic thioether linkage, the thioether linkage in **20b** was aliphatic. The result was that the T_g values of these polymers were very similar to those of polymers **9a** and **12d**. The T_g of the *p*-polyphenylenesulfide (**9a**) was found to be 86°C, while the T_g of polymer **20a** was 89°C. In addition, it was shown earlier that the T_g of polymer **12d** was 33°C, and the incorporation of aliphatic thioether units into polymer **20b** resulted in a T_g at 38°C. Since the glass transition temperatures of the polyaromatic ethers described earlier ranged from 113 to 165°C, it can be concluded that the glass transition temperatures of mixed polyether/thioethers are more highly influenced by the sulfur linkages than the oxygen linkages. DSC of polymers **16a** and **16b** revealed that these amine/thioether polymers possessed higher glass transition temperatures than did their ether/thioether analogs. The T_g of polymer **16b** (109°C) was 4°C lower than that of **16a**, in light of the longer aliphatic chains in its backbone.

III. STAR-SHAPED POLYAROMATIC ETHERS

Dendrimers and star polymers containing redox active sites have been utilized in the design of new types of catalysts, sensors, bioelectronic devices, and molecular batteries.[47–50] Highly branched polymers containing arenes coordinated to organometallic moieties have been prepared with chromium tricarbonyl,[51] cyclopentadienyliron,[52–56] and pentamethylcyclopentadienylruthenium moieties.[57] Astruc and

coworkers have used this class of complex to prepare polyfunctional cores, which were subsequently used to synthesize dendritic materials containing various organic and organometallic moieties within their structures.[52–54] The resulting organometallic materials included the arene complexes at the core and/or the termini of the branches; however, there were no examples of polymers with organometallic complexes throughout the molecules.

The success associated with the controlled synthesis of aromatic ethers using arene complexes of cyclopentadienyliron makes this methodology attractive for the design of branched molecules. Reaction of complexes **1** and **21** with phloroglucinol (**22**) resulted in the isolation of trimetallic complexes **23** and **24** in 78–90% yields as yellow and beige solids, respectively (Scheme 7).[33,34] Complex **23** is an excellent precursor for larger star-shaped complexes.

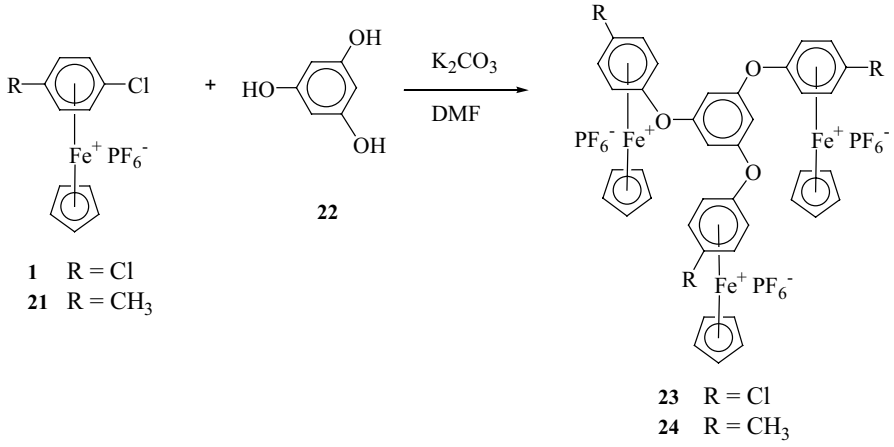

1 R = Cl
21 R = CH_3

23 R = Cl
24 R = CH_3

Scheme 7

It is important to note that only one chloro group of the *p*-dichlorobenzene complex (**1**) was displaced during the initial reaction, which was confirmed by ^{1}H and ^{13}C NMR as well as elemental analysis.[34] Figure 17 shows the ^{1}H and ^{13}C NMR spectra of complex **23** in acetone-d_6. The ^{1}H NMR spectrum shows that only one cyclopentadienyl resonance integrating for 15 protons is present at 5.37 ppm, while the metal-coordinated arene protons appear as two sets of doublets at 6.73 and 6.81 ppm. The three protons on the trisubstituted central aromatic ring resonate as a singlet at 7.49 ppm. In the ^{13}C NMR spectrum, the cyclopentadienyl resonance appears at 80.31 ppm, while the complexed aromatic CH carbons resonate at 78.11 and 87.83 ppm, and the quaternary complexed aromatic carbons are observed at 105.39 and 133.59 ppm, respectively. The uncomplexed aromatic CH carbons resonate at 111.85 ppm, while the three equivalent quaternary aromatic carbons are seen at 157.35 ppm.

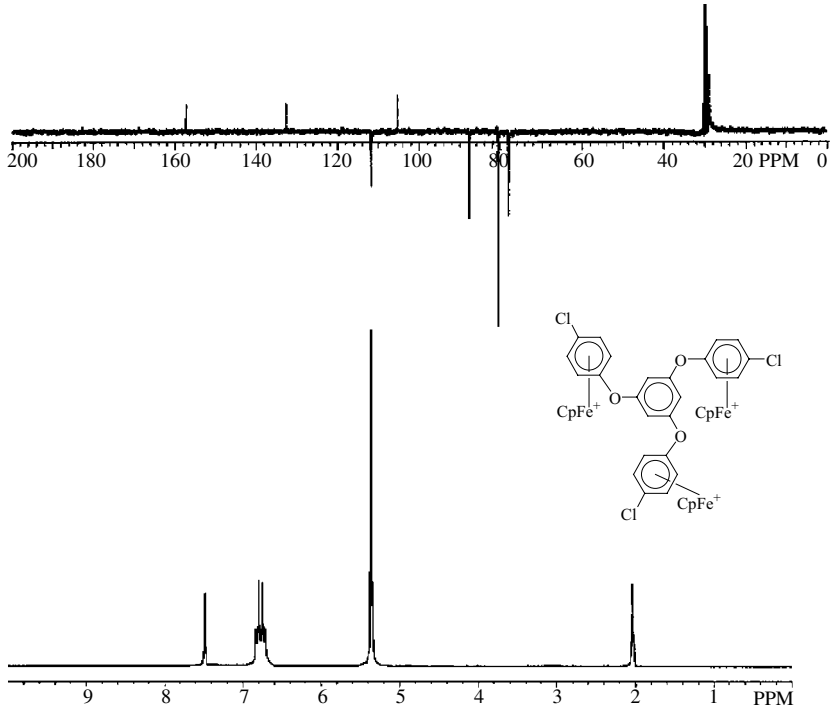

Figure 17 ^{1}H and ^{13}C NMR spectra of complex **23** in acetone-d_6.

The electrochemical properties of the cyclopentadienyliron-coordinated star-shaped complexes (**23** and **24**) were examined using cyclic voltammetry (Fig. 18).[34] The cyclic voltammetric studies were carried out in DMF from −40 to +20°C at sweep rates of 0.1–5 V/s. The $E_{1/2}$ value corresponding to reduction of complex **23**, containing terminal chloro groups, was −0.99 V, while the $E_{1/2}$ value corresponding to reduction of complex **24** was −1.41 V at −40°C, $\nu = 0.1$ V/s. This indicates that electron-withdrawing groups attached to the complexed arenes results in less negative reduction potentials. The voltammograms of complexes **23** and **24** each showed three concurrent one-electron reduction processes, which indicates that the iron moieties behave as isolated redox centers.

Scheme 8 shows the synthesis of organometallic complexes containing terminal phenolic groups (**26–29**) by reaction of the chlorotoluene complex (**21**) with various dinucleophiles. These molecules were synthesized for reaction with the star-shaped complex **23** in order to prepare hexametallic complexes.

Reaction of complexes **26–29** with the trimetallic complex **23** was achieved at room temperature in DMF using potassium carbonate as the base. The resulting star-shaped polymers were isolated in very good yields.[34] Any unreacted starting materials were removed from the products by passing them through an alumina column with acetone. Scheme 9 shows the structures of the star polymers containing six metallic moieties pendent to their branches.

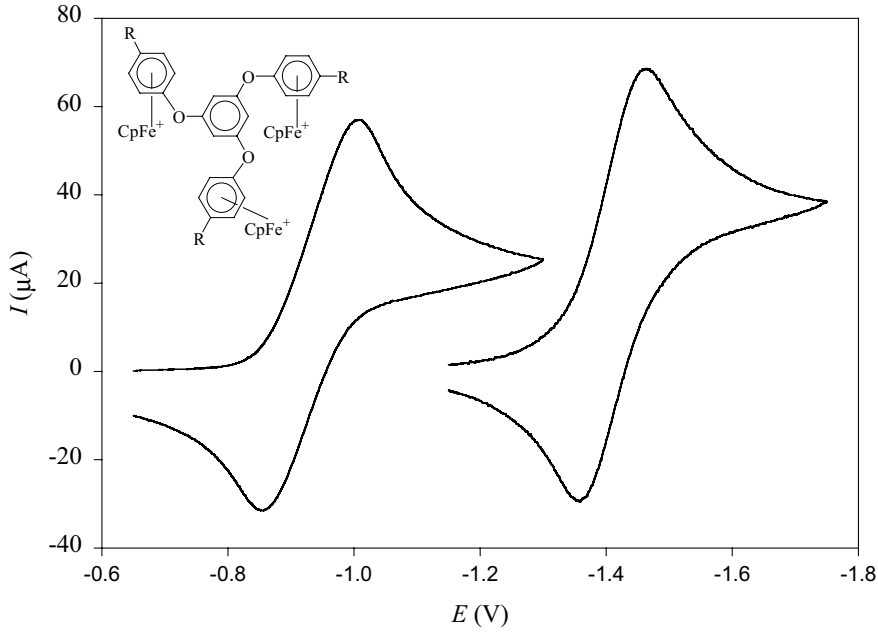

Figure 18 Cyclic voltammograms of complexes **23** (left, R = Cl) and **24** (right, R = CH_3).

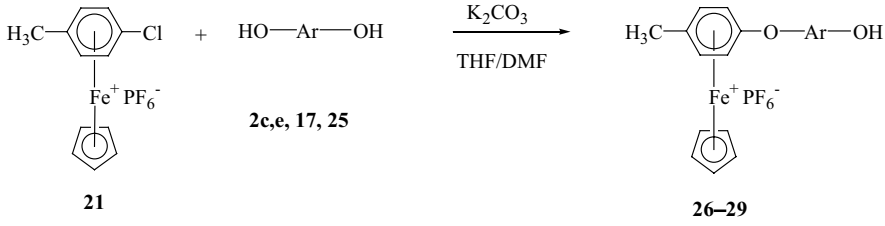

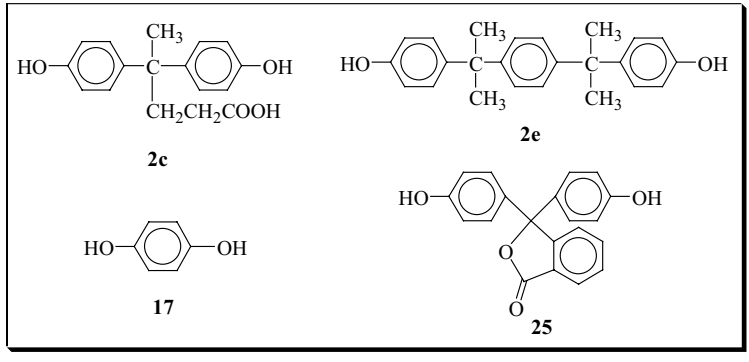

Scheme 8

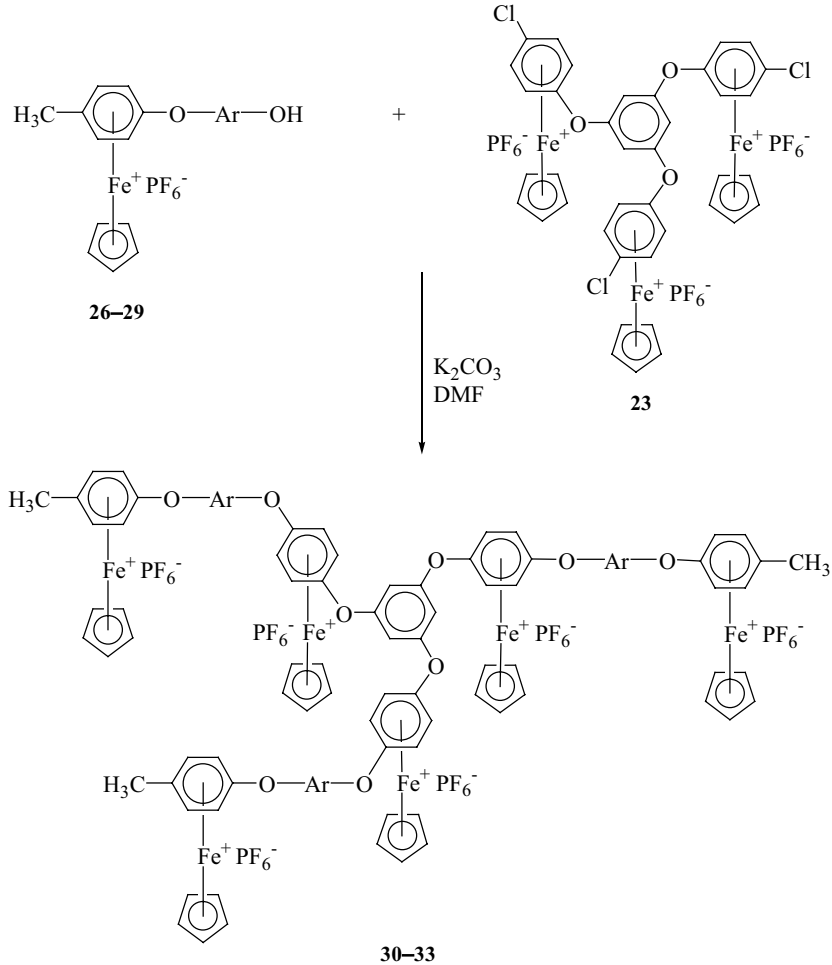

Scheme 9

The ^{1}H NMR spectrum of complex **27** (Fig. 19) shows two methyl groups at 1.62 and 1.67 ppm corresponding to the isopropylidene groups and the methyl on the complexed aromatic ring at 2.48 ppm. There is one cyclopentadienyl resonance at 5.20 ppm and the complexed aromatic protons are seen as two sets of doublets at 6.29 and 7.22 ppm. The protons on the uncomplexed aromatic rings resonate as four sets of doublets at 6.73, 7.07, 7.22, and 7.71 ppm and a singlet at 7.17 ppm. Following reaction with the core molecule (**23**), the NMR spectrum of the hexametallic complex **31** was obtained. The methyls of the isopropylidene groups appear at 1.68 and 1.70 ppm, while the methyl protons of the complexed toluene rings resonate as a singlet at 2.47 ppm. The protons of the two nonequivalent cyclopentadienyl rings appear at 5.19 and 5.28 ppm, while the complexed aromatic protons appear at 6.29 and 6.53 ppm as multiplets. The uncomplexed aromatic protons appear as two broad peaks at 7.21 ppm and 7.31–7.45 ppm.

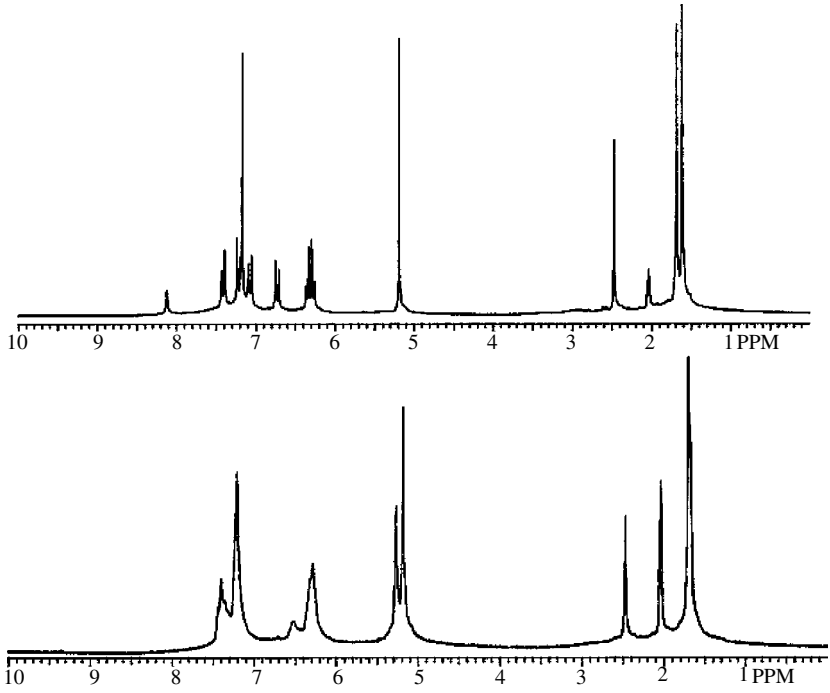

Figure 19 ^{1}H NMR spectra of complexes **27** (top) and **31** (bottom) in acetone-d_6.

The cyclic voltammogram of complex **32** is shown in Figure 20.[34] While the CVs of complexes **23** and **24** showed single redox processes corresponding to three concurrent one-electron reductions, the CV of complex **32** showed that two distinct redox processes were occurring. These two processes can be attributed to reduction of the inner three and outer three iron centers. The $E_{1/2}$ values for these two redox processes occurred at −1.20 and −1.30 V, respectively. This cyclic voltammogram was obtained in DMF at −40°C with a sweep rate of 0.1 V/s.

Scheme 10 shows the synthesis of complex **34**, containing three phenolic groups. This complex was synthesized by displacing the terminal chloro groups of complex **23** with an excess of hydroquinone (**17**) in the presence of potassium carbonate.

The synthesis of higher molecular weight polymers was accomplished using hydroquinone-based systems. The syntheses of linear aromatic ether complexes containing two, three, and four cyclopentadienyliron cations pendent to their structures are shown in Scheme 11. Reaction of complexes **36** and **38** with an excess of hydroquinone resulted in the isolation of the aryl ether oligomers **37** and **39**. Complexes **36** and **38** were isolated as beige powders in 87 and 94% yields, respectively. These complexes contain terminal phenolic groups that can be further reacted with chloroarene complexes. These complexes (**36**, **38**, and **40**) each contain one terminal chloroarene complex that can be reacted with the triphenolic star complex **34** to produce larger star polymers. Complexes **36**, **38**, and **40** were isolated as yellow solids in 90–93% yields.

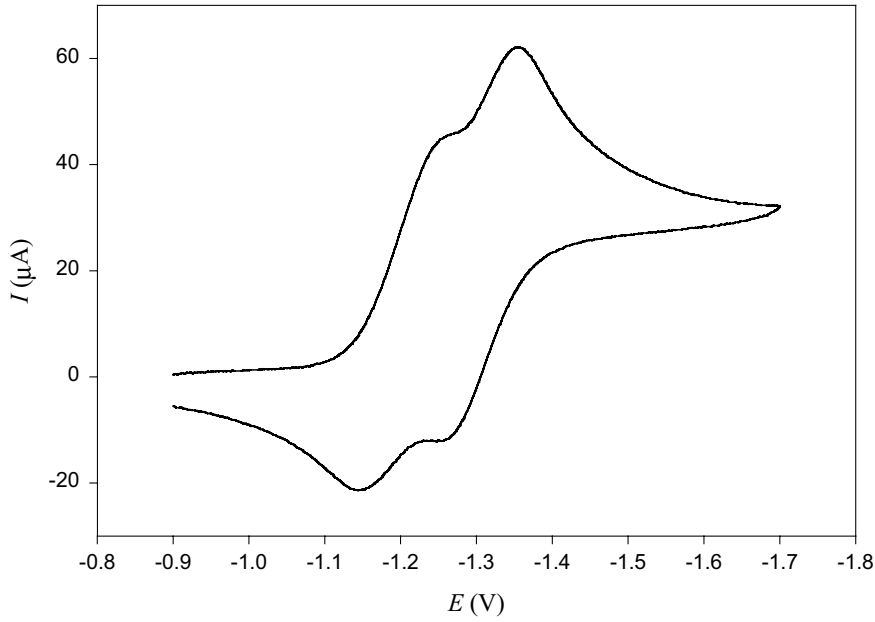

Figure 20 Cyclic voltammogram of hexametallic star complex **32** in DMF.

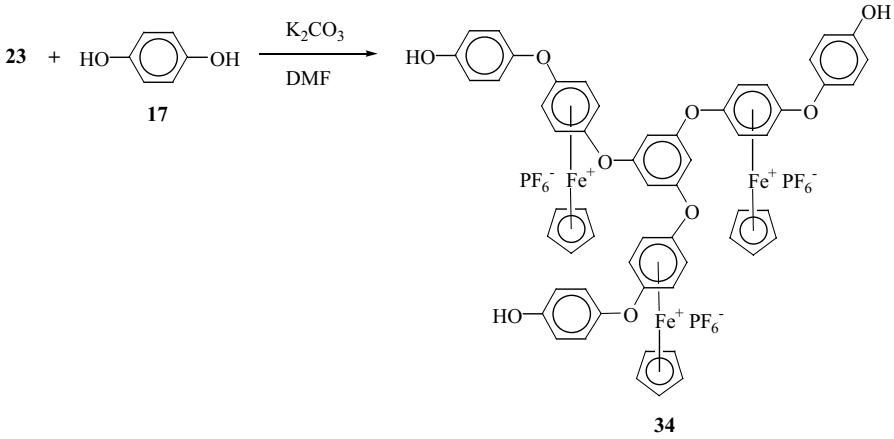

Scheme 10

Complex **34** was subsequently reacted with the chloroarene complexes **36**, **38**, and **40**, resulting in the isolation of star polymers **41–43** containing 9, 12, and 15 metallic moieties pendent to their backbones, respectively. The synthesis of these polymetallic stars is shown in Scheme 12. It was found that the solubility of these polymers decreased with increasing molecular weight; however, all polymers could be solubilized in polar aprotic solvents such as DMF and DMSO.

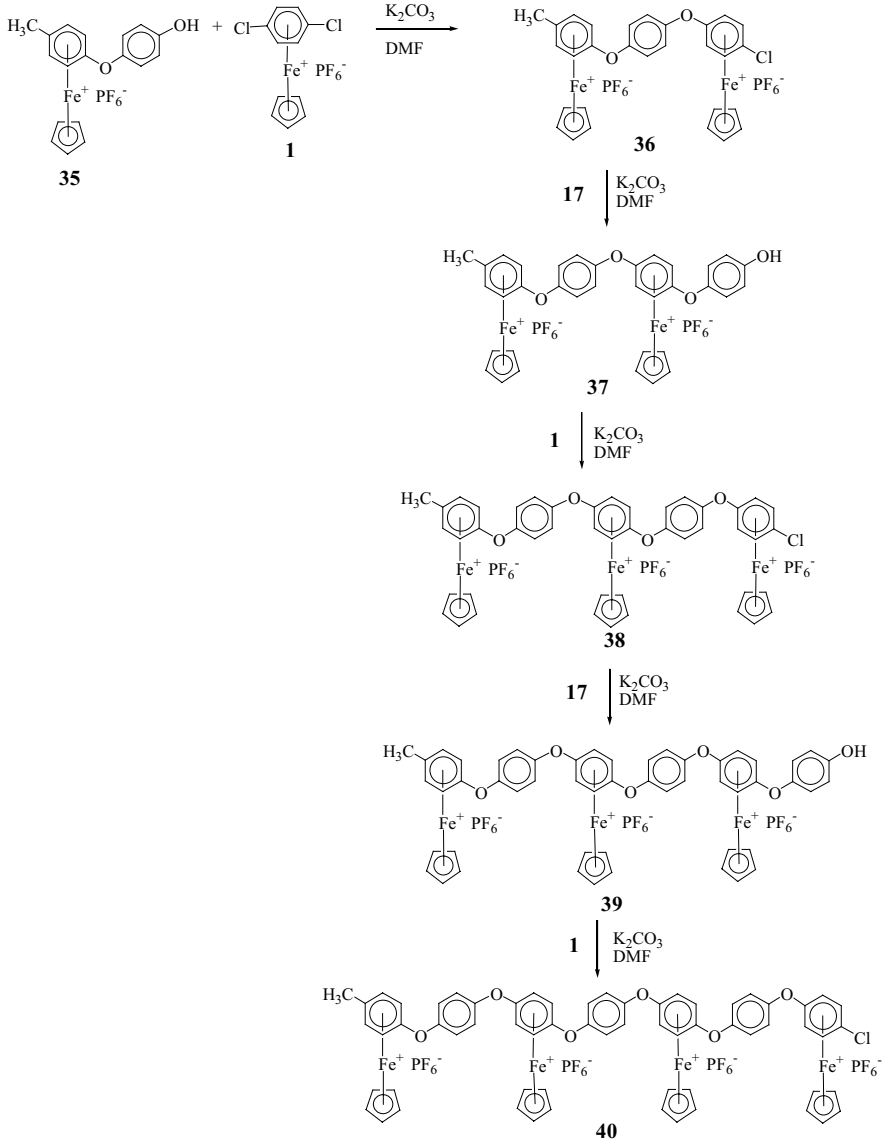

Scheme 11

The electrochemical properties of the star-shaped complexes were examined using cyclic voltammetry.[34] It is important to note that increasing the size of the oligomers resulted in broader redox waves, due to overlapping reduction processes. For example, while the CV of complex **32** (containing six organoiron units) showed two distinct redox waves as a scan rate of 0.1 V/s, the CV of complex **41** (containing nine organoiron units) showed only one broad reduction wave at a scan rate of 0.1 V/s (Fig. 21). The $E_{1/2}$ of this reduction process occurred at −1.30 V.

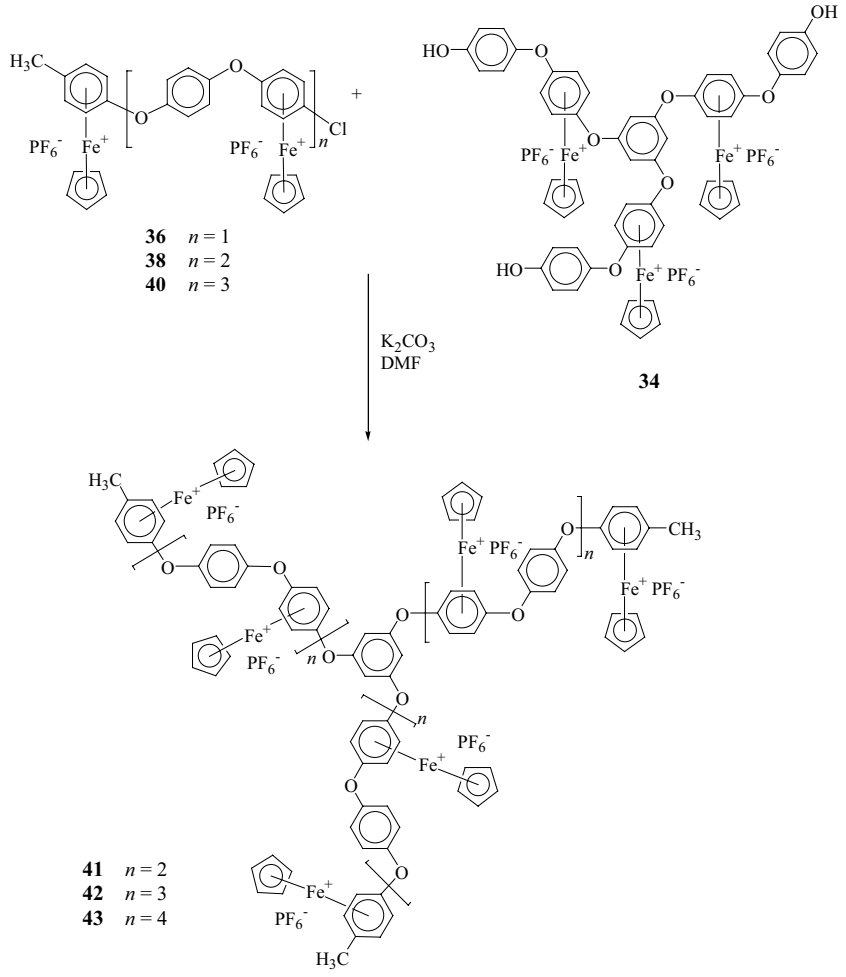

Scheme 12

The cyclic voltammogram of the star-shaped complex containing 12 metallic moieties in its structure (**42**) is shown in Figure 22. The reduction wave is very broad because of overlapping redox processes; however, the reduction peaks for this complex became narrower at higher scan rates. The $E_{1/2}$ value corresponding to reduction of the iron centers in this complex was -1.25 V at a scan rate of 0.1 V/s.

The redox wave of complex **43**, containing 15 pendent metallic moieties, is shown in Figure 23. In contrast to the CV of **42**, the cyclic voltammogram of complex **43** appears to be much narrower. This fairly broad redox wave at $E_{1/2} = -1.34$ V corresponds to one-electron reductions of each of the 15 metal centers. This CV appears to be narrower because more iron centers are equivalent (or quasiequivalent) because of the larger number of complexed aromatic rings containing diarylether linkages. Because of the greater number of these complexes relative to the terminal toluene complexes, these redox waves predominate.

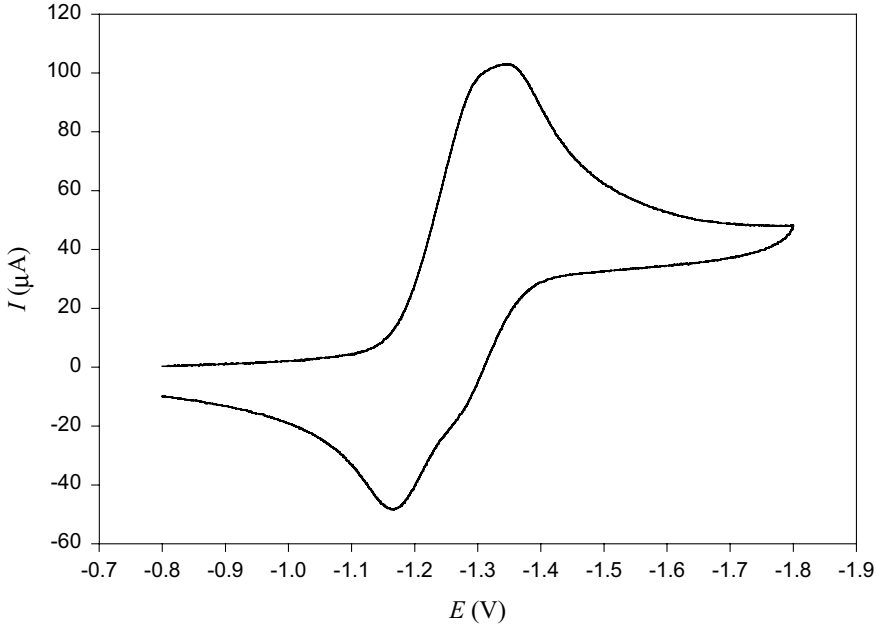

Figure 21 Cyclic voltammogram at glassy carbon of **41** with nine metallic moieties in 0.1 M TBAP in DMF, $\nu = 0.1$ V/s at −40°C.

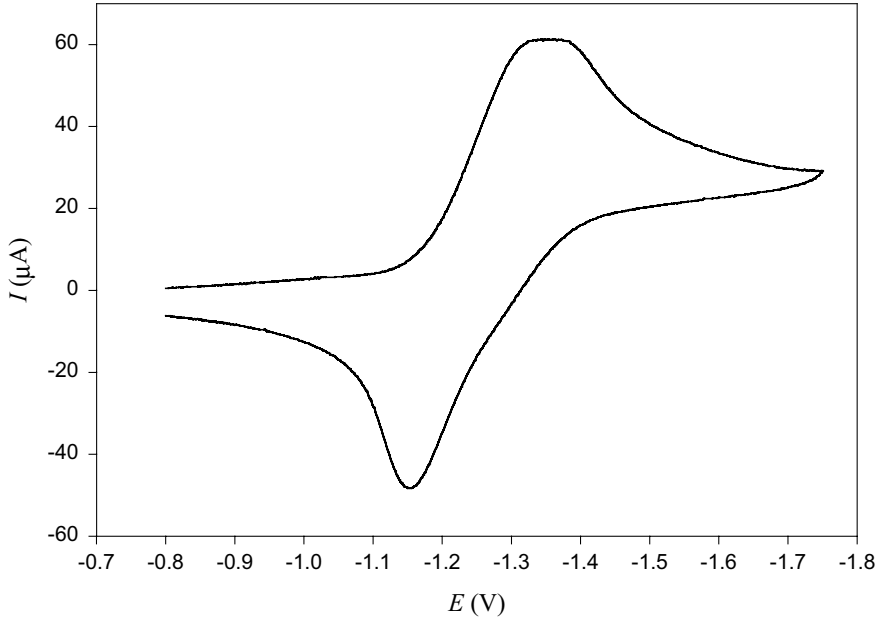

Figure 22 Cyclic voltammogram at glassy carbon of complex **42** with 12 metallic moieties in 0.1 M TBAP in DMF, $\nu = 0.1$ V/s at −40°C.

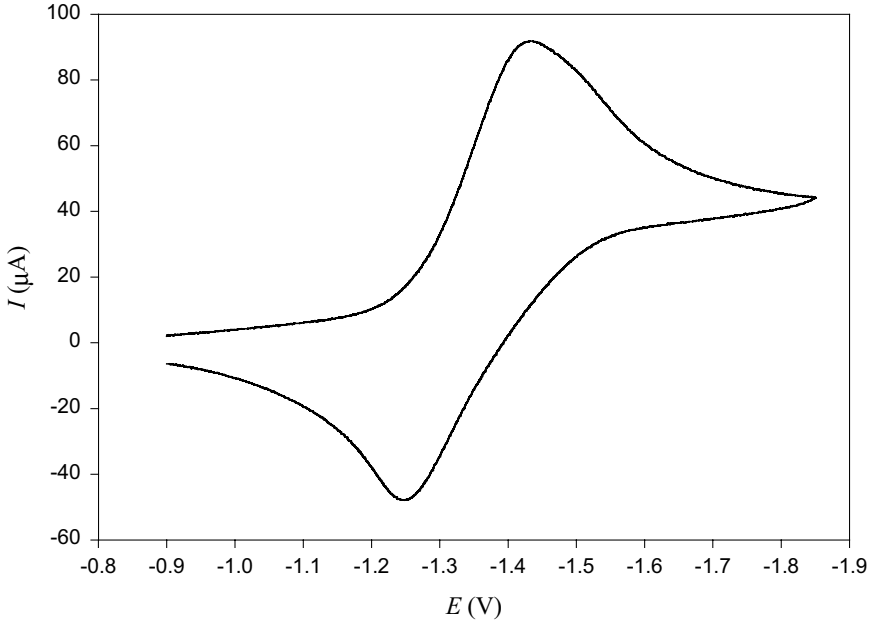

Figure 23 Cyclic voltammogram at glassy carbon of **43** with 15 metallic moieties in 0.1 M TBAP in DMF, $\nu = 0.1$ V/s at −40°C.

IV. POLYMERS CONTAINING NEUTRAL AND CATIONIC CYCLOPENTADIENYLIRON MOIETIES IN THEIR STRUCTURES

The synthesis of complexes containing terminal chloroarene functionalities (**46**, **47**) is described in Scheme 13.[35] These complexes were prepared by reaction of *p*-dichlorobenzene cyclopentadienyliron hexafluorophosphate with an equimolar amount of 4-hydroxybenzylalcohol (**44**) or 2-mercaptoethanol (**45**). Complexes **46** and **47** were isolated in 73 and 89% yields, respectively. These complexes were subsequently reacted with 1,1′-ferrocenedicarbonyl chloride (**48**) in the presence of pyridine, allowing for the isolation of trimetallic complexes **49** and **50** in 76 and 72% yields.

Figure 24 shows the ^{1}H and ^{13}C NMR spectra of complex **49**. The methylene protons resonate at 5.35 ppm, the Cp resonance of the cationic iron complexes appear at 5.33 ppm, and the ferrocenyl resonances appear at 4.50 and 4.82 ppm. The complexed aromatic protons appear as two sets of doublets at 6.49 and 6.79 ppm, while the uncomplexed aromatic protons appear as two doublets at 7.41 and 7.73 ppm. In the ^{13}C NMR spectrum, the methylene resonance appears at 65.56 ppm. The CH carbons of the ferrocenyl Cp rings appear at 72.19 and 73.65 ppm, while the carbons *ipso* to the carbonyl appear at 73.53 ppm. The Cp carbons coordinated to the cationic iron center resonate at 80.25 ppm. The complexed aromatic (CH) carbons resonate at 76.97 and 87.56 ppm, while the quaternary complexed aromatic carbons appear at 104.74 and 133.37 ppm. The uncomplexed aromatic carbons appear at 121.51 and 131.54 ppm, and the quaternary aromatic carbons resonated at 136.09 and 153.52 ppm.

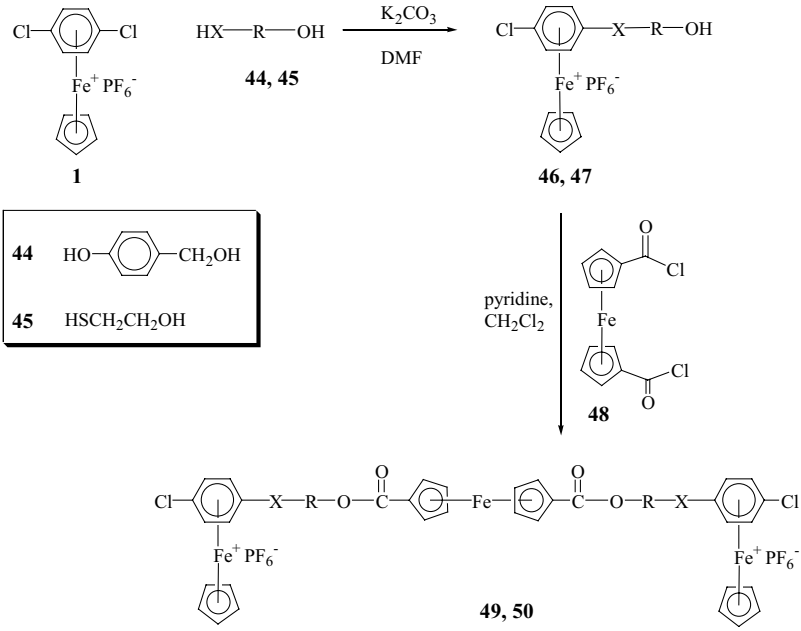

Scheme 13

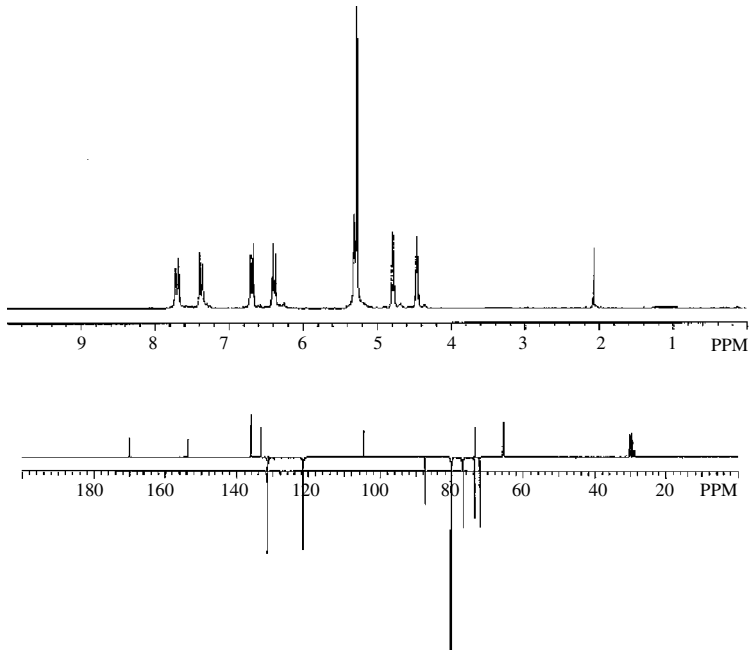

Figure 24 ^{1}H and ^{13}C NMR spectra of complex **49** in acetone-d_6.

The electrochemical properties of the trimetallic monomers were examined using cyclic voltammetry. It has been established that cationic cyclopentadienyliron complexes undergo reduction processes, while ferrocene and functionalized ferrocenes undergo oxidation processes. Figure 25 shows the cyclic voltammogram of complex **49**. The $E_{1/2}$ value obtained for the oxidation of the neutral iron center was 0.994 V, and the $E_{1/2}$ value obtained for the reduction of the two terminal cationic iron centers was –1.12 V.

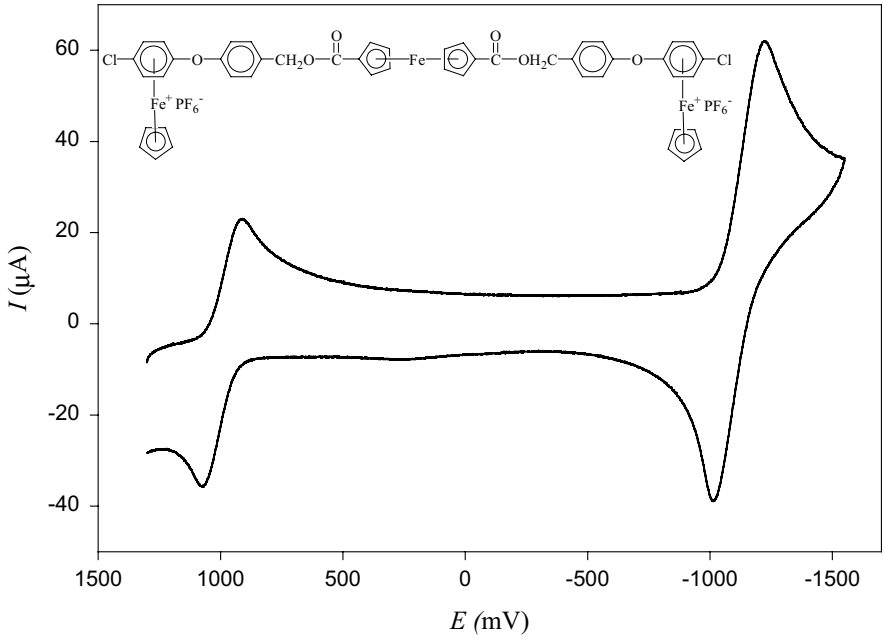

Figure 25 Cyclic voltammogram at glassy carbon of **49** in 0.1 M TBAP in propylene carbonate, $\nu = 0.2$ V/s at −20°C.

Monomers **49** and **50** were subsequently reacted with **2d**, **7,** and **10d** in the presence of potassium carbonate in DMF, resulting in the formation of polymers **51a–f** as shown in Scheme 14.[35] These polymers are unique in that they bear neutral ferrocenyl units in their backbones and cationic cyclopentadienyliron moieties pendent to their backbones. These polymers were isolated as orange solids in yields ranging from 86 to 91%. These organoiron polymers demonstrated good solubility in polar organic solvents such as DMF and DMSO.

Figure 26 shows the ^{1}H and ^{13}C NMR spectra of polymer **51e**. The ^{1}H NMR spectrum shows two peaks at 4.52 and 4.73 ppm, corresponding to the ferrocenyl cyclopentadienyl protons, while the singlet at 5.11 ppm corresponds to the cyclopentadienyl protons coordinated to the cationic iron center. In addition, the presence of two sets of doublets between 7.49 and 7.63 ppm confirms the incorporation of the

aromatic thioether bridges into the polymer backbone. In the ^{13}C NMR spectrum, the CH carbons of the ferrocenyl cyclopentadienyl rings resonate at 70.89 and 72.68 ppm, while the quaternary cyclopentadienyl carbons can be seen at 71.37 ppm, and the cyclopentadienyl carbons pendent to the polymer backbone appear at 79.03 ppm.

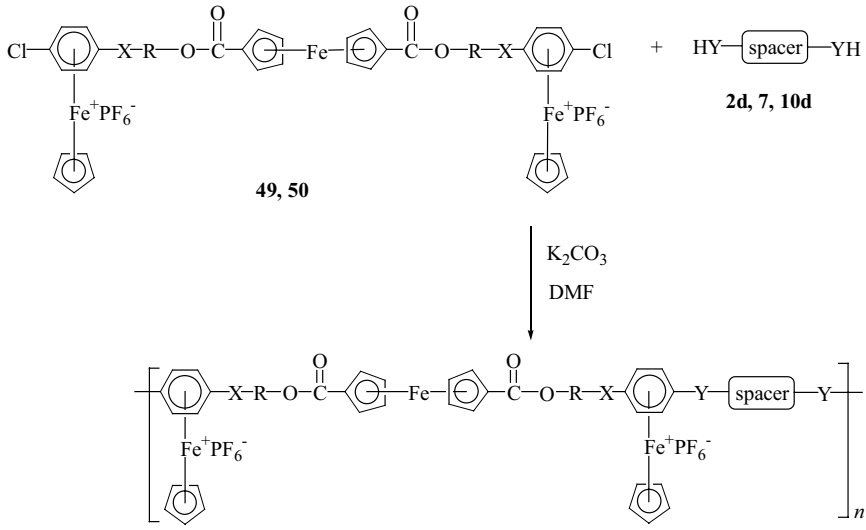

51a X=O, R=$C_6H_4CH_2$, Y-spacer-Y = $OC_6H_4C(CH_3)_2C_6H_4O$
51b X=O, R=$C_6H_4CH_2$, Y-spacer-Y =$SC_6H_4SC_6H_4S$
51c X=O, R=$C_6H_4CH_2$, Y-spacer-Y = $S(CH_2)_8S$
51d X=S, R=CH_2CH_2, Y-spacer-Y = $OC_6H_4C(CH_3)_2C_6H_4O$
51e X=S, R=CH_2CH_2, Y-spacer-Y = $SC_6H_4SC_6H_4S$
51f X=S, R=CH_2CH_2, Y-spacer-Y = $S(CH_2)_8S$

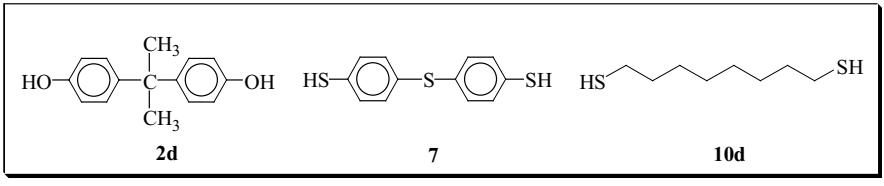

Scheme 14

Photolysis of polymers **51a–f** (Scheme 15) resulted in loss of the $CpFePF_6$ moieties, and polymers **52a–f**, containing only neutral ferrocene groups in their backbones, were isolated.[35] This methodology represents a new route to the production of ferrocene-based polymers containing aryl ether and thioether spacers.

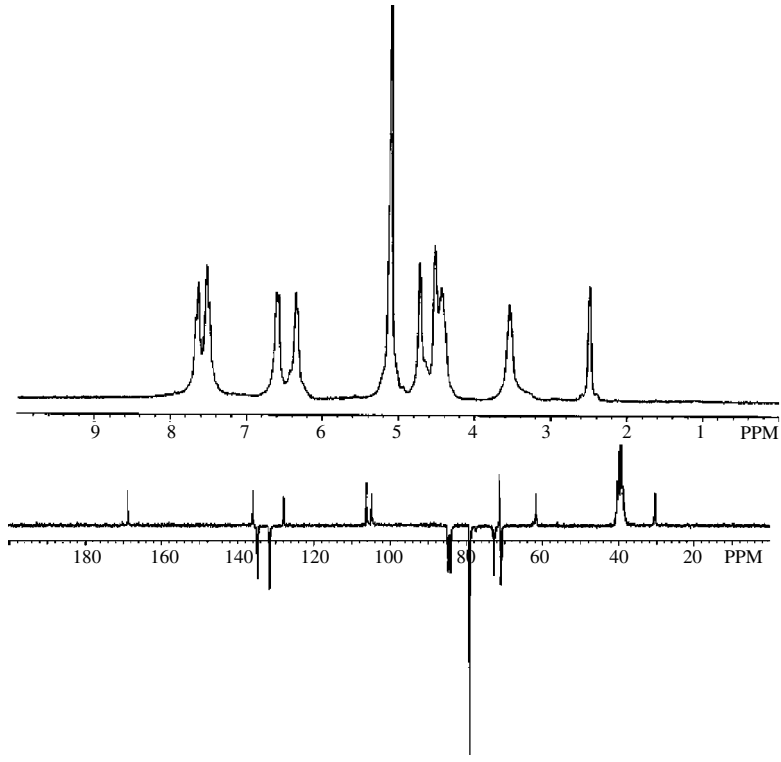

Figure 26 ^{1}H and ^{13}C NMR spectra of polymer **51e** in DMSO-d_6.

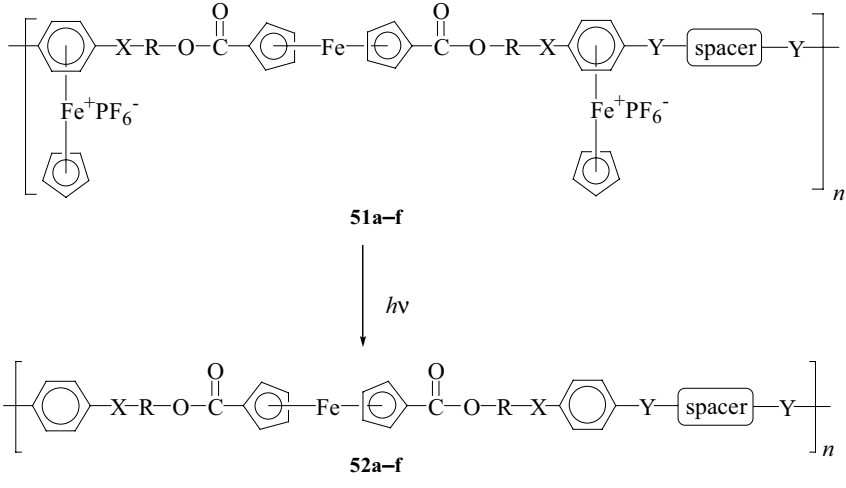

Scheme 15

^{1}H and ^{13}C NMR analysis of these polymers clearly showed that the cyclopentadienyl resonances corresponding to the cyclopentadienyliron cations were no longer present. However, the cyclopentadienyl resonances corresponding to the neutral organoiron groups were still observed. Figure 27 shows the ^{1}H and ^{13}C NMR spectra of polymer **52a**. The ferrocenyl cyclopentadienyl resonances are present at 4.24 and 4.75 ppm, and the complexed aromatic protons that were seen in polymer **51a** have shifted downfield. The peak at 5.18 ppm corresponds to the methylene protons, and the singlet at 1.63 ppm corresponds to the methyl protons. The aromatic protons appear as three sets of doublets and two singlets between 6.86 and 7.34 ppm. The ^{13}C NMR spectrum of polymer **52a** shows the methyl resonance at 30.97 ppm, and the quaternary carbons of the isopropylidene groups appear at 41.99 ppm. The methylene carbon resonance appears more downfield at 65.70 ppm because of its proximity to the ester functionality. The ferrocenyl (CH) carbons appear at 71.49 and 72.88 ppm, while the quaternary ferrocenyl carbon appears at 72.60 ppm. There are six aromatic carbons between 117.68 and 130.27 ppm, and six quaternary aromatic carbons between 130.71 and 157.94 ppm. Finally, the carbonyl carbon appears furthest downfield at 170.22 ppm.

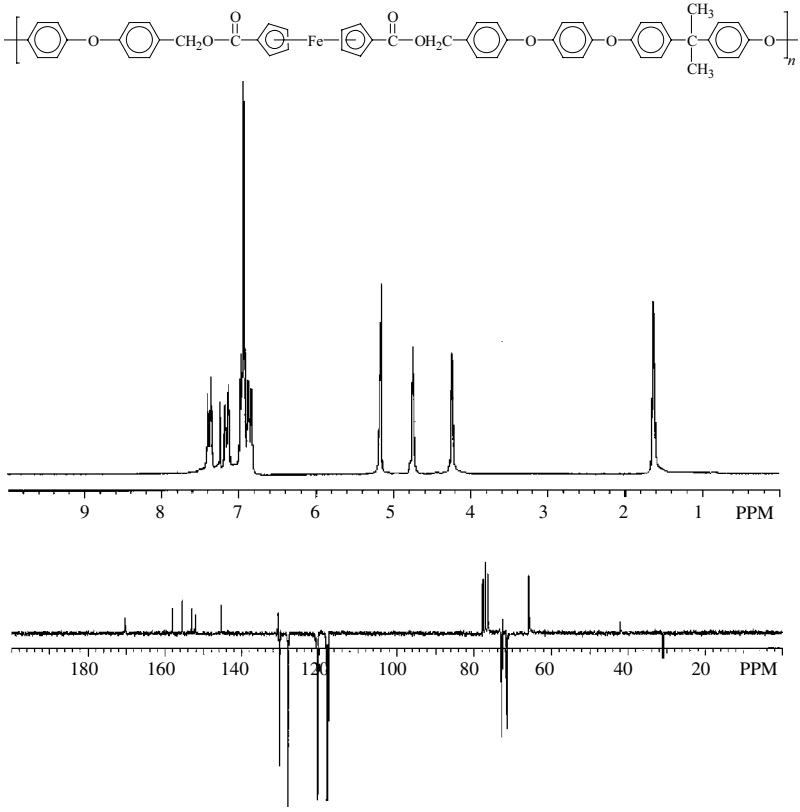

Figure 27 ^{1}H and ^{13}C NMR spectra of polymer **52a** in $CDCl_3$.

The cyclic voltammogram of polymer **51b** is shown in Figure 28. It was determined that the oxidation of the neutral iron centers occurred at $E_{1/2} = 1.03$ V. In contrast, reduction of the cationic iron centers occurred at $E_{1/2} = -1.02$ V.

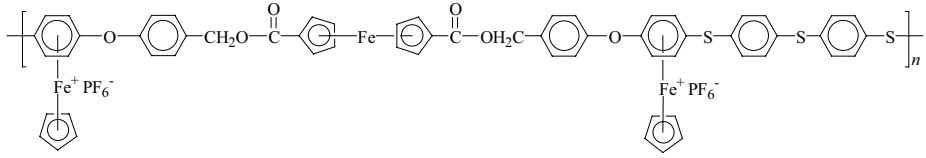

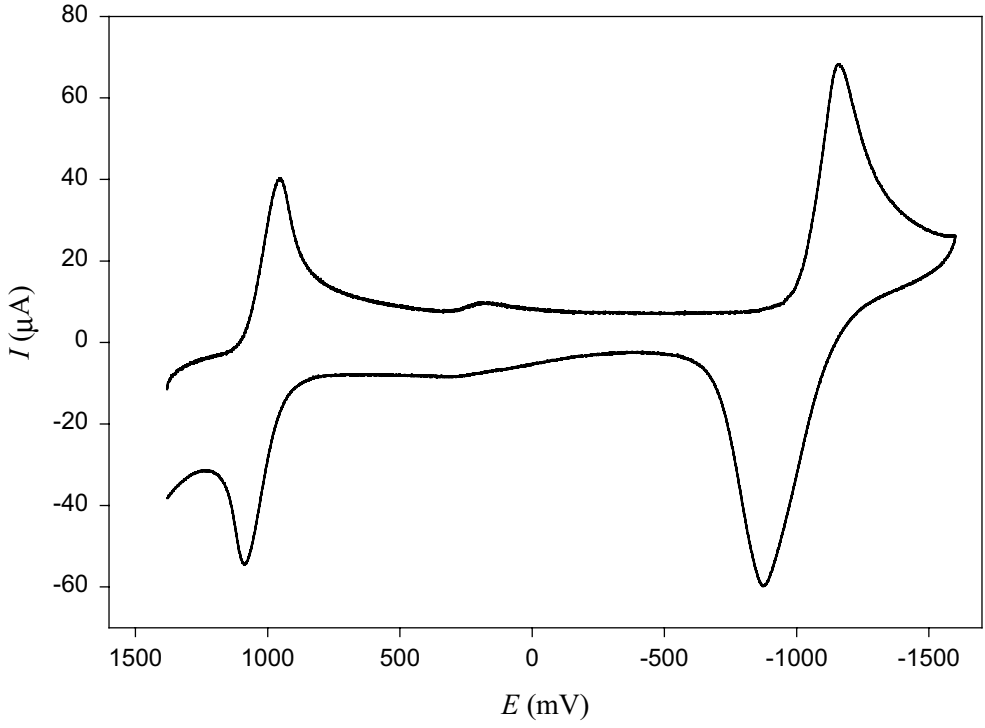

Figure 28 Cyclic voltammogram at glassy carbon of **51b** in 0.1 M TBAP in propylene carbonate, $\nu = 0.2$ V/s at -10°C.

Electrochemical analysis of the photolyzed polymers was also performed. Figure 29 shows the cyclic voltammogram of polymer **52b**, which was obtained in dichloromethane. It can be seen that oxidation of the iron centers in this polymer occurred at $E_{1/2} = 0.609$ V.

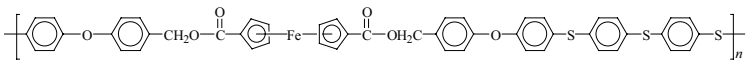

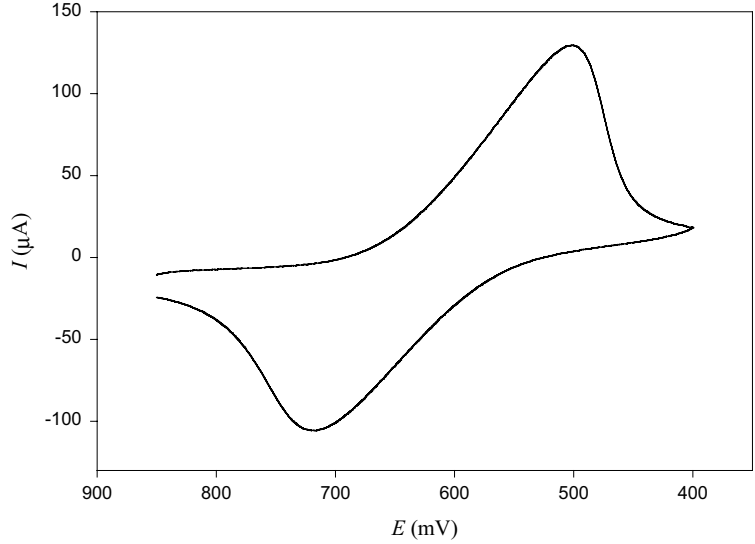

Figure 29 Cyclic voltammogram at glassy carbon of **52b** in 0.1 M TBAP in dichloromethane, $\nu = 0.1$ V/s at $-30°C$.

V. POLYMERS CONTAINING AZOBENZENE CHROMOPHORES IN THEIR SIDECHAINS

Scheme 16 shows the synthesis of azobenzene-derivatized monomers (**55a–c**) by reaction of complex **53** with the alcohol-functionalized chromophores (**54a–c**).[36] The resulting monomers were isolated in 87–90% yields. Reaction of monomers **53** or **55a–c** with dinucleophilic reagents provides a route to polymers functionalized with carboxylic acid or azobenzene groups.

It was observed that the colors of complexes **55a–c** were orange, orange-red, and red, respectively, while complex **53** is light beige-yellow. UV–Vis analysis of complexes **55a–c** showed that they absorbed at 421, 452, and 491 nm, respectively, while the wavelength maximum for complex **53** was around 273 nm.[36]

Figure 30 shows the ^{1}H and ^{13}C NMR spectra of complex **55b**. The methyl protons of the *N*-ethyl chain appear as a triplet at 1.23 ppm, while the adjacent methylene protons appear as a quartet at 3.59 ppm. The methyl of the acetyl group appears as a singlet at 2.61 ppm, while the protons of the methyl group adjacent to the quaternary aliphatic carbon resonates as a singlet at 1.67 ppm. The other methylene resonances in this complex appear at 2.14, 2.46, 3.79, and 4.33 ppm. The cyclopentadienyl protons resonate as a singlet at 5.32 ppm, while the complexed aromatic protons appear as two sets of doublets at 6.42 and 6.74 ppm. The uncomplexed aromatic protons appear as six sets of doublets between 6.96 and 8.09 ppm. The doublet furthest upfield

corresponds to the aromatic protons alpha to the *N,N*-dialkyl group, while the doublet resonating furthest downfield is assigned to the protons alpha to the acetyl group.

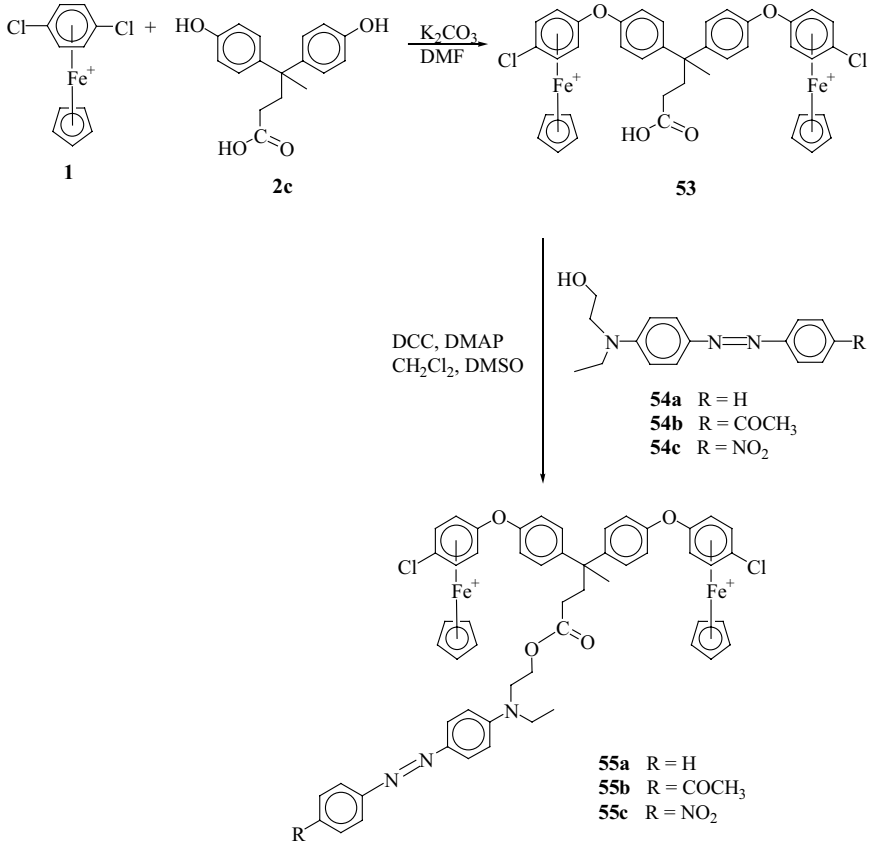

Scheme 16

The ^{13}C NMR spectrum of complex **55b** shows three methyl resonances at 12.31, 26.83, and 27.72 ppm; five methylene resonances at 30.67, 37.02, 46.16, 48.96, and 62.29 ppm; and a quaternary aliphatic carbon at 45.50 ppm. The cyclopentadienyl carbons appear at 80.31 ppm and the complexed aromatic carbons resonate at 76.86, 87.66, 104.70, and 133.73 ppm. There are six aromatic CH carbons resonating between 112.36 and 130.50 ppm and six quaternary aromatic carbons observed between 137.91 and 156.30 ppm. Finally, the carbonyl resonances can be seen at 173.50 and 197.34 ppm.

Initial polymerization studies were performed using monomer **53** containing the pendent carboxylic acid group with dinucleophiles **2d**, **7**, and **10d** as shown in Scheme 17. The resulting polymers (**56a–c**) exhibited good solubility in polar aprotic solvents such as DMF and DMSO. These polymers were also soluble in aqueous solutions of sodium hydroxide.

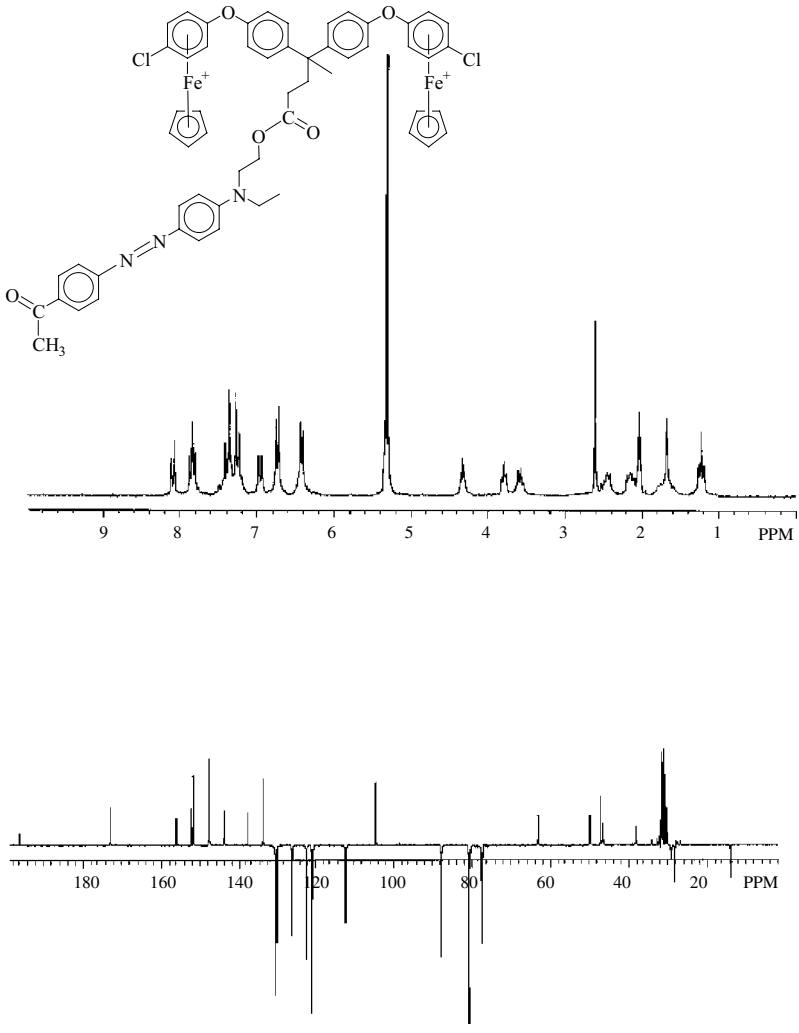

Figure 30 ^{1}H and ^{13}C NMR spectra of complex **55b** in acetone-d_6.

Figure 31 shows the ^{1}H NMR spectrum of polymer **56c**. The methyl protons appear at 1.66 ppm, and the methylene protons in the polymer backbone resonate at 1.34, 1.56, and 3.34 ppm as broad singlets. The methylene protons in the polymer sidechain appear as broad singlets at 2.06 and 2.40 ppm. The cyclopentadienyl protons appear as a singlet at 5.12 ppm, indicating that the polymerization reaction was successful. The complexed aromatic protons of this polymer appear as two sets of doublets at 6.31 and 6.41 ppm. Finally, the uncomplexed aromatic protons appear as two broad doublets at 7.25 and 7.37 ppm.

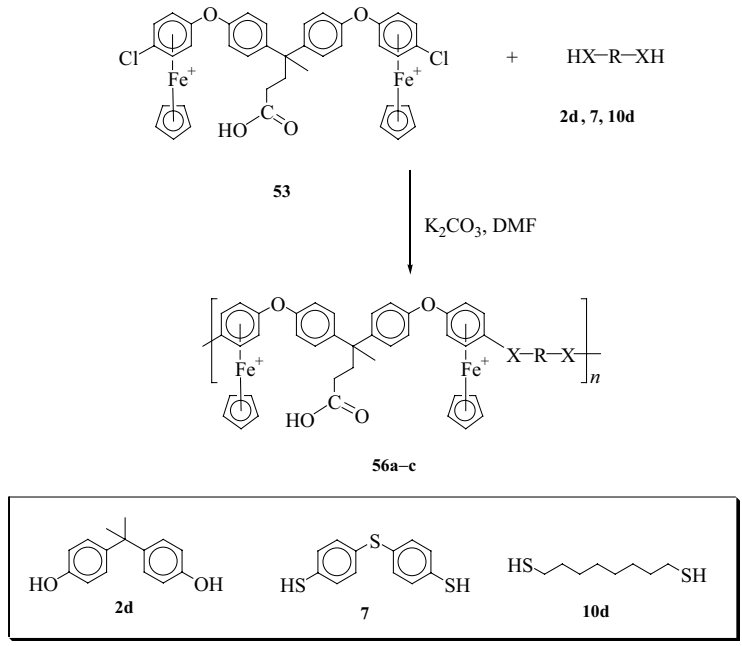

Scheme 17

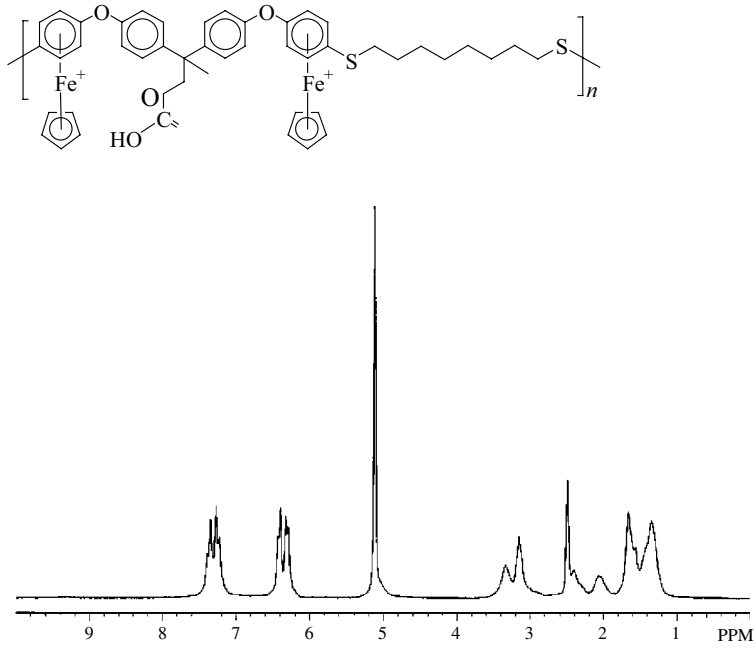

Figure 31 ^{1}H NMR spectrum of polymer **56c** in DMSO-d_6.

The azobenzene-functionalized complexes **55a–c** (Scheme 18) were also reacted with nucleophiles **2d**, **7**, and **10**, resulting in the isolation of polymers **57a–c**, **58a–c,** and **59a–c** in excellent yields.[36] These cyclopentadienyliron-coordinated polyaromatic ethers or ether/thioethers containing azobenzene chromophores in their sidechains displayed fair to excellent solubility in polar organic solvents such as DMF, DMSO, and acetonitrile. The polymers prepared using bisphenol A (**2d**) possessed the highest solubility, while polymers prepared with 4,4′-thio-*bis*-benzenethiol (**7**) and 1,8-octanedithiol (**10d**) often formed gels.

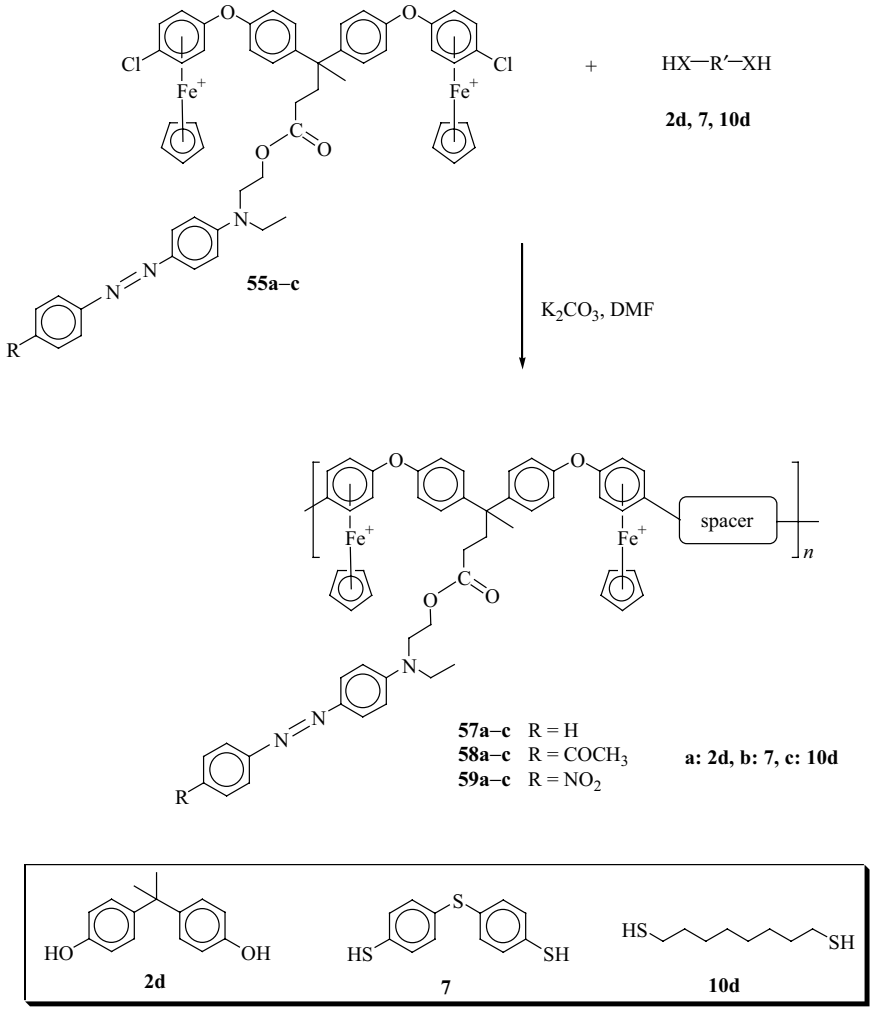

Scheme 18

Polymers **57a–c**, **58a–c**, and **59a–c** were demetallated using photolytic techniques to give polymers **60a–c**, **61a–c**, and **62a–c** in moderate yields (Scheme 19).

The molecular weights of the organic polymers were determined using gel permeation chromatography. The weight-average molecular weights of these polymers (**60a–c**, **61a–c**, **62a–c**) were estimated to range from 8400 to 20,500, with polydispersities ranging from 1.16 to 2.64. It is important to note that the molecular weights of these polymers were limited by their poor solubilities in many cases. From the GPC values obtained from **57a–c**, **58a–c**, and **59a–c**, the molecular weights of the corresponding organoiron polymers were estimated to range from 13,400 to 31,600.

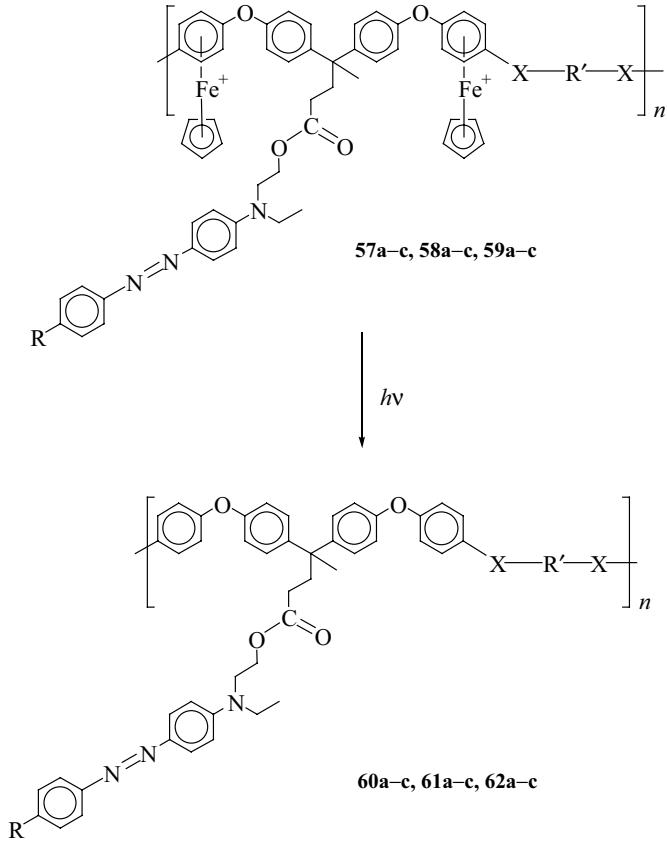

Scheme 19

The thermal properties of the carboxylic acid-functionalized polymers were compared with the azo-functionalized polymers in order to examine the effects of the azobenzene sidechains. In addition, a comparison of the thermal properties of the metallated and demetallated azo-functionalized polymers could provide information on the influence of the cyclopentadienyliron moieties on these materials. Thermal analysis of these polymers was performed using thermogravimetric analysis and differential scanning calorimetry.

Thermogravimetric analysis of all the metallated polymers showed weight losses between 220 and 240°C, indicative of cleavage of the $CpFe^+$ moieties pendent to their backbones. The azo dye-functionalized polymers underwent secondary weight losses between 250 and 290°C, which were attributed to decomposition of the polymer side chains; however, these weight losses were not always distinct, and overlapped with other weight losses. Further decomposition steps were observed starting around 420–460°C in the azo-functionalized polymers. The carboxylic acid functionalized polymers experienced only two weight losses: the first due to decomposition of the organoiron groups and the second, to polymer decomposition.

Differential scanning calorimetry was utilized to determine the glass transition temperatures of the organometallic and organic polymers. In general, the metallated polymers exhibited much higher glass transition temperatures than did the organic polymers. The polymers with aromatic spacers in their backbones possessed higher T_g values than did polymers incorporating aliphatic spacers in their backbones, in both their metallated and demetallated states. The glass transition temperatures of the carboxylic acid substituted polymers were generally higher than those of their azo-substituted analogs for the polymers with aromatic backbones. Figure 32 shows the DSC thermogram of polymer **56c**. The T_g of this polymer occurred at 123°C, compared to 203 and 195°C for polymers **56a** and **56b**, respectively.

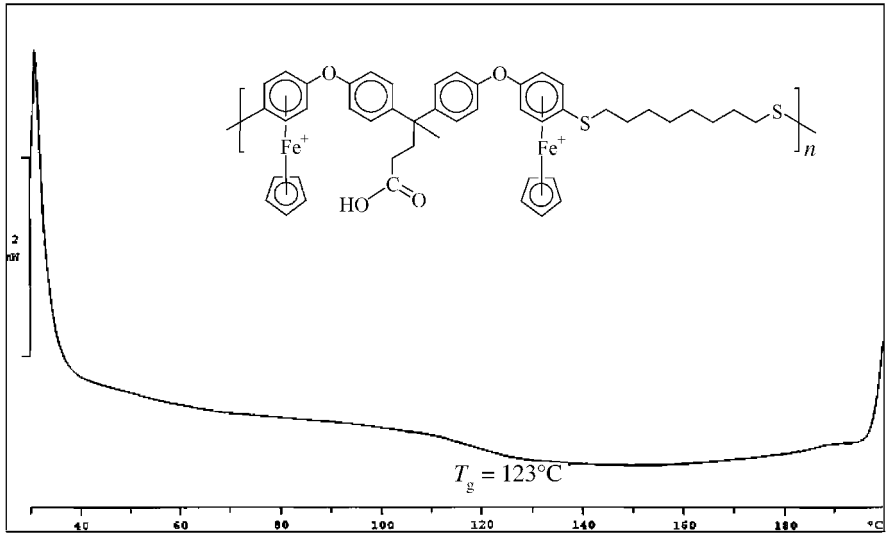

Figure 32 DSC trace of polymer **56c**.

Figure 33 shows the thermogram of organoiron polymer **57c**, which has the same organic backbone as **56c**, but incorporates azobenzene units in its sidechains. The T_g of **57c** occurs at 114°C. On demetallation, the T_g values of the organic

polymers were much lower than their organoiron counterparts. For example, polymer **60c** had a T_g at 59°C, and the thermogram of this polymer is shown in Figure 34. The glass transition temperatures of the organic polymers with aryl ether spacers occurred between 111 and 123°C, while the polymers with alternating aryl ether and thioether spacers occurred between 101 and 115°C.

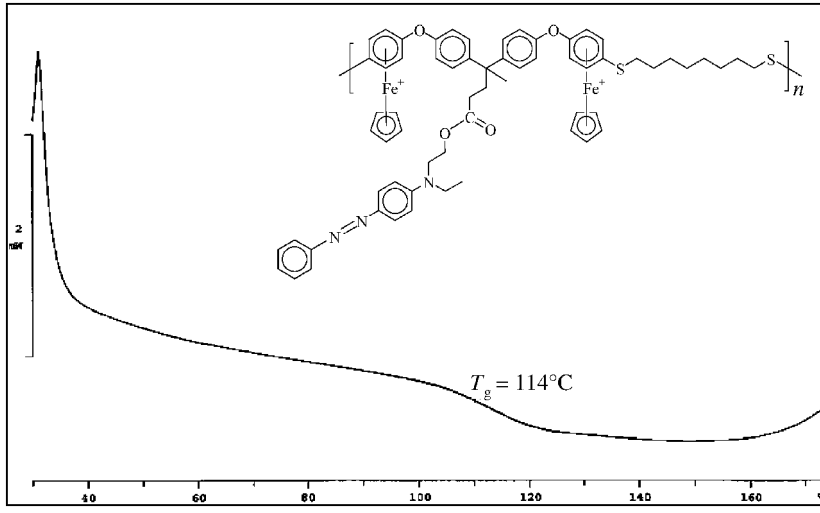

Figure 33 DSC trace of polymer **57c**.

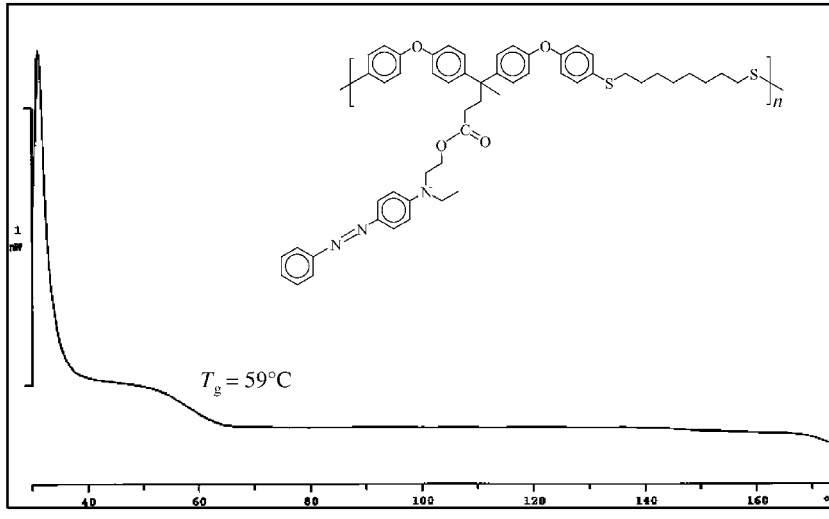

Figure 34 DSC trace of polymer **60c**.

VI. CONCLUSIONS

The use of arene cyclopentadienyliron complexes in monomer and polymer synthesis was described. Chloroarene complexes undergo facile nucleophilic aromatic substitution reactions with *bis*-phenols and *bis*-thiols to produce polymers with ether and thioether spacers in their backbones. This represents an alternative route to the synthesis of polyaromatic ethers and thioethers using mild reaction conditions. An added benefit to utilizing this metal-mediated methodology is that the resulting organometallic polymers displayed good solubility in polar organic solvents such as acetone, dichloromethane, acetonitrile, dimethylformamide, and dimethyl sulfoxide. In contrast, on removal of the metallic moieties pendent to the polymer backbones using photolytic means, many of the resulting organic polymers were insoluble in common organic solvents.

By altering the nature of the spacers in the polymer backbones, it was possible to alter the thermal properties of these materials. It was found in all studies that the glass transition temperatures of polymers with aromatic backbones were higher than those of polymers with aliphatic spacers in their backbones. It was also determined that ether linkages resulted in higher glass transition temperatures than did thioether linkages. The glass transition temperatures of cyclopentadienyliron-coordinated polymers were also examined for some of the classes of polymers. These organometallic complexes increased the T_g values of polyethers and thioethers significantly. All polymers displayed good thermal stability following degradation of the organometallic moieties pendent to the polymer backbones. However, the incorporation of azobenzene groups in the sidechains of polyethers and thioethers decreased their thermal stability. It was also noted that these polymers were bright orange or red compared to other classes of organoiron polymers that were beige, yellow or light orange.

The electrochemical properties of the cyclopentadienyliron-coordinated polymers were examined using cyclic voltammetry. These polymers underwent reversible reduction processes from 18-electron species to 19-electron species. It was also possible to effect a second reduction step for some of these organometallic polymers, resulting in the formation of anionic 20-electron species. By incorporating neutral ferrocene moieties into the backbones of polyethers and thioethers, it was also possible to oxidize these polymers. Polymers containing cationic cyclopentadienyliron moieties pendent to their backbones and neutral cyclopentadienyliron moieties within their backbones were found to undergo independent redox processes. Following cleavage of the cyclopentadienyliron cations from these polymers, the electrochemical oxidation of the neutral iron centers in these polymers was examined.

VII. REFERENCES

1. R. J. Cotter, *Engineering Plastics: A Handbook of Polyarylethers*, Gordon and Breach, New York, 1995.
2. J. R. Fried, *Polymer Science and Technology*, Prentice-Hall PTR, Englewood Cliffs, NJ, 1995.

3. L. C. Lopez, G. L. Wilkes, *J. Macromol. Sci., Rev. Macromol. Chem. Phys.* **C29,** 83 (1989).
4. R. D. Pike, D. A. Sweigart, *Coord. Chem. Rev.* **187,** 183 (1999).
5. A. S. Abd-El-Aziz, S. Bernardin, *Coord. Chem. Rev.* **203,** 219 (2000).
6. A. S. Abd-El-Aziz, C. R. de Denus, M. J. Zaworotko, L. R. MacGillivray, *J. Chem. Soc. Dalton Trans.* 3375 (1995).
7. A. J. Pearson, A. M. Gelormini, *J. Org. Chem.* **59,** 4561 (1994).
8. A. S. Abd-El-Aziz, K. M. Epp, C. R. de Denus, G. Fisher-Smith, *Organometallics* **13,** 2299 (1994).
9. A. S. Abd-El-Aziz, *Coord. Chem. Rev.* **233–234,** 177 (2002).
10. A. S. Abd-El-Aziz, C. R. de Denus, M. J. Zaworotko, C. V. K. Sharma, *Chem. Commun.* 265 (1998).
11. A. J. Pearson, A. M. Gelormini, M. A. Fox, D. Watkins, *J. Org. Chem.* **61,** 1297 (1996).
12. A. J. Pearson, A. M. Gelormini, *Macromolecules* **27,** 3675 (1994).
13. A. S. Abd-El-Aziz, C. R. de Denus, E. K. Todd, S. A. Bernardin, *Macromolecules* **13,** 5000 (2000).
14. A. S. Abd-El-Aziz, A. L. Edel, K. M. Epp, H. M. Hutton, *New J. Chem.* **23,** 569 (1999).
15. A. S. Abd-El-Aziz, A. L. Edel, L. J. May, K. M. Epp, H. M. Hutton, *Can. J. Chem.* **77,** 1797 (1999).
16. A. S. Abd-El-Aziz, L. J. May, A. L. Edel, *Macromol. Rapid Commun.* **21,** 598 (2000).
17. J. -I. Jin, R. Kim, *Polym. J.* **19,** 977 (1987).
18. A. A. Dembek, R. R. Burch, A. E. Feiring, *J. Am. Chem. Soc.* **115,** 2087 (1993).
19. M. E. Wright, *Macromolecules* **22,** 3256 (1989).
20. M. E. Wright, L. Lawson, R. T. Baker, D. C. Roe, *Polyhedron* **11,** 323 (1992).
21. M. E. Wright, C. K. Lowe-Ma, *Inorg. Chim. Acta* **232,** 223 (1995).
22. R. Atencio, L. Brammer, S. Fang, F. C. Pigge, *New J. Chem.* **23,** 461 (1999).
23. L. Brammer, J. C. Mareque Rivas, R. Atencio, S. Fang, F. C. Pigge, *J. Chem. Soc., Dalton Trans.* 3855 (2000).
24. Y. Morisaki, H. Chen, Y. Chujo, *Polym. Bull.* **48,** 243 (2002).
25. S. I. Yaniger, D. J. Rose, W. P. McKenna, E. M. Eyring, *Macromolecules* **17,** 2579 (1984).
26. H. Nishihara, H. Funaki, T. Shimura, K. Aramaki, *Synth. Met.* **55–57,** 942 (1993).
27. S. I. Yaniger, D. J. Rose, W. P. McKenna, E. M. Eyring, *Appl. Spectrosc.* **38,** 7 (1984).
28. H. Funaki, K. Aramaki, H. Nishihara, *Chem. Lett.* 2065 (1992).
29. H. Funaki, K. Aramaki, H. Nishihara, *Synth. Met.* **74,** 59 (1995).
30. A. S. Abd-El-Aziz, T. H. Afifi, E. K. Todd, G. Z. Ma, *Polym. Prepr. Am. Chem. Soc., Div. Polym. Chem.* **42**(2), 450 (2001).
31. A. S. Abd-El-Aziz, E. K. Todd, K. M. Epp, *J. Inorg. Organomet. Polym.* **8,** 127 (1998).
32. A. S. Abd-El-Aziz, E. K. Todd, G. Z. Ma, *J. Polym. Sci., Part A, Polym. Chem.* **39,** 1216 (2001).
33. A. S. Abd-El-Aziz, E. K. Todd, T. Afifi, *Polym. Prepr., Am. Chem. Soc., Div. Polym. Chem.* **42**(2), 597 (2001).
34. A. S. Abd-El-Aziz, E. K. Todd, T. H. Afifi, *Macromol. Rapid Commun.* **23,** 113 (2002).
35. A. S. Abd-El-Aziz, E. K. Todd, R. M. Okasha, T. E. Wood, *Macromol. Rapid Commun.* **23,** 743 (2002).
36. A. S. Abd-El-Aziz, T. Afifi, W. Budakowski, K. Friesen, E. K. Todd, *Macromolecules* **35,** 8929 (2002).
37. A. S. Abd-El-Aziz, E. K. Todd, *Polym. Mater., Sci. Eng.* **86,** 103 (2002).
38. A. S. Abd-El-Aziz, R. M. Okasha, J. Hurd, E. K. Todd, *Polym. Mater., Sci. Eng.* **86,** 91 (2002).

39. C. R. de Denus, L. M. Hoffa, E. K. Todd, A. S. Abd-El-Aziz, *J. Inorg. Organomet. Polym.* **10,** 189 (2000).
40. A. A. Dembek, P. J. Fagan, M. Marsi, *Macromolecules* **26,** 2292 (1993).
41. A. A. Dembek, P. J. Fagan, M. Marsi, *Polym. Mater. Sci. Eng.* **71,** 158 (1994).
42. J. A. Segal, *J. Chem. Soc. Chem. Commun.* 1338 (1985).
43. Unpublished results.
44. D. Astruc, *Electron Transfer and Radical Processes in Transition-Metal Chemistry*, VCH, New York, 1995.
45. A. S. Abd-El-Aziz, C. R. de Denus, K. M. Epp, S. Smith, R. J. Jaegr, D. T. Pierce, *Can. J. Chem.* **74,** 650 (1996).
46. A. S. Abd-El-Aziz, K. Winkler, A. S. Baranski, *Inorg. Chim. Acta* **194,** 207 (1992).
47. D. Astruc, F. Chardac, *Chem. Rev.* **101,** 2991 (2001).
48. C. Valerio, S. Rigaut, J. Ruiz, J. -L. Fillaut, M. -H. Delville, D. Astruc, *Bull. Pol. Acad. Sci.* **46,** 309 (1998).
49. I. Cuadrado, M. Moran, C. M. Casado, B. Alonso, J. Losada, *Coord. Chem. Rev.* **193–195,** 395 (1999).
50. M. A. Hearshaw, A. T. Hutton, J. R. Moss, K. J. Naidoo, *Advances in Dendritic Macromolecules*, G. R. Newkome, ed., JAI Press, Greenwhich, CT, 1999, Vol. 4, p. 1.
51. F. Lobete, I. Cuadrado, C. M. Casado, B. Alonso, M. Morán, J. Losada, *J. Organomet. Chem.* **509,** 109 (1996).
52. S. Rigaut, M. -H. Delville, D. Astruc, *J. Am. Chem. Soc.* **119,** 11132 (1997).
53. F. Moulines, L. Djakovitch, R. Boese, B. Gloaguen, W. Thiel, J. -L. Fillaut, M. -H. Delville, D. Astruc, *Angew. Chem. Int. Ed. Engl.* **32,** 1075 (1993).
54. H. A. Trujillo, C. M. Casado, J. Ruiz, D. Astruc, *J. Am. Chem. Soc.* **121,** 5674 (1999).
55. C. Valério, F. Moulines, J. Ruiz, J. -C. Blais, D. Astruc, *J. Org. Chem.* **65,** 1996 (2000).
56. V. Sartor, S. Nlate, J. -L. Fillaut, L. Djakovitch, F. Moulines, V. Marvaud, F. Neveu, J. -C. Blais, J. -F. Letard, D. Astruc, *New J. Chem.* **24,** 351 (2000).
57. J. W. Kriesel, S. Konig, M. A. Freitas, A. G. Marshall, J. A. Leary, T. D. Tilley, *J. Am. Chem. Soc.* **120,** 12207 (1998).

CHAPTER 11

Polymerization of Olefinic Monomers Functionalized with Cationic Cyclopentadienyliron Arene Complexes

Alaa S. Abd-El-Aziz,* Erin K. Todd, and Rawda M. Okasha

Department of Chemistry, The University of Winnipeg, Winnipeg, Manitoba, Canada

CONTENTS

Macromolecules Containing Metal and Metal-like Elements, Volume 2: Organoiron Polymers, Edited By Alaa S. Abd-El-Aziz, Charles E. Carraher, Jr., Charles U. Pittman, Jr., John E. Sheats, and Martel Zeldin
ISBN 0-471-45078-2

I. INTRODUCTION

In 1955, Arimoto and Haven reported the first example of an organoiron polymer via the radical-initiated polymerization of vinylferrocene.[1] Since that time there have been numerous studies outlining the polymerization of olefins substituted with organoiron complexes.[2–13] In the 1970s, Pittman and coworkers reported that a number of olefin monomers functionalized with the ferrocene group could be copolymerized with organic monomers such as styrene, methyl methacrylate, *N*-vinylpyrrolidone, and acrylonitrile.[8–13] More recently, Schrock and coworkers described the ring-opening metathesis polymerization (ROMP) of norbornenes functionalized with ferrocenyl groups.[14,15] While ferrocene-based systems are by far the most prevalent, there have also been a number of studies outlining the olefin polymerization of other classes of organoiron monomers. For example, Mapolie and coworkers have reported the polymerization of a monomer containing a cyclopentadienyliron dicarbonyl complex with an iron–carbon σ bond.[16] The homo- and copolymerization of π-(2,4-hexadienyl acrylate)tricarbonyliron has also been reported.[17,18]

Since the mid-1990s, arene complexes of cyclopentadienyliron have emerged as efficient precursors to functionalized materials.[19–26] Many of our studies in this area involved the metal-mediated nucleophilic aromatic substitution polymerization of dichloroarene complexes with dinucleophiles.[19–23] The cyclopentadienyliron moieties have also been cleaved from the polymer backbones to yield the corresponding organic polymers using techniques such as photolysis, pyrolysis, and electrolysis. The cyclopentadienyliron-coordinated materials possessed enhanced solubility relative to their organic analogs and good thermal stability.[20] Novel monomers have also been synthesized using the electron-withdrawing power of the cyclopentadienyliron moiety.[27–30] Polymethacrylates containing CpFe cations in their sidechains were the first class of organoiron polymers that we prepared via olefin polymerization.[31] We have subsequently investigated the radical polymerization of styrene monomers functionalized with arenes π-coordinated to cyclopentadienyliron cations.[31,32] We have also reported that cyclopentadienyliron complexes of chloroarenes can be utilized to prepare aromatic and aliphatic ether-functionalized norbornene monomers.[28–30,33,34] In our initial studies of these materials, the cationic organoiron complexes were cleaved

from the monomers prior to polymerization.[28–30] However, we have reported that cationic organoiron norbornenes also undergo ROMP to produce organoiron polynorbornenes.[33,34] In this chapter we review some of the results obtained on the polymerization of cyclopentadienyliron complexes functionalized with olefins.

II. METHACRYLATES

A. Radical Polymerization of the Methacrylate Groups

Our interest in the design of aryl ether and thioether monomers and polymers using arene cyclopentadienyliron complexes prompted our investigation into the synthesis of methacrylate monomers functionalized with aryl ether groups.[31] Initially, two complexes with terminal carboxylic acid groups were synthesized so that they could undergo reaction with a methacrylate monomer containing a terminal hydroxyl group. Scheme 1 shows the synthesis of complexes **3a** and **3b** via reaction of complexes **1a** and **1b** with **2**, followed by decomposition of the imine groups with HCl. The resulting aldehyde complexes (**3a** and **3b**) were subsequently oxidized with chromium trioxide and sulfuric acid to produce complexes **4a** and **4b**. Reaction of these carboxylic acids with thionyl chloride produced the corresponding acid chloride complexes, which were reacted in situ with 2-hydroxyethyl methacrylate (**5**), to produce the methacrylate organoiron monomers **6a** and **6b** in 92 and 89% yields, respectively.

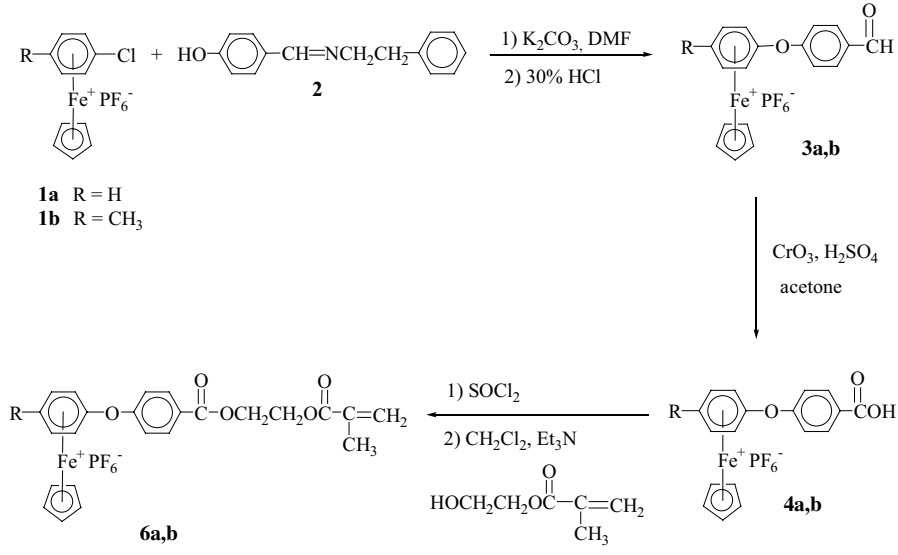

Scheme 1

NMR analysis of the monomers confirmed that the condensation reactions between the carboxylic acid-functionalized complexes and 2-hydroxyethyl methacrylate were successful. Figure 1 shows the ^{1}H NMR spectrum of monomer **6b**. The singlet at 1.91 ppm corresponds to the protons of the methyl group attached to the olefinic carbon, while the singlet at 2.51 ppm corresponds to the methyl protons on the complexed aromatic ring. The multiplets at 4.52 and 4.62 ppm are assigned as the methylene protons. The singlet at 5.25 corresponds to the cyclopentadienyl resonance, and the multiplet at 6.44 ppm corresponds to the four complexed aromatic protons. The two singlets at 5.65 and 6.09 ppm are the olefinic protons, and the doublets at 7.42 and 8.15 ppm correspond to the uncomplexed aromatic protons.

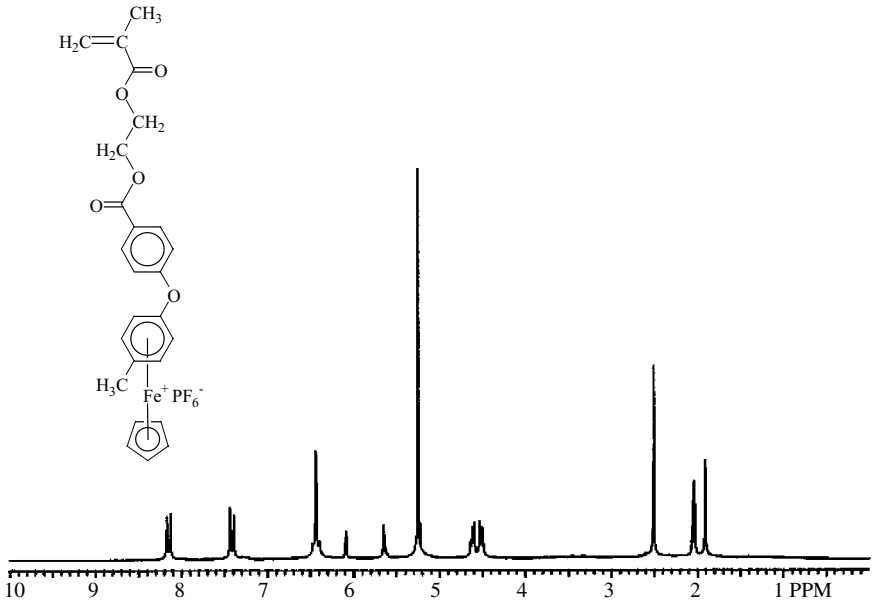

Figure 1 ^{1}H NMR spectrum of monomer **6b** in acetone-d_6.

Polymerization of monomers **6a** and **6b** was accomplished using the radical initiator 2,2′-azo-*bis*(2-methylpropionitrile) (AIBN). Scheme 2 shows these polymerization reactions, which allowed for the production of polymethacrylates **7a** and **7b**. The polymerization reactions were conducted in refluxing acetone for 24 hours, and then poured into a water/methanol solution. The resulting polymethacrylates with organoiron sidechains were isolated in good yields as yellow solids. On the basis of interactions between the cationic iron complexes and GPC columns, the molecular weights of the polymethacrylates were determined following cleavage of the cyclopentadienyliron moieties from the polymer sidechains. Polymers **7a** and **7b** were subjected to photolytic demetallation, resulting in the isolation of the organic polymethacrylates **8a** and **8b**.

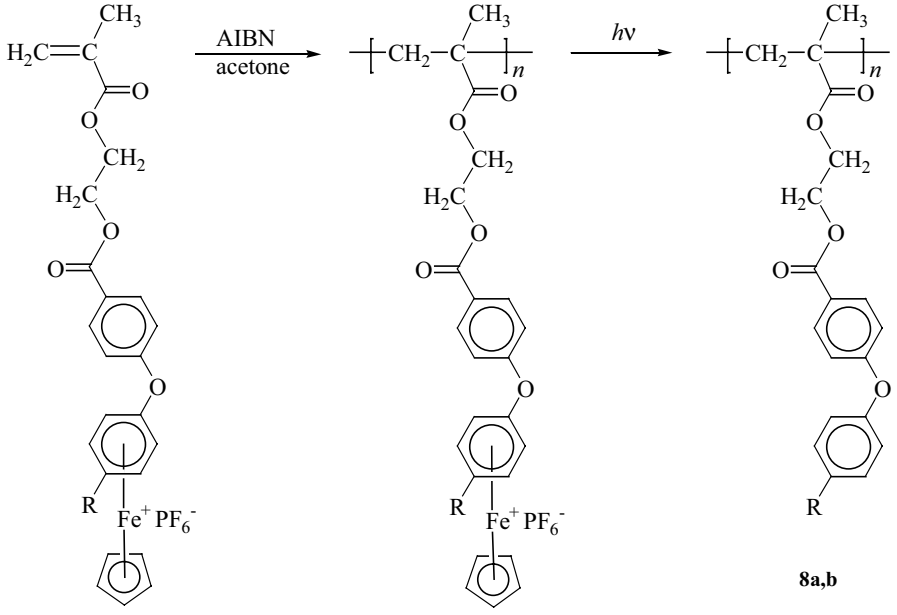

6a,b **7a,b** **8a,b**

Scheme 2

NMR analysis of the polymethacrylates was very useful in determining the success of the polymerization reactions. The loss of the olefinic resonances in the ^{1}H and ^{13}C NMR spectra and the appearance of new peaks further upfield were indicative of the spectra of these polymers. The ^{1}H NMR spectrum of polymer **7b** is shown in Figure 2a. It can be seen that the olefinic resonances are no longer present at 5.65 and 6.09 ppm; however, there are broad peaks between 0.53 and 1.90 ppm that correspond to the methylene protons in the polymer backbone and the methyl protons attached to the polymer backbone. The methyl on the complexed aromatic ring appears as a singlet at 2.47 ppm, while the methylene protons in the polymer sidechains appear at 4.32 and 4.55 ppm as broad singlets. The cyclopentadienyl protons appear as a singlet at 5.18 ppm, while the complexed aromatic protons resonate at 6.36 ppm. The uncomplexed aromatic protons appear as broad singlets at 7.37 and 8.07 ppm. The ^{1}H NMR spectrum of polymer **8b** (Fig. 2b) shows that the cyclopentadienyliron moieties were cleaved from the polymer backbones. Also, on demetallation, the complexed aromatic protons shifted downfield.

The polymethacrylates with aryl ether sidechains coordinated to cyclopentadienyliron moieties (**7a** and **7b**) were investigated using thermogravimetric analysis.[35] Both of these polymers showed two weight loss steps in their thermograms. The first weight losses, between 218 and 248°C, corresponded to loss of the cyclopentadienyliron moieties, while the second weight losses corresponded to degradation of the polymer backbones. The polymethacrylate backbones were stable until ~320°C,

at which point the polymers underwent a 40% weight loss. Figure 3 shows the TGA thermogram of polymer **7b**. Thermal analysis of the demetallated polymethacrylates (**8a** and **8b**) was performed using thermogravimetric analysis and differential scanning calorimetry. These polymers experienced weight losses beginning starting between 314 and 347°C accounting for between 62 and 76% of the polymers' masses. Differential scanning calorimetry of **8a** and **8b** showed that they have glass transition temperatures at 64 and 71°C, respectively.

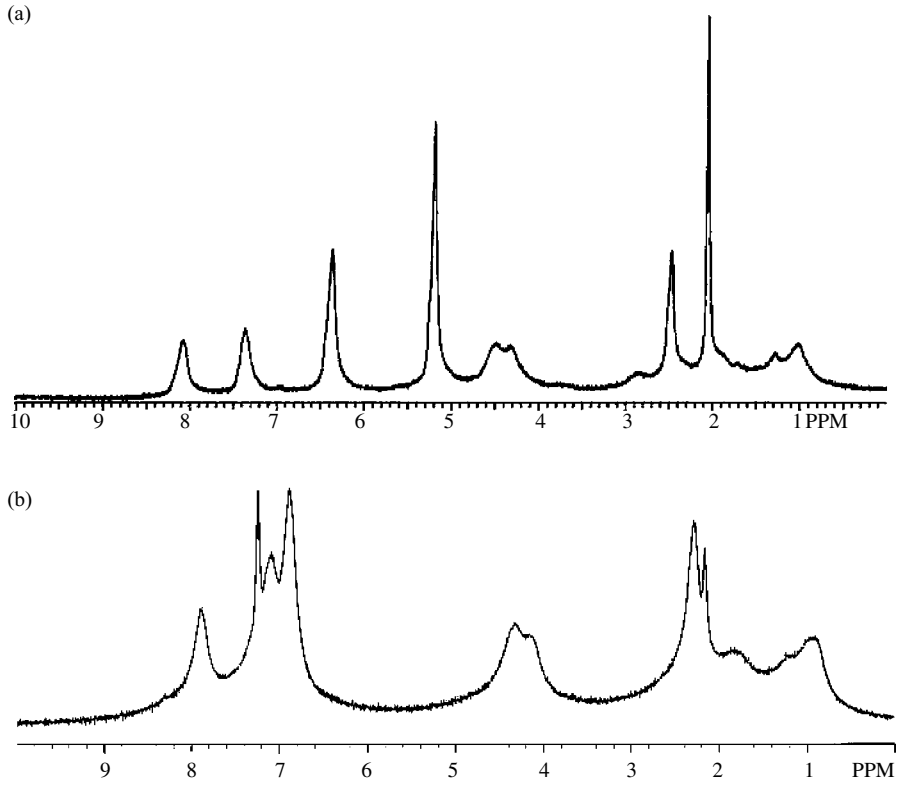

Figure 2 (a) ^{1}H NMR spectrum of metallated polymethacrylate 7b in acetone-d_6; (b) ^{1}H NMR spectrum of organic polymethacrylate **8b** in $CDCl_3$.

The molecular weights of the organic polymethacrylates were determined using gel permeation chromatography. A calculation was performed in order to determine the molecular weights of their corresponding organoiron polymers. While polymer **8a** has a weight average molecular weight of 17,800, its metallated analog (**7a**) would have had a M_w of 32,300. Similarly, the weight-average molecular weight of polymer **8b** is 48,500, which corresponds to a M_w of 86,400 for its metallated analog (**7b**). The degrees of polymerization for these polymers were calculated to be 55 and 143, respectively.

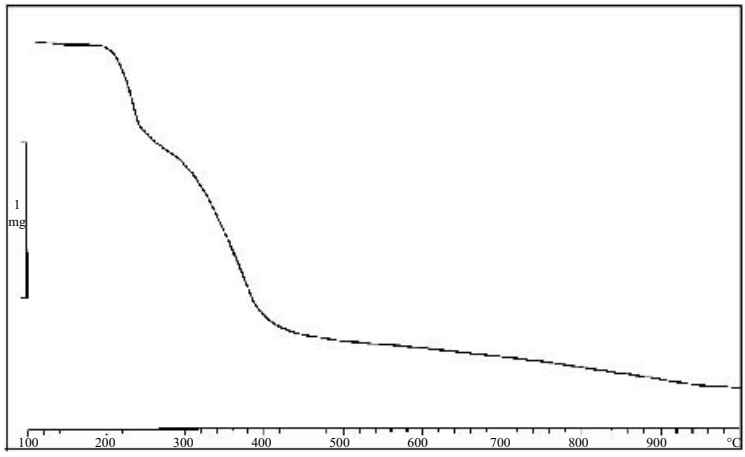

Figure 3 TGA thermogram of metallated polymethacrylate **7b**.

The electrochemical properties of the polymethacrylates containing organoiron groups in their sidechains were examined using cyclic voltammetry.[35] Figure 4 shows the cyclic voltammogram of polymer **7b** obtained at −50°C with a scan rate of 1 V/s. There are two reduction steps that can be observed in this polymer. The first reduction ($E_{1/2}$ = −1.24 V) corresponds to reduction of the 18-electron cationic iron centers to neutral 19-electron species. The second reduction step ($E_{1/2}$ = −1.94 V) corresponds to the reversible formation of the anionic 20-electron iron complexes.

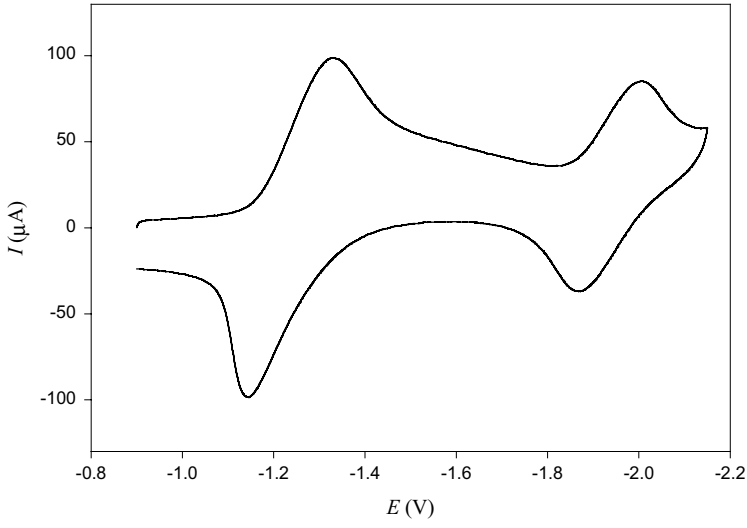

Figure 4 Cyclic voltammogram of polymer **7b** in DMF at −50°C obtained with a scan rate of 1 V/s.

The design of diiron complexes functionalized with methacrylate units was also achieved using complex **9**. The synthesis of complex **9** was previously reported by the reaction of the 1,4-dichlorobenzene complex of cyclopentadienyliron with 4,4-*bis*(4-hydroxyphenyl)valeric acid.[36] Scheme 3 shows the synthesis of monomer **11** via condensation of an acid chloride complex (**10**) with 2-hydroxyethyl methacrylate (**5**). Monomer **11** was isolated as a yellow precipitate in excellent yield.

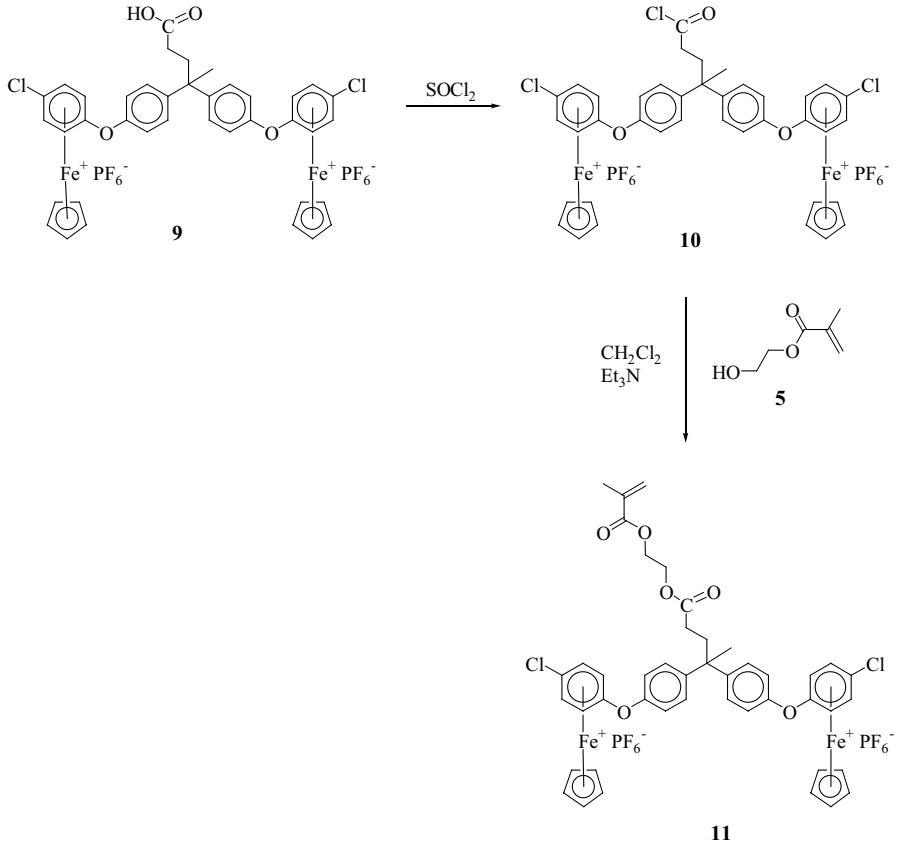

Scheme 3

The ^{1}H NMR spectrum of monomer **11** is shown in Figure 5. The methyl of the methacrylate unit appears as a singlet at 1.73, and the protons of the other methyl group resonate at 1.90 ppm. The methylene protons at 2.20 and 2.54 are triplets, each integrating for two protons, while the two methylenes between the esters appear as a singlet integrating for four protons at 4.33 ppm. The cyclopentadienyl protons resonate as a singlet at 5.37 ppm, and the olefinic protons appear as two peaks at 5.65 and 6.06 ppm. The complexed aromatic protons appear as two sets of doublets at 6.50 and 6.81, and the uncomplexed aromatic protons are also split into two sets of doublets at 7.32 and 7.47 ppm.

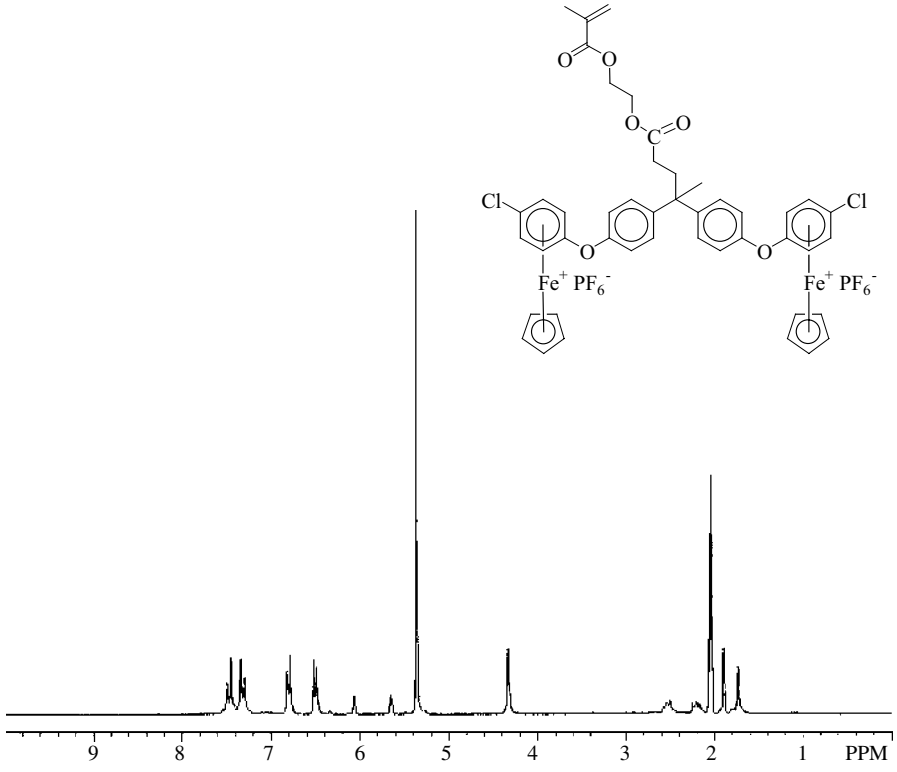

Figure 5 ^{1}H NMR spectrum of methacrylate monomer **11** in acetone-d_6.

Following isolation of the methacrylate complex **11**, this monomer was polymerized in the presence of AIBN as shown in Scheme 4 to produce polymer **12**. Polymethacrylate **12** displayed good solubility in acetonitrile, DMF and DMSO. Polymethacrylate **12** was subsequently demetallated using photolytic techniques to yield the organic polymer **13**.

NMR analysis of **12** confirmed that the polymerization reaction had been successful. The ^{1}H NMR spectrum of polymer **12** obtained in deuterated acetonitrile is shown in Figure 6. The methyl and methylene protons attached to the polymer backbone appear as a broad multiplet within 0.82–1.26 ppm, while the other methyl protons and the methylene protons in the polymer backbone overlap between 1.64 and 1.93 ppm. The two methylene spacers next to the quaternary carbon appear as broad singlets at 2.07 and 2.43 ppm, while the two methylene groups sandwiched between the ester groups appear as a broad singlet at 4.11 ppm. The cyclopentadienyl resonance appears as a singlet at 5.09 ppm, and the complexed aromatic protons are found as broad singlets at 6.15 and 6.47 ppm. The uncomplexed aromatic protons resonate at 7.01 and 7.33 ppm. The most significant feature of this spectrum is the absence of olefinic peaks between 5.5 and 6.1 ppm.

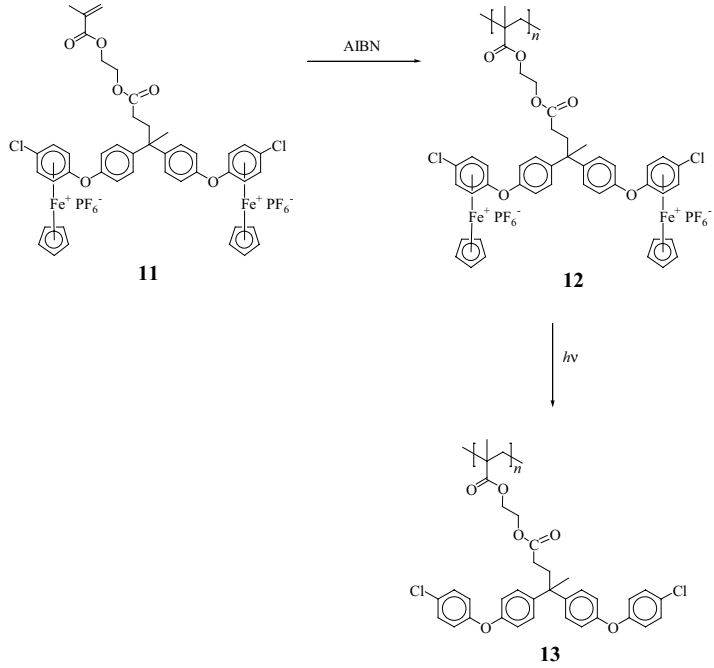

11 **12** **13**

Scheme 4

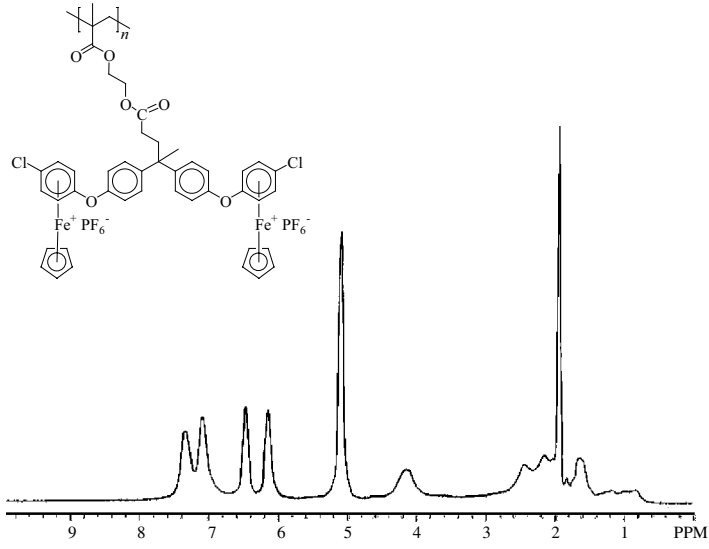

Figure 6 ^{1}H NMR spectrum of polymethacrylate **12** in acetonitrile-d_3.

Following photolysis, the weight-average molecular weight of polymer **13** was determined to be 12,100 by GPC with a polydispersity of 1.38. From this value, the molecular weight if the organoiron polymethacrylate (**12**) was calculated to be 22,500. This corresponds to a degree of polymerization of approximately 20. In contrast, polymethacrylates **7a** and **7b** had degrees of polymerization ranging from 55 to 143. The lower solubility and bulkier sidechains in the metallated polymethacrylate **12** may have prevented the production of higher molecular weight polymers.

The cyclic voltammogram of the organoiron-coordinated polymethacrylate **12** is shown in Figure 7. This CV shows the reversible reduction of the iron centers in the polymer occurring at $E_{1/2} = -1.18$ V.

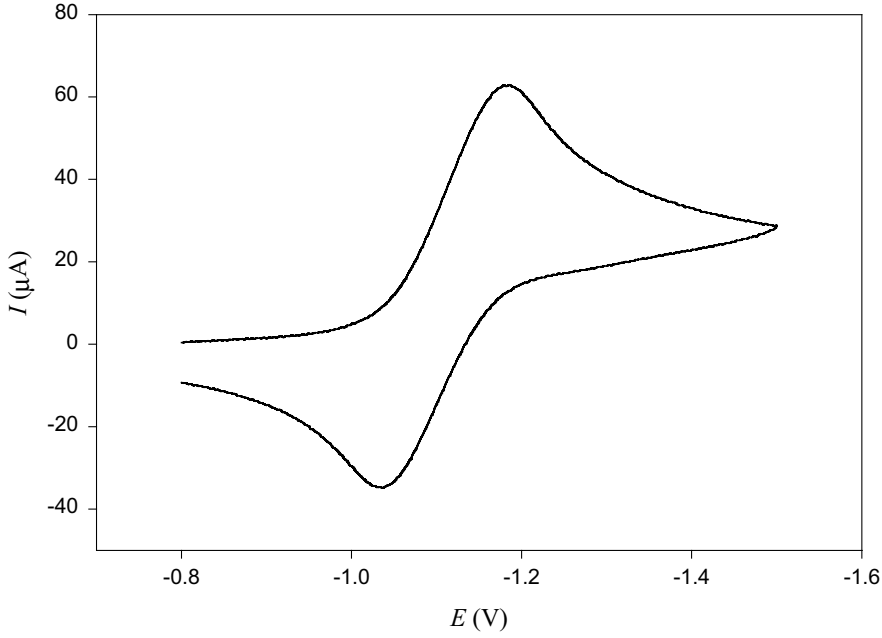

Figure 7 Cyclic voltammogram of methacrylate polymer **12** in DMF at −40°C.

B. Substitution Polymerization of Chloroarene Complexes

It was also of interest to examine the polymerization of monomer **11** via nucleophilic displacement of the chloro groups with oxygen- and sulfur-based nucleophiles.[32] Our previous studies have shown that these reactions proceed under mild reaction conditions to yield soluble polycationic organoiron polymers.[19–23] Scheme 5 shows the reaction of **11** with **14a** and **14b** to produce polymers **15a** and **15b**.

Polymers **15a** and **15b** were isolated as light yellow precipitates in 92 and 93% yields, respectively. These cyclopentadienyliron-coordinated polymers exhibited good

solubility in polar aprotic solvents such as DMF and DMSO. NMR analysis revealed that the S_NAr polymerization reactions had been successful and that the olefinic groups had not polymerized under the conditions of these reactions.[35] Figure 8 shows the ^1H NMR spectrum of polymer **15a**, which was obtained in deuterated DMSO. The protons of the three methyl groups attached to the polymer backbone appear at 1.65 and 1.71 ppm, while the methyl resonance of the methacrylate unit appears at 1.85 ppm. The methylene spacers next to the quaternary carbon in the polymer backbone can be found at 2.15 and 2.39 ppm, and the protons of the two methylene spacers between the ester groups appear as a singlet at 4.26 ppm. The cyclopentadienyl protons resonate as a singlet at 5.21 ppm and the complexed aromatic protons have collapsed into a singlet integrating for eight protons at 6.26 ppm. The olefinic protons appear at 5.68 and 6.00 ppm as singlets, and the uncomplexed aromatic protons appear as a doublet at 7.23 ppm and a multiplet from 7.32 to 7.42 ppm.

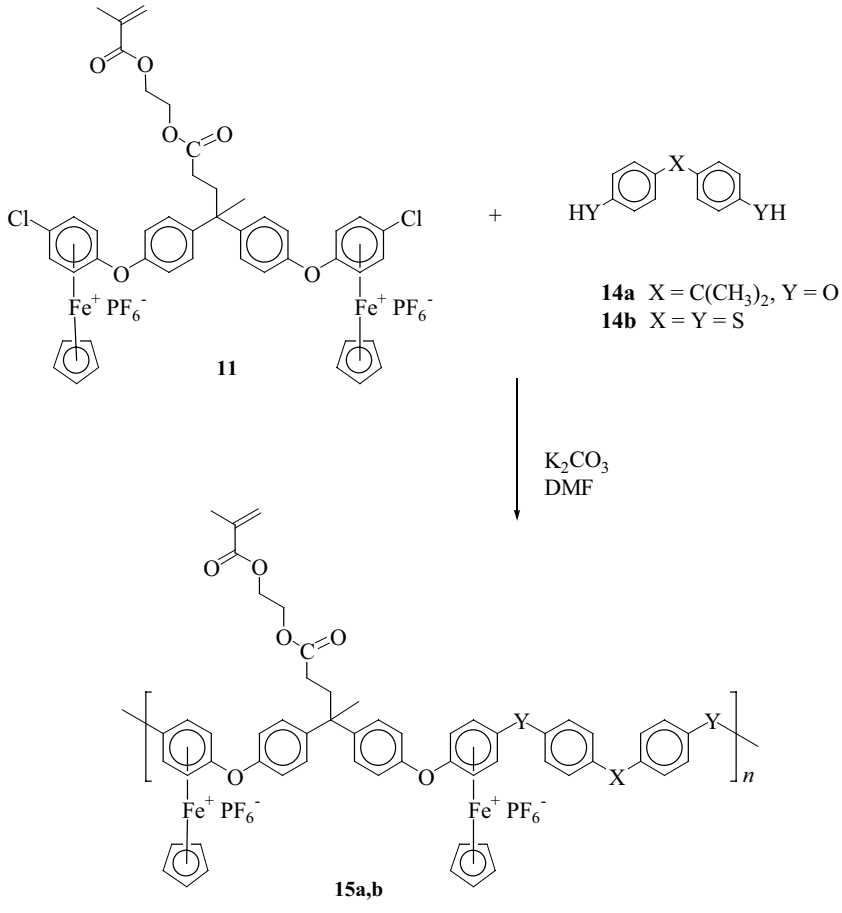

Scheme 5

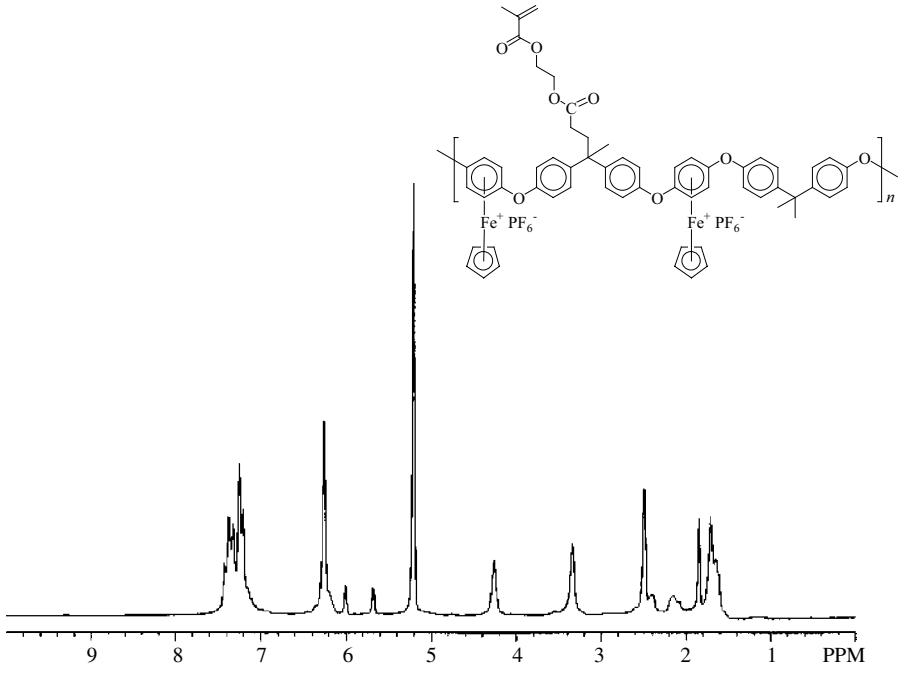

Figure 8 ^{1}H NMR spectrum of polymethacrylate **15a** in DMSO-d_6.

The thermal stability of these polyaromatic ethers and ether–thioethers functionalized with methacrylate groups was examined using thermogravimetric analysis. The polymers displayed typical thermograms in that there were weight losses corresponding to loss of the metallic moieties from 225 to 260°C, followed by secondary weight losses due to polymer degradation. These polymers continued to gradually lose weight after the second major weight loss, as can be seen in the thermogram of polymer **15a** in Figure 9. The backbones of polymers **15a** and **15b** began to degrade at 474 and 460°C, respectively, and lost 30 and 23% of their mass during these weight losses.

In order to examine the molecular weights of polymers **15a** and **15b**, they were photolyzed as shown in Scheme 6, resulting in the isolation of organic polymers **16a** and **16b**. These polymers displayed moderate solubility in tetrahydrofuran and chloroform; however, their solubilities decreased on drying.

Following NMR identification of these polymers, gel permeation chromatography of polymers **16a** and **16b** was performed in order to determine their molecular weights and molecular weight distributions. It was determined that polymer **16a** had a weight average molecular weight of 9800 with a polydispersity of 1.31. This corresponds to a molecular weight of approximately 17,200 for its metallated analog polymer **15a**. Polymer **16b** exhibited poorer solubility, and its M_w was found to be 8300, with a PDI of 1.65. This corresponds to a weight-average molecular weight of approximately 13,800 for polymer **15b**.

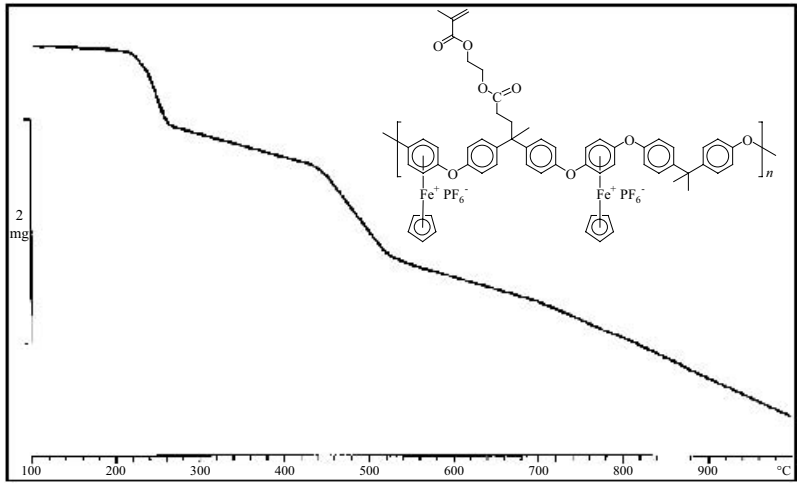

Figure 9 TGA thermogram of polymer **15a**.

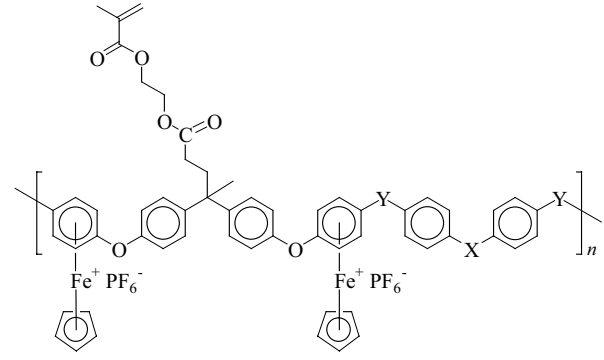

15a,b

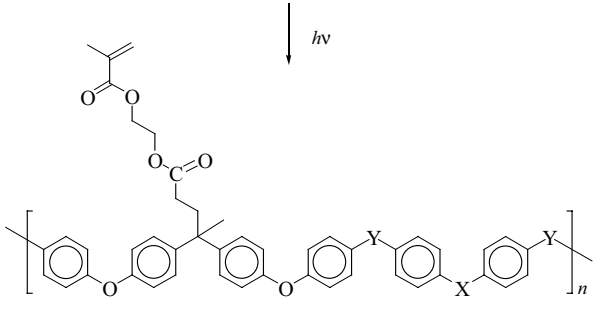

16a,b

Scheme 6

C. Crosslinking

The polymers with methacrylate functionalities in their sidechains (**15a** and **15b**) were also subjected to radical polymerization reactions with AIBN to produce crosslinked polymers as shown in Scheme 7.

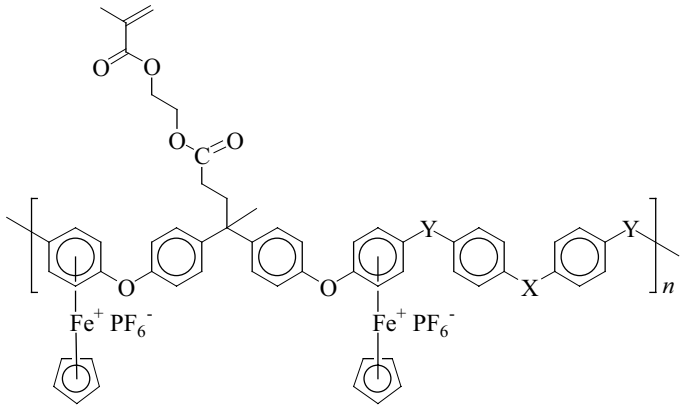

15a,b

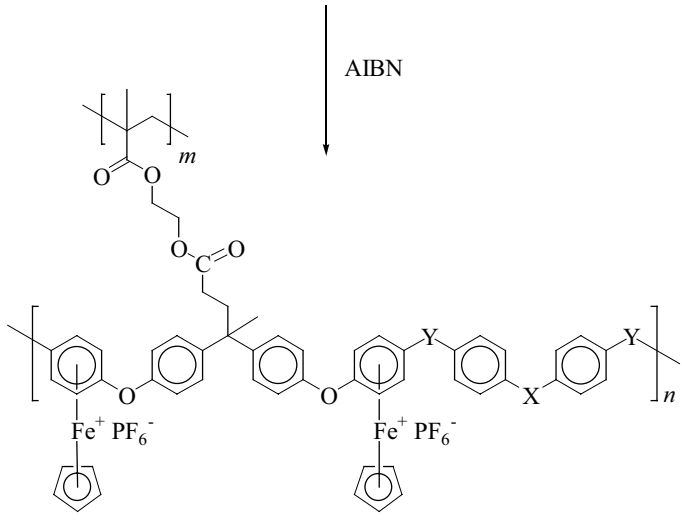

17a,b

Scheme 7

These polymerization reactions were carried out in a number of different solvents depending on the solubility of the starting polymer.[35] Ideally, acetone was used; however, most of the polymers were not completely soluble in acetone. Acetonitrile was also used; however, attempts were also made with DMF and DMSO. The

polymerization reactions were terminated when the polymers precipitated from solution. The polymers were gels or completely insoluble in polar aprotic solvents. NMR analysis of the gels confirmed that there were no olefinic peaks present in the polymers; however, the spectra were very broad.

TGA analysis of the crosslinked polymers was performed; however, there were no substantial differences between the thermograms of the linear and crosslinked polymers. Figure 10 shows the TGA thermograms of polymers **15b** and **17b**. Although there is a slight difference between the two thermograms, weight losses were within 10–20°C of each other.

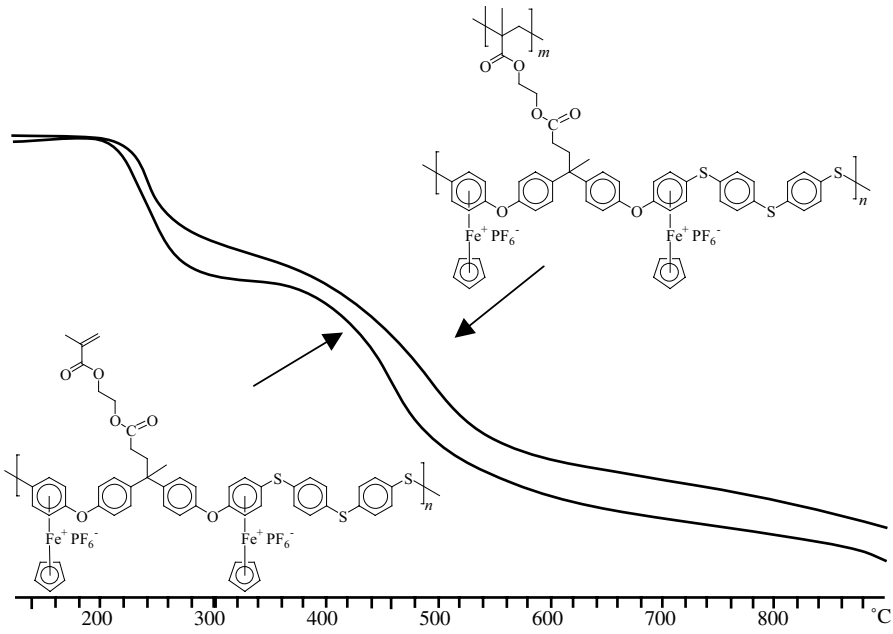

Figure 10 TGA thermograms of polymers **15b** and **17b**.

III. STYRENES

A. Radical Polymerization of the Styrene Groups

Scheme 8 shows the synthesis of the styrene monomer **19** by reaction of the carboxylic acid complex **9** with 4-vinylbenzylchloride (**18**).[32] Complex **19** was isolated in excellent yield as a yellow precipitate.

Monomer **19** was analyzed using ^{1}H and ^{13}C NMR spectroscopy.[35] The olefinic portion of complex **19** displays an *ABX*-type pattern in its ^{1}H NMR spectrum since the protons of the methylene group are not chemically equivalent. Figure 11 shows the numbering system used for identifying the olefinic protons in this compound.

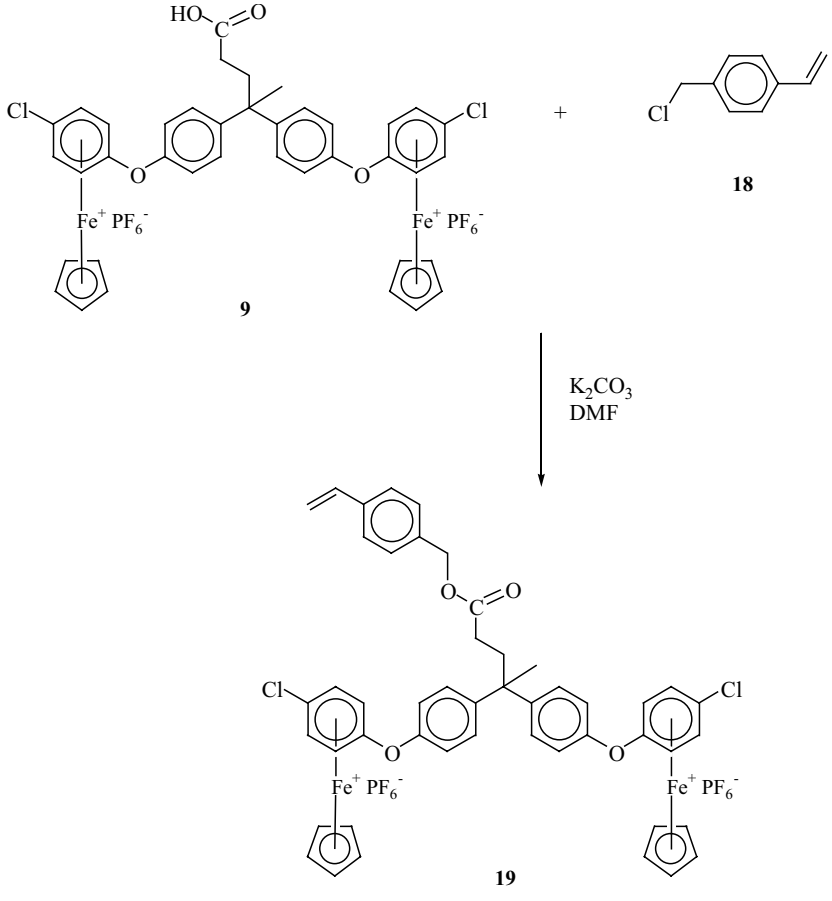

Scheme 8

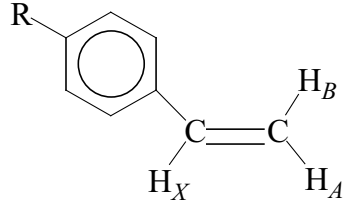

Figure 11 Labeling of styrene functional group.

Figure 12 shows the ^{1}H and ^{13}C NMR spectra of monomer **19**. In the ^{1}H spectrum, proton H_A appears as a doublet at 5.30 ppm due to coupling ($J = 13.3$ Hz) between H_A and H_X. Although there is also coupling between H_A and H_B, this coupling is very small and was not observed. Proton H_B appears as a

doublet at 5.81 ppm due to coupling ($J = 17.6$ Hz) between H_B and H_X. Finally, H_X resonates as two sets of doublets; however, the complexed aromatic protons overlap one of the doublets. The doublet that is visible appears at 6.71 ppm with a coupling constant of 10.9 Hz. The methyl group appears as a singlet at 1.73 ppm, and the two aliphatic methylene groups appear as triplets at 2.24 and 2.57 ppm. The benzylic methylene group appears as a singlet at 5.08 ppm, and the cyclopentadienyl resonance is seen at 5.35 ppm. The complexed aromatic protons resonate as two sets of doublets at 6.48 and 6.79 ppm, while the uncomplexed aromatic protons appear as three sets of doublets at 7.31, 7.35, and 7.47 ppm.

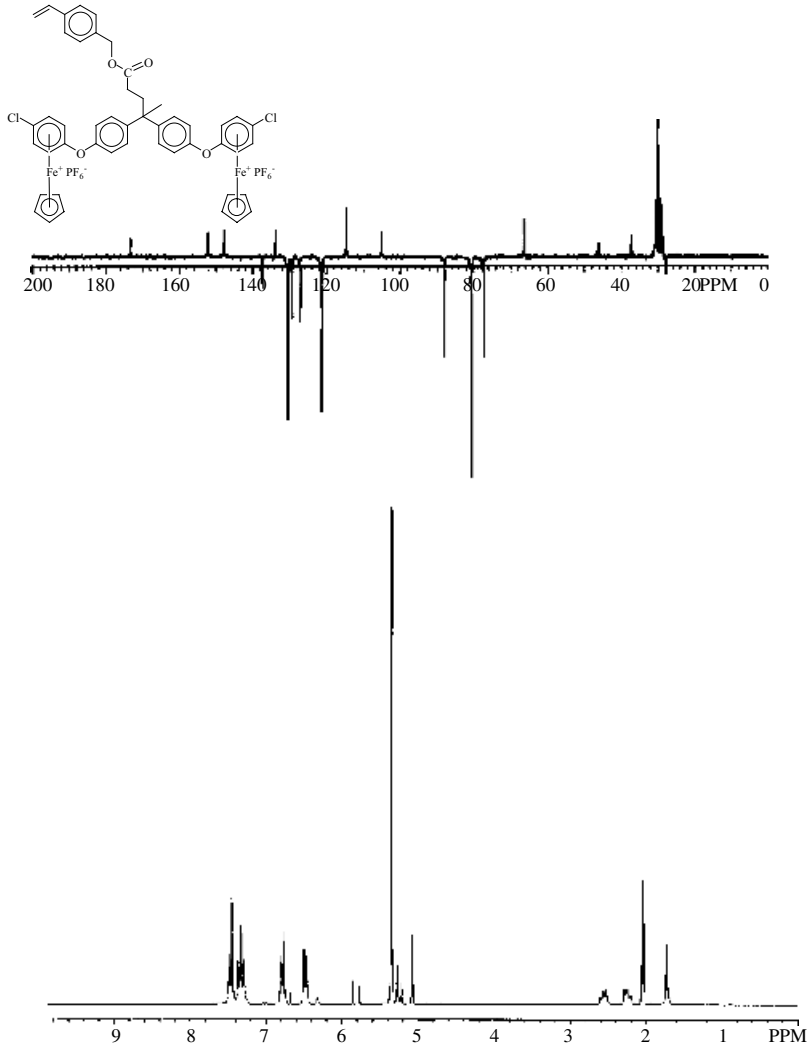

Figure 12 ^{1}H and ^{13}C NMR spectra of monomer **19a** in acetone-d_6.

In the ^{13}C NMR spectrum of monomer **19**, the olefinic carbons appear at 114.56 ppm for the methylene carbon and 137.19 ppm for the methine carbon. The methyl resonance appears at 27.82 ppm, while the quaternary aliphatic carbon is found at 46.20 ppm and the CH_2 groups appear at 28.64, 37.04, and 66.24 ppm. The cyclopentadienyl resonance appears at 80.37 ppm, and the complexed aromatic carbons resonate at 77.04, 87.74, 104.74, and 133.75 ppm. There are four aromatic (CH) carbons at 121.21, 127.00, 129.19, and 130.54 ppm, and four quaternary aromatic carbons at 136.84, 138.11, 147.81, and 151.91 ppm. Finally, the carbonyl carbon appears at 173.38 ppm.

Monomer **19** was subsequently polymerized in the presence of AIBN as shown in Scheme 9 to produce polymer **20**, which was isolated as its hexafluorophosphate salt. This polymer exhibited fairly low solubility in polar organic solvents and often formed gels. The cyclopentadienyliron-functionalized polystyrene (**20**) was analyzed using NMR, IR, and TGA. This organoiron polymer was subsequently demetallated in order to examine its molecular weight; however, the organic analog (**21**) was insoluble.

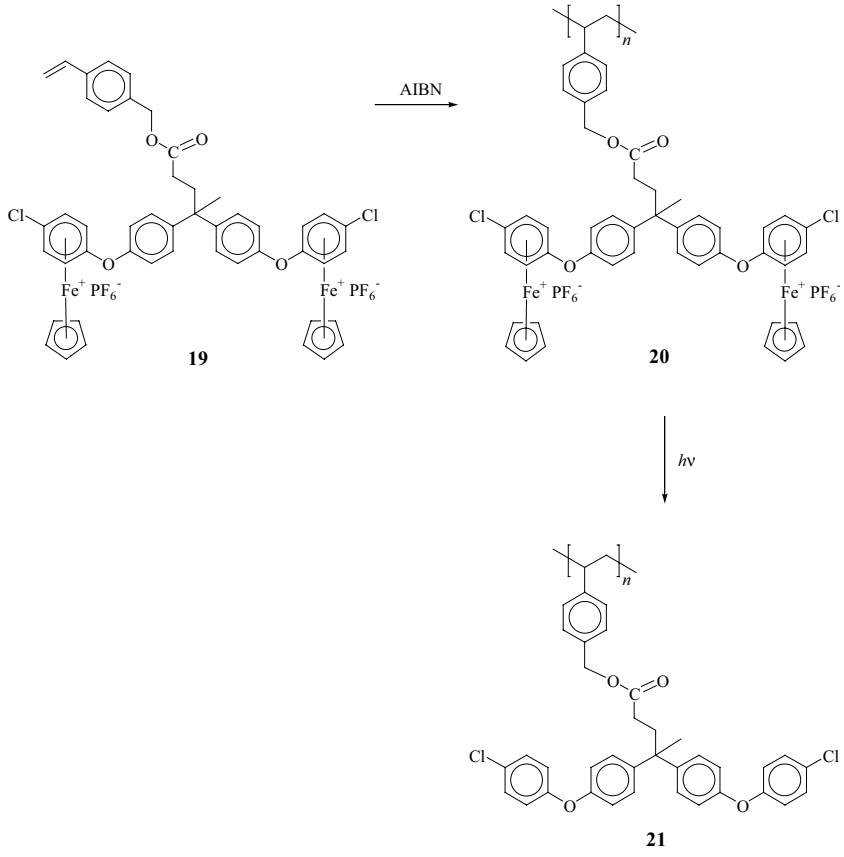

Scheme 9

The TGA thermograms of the styrene monomer (**19**) and its corresponding cyclopentadienyliron-coordinated polymer (**20**) are shown in Figure 13.[35] Monomer **19** exhibits three distinct weight losses starting at 217, 437, and 550°C, while polymer **20** shows only two distinct weight loss steps starting at 226 and 433°C. Although the first two weight losses occur at approximately the same temperatures, the functionalized polystyrene displays superior weight retention at higher temperatures.

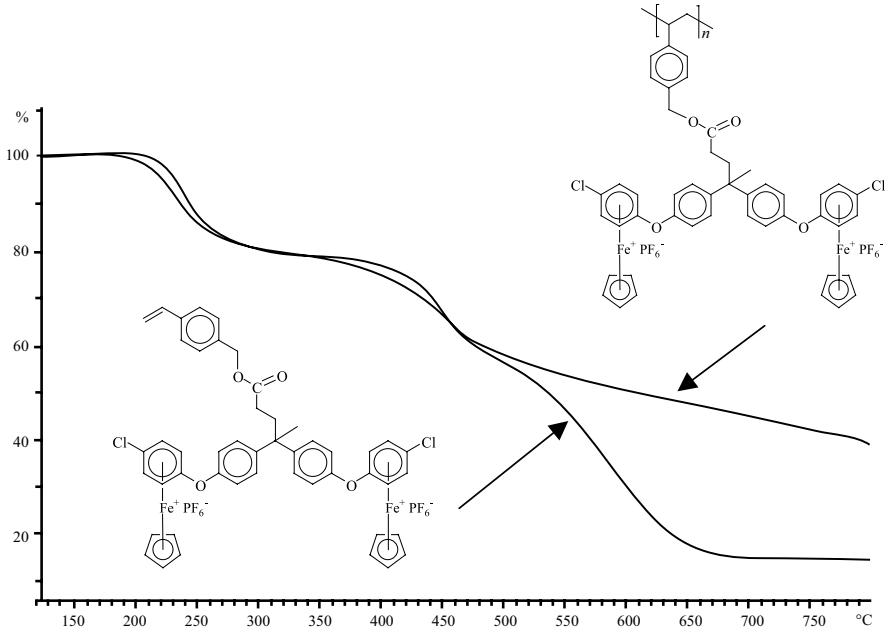

Figure 13 Thermogravimetric analysis of styrene monomer **19** and polymer **20**.

B. Substitution Polymerization of Chloroarene Complexes

The next step of this investigation was to examine the polymerization of monomer **19** via nucleophilic aromatic substitution reactions with dinucleophiles **14a** and **14b**.[32] Scheme 10 shows the synthesis of polymers **22a** and **22b** using this methodology.

These cyclopentadienyliron-coordinated polymers displayed very good solubility in polar aprotic solvents such as DMF and DMSO. They were isolated as beige and yellow precipitates in excellent yields and were analyzed using spectroscopic, thermal, and electrochemical methods.

The interesting feature of the ^{1}H NMR spectra of these organometallic polymers is that while some of the olefinic resonances were overlapped with the complexed aromatic resonances in monomer **19**, all of these peaks can be observed in the spectra of the polymers. Figure 14 shows the ^{1}H NMR spectrum of polymer **22a**. The olefinic proton at 5.23 now overlaps slightly with the cyclopentadienyl

resonance at 5.20 ppm; however, there is a doublet at 5.83 and a doublet of doublets at 6.72 ppm that are identified as the vinyl protons. The multiplet around 1.65 ppm corresponds to the methyl protons, while the small peaks at 2.20 and 2.46 ppm correspond to the methylene spacers. The methylene protons adjacent to the styrene group appear as a singlet at 5.04 ppm integrating for two hydrogens. The complexed aromatic protons have collapsed into a singlet, while the uncomplexed aromatic peaks appear as four sets of doublets at 7.23, 7.32, 7.36, and 7.46 ppm.

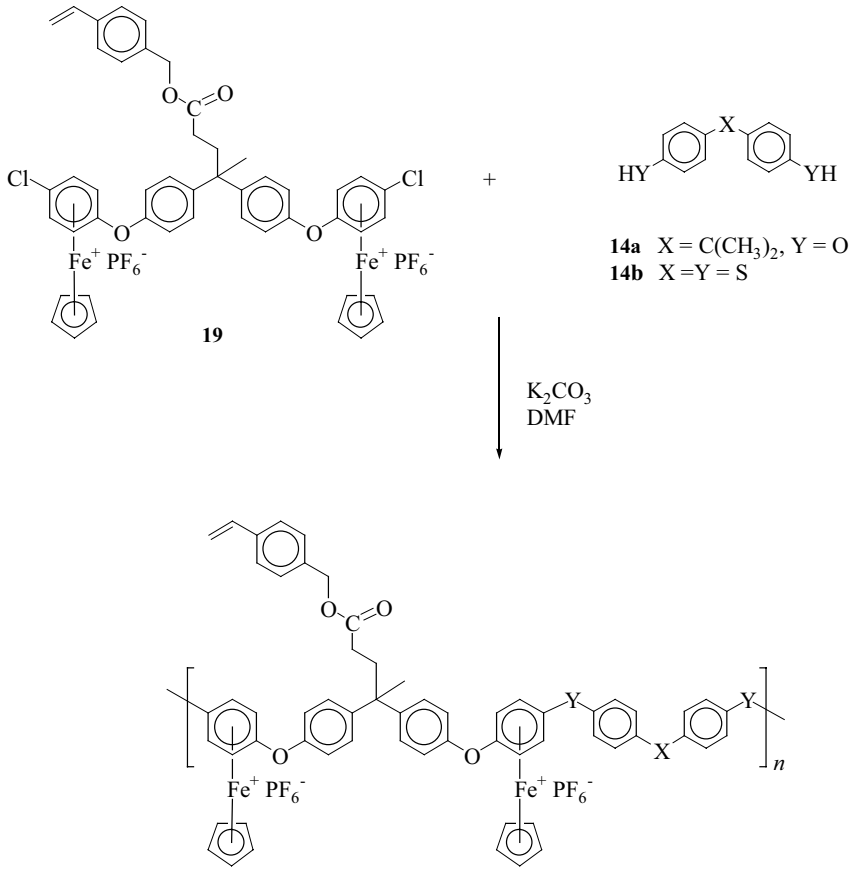

Scheme 10

The ^{13}C NMR spectrum of polymer **22a** is also shown in Figure 14. There are two methyl resonances at 26.94 and 30.63 ppm, and two corresponding quaternary aliphatic carbon peaks at 42.16 and 44.99 ppm. The three aliphatic methylene peaks appear at 29.71, 35.89, and 65.34 ppm, while the olefinic methylene and methine resonances appear at 114.64 and 136.14 ppm, respectively. The cyclopentadienyl carbons can be found at 77.83 ppm, and the complexed aromatic (CH) carbons

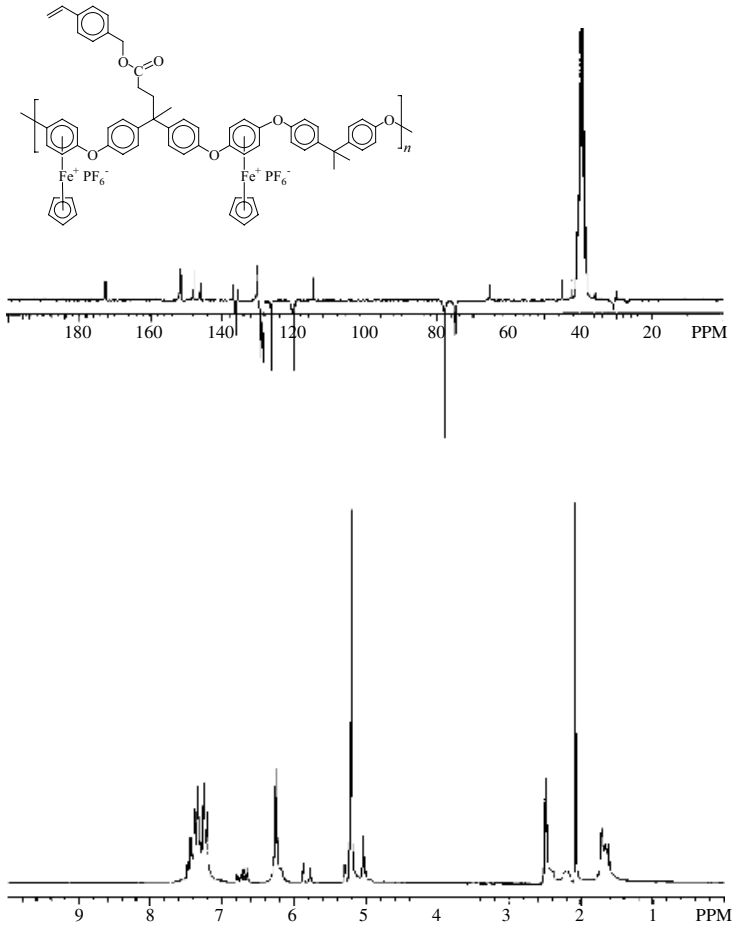

Figure 14 ^{1}H and ^{13}C NMR spectra of polystyrene **22a** in DMSO-d_6.

appear at 74.90 and 75.07 ppm. The corresponding complexed quaternary carbon resonances are found at 129.97 and 130.18 ppm. The aromatic carbon peaks appear between 119.93 and 129.20 ppm, and the quaternary aromatic resonances appear between 135.66 and 151.61 ppm. The carbonyl from the ester group is seen furthest downfield at 172.67 ppm.

TGA analysis of these organoiron polymers with styrene groups in their sidechains revealed the presence of two distinct weight loss steps. Figure 15 shows the thermogram of polymer **22a**. The first weight loss was attributed to decomplexation of the cyclopentadienyliron moieties from the polymer sidechains, while the second weight loss was due to degradation of the polymer backbone and sidechains.

The cyclic voltammetric properties of polymer **22a** were examined in DMF using *tetra*-butylammonium perchlorate as the supporting electrolyte. Figure 16 shows the CV obtained at −50°C with a scan rate of 2 V/s. It can be seen that the reduction process for this polymer is reversible and occurs at $E_{1/2} = -1.20$ V.

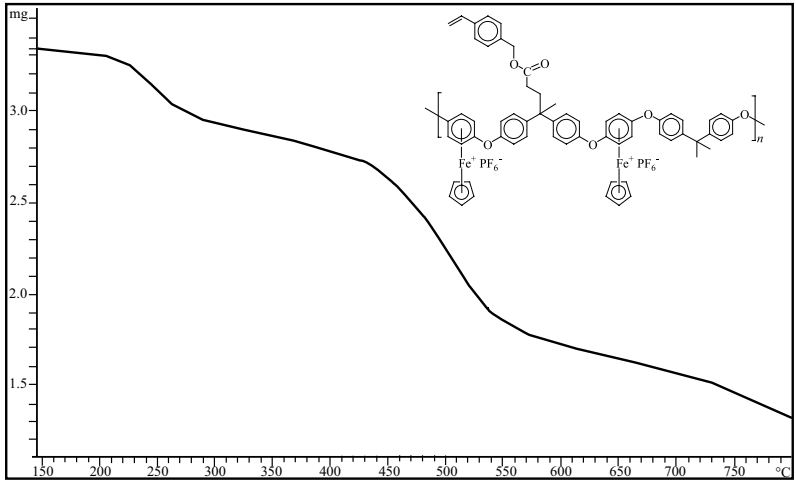

Figure 15 Thermogravimetric analysis of cyclopentadienyliron-coordinated polyether **22a**.

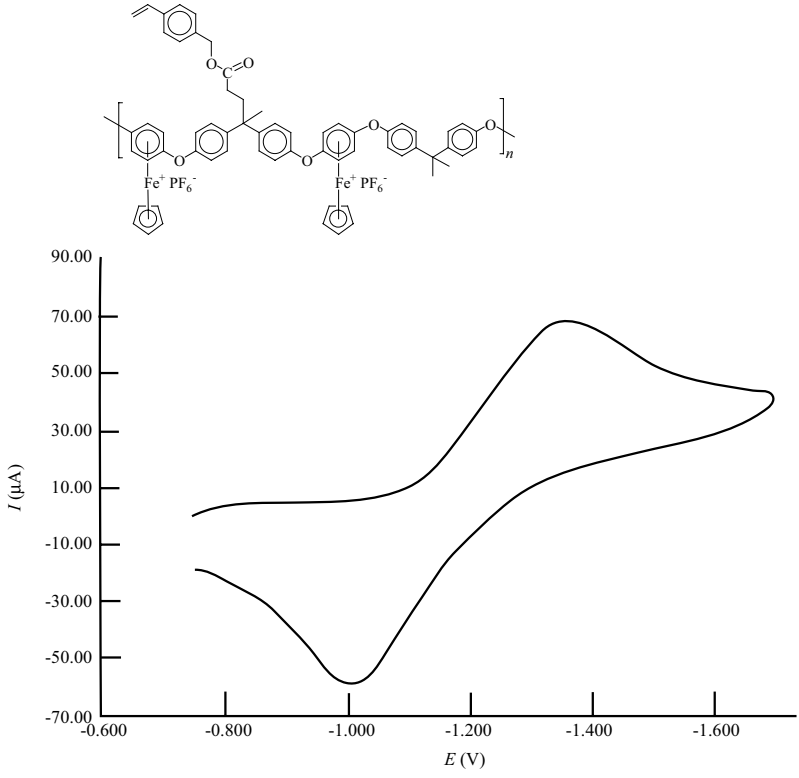

Figure 16 Cyclic voltammogram of **22a** at −50°C in DMF.

Scheme 11 shows the photolysis of the cyclopentadienyliron-coordinated polyaromatic ether and ether/thioether containing styrene units in their sidechains (**22a**, **22b**), allowing for the isolation of the corresponding organic polymers **23a** and **23b**.

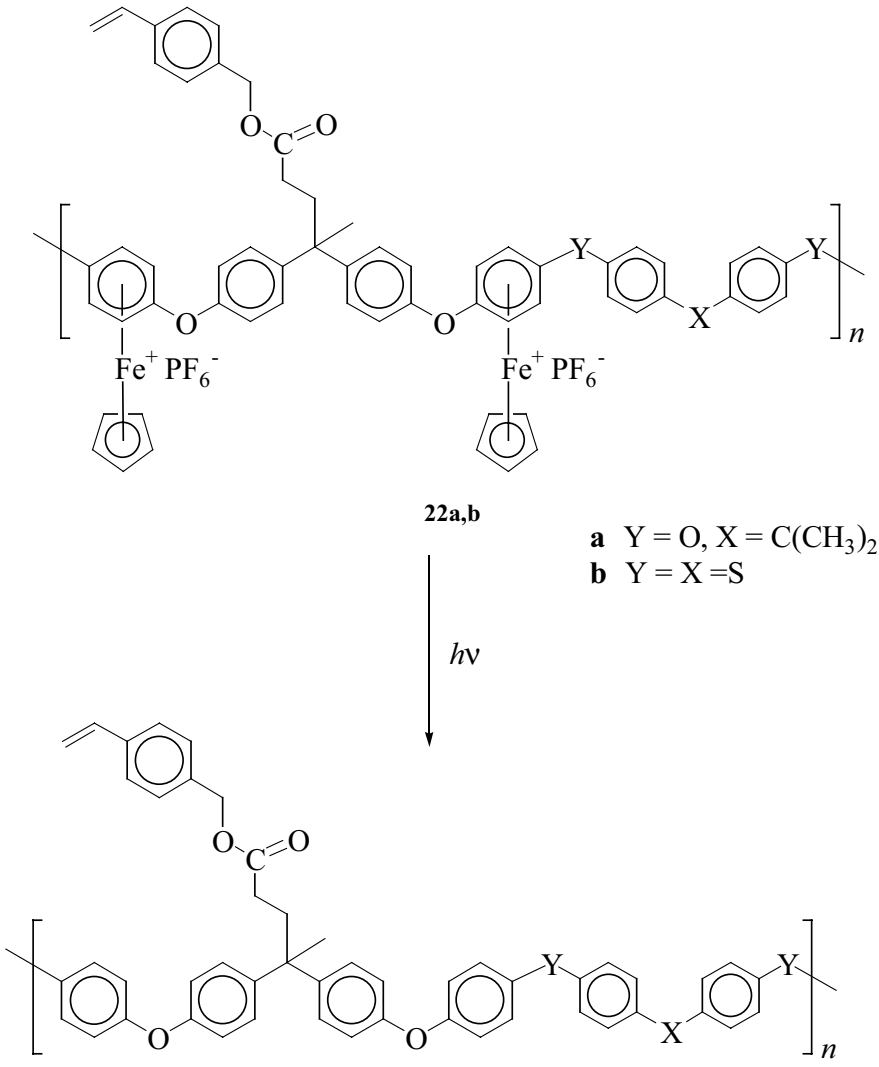

22a,b

a Y = O, X = $C(CH_3)_2$
b Y = X = S

23a,b

Scheme 11

While polymer **23a** displayed fair solubility in chloroform and tetrahydrofuran, polymer **23b** exhibited poor solubility in the common solvents that it was tested in. The molecular weights of the demetallated polymers were also determined using GPC. It was found that the weight-average molecular weights of polymers **23a** and **23b** were 13,500 and 6300 with PDI values of 1.21 and 1.15, respectively. These molecular weights correspond to 22,800 for polymer **22a** and 10,500 for polymer **22b**.

Figure 17 shows the ^{1}H NMR spectrum of polymer **23a**. The two methyl groups appear as overlapping singlets at 1.57 and 1.64 ppm, integrating for three and six protons, respectively. Two methylene resonances are seen at 2.16 and 2.56 ppm, while the methylene protons attached to the styryl group appears as a singlet at 5.02 ppm. There are two doublets at 5.23 and 5.72 ppm that correspond to the protons of the olefinic methylene group. The olefinic methine proton appears as a multiplet between 6.62 and 6.84 ppm, while the uncomplexed aromatic protons resonate between 6.86 and 7.34 ppm.

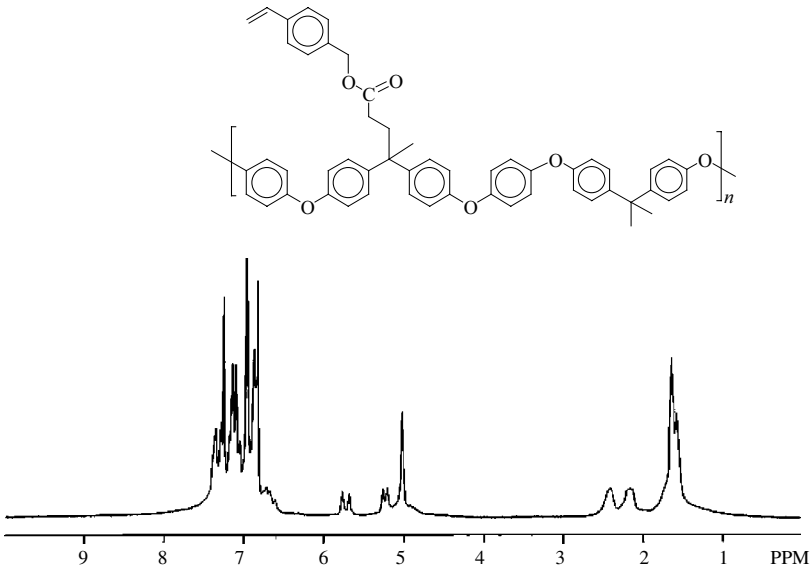

Figure 17 ^{1}H NMR spectrum of polymer **23a** in $CDCl_3$.

C. Crosslinking

Polymerization of the styrene groups in the sidechains of polymers **23a** and **23b** was also examined. Scheme 12 shows the synthesis of the crosslinked organoiron polymers **24a** and **24b**. The crosslinking reactions had the desired effect of making the soluble linear polymers insoluble. Since the linear polymers were stable with their styrene functionalized sidechains, this could allow for the processing of a soluble polymer, which could subsequently be rendered insoluble by crosslinking.

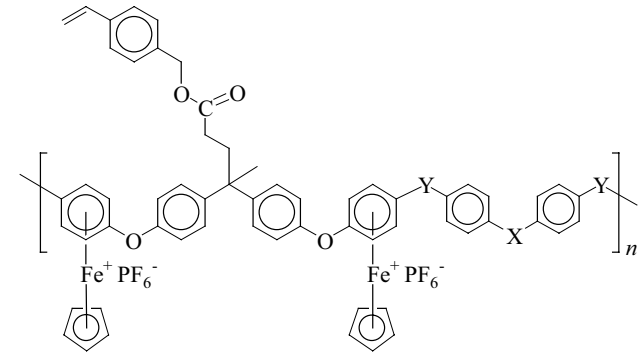

23a,b

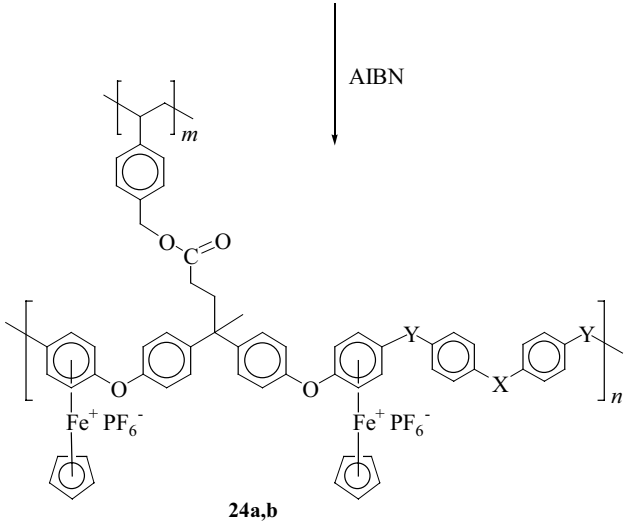

24a,b

Scheme 12

IV. NORBORNENES

A. Ring-Opening Metathesis Polymerization of the Norbornene Groups

Norbornene monomers functionalized with aromatic or aliphatic ether groups have been prepared using cyclopentadienyliron complexes.[28–30] Our initial investigation into these materials showed that the use of organoiron arene complexes was an efficient method to prepare these classes of functionalized norbornene monomers. Following photolysis of complexes **25–27**, the corresponding organic monomers underwent ring-opening metathesis polymerization using either ruthenium chloride or Grubbs' catalyst.

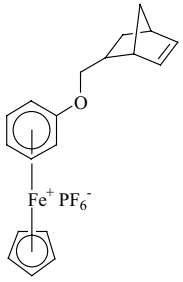

25

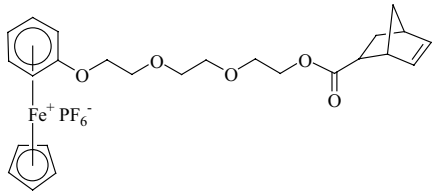

26

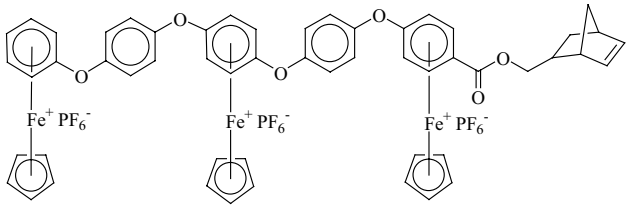

27

We have reported that norbornene monomers functionalized with arene complexes also undergo ring-opening metathesis polymerization to produce the corresponding cyclopentadienyliron-coordinated polynorbornenes. Scheme 13 shows the synthesis of polymers containing aromatic ether sidechains functionalized with organoiron moieties.[33]

NMR analysis of the monomers was accomplished using one- and two-dimensional techniques in order to identify their *exo* and *endo* isomers. Figure 18 shows the labeling scheme utilized in the identification of the protons of the *exo* and *endo* isomers.

Figure 19 shows the HH COSY NMR spectrum of monomer **32a**. The cyclopentadienyl protons resonated at 5.25 ppm, while the complexed aromatic protons were found at 6.3–6.5 ppm. The uncomplexed aromatic protons resonated further downfield between 7.2 and 7.5 ppm, while the olefinic protons of the norbornene unit were found in the range of 6.12–6.26 ppm. The aliphatic norbornene protons were found furthest upfield between 1.39 and 3.38 ppm.

For the identification of the *endo* isomer, the olefinic protons (H_6 and H_5) were first assigned based on their strong coupling to each other, as well as their couplings to the bridgehead protons H_1 and H_4, respectively. Protons H_6 and H_5 each appear as a doublet of doublets, with H_5 resonating at 6.26 ppm ($J_{5,6}$=5.48 Hz, $J_{4,5}$=2.93 Hz) and H_6 appearing 6.12 ppm ($J_{5,6}$=5.48 Hz, $J_{1,6}$=2.58 Hz). The bridgehead protons H_1 and H_4 appeared as broad singlets at 3.38 and 2.97 ppm, and also displayed weak long-range coupling with each other. The multiplet resonating between 3.33 and

3.36 ppm was assigned to H_2 on the basis of its connectivity with H_1, as well as $H_{3,x}$ and $H_{3,n}$. The H_3 protons ($H_{3,x}$=2.03–2.06 ppm, $H_{3,n}$=1.39–1.52 ppm) were also assigned on the basis of their characteristic strong coupling with each other ($J_{3,x;3,n}$=11–13 Hz), as well as their connectivity with H_4. The bridge protons, H_{7a} and H_{7s}, also exhibited strong coupling with each other ($J_{7,a;7,s}$=8.40 Hz), and resonated as a multiplet between 1.39 and 1.52 ppm ($H_{7,a}$) and a doublet at 1.58 ppm ($H_{7,s}$).

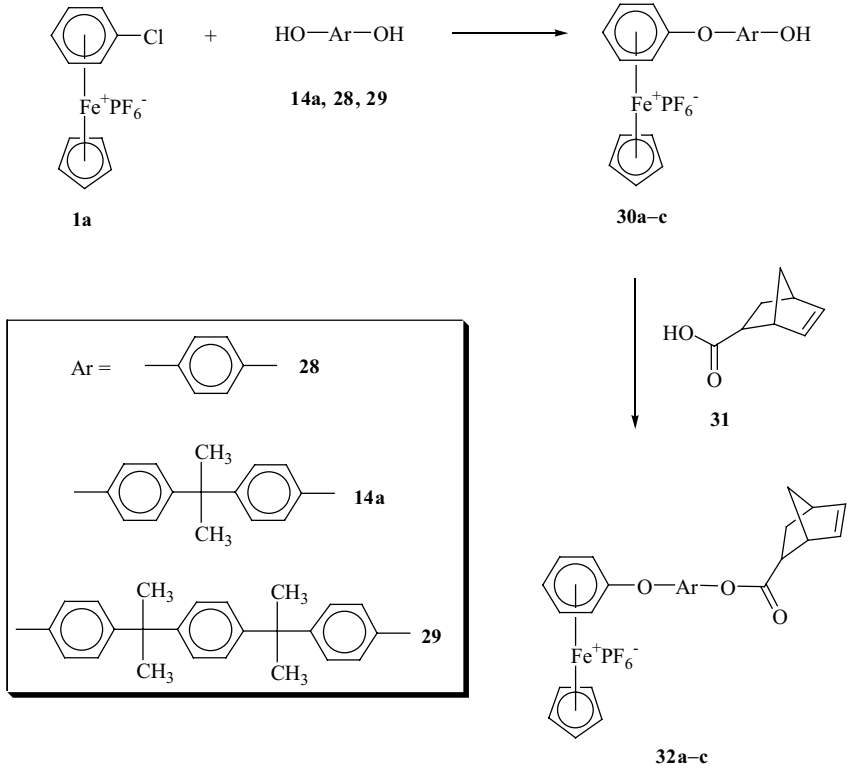

Scheme 13

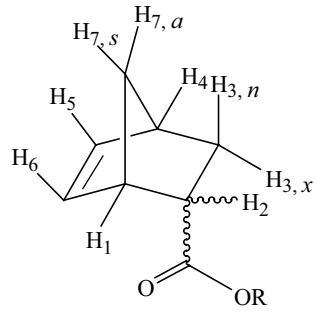

Figure 18 Labeling of norbornene protons.

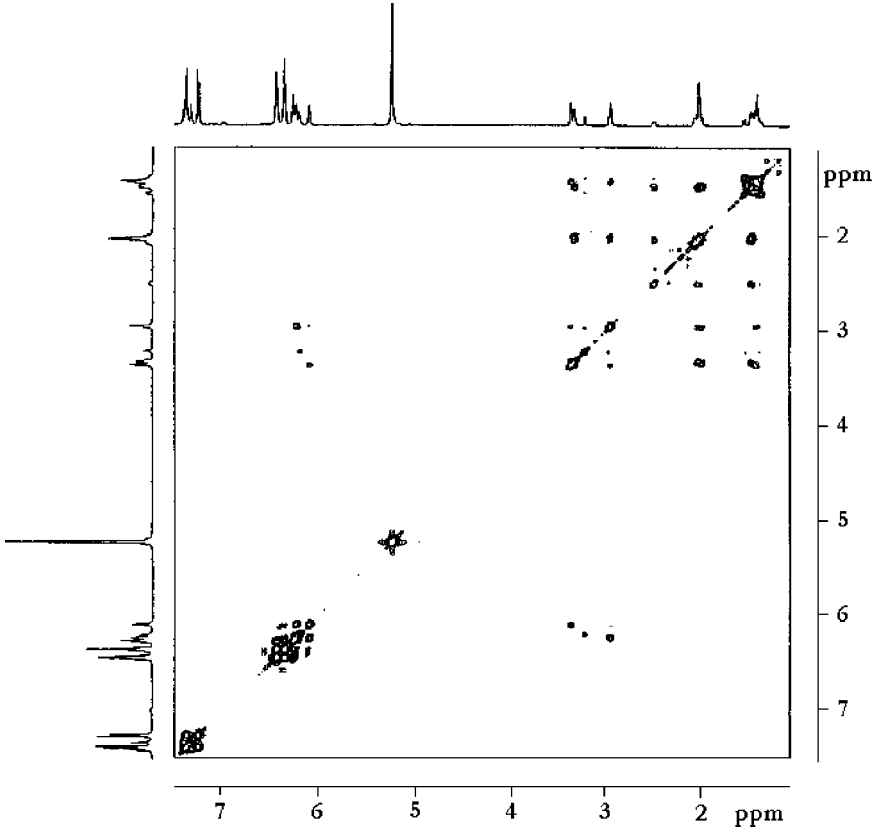

Figure 19 HH COSY NMR spectrum of monomer **32a**.

The protons of the *exo* isomer were identified using the same strategy. The olefinic protons (H_6 and H_5) were assigned to the multiplet resonating between 6.20 and 6.23 ppm. The distinctive couplings between H_6 and H_5 with the bridgehead protons (H_1 and H_4) allowed for the assignment of H_1 to the singlet at 3.24 ppm, and H_4 to the broad singlet appearing at 3.17 ppm. Proton $H_{3,x}$ (2.03–2.06 ppm) was identified via its coupling with the bridgehead proton H_4; however, $H_{3,n}$ could not be found using H_4 since coupling between these protons was not observed in the *exo* isomer. Using the characteristic strong coupling between the two H_3 protons, as well as their coupling with H_2, it was found that $H_{3,n}$ resonates within the multiplet between 1.39 and 1.52 ppm. Using this information, it was also found that H_2 appeared as a doublet of doublets at 2.52 ppm ($J_{2;3,x}$=8.57 Hz, $J_{2;3,n}$=2.52 Hz). Finally, the H_7 protons were assigned to the multiplet resonating between 1.39 and 1.52 ppm.

Ring-opening metathesis polymerization of monomers **32a–c** with *bis*(tricyclohexylphosphine)benzylidene ruthenium(IV) dichloride (Grubbs' catalyst)[36] allowed for the isolation of polynorbornenes **33a–c** as shown in Scheme 14. These polymerization reactions were carried out using a monomer:catalyst ratio of

20–1 over a period of 2 h.[33] These polymers precipitated from the dichloromethane solution during this time, and the reactions were terminated on the addition of ethyl vinyl ether. Following analysis of the metallated polynorbornenes, the cyclopentadienyliron cations were cleaved from the polymer sidechains by photolysis. This resulted in the isolation of polymers **34a–c** as beige solids. These organic polymers had weight-average molecular weights ranging from 11,600 to 14,800 with polydispersities ranging from 1.24 to 1.56.

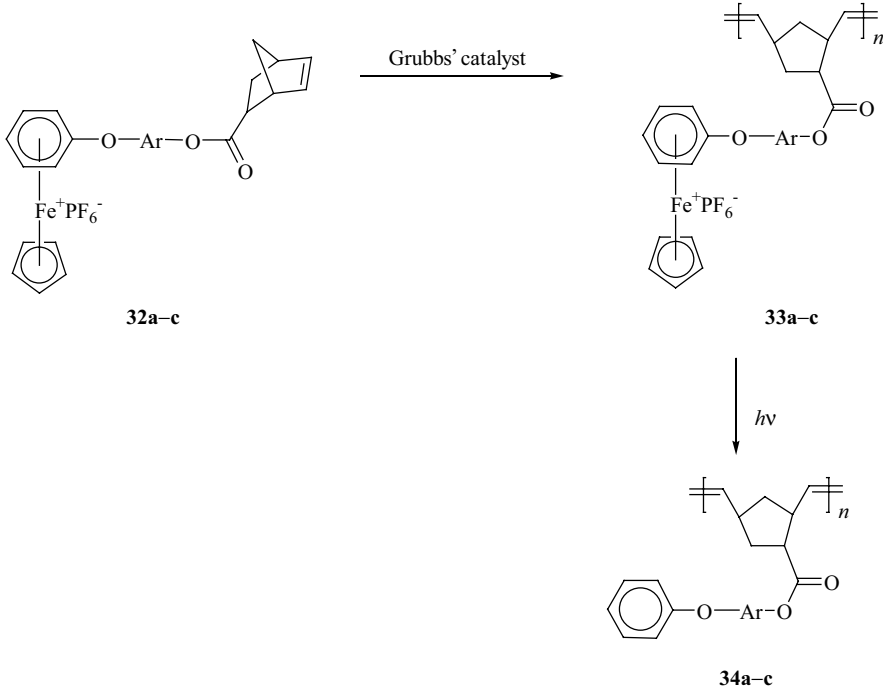

32a–c **33a–c** **34a–c**

Scheme 14

Thermogravimetric analysis of the metallated polynorbornenes (**33a–c**) showed two distinct weight loss steps. The primary weight losses around 210–250°C correspond to degradation of the cyclopentadienyliron hexafluorophosphate moieties, while the secondary weight losses correspond to decomposition of the polymer backbones and sidechains. Figure 20 shows the TGA thermograms of polymer **33a** and its organic counterpart **34a**. The onsets for weight loss of polymer **33a** occurred at 225 and 412°C, while a single weight loss for **34a** began at 408°C. DSC analysis of the organic polymers (**34a–c**) showed that these materials had glass transition temperatures between 59 and 81°C.

It was also possible to design norbornene monomers functionalized with two cyclopentadienyliron arene complexes.[33,34] Scheme 15 shows the synthesis of complex **36** via reaction of the diiron complex **9** with *endo,exo*-5-norbornene-2-methanol (**35**). While this monomer could itself be ring-opened, it could also be reacted with various phenolic compounds (**37a–c**) to produce longer aromatic ether spacers.

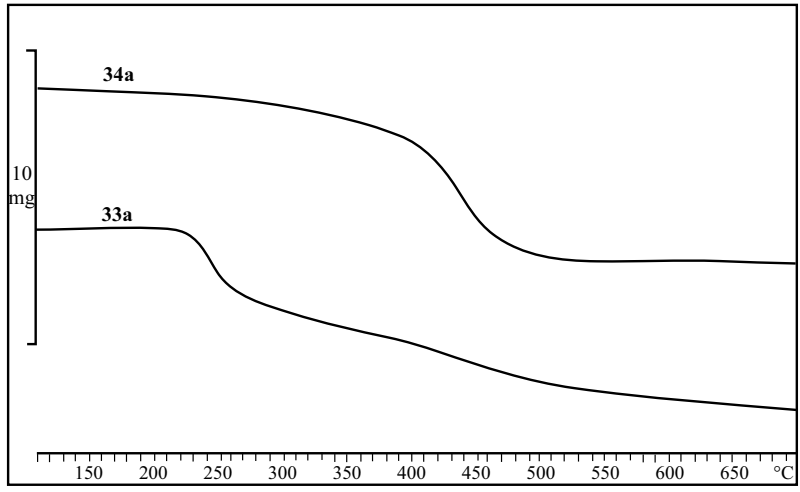

Figure 20 TGA thermograms of metallated polynorbornene **33a** (bottom) and its organic analog **34a** (top).

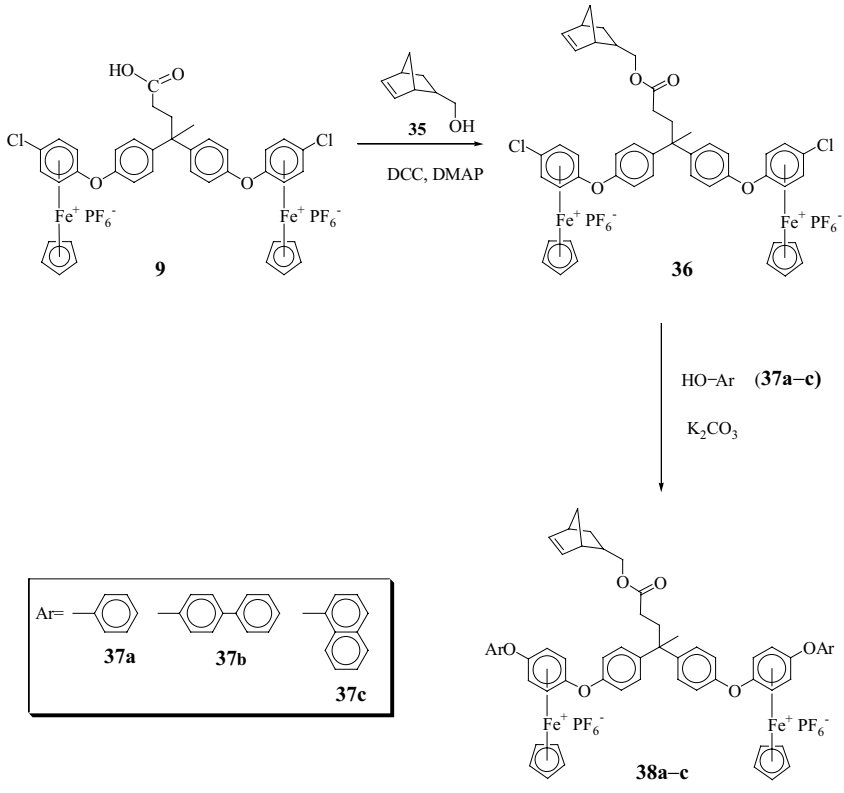

Scheme 15

These monomers were analyzed using one- and two-dimensional NMR prior to polymerization in order to identify the isomeric mixture of compounds **36** and **38a–c**. Scheme 16 shows the polymerization of monomers **36** and **38a–c** using Grubbs catalyst. Polymers **39** and **40a–c** were isolated as brown solids in yields ranging from 70 to 75% and analyzed using spectroscopic, thermal, and electrochemical methods. Following cleavage of the metallic moieties from the polymer sidechains, the molecular weights of the organic polynorbornenes were found to range from 12,800 to 20,300, which corresponds to M_w values of 24,000–32,700 for the organoiron polymers **39** and **40a–c**. The glass transition temperature of **41** was 92°C, while the T_g values of **42a–c** ranged from 75 to 76°C.

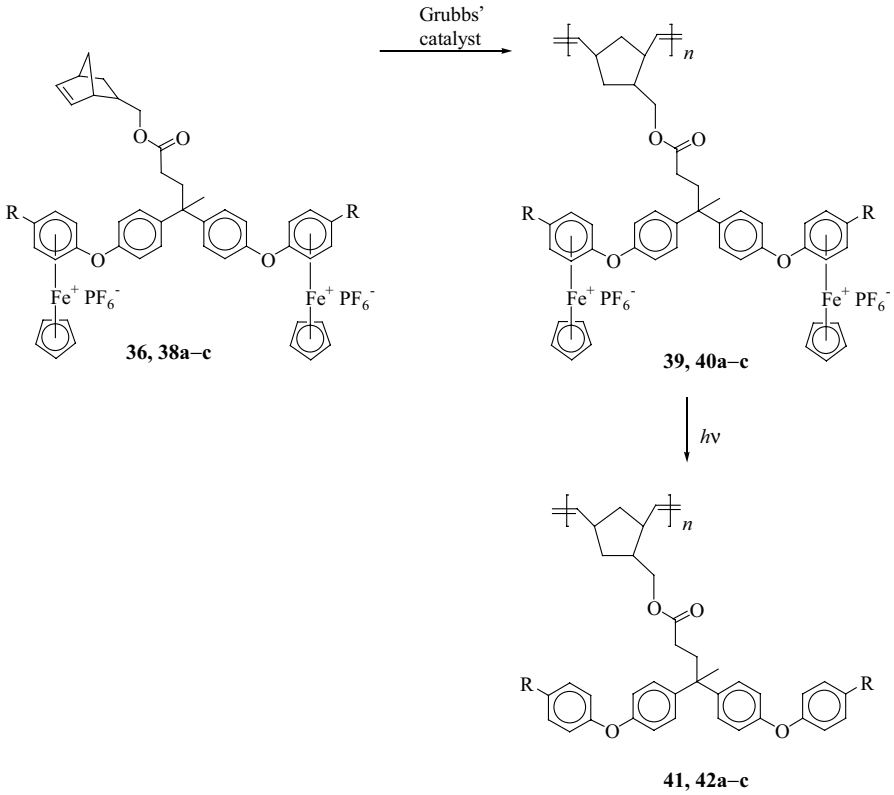

Scheme 16

Figure 21 shows the cyclic voltammogram of polymer **40a** obtained in DMF at −30°C. The iron centers of this polymer underwent reversible reduction at −1.22 V using a scan rate of 2 V/s.

The length of the spacer between the polynorbornene backbone and the aromatic portion of the side chains was also examined.[34] Scheme 17 shows the strategy

used to prepare monomers **45a–c** using three aliphatic diols. Initially, complex **9** was reacted with an excess of 1,2-ethanediol, 1,6-hexanediol, or 1,12-dodecanediol to produce complexes **44a–c**. These diol complexes were subsequently reacted with *exo,endo*-5-norbornene-2-carboxylic acid to give monomers **45a–c**.

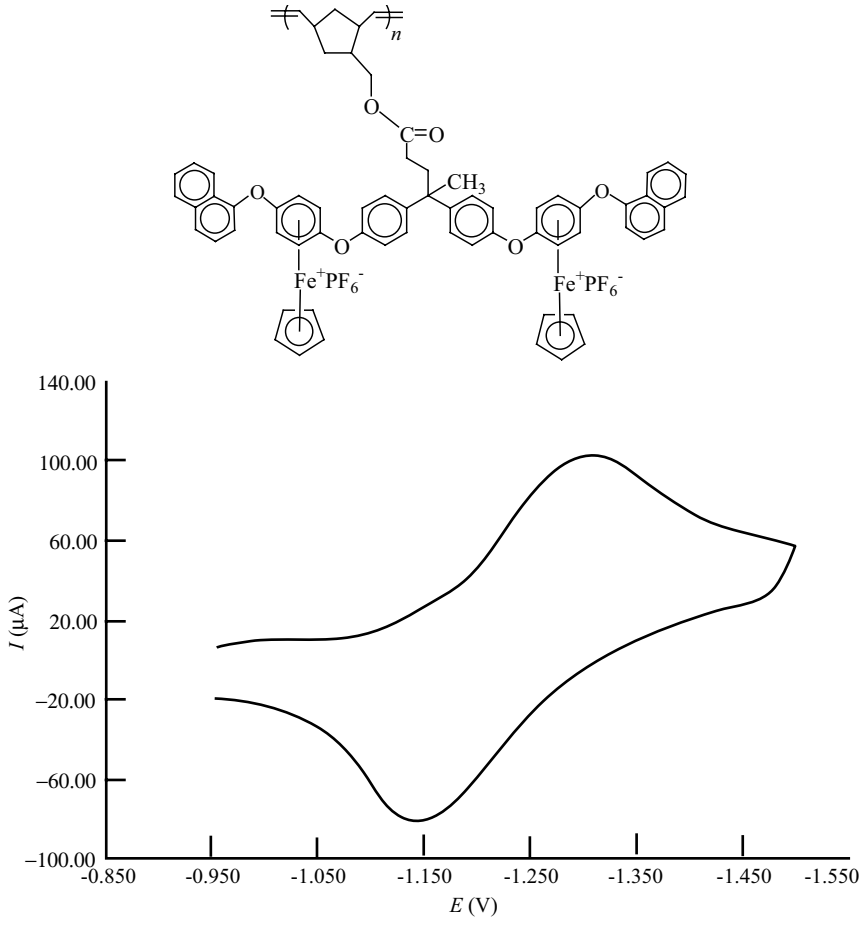

Figure 21 Cyclic voltammogram of **40a** in DMF.

Polymerization of monomers **45a–c** was carried out using a monomer to catalyst ratio of 20 to 1 (Scheme 18). This allowed for the isolation of polynorbornenes **46a–c** in good yields. These polymers were subsequently demetallated to give polymers **47a–c**. It was determined that these polymers had weight average molecular weights ranging from 10,600 to 18,600 with PDI values ranging from 1.3 to 1.6.

Thermogravimetric analysis of these polymers was accomplished in order to examine their thermal stability. Figure 22 shows the TGA thermogram of polymer **46c**. It can be seen that there are two weight losses starting at 215 and 395°C. These weight losses account for degradation of the organometallic moieties, and the organic portions of the polymers, respectively.

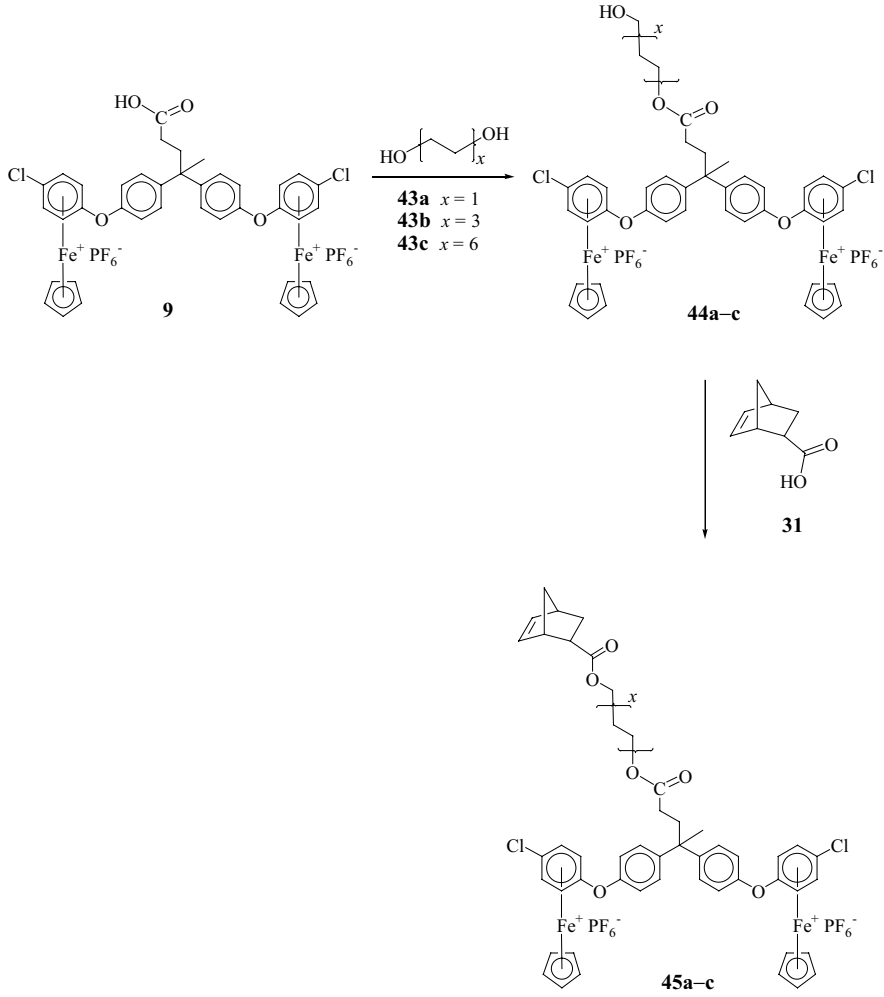

Scheme 17

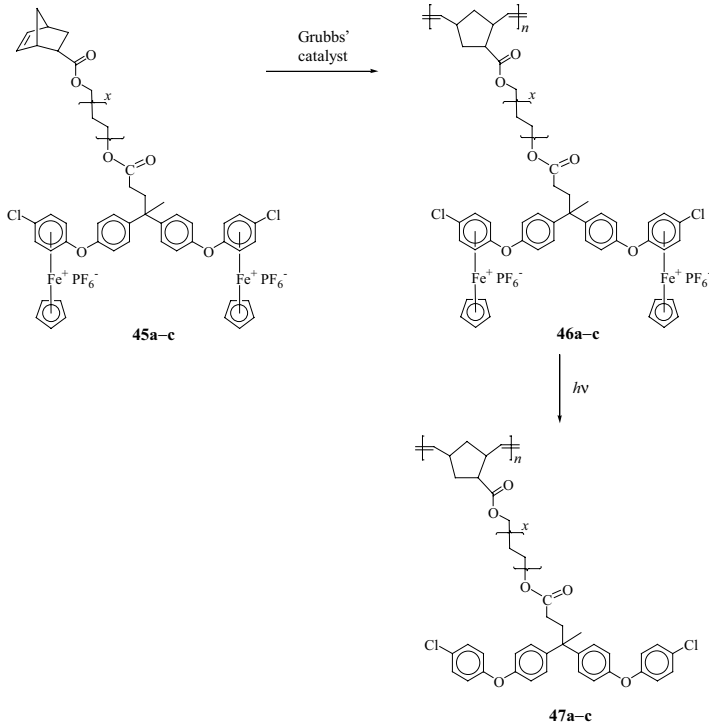

Scheme 18

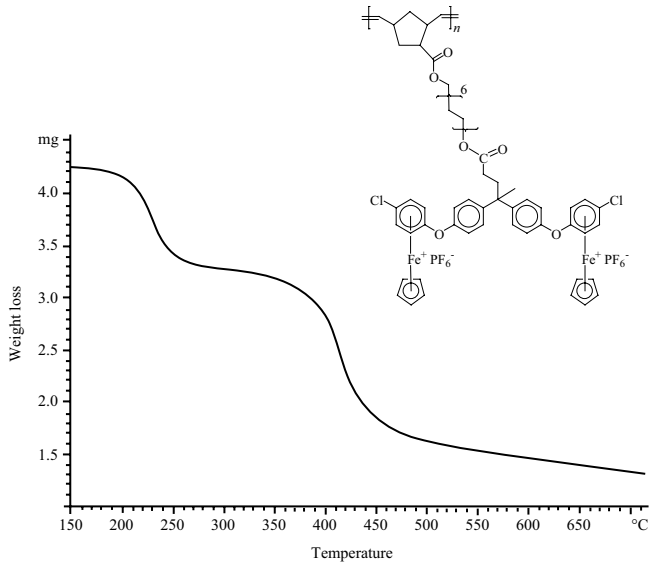

Figure 22 TGA thermogram of polynorbornene **46c**.

B. Substitution Polymerization of Chloroarene Complexes

Polyaromatic ethers and ether–thioethers with norbornene substituents in their side chains were also synthesized by reaction of monomer **36** with dinucleophiles **14a** and **14b** using the strategy shown in Scheme 19. The resulting organoiron polymers exhibited good solubility in polar organic solvents and were isolated in excellent yields.

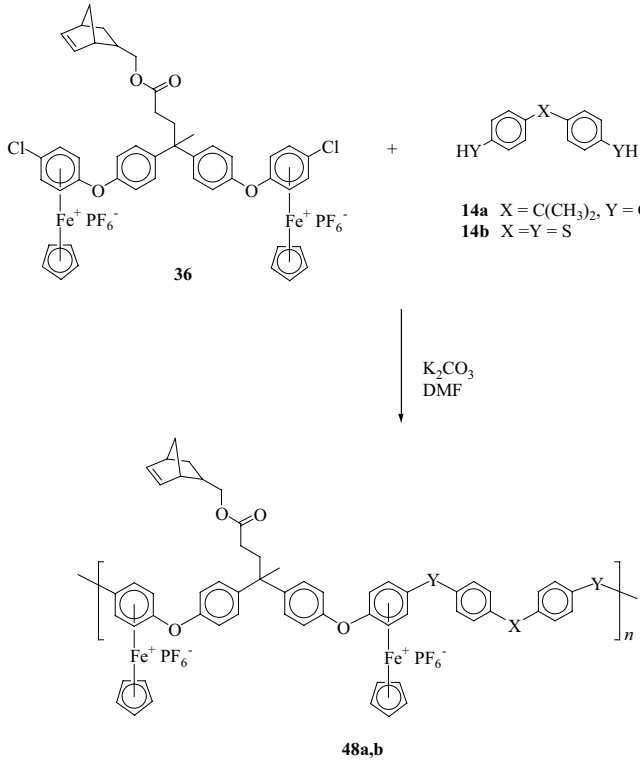

Scheme 19

Polymers **48a** and **48b** were analyzed using NMR, TGA, and cyclic voltammetry. Thermogravimetric analysis showed that following cleavage of the metallic moieties from the polymer sidechains, these materials exhibited good weight retention. Figure 23 shows the TGA thermogram of the organoiron polyether–thioether with norbornene units in its sidechain (**48b**).

The electrochemical properties of these cyclopentadienyliron-coordinated polyethers and ether-thioethers with norbornene units in their side chains were examined using cyclic voltammetry. Figure 24 shows the CV of polymer **48b** at 0°C obtained with a sweep rate of 1 V/s in DMF. Reduction of the cationic 18-electron iron centers to the corresponding neutral 19-electron species occurred at $E_{1/2} = -1.08$ V.

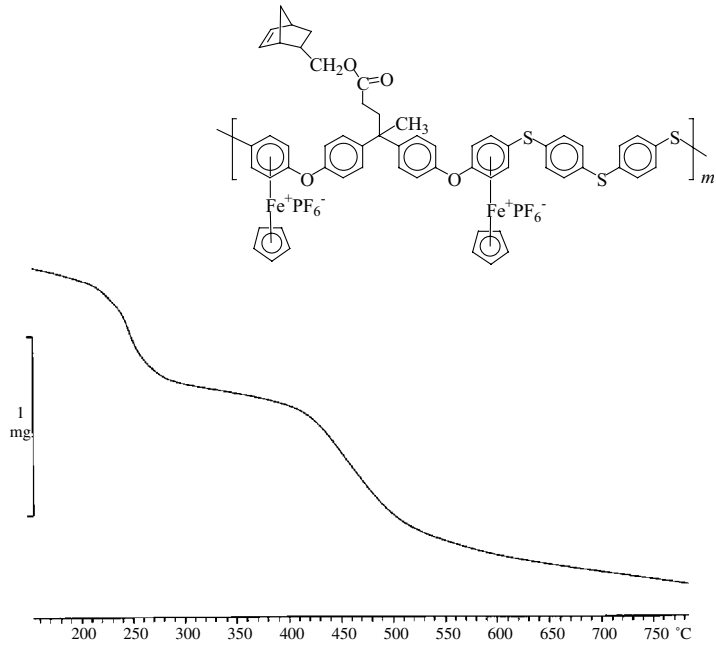

Figure 23 TGA thermogram of metallated polymer **48b**.

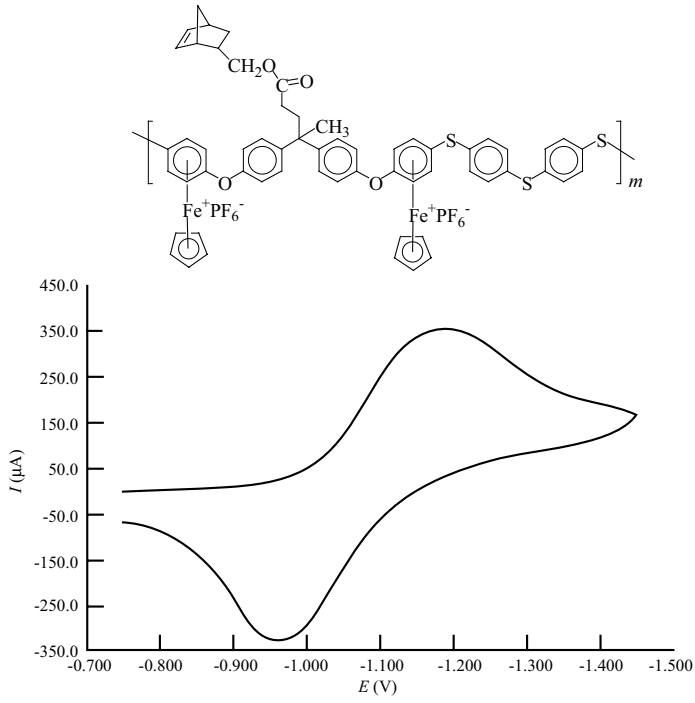

Figure 24 Cyclic voltammogram of polymer **48b** in DMF.

The organoiron polymers **48a** and **48b** were subjected to photolytic demetallation to produce the corresponding organic polymers with norbornene groups in their sidechains as shown in Scheme 20. GPC analysis showed that these organic polymers had molecular weights of ~10,000.

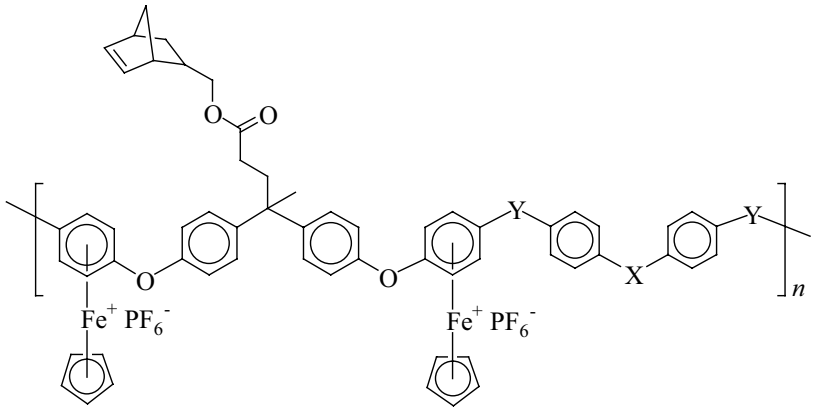

48a,b

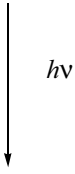

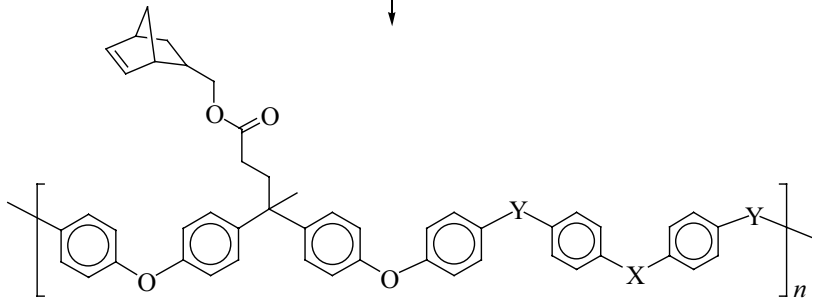

49a,b

Scheme 20

C. Crosslinking

Polymers **48a** and **48b** were also subjected to ring-opening metathesis polymerization reactions to produce crosslinked polymers **50a** and **50b**. Scheme 21 shows the structure of these polynorbornene networks. These polymers were insoluble in all organic solvents tested.

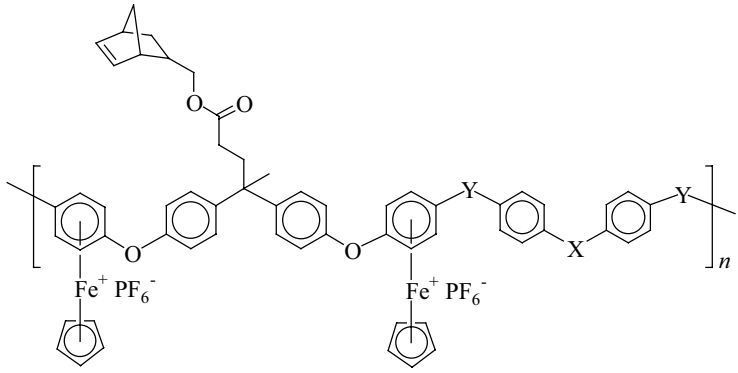

48a,b

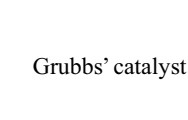

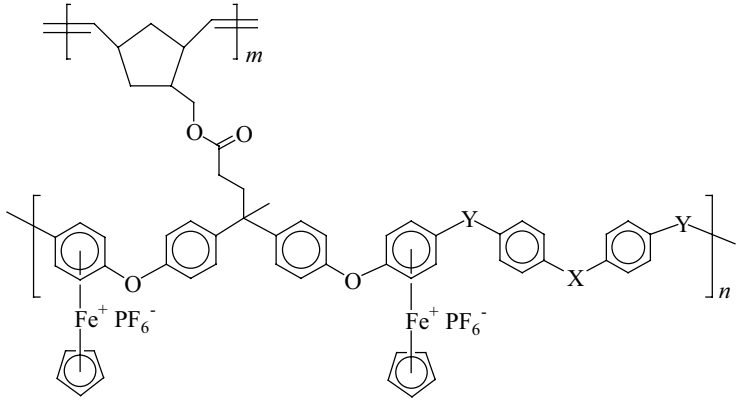

50a,b

Scheme 21

V. CONCLUSIONS

The polymerizations of three different classes of organoiron monomers containing olefins in their structures were examined. Methacrylate-functionalized monomers substituted with aromatic ether complexes were initially subjected to polymerization using AIBN as the initiator. This allowed for the isolation of high molecular weight soluble polymethacrylates bearing cyclopentadienyliron cations in their sidechains. Styrene-substituted monomers were also polymerized in the presence of a radical initiator; however, the resulting organoiron polystyrenes exhibited much lower solubility in polar aprotic solvents. Norbornene-based organoiron monomers were subjected to

ring-opening metathesis polymerization reactions to yield the corresponding polynorbornenes using Grubbs' catalyst. The polymethacrylates, polystyrenes, and polynorbornenes were studied using spectroscopic, thermal, and electrochemical means. Thermogravimetric analysis showed that these materials underwent initial weight losses at ~225°C corresponding to loss of the metallic moieties from the polymer sidechains, and second weight losses between 320 and 450°C corresponding to degradation of the polymer backbones. Cyclic voltammetric studies revealed that the cationic 18-electron iron centers pendent to the polymer sidechains underwent reversible reduction processes to produce neutral 19-electron species. Further reduction to the anionic 20-electron iron complexes was also observed. These polymers were subjected to photolysis, resulting in cleavage of the cyclopentadienyliron cations from the polymer sidechains.

Methacrylate, styrene, and norbornene substituted monomers containing chloroarene complexes in their structures were also subjected to nucleophilic aromatic substitution polymerization with phenolic and thiophenolic dinucleophiles to produce the corresponding polyaromatic ethers and ether–thioethers with acyclic or cyclic olefins in their sidechains. These polymers displayed very good solubility in polar solvents at room temperature. Demetallation of these polymers resulted in a decreased solubility for the polyaromatic ether–thioethers. NMR analysis of these polymers showed that the olefinic groups were not polymerized during these processes. The aromatic polymers prepared by nucleophilic aromatic substitution reactions possessed higher thermal stability than the polymers prepared by radical or ring-opening metathesis polymerization reactions. The polyaromatic ethers and ether–thioethers were crosslinked through their olefinic groups, resulting in the isolation of insoluble organoiron networks.

VI. REFERENCES

1. F. S. Arimoto, A. C. Haven, Jr., *J. Am. Chem. Soc.* **77,** 6295 (1955).
2. M. Baumert, J. Frohlich, M. Stieger, H. Frey, R. Mulhaupt, H. Plenio, *Macromol. Rapid Commun.* **20,** 203 (1999).
3. N. Kuramoto, Y. Shishido, K. Nagai, *J. Polym. Sci. Part A, Polym. Chem.* **35,** 1967 (1997).
4. Y. Yang, Z. Xie, C. Wu, *Macromolecules* **35,** 3426 (2002).
5. M. E. Wright, E. G. Toplikar, *Macromolecules* **27,** 3016 (1994).
6. A. Wiesemann, R. Zentel, G. Lieser, *Acta Polym.* **46,** 25 (1995).
7. R. Deschenaux, F. Turpin, D. Guillon, *Macromolecules* **30,** 3759 (1997).
8. C. U. Pittman, Jr., J. C. Lai, D. P. Vanderpool, *Macromolecules* **3,** 105 (1970).
9. J. C. Lai, T. D. Rounsefell, C. U. Pittman, Jr., *Macromolecules* **4,** 155 (1971).
10. C. U. Pittman, Jr., R. L. Voges, W. R. Jones, *Macromolecules* **4,** 291 (1971).
11. C. U. Pittman, Jr., P. Grube, *J. Polym. Sci. Part A1*, **9,** 3175 (1971).
12. D. O. Cowan, J. Park, C. U. Pittman Jr., Y. Sasaki, T. K. Mukherjee, N. A. Diamond, *J. Am. Chem. Soc.* **94,** 5110 (1972).
13. C. U. Pittman Jr., B. Surynarayanan, *J. Am. Chem. Soc.* **96,** 7916 (1974).
14. D. Albagli, G. Bazan, M. S. Wrighton, R. R. Schrock, *J. Am. Chem. Soc.* **114,** 4150 (1992).

15. D. Albagli, G. Bazan, R. R. Schrock, M. S. Wrighton, *J. Am. Chem. Soc.* **115,** 7328 (1993).
16. S. F. Mapolie, J. R. Moss, G. S. Smith, *J. Inorg. Organomet. Polym.* **7,** 233 (1997).
17. C. U. Pittman, Jr., O. E. Ayers, S. P. McManus, *J. Macromol. Sci. Chem.* **A7**(8), 1563 (1973).
18. C. U. Pittman, Jr., *Macromolecules* **7,** 396 (1974).
19. A. S. Abd-El-Aziz, E. K. Todd, K. M. Epp, *J. Inorg. Organomet. Polym.* **8,** 127 (1998).
20. A. S. Abd-El-Aziz, E. K. Todd, G. Z. Ma, *J. Polym. Sci. Part A: Polym. Chem.* **39,** 1216 (2001).
21. C. R. de Denus, L. M. Hoffa, E. K. Todd, A. S. Abd-El-Aziz, *J. Inorg. Organomet. Polym.* **10,** 189 (2000).
22. A. S. Abd-El-Aziz, T. H. Afifi. W. R. Budakowski, K. J. Friesen, E. K. Todd, *Macromolecules* **35,** 8929 (2002).
23. A. S. Abd-El-Aziz, E. K. Todd, R. M. Okasha, T. E. Wood, *Macromol. Rapid Commun.* **23,** 743 (2002).
24. H. Funaki, K. Aramaki, H. Nishihara, *Synth. Met.* **74,** 59 (1995).
25. A. S. Abd-El-Aziz, T. H. Afifi, E. K. Todd, G. Z. Ma, *Polym. Prepr.* (*Am. Chem. Soc., Div. Polym. Chem.*) **42**(2), 450 (2001).
26. A. S. Abd-El-Aziz, E. K. Todd, T. H. Afifi, *Macromol. Rapid Commun.* **23,** 113 (2002).
27. A. S. Abd-El-Aziz, C. R. de Denus, E. K. Todd, S. A. Bernardin, *Macromolecules* **33,** 5000 (2000)
28. A. S. Abd-El-Aziz, A. L. Edel, K. M. Epp, H. M. Hutton, *New J. Chem*. **23,** 569 (1999).
29. A. S. Abd-El-Aziz, A. L. Edel, L. May, K. M. Epp, H. M. Hutton, *Can. J. Chem.* **77,** 1797 (1999).
30. A. S. Abd-El-Aziz, L. May, A. L. Edel, *Macromol. Rapid Commun.* **21,** 598 (2000).
31. A. S. Abd-El-Aziz, E. K. Todd, G. Z. Ma, J. DiMartino, *J. Inorg. Organomet. Polym.* **10,** 265 (2000).
32. A. S. Abd-El-Aziz, E. K. Todd, *Polym. Mater. Sci. Eng.* **86**(1), 103 (2002).
33. A. S. Abd-El-Aziz, L. J. May, J. A., R. M. Okasha, *J. Polym. Sci. Part A, Polym. Chem.* **39,** 2716 (2001).
34. A. S. Abd-El-Aziz, R. M. Okasha, J. Hurd, E. K. Todd, *Polym. Mater. Sci. Eng.* **86**(1), 91 (2002).
35. A. S. Abd-El-Aziz, E. K. Todd, manuscript in preparation.
36. P. Schwab, M. B. France, J. W. Ziller, R. H. Grubbs, *Angew. Chem. Int. Ed. Engl.* **34,** 2039 (1995).

Macromolecules Containing Metal and Metal-like Elements, Volume 2: Organoiron Polymers, Edited By Alaa S. Abd-El-Aziz, Charles E. Carraher, Jr., Charles U. Pittman, Jr., John E. Sheats, and Martel Zeldin
ISBN 0-471-45078-2

Index

M

T